Dynamic Capacity Enhancement Using a Smart Antenna In Mobile Telecommunication Networks

Freeborn Bobor-Oyibo

A thesis submitted in partial fulfilment

of the requirements of the

University of Northumbria at Newcastle for the degree of

Doctor of Philosophy

Research undertaken in the

School of Computing, Engineering and Information Sciences

November 2011

Table of Contents

ABSTRACT

This work describes an investigation into the performance of antennas for mobile base station applications and techniques for improving the coverage and capacity within a base station cell. The work starts by tracing the development of mobile systems, both in technical and commercial terms, from the earliest analogue systems to present day broadband systems and includes anticipated future developments. This is followed by an outline of how smart antenna systems can be utilised to improve cell coverage and capacity.

A novel smart antenna system incorporating an array of slant $\pm 45^0$ dual- polarised stacked patch elements four columns wide excited by a novel multi-beam forming and beam shaping network has been designed, simulated and implemented. It is found that for an ideal smart antenna array, four narrow overlapping beams, one wide "broadcast channel" beam and right and left shaped beams can be provided. Results are presented for the simulation of the smart antenna system using CST EM simulation software which inherently includes mutual coupling and the effects of a truncated ground plane on the element patterns. The results show some significant changes to the desired set of coverage patterns and various mutual coupling compensation techniques have been reviewed.

An improved design technique has been developed for compensating the performance degrading effects of mutual coupling and finite ground plane dimensions in microstrip antenna arrays. The improved technique utilises combination of two previously known techniques: complex excitation weights compensation by inversion of the array mutual coupling scattering matrix and the incorporation of a WAIM (wide angle impedance matching) sheet. The technique has been applied to a novel multi-beam smart antenna array to demonstrate the efficacy of the technique by electromagnetic simulation. In addition, a demonstrator array has been constructed and tested which has yielded a positive conformation of the simulation results. For the developed demonstrator array which provides seven different beams, beams "footprints" have been predicted both for free space propagation and for urban propagation to evaluate the dynamic capacity performance of the smart antenna in a 3G mobile network. The results indicate that sector capacity can be dynamically tailored to user demand profiles by selection of the appropriate beam patterns provided by the novel smart antenna system.

LIST OF FIGURES

LIST OF TABLES

GLOSSARY OF ABBREVIATIONS

2G	Second generation
3G	Third generation
3GPP	Third generation partnership project
AS	Angular spread
AUT	Antenna under test
BFN	Beam forming network
BSC	Base station controller
BSS	Base station subsystem
BTS	Base transceiver station
CDMA	Code Division Multiple Access
dB	decibel
DBF	Digital beam forming
DL	Downlink
DS-CDMA	Direct sequence code division multiple access
DSP	Digital signal processor
E_b/N_0	Energy per bit divided by noise per hertz
EM	Electromagnetic
FDD	Frequency division duplex
FDMA	Frequency Division Multiple access
GSM	Global System for Mobile Communication
HSDPA	High speed downlink packet access
HSDPA	High speed downlink packet access
IM	Interference margins
IM_{UL}	Interference margin at the uplink
ISI	Inter-symbol interference
ITU	International telecommunication union

Kbps	Kilo bits per second
KPI	Key performance indicator
LS Beam	Left shaped beam
Mbps	Mega bits per second
MC	Mutual coupling
MHz	Mega hertz
MIC	Microwave integrated circuit
MIMO	multiple input multiple output
MMIC	Monolithic microwave integrated circuit
MS	Mobile station
MSC	Mobile Switching Centre
NP	Noise power
OVSF	Orthogonal spreading factor codes
PAS	Power azimuth spread
PCB	Printed circuit board
PIM	Phase intermodulation
PL	Path loss
PSTN	Public switching telephone network
QoS	Quality of service
RF	Radio frequency
RNC	Radio network controller
RNS	Radio network subsystems
RS Beam	Right shaped beam
S	Signal
S/N	Signal to noise ratio
SCDMA	Synchronous Code Division Multiple Access
SDMA	Space division multiple access

SIM	Subscriber identity module
SNIR	Signal to Noise Interference Ratio
SR	Spread rate
T/R	Transmit and Receive
TDD	Time division duplex
TDMA	Time Division Multiple access
TD-SCDMA	Time Division Synchronous Code-Division Multiple –Access
TRXS	Transceiver
Tv	Television
UK	United Kingdom
UL	Uplink
UMTS	Universal Mobile Telecommunications System
UTRAN	Universal terrestrial radio access network
VET	Variable electrical tilt
WAIM	Wide Angle Impedance Matching
WCDMA	Wide Code Division Multiple Access

GLOSSARY OF SYMBOLS

μ	Mean
α	Orthogonality factor
φ	Phase shift associated with a transmission line
ξ	Sectorisation gain
σ	Standard deviation
$\Delta\varphi$	Set of different inter-element phase shifts
$\Delta\phi_1$	First variable phase shifter
$\Delta\phi_2$	Second variable phase shifter
$\Delta\phi_3$	Third variable phase shifter
Γ_A	Active reflection coefficient
ε_{eff}	Effective dielectric constant
Δh_b	Difference between base station height and building height
Δh_m	Difference between the building height and mobile antenna height
$\Delta Ø$	variable phase in degree
ε_r	dielectric constant
$[a_i]$	Complex incident voltage wave
$[a_i']$	Compensated excitation voltage wave
$[a_n]$	n^{th} excitation complex weight
$[b_i]$	Complex reflected voltage wave
$[b_n]$	n^{th} complex reflected complex weight
$[S_{ij}]$	S-parameters
[u]	Unit vector
$[v_i]$	Element excitation voltage wave
$a^{[\,]}$	Sampled amplitude
a_1	Output complex weight at port one of the beam shaping network

$a_{2,}$	Output complex weight at port two of the beam shaping network
a_3	Output complex weight at port three of the beam shaping network
$a_{4,}$	Output complex weight at port four of the beam shaping network
AF(Ø)	Horizontal array factor
$A_m e^{j\phi m}$	N beam port weight
B	Channel bandwidth in hertz
B1L	first left narrow beam
B1R	first right narrow beam
B2L	second left narrow beam
B2R	second right narrow beam
C	Capacity in bits per second
D	Antenna under test aperture
d	Average separation between buildings
E(Ø)	Azimuth radiation pattern in the far field
Ee(Ø)	Horizontal pattern of the column element
E_x	Electric field component in the x-direction
E_y	Electric field component in y-direction
F	Transfer function
f_c	Centre frequency
f_H	Higher band frequency
f_L	Lower band frequency
G(θ,Ø)	Gain of a transmitter antenna in the direction of receiving antenna
G_a	Antenna gain
G_{AUT}	Gain of antenna under test
L_{fast}	Loss due to fast fading
G_{SGH}	Gain of standard horn antenna
L_{slow}	Loss due slow fading

i	interference
$I_n(t)$	Interference signal source
K	Constant
L_{fs}	Free space propagation loss
L_{msd}	Multiple screen diffraction loss
L_{rts}	Rooftop to street loss
MS_j	j^{th} mobile station
Node B	Third generation base station
n_s	Number of sectors
$\emptyset^{[\ ]}$	Sampled phase
P_1	Power at port one
P_2	Power at port two
P_3	Power at port three
P_4	Power at port four
PL_j	Path loss from the j^{th} mobile user
P_r	Receive power
$P_{rflected}$	Total reflected power
P_t	Transmitted power
Q_m	Factor which depends on the relative height of base station antenna
R	Straight line between transmitter and receiver
R_j	User j^{th} bit rate
$S_j(t)$	j^{th} port signal ports
ν_j	Service activity factor
W	chip rate
w_n	array complex weight
$w_n e^{j\psi}$	Total complex weight needed to form shaped beam
x	Horizontal distance between the mobile and diffracting edges

$y(t)$	Output signal with time
y_j	Total signal appearing at port j
Z_0	characteristic input impedance
Z_1	Through line impedance
Z_2	Branch line impedance
Z_{in}	Input impedance
η	Load factor
λ_0	Wavelength in free space
λ_g	wavelength in dielectric
Φ_n	n number of arbitrary angle

DEDICATION

The Lord has blessed me with a wonderful family to whom this thesis is dedicated.

To my wife Mrs Elizabeth Okiemute Oyibo and our children Precious, David and Joseph

ACKNOWLEDGEMENTS

I wish to express my thanks to God for his providential care lavished on me during the course of this research. My special thanks go to my supervisors Professor David Smith and Professor Stephen J. Foti for their guide and advice on every step and stages of this research. I would also like to thank Professor Stephen J. Foti again for proof reading this thesis.

My sincere thanks also go to Dr. Gillian Brooks and the entire academic and technical members of Northumbria Communication Research Laboratory for helping me out from time to time. I specially thank my family, especially my wife - Elizabeth, for their constant support, patience, understanding and encouragement throughout the duration of this work.

DECLARATION

I declare that the work contained in this thesis has not been submitted for any other award and that it is all my own work. I also confirm that this work fully acknowledges opinions, ideals and contributions from the work of others.

Name: Freeborn Bobor-Oyibo

Signature:

Date:

Chapter 1 - INTRODUCTION

1.1 Background

The era of Wireless communication began with the work of Heinrich Hertz in 1886 when he first demonstrated wireless technology. In 1901 the first practical application of radio wave to communicate over a long distance was demonstrated by Guglielmo Marconi. Since then communication has not been inherently limited to users' equipment and wires only, instead a freedom to roam and still communicate was possible, however only relatively few individuals were able to enjoy this type of communication [1-2]. The increasing demand for mobile telecommunication services has made mobile telecommunication evolve through the years [3-9].

The First generation of mobile telecommunication technology was analogue and it was introduced in the 1980s mainly for voice services communication only [3-4]. Second generation (2G) mobile telecommunication technology was digital and was introduced in 1990, with increased features to provide voice services and basic data transmission services [5]. To support more multimedia services like video messaging and to provide improved quality of service and higher data rates compared to second generation mobile telecommunications, third generation (3G) technology was introduced. Third generation technology is digital, with the capability to provide various forms of multimedia services like video telephoning, good quality of service and can be used anywhere in the world [5-9]. It has higher data transmission rates and enhanced features for more efficient use of the precious spectrum resource compared to 2G. 3G mobile telecommunication can provide higher data rates of about 384 kbps to 2Mbps compared to GSM (Global systems for mobile communication) network that is offering between 10 kbps to 20 kbps only[1-2].

Today, mobile telecommunications represent the dominant percentage of all telecommunication subscriptions around the world. Research has shown that during the early part of this decade, the number of mobile telecommunication subscribers has surpassed that of conventional fixed lines telecommunication [10-13].

The field of wireless communications is developing at a fast rate, covering many technical areas and it has a wide influence on various aspects of human endeavour. At the end of 2011, worldwide cellular subscription passed 6 billion and the rapid growth is expected to last for many years [14]. The worldwide activities in this fast growing industry are perhaps an indication of its importance to human development. The growth of this industry has exceeded all estimates and forecasts. Indeed the question has not been where the demand

is, but instead the question has been how the demands of subscribers can be met. With the demand for mobile communication services increasing at an exponential rate there is a need to: increase capacity, extend coverage and improve transmission quality for network providers to effectively accommodate the increased wireless traffic in their networks and to satisfy customer expectations [6, 9, 15-16].

To accommodate the increase in mobile subscriber demand, 3GPP has developed fourth generation (4G) radio access technology and Long Term Evolution (LTE), which employs the MIMO-OFDM radio interface. 4G is anticipated to solve still-remaining problems of 3G systems and to provide a wide variety of new services, from high-quality voice and high-definition video to high data rate of about up to 1Gb/s in wireless channel [12]. However, as WCDMA is expected to remain the leading mobile Internet machinery for a number of years, the WCDMA standard continues to expand, especially in the High Speed Packed Access (HSPA) subsystem.

1.2 Research Motivation and Justification

The ever increasing numbers of mobile communication subscribers has placed challenges on mobile network providers to maintain coverage, capacity and quality of service for its users [7, 15-17]. A number of different techniques are being investigated to assist with these challenges and the use of smart antennas is one area currently under investigation. Currently, each base station (mobile phone mast) typically incorporates three fixed beam sector antennas, each providing coverage over a 120-degree sector [18]. However, this approach wastes power in directions away from users and accepts interference from directions of all users. Furthermore, in 2G networks coverage and capacity are independent; however, in 3G networks employing wide-band code-division multiple-access (WCDMA) capacity and coverage are no longer independent[19]. This is due to the fact that as more users access a particular base station additional noise is added to other user channels because all digital codes are not perfectly orthogonal. This gives rise to an effect known as “cell breathing”. Since the edge of cell coverage is defined by a specific minimum signal-to-interference plus noise ratio (SINR), then as the noise floor increases, when additional users access the particular cell, the SINR drops below the minimum level; hence, the user must move closer to the cell centre to regain the minimum SINR. Clearly the cell has shrunk. Since this effect is dynamic (dependent upon the instantaneous number of users accessing the base station), it is therefore desirable to incorporate antennas, which

provide multiple simultaneous narrow beams and shaped beams which suppress interference to overcome the above problems [18-22].

1.2.1 Traditional Techniques to Increase Coverage and Capacity

The conventional ways of increasing coverage and capacity are to acquire additional carriers, mast head amplifiers and active antennas [23], higher order receive diversity, transmit diversity [9, 21, 24-25], higher sectorisation [15-16, 20, 25], infrastructural sharing and adding more cells [25-26]. For all the methods listed above there are associated problems. In the case of cell addition, cells are very expensive not only in terms of equipment but also real estate cost, regulatory fees and potential legal fees associated with fighting objections from local residents who do not want mobile base stations nearby (protests arise from regulatory and political issues as to the RF signal exposure limits, abutting owner veto's against new masts and prohibitions of new sites on public buildings). Additionally, such systems are fixed and cannot easily adapt to changing demands.

Traffic load imbalance places additional challenges on mobile telecommunication network providers this occur due to the movement of mobile users and their variable capacity demands in a mobile communication network. Just as traffic users can be highly concentrated in an area, it can also happen in a sector of a cell in a network. Most areas with high traffic density are often time-variant; consider football stadiums and or other sports grounds which present high user density during the hours of the game, but light traffic after the football match [28-29]. The problem is that traffic in the most highly loaded sector would jam up the capacity in the other light load sectors. This causes the unused capacity to be locked up and the cell site reaching its capacity limit prematurely. Various methods have been used to correct the problem of load imbalance from the first generation of wireless communications to the third generation, and the most commonly reported techniques are cell splitting [25], channel borrowing, channel sharing [30-32], dynamic channel allocation [33], new soft handover schemes [34], cell overlay [35], use of variable tilted antennas [36-37], dynamic cell-size control [38] and dynamic sectorisation [39] etc. It is necessary to note that all the listed techniques have their limitations. Re-sectorisation and overlay of a cell site tend to increase call handover in mobile telecommunication networks [23].

Smart antennas have emerged as one of the most promising techniques that can solve the problem of capacity, coverage and high quality transmission and traffic load imbalance [15, 23, and 40]. Each of the simultaneous narrow beams of a smart antenna concentrate

transmitted power to a specific user and only “looks” in the direction of the user for the received signal, thus minimising interference from other users. Hence, cell breathing is greatly reduced [15-16, 23]. This ensures that the user receives the optimum quality of service and maximum coverage from a base station. A major feature of smart antennas is the ability to dynamically change the beam characteristics [16]. The use of smart antennas provides a higher capacity in wireless networks, combats multi-path, co-channel interference impairment and also reduces to less than half, the number of base stations required for wireless communication systems (if deploying a new network), thereby increasing both the performance and capacity of wireless network systems [15, 40].

Despite the numerous advantages promised by the smart antenna, migration of this technology into mobile networks has been slow [23]. Various reasons have been given to explain why it has not been fully used. The reasons have ranged from the fact that smart antennas were not planned in second-generation systems, smart antennas require very large panels, the benefits of smart antenna systems proved hard to quantify, the cost of the smart antenna is too high and many appliqué systems disabled the space-diversity reception feature on second-generation systems [23]. However, time division synchronous code-division multiple-access (TD-SCDMA**)** proposed by China Academy of Telecommunication Technology, which was accepted by the International Telecommunication Union(ITU) in November 1999 as one of the 3G standards, is the only system that requires all base stations to use smart antennas. It has been proven that the TD-SCDMA and SCDMA system with smart antennas greatly increases capacity, coverage and quality of service to subscribers [42]. The question is how can it be fully utilized to the optimum techno-economic advantage?

The majority of current studies of smart antennas has been directed towards the quantification of the capacity smart antennas can offer, direction of arrival, angle of arrival, smart antenna algorithm and propagation effects [43-49]. Therefore to accommodate the current demand for services from mobile communication users and solve the problem of traffic load imbalance, there is a need for new intelligent or self-optimized and highly efficient systems. In the pursuit of a cost effective technique that will solve this problem, attention has recently turned to smart antenna systems and many articles have been published [29, 50-55]. In [52] it has been proposed that one way of achieving load balancing is to modify the antenna orientation and angular beam width of each sector to unify the traffic, this is possible using smart antennas. In [53] the author uses a cooperative

negotiation technique and semi-smart antenna to provide dynamic geographic load balancing for mobile cellular networks. The negotiation was used as an intelligent control to adjust the cell sizes and shapes of the whole cellular network. Reference [54] uses a case-base reasoning with semi-smart antenna to change the cell size and shape for load balancing. The technique built up a case library that stores typical traffic patterns and the corresponding antenna patterns so that when a cell is overloaded the network can react quickly by adjusting the size and shape of the cell to balance the load. The technique is effective but complex. The use of a smart antenna to increase uplink capacity of a CDMA mobile telecommunication network was reported in [55]. The method maximizes capacity by using a switched beam smart antenna system with an adaptive sectoring algorithm to combine a subset of the switched beams in the base stations of mobile telecommunication networks. The adaptive sectoring algorithm relieves the sector load as soon as the outage probability begins to increase and then divides the mobile users between the three sectors. The techniques according to [55] is claimed to be effective because it shows that no sector has outage probability that is above 1% compared to that of fixed three-sector base station of a mobile telecommunication network. However it should be noted that their result presented in the paper is that of simulation and the authors acknowledge that it remains to test this concept in real traffic scenarios. The use of smart antennas to dynamically optimize the network for enhancement of coverage in sub-sectors while maintaining capacity has not been investigated.

1.2.2 Outline of New Smart Antenna System

By employing a multiple switched beam smart antenna which can provide beam shaping, an intelligent sector optimisation of varying azimuth beam shape can be established. The developed technique, multiple switched beam smart antennas with beam shaping network can be used to dynamically optimise sector coverage and capacity, especially for hotspots in mobile networks cell sectors. Furthermore, base stations currently equipped with one transceiver per sector per polarisation with a conventional sector antenna and the new antenna system would not be required to add transceivers when the proposed design is implemented. In this project a smart antenna that will dynamically optimise a cell sector to relieve congestion at a single hotspot cell sector have been designed, simulated and implemented. To appreciate the contribution of the subject research to the enhancement of capacity in mobile telecom networks, it is important to note that previous multiple access techniques to increase capacity have exploited the time domain (TDMA), the frequency

domain (FDMA) and the digital signal processing domain (WCDMA). The single remaining domain for significant capacity improvement to be realised is that of the *spatial* domain. What is desired is an antenna system that essentially provides spatial filtering, i.e. the antenna must be capable of providing a specific radiation pattern level as a function of spatial angle. In addition, because the mobile network "traffic" is continuously changing as users move and demand varying data rates dependent upon the multi-media services that they may request, the required shaped radiation pattern must be dynamically variable. The proposed antenna system achieves this requirement in a very cost-effective manner and the "optimisation" provided may be considered a *soft optimisation* which essentially operates in an open loop manner by monitoring the traffic channel monitor data. Hence, the capacity in a given coverage area can be optimally distributed to both high data rate and low data rate (i.e. voice only) users simultaneously.

1.3 Research Objective

This research work is aimed at designing, analysing, simulating and proving smart antenna concepts that will dynamically optimise cell sector coverage and capacity of mobile telecommunication networks, especially for hotspots in the mobile network cell sector, without increasing the network base station radio frequency electronics. To achieve this, the research objectives are outlined as follows:

- Review 2G and 3G mobile communication networks using traditional antennas and identify current challenges of mobile network operators.
- Review the fundamental properties of smart antenna technology.
- Design and analyse a smart antenna system that will dynamically optimise coverage and capacity over a 120^0 sector.
- Simulate the dynamic operating states of the antenna system over the 3G frequency band.
- Analyse the effects of mutual coupling on the smart antenna system radiation pattern and return loss performance and compensation, if possible.
- Implement the beam shaping, multi-beam forming networks and array antenna (with a reduced size array – one element in place of each 10 element column – to

produce the desired azimuth radiation patterns) as a *demonstrator* to prove the concept.

- Experimentally test the demonstrator and extrapolate the smart antenna performance (i.e. a four column, ten elements per column array) using the measured results from the demonstrator.

- Develop an analytical model that can be applied to predict the mobile user's antenna received power footprint contour (on the downlink) and determine capacity versus coverage.

- Review network planning strategy with the proposed smart antenna and investigate strategic deployment of the smart antenna system in mobile telecommunication networks.

1.4 Thesis Organization

This thesis report is arranged into eleven chapters, following the introduction chapter is chapter two which presents the basic structure of current mobile telecommunication networks (GSM and UMTS). 2G and 3G network architectures with their distinguishing features, conventional tri-sector antenna system and capacity limitations of current 3G systems are presented in this chapter. The fundamentals of smart antenna technology along with benefits and cost/performance trade-offs are also mentioned in chapter three. Alternative multiple fixed beam forming networks and the major building blocks of the multiple switched beam smart antenna system is discussed. Modelling and analysis of the proposed smart antenna concept is presented in chapter four.

Chapter five presents the design of the fundamental components of the smart antenna system. The antenna array element, array antenna and the feed (Butler matrix and beam shaping network) network design is presented in this chapter.

The simulation results of all the fundamental components of the smart antenna system designed in chapter five is presented in chapter six. The full network simulation result at the uplink of the chosen frequency band is also presented in this chapter.

Chapter seven analyses the effects of mutual coupling on antenna array and techniques to mitigate the mutual coupling effects. This chapter highlights the performance limitation of compensation of excitation weights (based on the inversion of the array scattering matrix)

to compensate mutual coupling effects in a small array antenna and presents alternative techniques to compensate mutual coupling. The chapter is concluded by investigating the effects of combined wide angle impedance matching (WAIM Sheet) techniques and modified weight compensation techniques to compensate mutual coupling.

Chapter eight gives a detailed description of the experiments used to measure the various components of the smart antenna demonstrator. The measured antenna radiation patterns, return loss, active reflection coefficient, insertion loss and the antenna gain is presented in this chapter.

Chapter nine presents analysis of received power footprint contour of the smart antenna system which is useful for radio network planners. The same chapter also discusses the estimated capacity versus antenna range that can be provided by the smart antenna system when used in 3G telecommunication system. Chapter ten provides an analogical overview of current network planning strategy and a basic radio network planning procedure for 3G and a strategic way to plan a radio network with the proposed smart antenna.

Chapter eleven discusses the key findings of this research, summarising and concluding comments and recommendations for future research are outlined.

1.5 Original Contributions

During the course of this research, the author has:

1. Investigated the use of multiple beam-forming networks, plus beam shaping networks with one transceiver per polarisation to dynamically enhance sub-sector coverage and maintain capacity of a cell sector in a mobile telecommunication network as detailed in chapter four.
2. Designed and simulated a smart antenna system incorporating an array of slant $\pm 45^0$ dual-polarised stacked patch elements, four columns (ten elements) wide excited by a multi-beam forming and beam shaping network with one transceiver per polarisation as detailed in chapter five and chapter six. It is demonstrated that using only three phase shifters within the beam shaping network provides dynamic beam flexibility. For an ideal array (i.e. no mutual coupling and cosine element pattern) four narrow overlapping beams, one wide “broadcast channel” beam and right and left shaped beams can be provided with one transceiver per polarisation. These are all detailed in chapter six.

3. Investigated the performance of the smart antenna system in the presence of mutual coupling and employed complex excitation weights compensation and WAIM (wide angle impedance matching) sheet techniques to compensate the effects of mutual coupling. This is presented in chapter seven.
4. Developed an improved design technique for compensating the performance degrading effects of mutual coupling and finite ground plane dimensions in microstrip antenna arrays, as discussed in chapter seven. The improved technique utilises two previously known techniques in combination (complex weight compensation and WAIM sheet), but iteratively optimised
5. Constructed and tested a demonstrator array to facilitate experimental verification of the simulation results which has yielded a positive conformation of the usefulness of the technique; these are all detailed in chapter eight.
6. For the developed smart antenna system which provides seven different beams (wide beam for broadcast channel, four narrow beams and left and right shaped beams), in chapter nine the beam "footprints" have been predicted both for free space propagation and for urban propagation (using COST 259 model) to evaluate the dynamic capacity performance of the smart antenna in a 3G mobile network.

These contributions are summarised in Fig.1.1 on the following page and have led to the publications listed in section 1.6.

Fig 1.1 Project roadmap & showing thesis contributions

1.6 List of publications

Journal Paper

[1] Freeborn Bobor-Oyibo, David Smith, Stephen J. Foti ‘‘Design and measurement of a multiple switched beam smart antenna with beam shaping capability using dual-polarized slant $\pm 45^0$stacked patch elements’’ Microwave and Optical Technology Letters (under review)

Conference

[2] F. Bobor-Oyibo, S. J. Foti, and D. Smith, "A multiple switched beam Smart antenna with beam shaping for dynamic optimisation of capacity & coverage in mobile telecommunication networks," in *Antennas, Propagation and EM Theory, 2008. ISAPE 2008, 8th International Symposium on*, pp. 356-359, 2008.

[3] F. Bobor-Oyibo, D. Smith, and S. J. Foti, "The effects of a finite ground plane on the characteristics of printed patch antennas with and without a suspended patch," in *Communication Systems Networks and Digital Signal Processing (CSNDSP), 7th International Symposium on*, pp. 111-114, *2010* .

[4] Freeborn Bobor-Oyibo, David Smith, Stephen J. Foti ‘‘Design and measurement of a multiple switched beam smart antenna with beam shaping capability using dual-polarized slant $\pm 45^0$stacked patch elements’’ Mediterranean microwave symposium procedings Tunisia 2011

[5] Freeborn Bobor-Oyibo(1), Stephen J. Foti(2), David Smith(3) , Okan Yurduseven(4) ‘‘A Smart Antenna System with Sub-Sector Dynamic Capacity Enhancement for Mobile Telecommunication Networks’’ 2012 IEEE International Workshop on Antenna Technology: Small Antennas and Unconventional Applications Tucson, Arizona, USA (accepted for publication December 2011)

[6] Okan Yurduseven*(1), David Smith (2), Freeborn Bobor-Oyibo (3), and Stephen J. Foti (4) ‘‘Design of a Highly Efficient Beam Scanning Asymmetric H-Plane Horn Antenna’’ 2012 IEEE International Workshop on Antenna Technology: Small Antennas and Unconventional Applications Tucson, Arizona, USA(accepted for publication December 2011)

Poster

[9] F. Bobor-Oyibo, D. Smith, and S. J. Foti, ‘‘Compensation of mutual coupling effects in a multiple switched beam smart antenna with beam shaping capability’’ Northumbria university conference, June 2011

Chapter 2 - OVERVIEW OF MOBILE TELECOMMUNICATIONS

2.1 Introduction

This chapter will provide a brief overview of 2G (GSM) and 3G basic mobile telecommunication systems. Coverage and capacity limitations in 3G systems and methods used to increase coverage, capacity and traffic load balancing especially in hotspot areas of a mobile telecommunication network will also be reviewed.

2.2 2G Mobile Telecommunication Networks

A very good treatment of the subject discussing technologies utilized in existing and current mobile telecommunication networks, the performance in terms of services, and evolution in wireless system development can be found in [56]. Throughout this thesis, the term “mobile” is used to denote a communications device on the move, including a mobile handset. To begin with, let us see the basic architecture of a GSM mobile communication network and how a typical mobile communications system involving land mobiles and base stations works [57, 58].

Mobile telecommunication networks are designed to serve large geographical areas with limited frequency bandwidth and it is different from the traditional fixed-line telecommunication network with characteristics of high operating frequencies. Fig 2.1 shows a basic GSM mobile telecommunication network system with three major sub-systems, which are: mobile station (Ms), base station sub-system (BSS) and the mobile switching centre (MSC). The mobile switching centre connects all the mobile phones to the public switching telephone network (PSTN). The mobile station (MS) is made up of two elements, the handset and subscriber identity module (SIM card). The SIM card provides the user access to the network and the most important task of the SIM card is authentication, (the process of validating the subscriber to the MS prior to the use of the network) radio transmission security and the storing of user’s data [1-3, 25, 56-58].The second major element of a mobile telecommunication network is the BSS. In GSM it consists of a base transceiver station (BTS) and a base station controller (BSC). The area served by a mobile communication network is divided into small areas called cells. Each of these cells contains base station transceivers which provide connection to the mobile station through the air interface. The BTS functions include generation of radio frequency (RF) carriers, modulation and demodulation of RF carriers, base band data processing error coding, etc. The BSC controls a number of BTSs [57-58] and handles signalling, traffic and operations and maintenance signals to and from all BTSs under its control. It has

some switching functionality which enables it to establish terrestrial to radio channel connections for traffic and signalling to mobiles. The switching functionality also enables it to carry out intra- and inter- BTS handovers without the intervention of the MSC. The third element is the MSC and its major function is that of switching and connecting mobile subscribers of a network to other network subscribers, fixed or mobile [58]. All the BSCs are connected to the MSC for control.

The frequency spectrum bandwidth available to GSM mobile telecommunication networks is utilized in a number of ways referred to as multiple access techniques. Mobile telecommunication network access techniques have a profound influence on the network capacity. The three major multiple access techniques used in GSM are FDMA, TDMA, and CDMA. In FDMA (frequency division multiple access) systems the available spectrum bandwidth is shared among the network subscribers by assigning different frequencies to various users. To reduce interference between two subscribers the frequency pair is separated by some amount of frequency (e.g. 45MHz and 80MHz in North American cellular system). TDMA (time division multiple access) is a digital transmission techniques, in which each user occupies a specific frequency but only communicates during an assigned time slot. The frequency is used by other users during other time slots. The TDMA technique improves the transmission and also increases capacity of the mobile telecommunication network. In CDMA (code division multiple access) techniques users are only separated by code and all users can occupy the same bandwidth [25, 57-58].

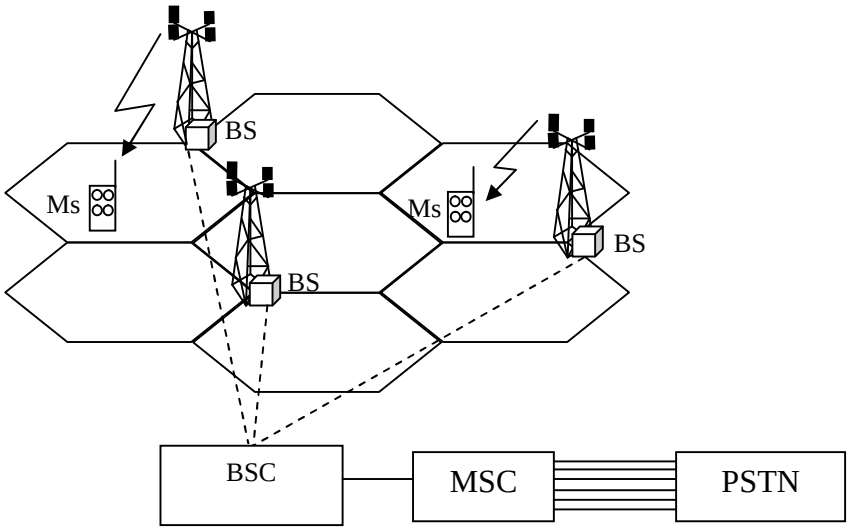

Fig .2.1: A basic GSM mobile communication network architecture [25]

2.3 3G System Overview

3G which is also referred to as Universal Mobile Telecommunications System (UMTS), is the mobile communication system that followed on from the 2G mobile communication system as 2G started to reach it limits in terms of spectral efficiency along with increasing demands for higher data rate services[25]. The need to improve the network capability and efficiency of spectrum utilization to provide higher data rate led to the introduction of 3G [3-8, 16, 25]. 3G has the ability to provide multimedia services especially internet services of about 144kb/s (Outdoor), 384kb/s (from outdoor to indoor) and 2Mb/s (indoor). It has a better quality of speech and other services compared to 2G. The 3G system that is based on WCDMA makes use of 5MHz of bandwidth in both uplink and downlink using frequency division duplex (FDD) [5-8, 16, 25]. It does not assign a specific frequency to a subscriber but rather every mobile user accesses the full available spectrum and discrimination is based on orthogonal digital codes.

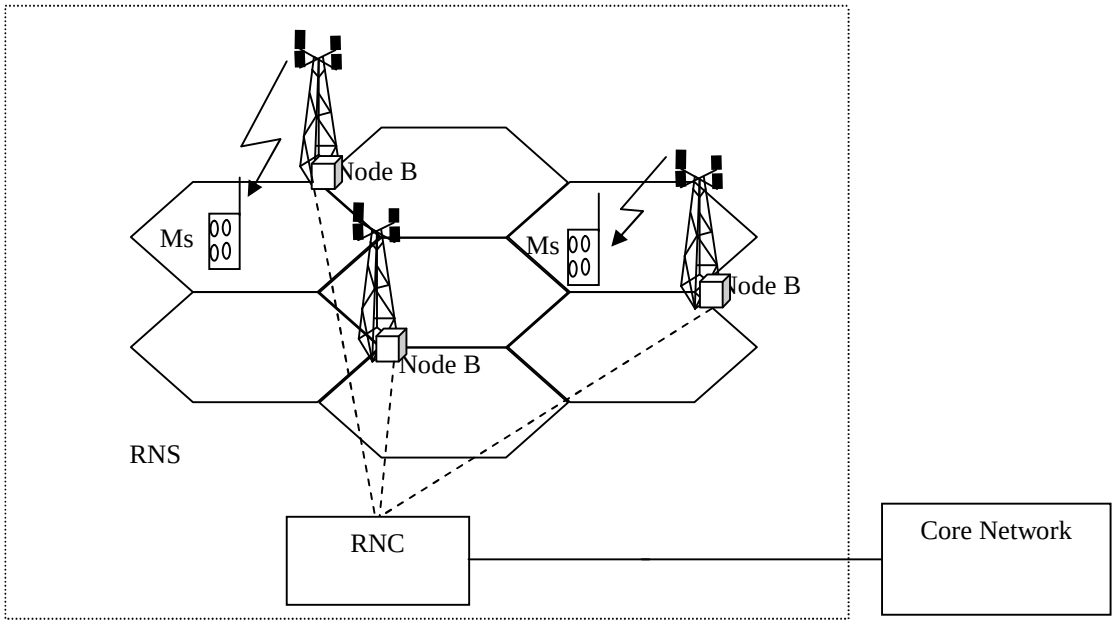

Fig .2.2: Basic UMTS network [25]

The basic architecture of a UMTS mobile telecommunication network based on a W-CDMA air interface [59] is shown in Fig 2.2. The architecture is divided into core network and radio network subsystems (RNS). The core network is responsible for performing switching and transmission functions to external networks. The RNS consists of a radio network controller (RNC) connected to one or several node Bs. The Node B is the base station transceiver and is controlled by the radio network controller (RNC) [59]. In 3G the frequency spectrum is utilized far more efficiently, and the data flow and its bit rate are not

dependent on time slots anymore [16, 25]. 3G has a completely new way to approach the term ‘Service’. All the services offered are different from that of 2G from technology platform point of view. One of the key requirements for UMTS is GSM/UMTS inter-operability, such as system handover whereby the radio access is able to switch from GSM to WCDMA and vice versa during the transmission. Three major standards are currently accepted for 3G and all are based on CDMA access technology (where each user occupies a signal on a particular frequency simultaneously with many other users, but is uniquely distinguishable by correlation with a special code used only by this user) which are CDMA2000, WCDMA and time division synchronous CDMA (TD-SCDMA) [3-4, 16 and 25].

2.3.1 CDMA2000

CDMA2000 is a wideband spread spectrum interface that uses CDMA access technology, but still maintains compatibility with IS-95 base station systems. It means that mobile handsets designed using the IS-95 standard can operate in a CDMA2000 system and vice versa. The CDMA2000 standard’s first component is called 1X radio transmission technology (1XRTT), the reason is that it uses an RF carrier of 1.25MHz like that of IS-95 base system, therefore it is also referred to as spread rate (SR)1. The major benefits of 1XRTT technology standard under the name of IS-2000[60-61] compared to IS-95A/B standard [62] are better forward error correction, fast forward link power control mechanism and multiple services and improved data service support.

2.3.2 WCDMA

WCDMA is the second 3G air interface based on direct-sequence CDMA (DS-CDMA). It uses a chip rate of 3.84Mcps compared to 1.2288Mcps of IS-95 and IS-2000 standards. It requires an RF carrier with 5-MHz bandwidth. The WCDMA air interface has two modes of operation which are: frequency division duplex (FDD) mode, where a pair of 5-MHz carrier is used, and a time division duplex (TDD), where only one carrier is used. Channelization is achieved through the use of orthogonal codes referred to as orthogonal spreading factor codes (OVSF), which are Walsh codes of variable lengths, like that of IS-95 and IS-2000, but source separation is achieved using gold codes[63-64]. To meet the demand for high data rates in multimedia services over a network supporting WCDMA, third generation partnership project (3GPP) has released a new high-speed data transfer protocol named HSDPA. The HSDPA is expected to provide significant improvements over the basic WCDMA data rate transmission [3-4].

2.3.3 TD-SCDMA

The TD-SCDMA operates on low-chip-rate carriers, with 1.6MHz carrier spacing instead of 5MHz for the other wideband standards. It allows end-user data rates up to 2Mb/s in optimal conditions [16, 41]. It uses Time division duplex and the number of timeslots used for uplink and downlink for communication can be adjusted dynamically by the system. TD-SCMA can accommodate uneven traffic with different service data rate requirement both for downlink and uplink than frequency the division duplex (FDD) scheme. One thing that is common to all mobile communication networks is the base transceiver station. In mobile telecommunication systems wires do not exist in a permanent form. The wires (by radiation) that allow communication with the network and its subscribers have to be created before communication can begin. The BTS is responsible to create the radio link that will enable connections to the MSs.

2.4 Capacity Limitations of Current 3G Systems

The capacity of a 3G mobile telecommunication network using WCDMA air interface is known to be interference limited (when there is no code limitation). An increase in the number of active users in the cell causes the total interference seen at the receiver to increase [8, 16, and 22]. This causes an increase in required received power as each user has to maintain a certain signal to interference ratio at the receiver for satisfactory performance. If the maximum capacity is limited by the amount of interference in the air interface, it is by definition a soft capacity, since there is no single fixed value for maximum capacity [63]. The load equation [65] is commonly used initially to estimate average capacity of a WCDMA network cell or sector. There are a number of elements that influence a WCDMA network load, which defines the maximum number of users per cell or per sector. The number of users and their bit rates is one of the elements that influence the total throughput of a cell or sector. The activity factor in speech and data series also affects the network loading. The most important contributor to the network load is the energy per bit divided by the Noise per Hertz (E_b/N_0) requirement, which depends at least on the service type, the data rate of the service, the propagation conditions, and the receiver performance [16, 65]. If a very good quality connection is desired, more bits are need for the error correction in order to guarantee the quality of the connection. Thus, when more bits are used for the error correction, the air interface load and the capacity for the traffic channels are decreased. The well known interference that influences the load of mobile communication network is the own-cell and other-cell interference [16]. Also, if the total

received noise is high, high transmitting powers are needed to guarantee communication and transmit power may be limited. The noise level in mobile communication networks also depends on the environment [16, 25 and 65].

2.4.1 Capacity Estimation in 3G System

Separate load equations are used to estimate the uplink and the downlink capacity of 3G mobile communication networks, but both include E_b/N_0 requirement, processing (bandwidth divided by information rate) gain, activity factor and inter-cell interference [16].

2.4.2 Uplink Load Equation

The uplink loading of a mobile telecommunication network can be estimated using this equation [65]:

$$\eta_{UL} = \sum_{j=1}^{N} \frac{\left(E_b/N_0\right)_j R_j v_j}{W}(1+i) \qquad (2\text{-}1)$$

Where η_{UL} is the uplink load factor, $R_j$is the MSj users bit rate, E_b/N_0 is the required Energy per bit divided by the Noise per Hertz, N is the number of users, v_j is the service activity, i is the interference and W is the bandwidth. From equation (2-1) the energy per bit divided by the Noise per Hertz (E_b/N_0) determines the capacity of a WCDMA access interface, as this decreases then capacity increases but of course the bit error rate gets worse. Any system that can reduce the E_b/N_0 without negative effect to the bit error rate will definitely increase the capacity of the WCDMA air interface [16, 65]. The uplink pole capacity (M_{UL}) is define as.

$$M_{UL} = \frac{W/R}{E_b/N_0 * v(1+i)} \qquad (2\text{-}2)$$

The uplink capacity is based on a formula called the pole capacity and it represents a theoretical limit of simultaneous calls a single sector could support if all the mobile users could maintain their transmit power level at their minimal values with perfect power control.

In calculating the power budget of the uplink, the uplink load factor defines the amount of uplink interference margin (IM_{UL}) in order to take into account the effect of cell breathing (cell shrinkage). It is estimated using this equation:

$$IM_{UL} = -10\log_{10}(1-\eta_{UL})\ \text{dB} \qquad (2\text{-}3)$$

The output power P_j is given by [65]

$$P_j = \frac{\frac{\left(E_b/N_0\right)_j R_j v_j}{W} NP * PL_j}{1-\eta_{UL}} \quad (2\text{-}4)$$

where NP is the noise power, PL_j is the path loss from the j^{th} mobile user to the base station antenna.

The interference margin has a direct relationship with the load factor for a cell or sector of a mobile telecommunication network. Interference margin, which is also called noise rise, indicates how much noise (mobile users) could be added to the noise floor of the receiver to reach the capacity limit. Interference margin, takes note of own-cell and other-cell interference and as the load increases to maximum, the interference margin approaches infinity as shown in the Fig.2.3 below [65]. As the interference margin is increased the coverage area will decrease (cell breathing). This is due to allowing more mobile users into the cell or sector causing more interference, thus reducing the uplink allowed total path loss. Typical interference margins range from 1 to 3dB corresponding to 20% to 50% loading [159-160].

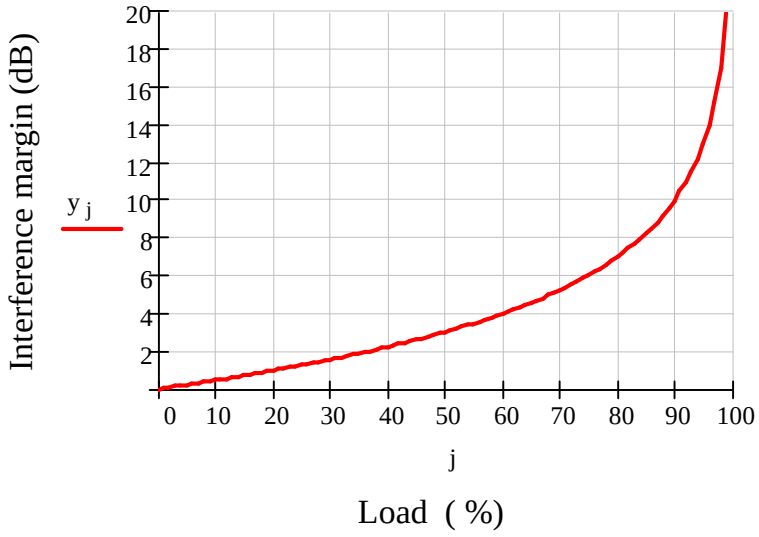

Fig. 2.3: Interference margin as a function of load

2.4.3 Downlink Load Equation

The downlink WCDMA capacity estimate follows the same procedure, but is different in behaviour. In contrast to the uplink loading, the orthognality between the codes affects the downlink loading. The link loss, soft handover, orthogonality of the codes is considered when estimating the downlink capacity. The downlink load equation is given by [65]

$$\eta_{DL} = \sum_{j=1}^{N} \frac{\left(E_b/N_0\right)_j R_j v_j}{W}\left[\left(1-\alpha_j\right)+i\right] \quad (2\text{-}5)$$

and the total transmit power at the base station is given by [65]

$$P_{DL} = \frac{\sum_{j=1}^{N} \frac{\left(E_b/N_0\right)_j R_j v_j * NP * PL_j}{W}}{1-\eta_{DL}} \quad (2\text{-}6)$$

Downlink pole capacity (M_{DL})

$$M_{DL} = \frac{W/R}{E_b/N_0 * v[(1-\alpha)+i]} \quad (2\text{-}7)$$

α_j is the orthogonality factor of j^{th} user (α_j=0.....1). The value of the orthogonality factor depends on the orthogonality of the codes. Orthogonality will be one when there is no multi-path propagation. Multipath propagation destroys orthogonality of the code, thereby increasing interference and finally increasing the downlink load seen by the system. Therefore, a system is needed to mitigate multipath propagation to increase the number of active users of the network [16, 65].

2.5 Conventional Techniques of Increasing Capacity with an Antenna

Conventional antennas for mobile telecommunication networks could be omni-directional antennas which radiate power in all directions or a directional antenna which directs its radiation within a particular angular cell range [15].

There are many types of antennas used in mobile telecommunication like wire antennas, aperture antennas and microstrip antennas etc. Each of these antennas has its own unique characteristics such as impedance, beam width, bandwidth, polarisation, side-lobe level and radiation pattern. Early mobile communication networks used omni-directional antennas for the network cell coverage, but these antennas wasted the limited power to all directions rather than the mobile network user direction. One of the main results is then an increase in interference. The need to improve network capacity and reduce interference

effects led to the development of sectorisation with directional antennas and receives and transmits diversity to reduce the effects of signal fading [15].

2.5.1 Sectorisation

Sectorised antenna systems take a traditional omni-directional cellular base state antenna system and subdivide it into sectors, each of which is served by a directional antenna. Each sector may be treated as a separate cell, which has a greater range than in the previous case [56]. The typical numbers of sectors are the tri-sector and six sector antenna system in mobile communication networks. Tri-sector means the cell has three directional antennas in the cell of the network. Sector antennas increase the possibility of frequency channel reuse (2G) in cellular systems by reducing potential interference across the original cell, and are widely used for this purpose [1-3, 56]. They also minimize or eliminate co-channel interference to neighbouring base stations since their beams are directional. In the case of a tri-sector, the directional antenna typically uses 120^0 10dB beam width. At a minimum, it can triple the capacity of any given coverage area when compared to the capacity that would be offered by deploying omni-directional antennas; however, the network is affected with frequent handovers.

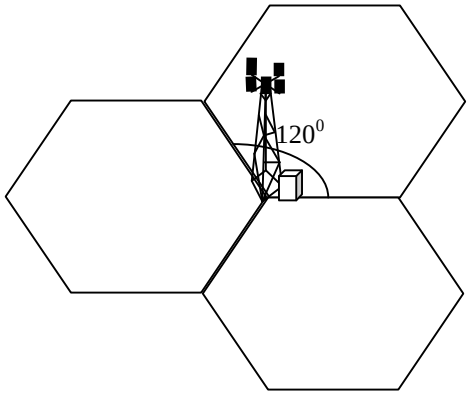

Fig.2.4: Traditional tri-sector base station

A tri-sector BTS (see Fig.2.4) requires at least three transceiver modules (six transceivers for the case of dual-polar antenna for diversity gain). The most important factor influencing the system performance of a sectorised site is the choice of the antenna. To a large extent this determines the levels of inter-cell interference, soft handover overhead and any changes in the maximum allowed propagation loss. The uplink loading of a sectorised base station can be estimated using this equation [16, 65],

$$\eta_{UL} = \sum_{j=i}^{N} \frac{1}{1+\frac{W}{\left(E_b/N_0\right)_j * R_j}} * \upsilon_j \left(1 + i * \frac{n_s}{\xi}\right) \quad (2\text{-}8)$$

where η_{UL} is the uplink load factor, $R_j$is the *MSj* users bit rate, E_b/N_0 is the required signal to interference ratio, *N* is the number of users, υ_j is the service activity, n_s is the numbers of sectors, W is the bandwidth and ξ is the sectorisation gain [16, 65].

2.5.2 Receive and Transmit Diversity

Typical current-generation GSM or 3G base station of mobile telecommunication networks are usually equipped with a two branch diversity receiving/transmitting antenna fed from either a single dual slant-polarised antenna (for polarisation diversity) or two separate vertically-polarised antennas (for spatial diversity) for the diversity scheme to reduce the effects of signal fading in the network.

A diversity scheme is essentially the combination of two or more uncorrelated signals and, since the probability of simultaneous fades on both channels is low, fading is reduced [9, 66]. If the diversity is obtained by using two receiving antennas separated by several wavelengths and combing the signals to reduce fading (for example, by maximal ratio combining) is space diversity [25]. It requires a separation distance *D* of 10-20λ for good de-correlation. Transmit diversity is used in the downlink of mobile telecommunication networks to improve performance of the network in terms of energy to noise ratio. Improvement in the downlink energy to noise ratio translates into improvement of both coverage and capacity of the downlink of the mobile telecommunication network. It is one of the key contributing technologies in defining the ITU allowed 3G system (WCDMA and cdma2000 air interface). The technology has the capability to improve the mobile user's receiver performance in a fading environment by presenting several independent copies of signals at the receiver of a communication link, where the probability of all the copies of the simultaneously transmitted signal to fade is very limited. Detail descriptions and comparisons of space and polarisation diversity can be found in [25, 67].

2.6 Traffic Load Balancing to increase Capacity

Another key problem of mobile telecommunication networks is traffic load imbalance across the network cell sites. This traffic load imbalance problem is as old as the history of mobile telecommunication networks [29, 33, 68, and 69-72]. Various techniques to balance traffic load and maintain coverage and capacity include:

2.6.1 Cell Splitting

With user growth in a particular mobile telecommunication network, a cell may become overloaded. This means that grade of service objectives are not being met due to a higher subscriber number greater than planned traffic levels during the busy hour. In these cases, congested cells can then be subdivided into smaller cells, each with its own base station. With smaller cells lower transmitter power and antennas with less height are used, thus permitting greater frequency reuse (in case of frequency division access techniques). These subdivided cells can also be split still further for even greater frequency reuse. By repeatedly splitting cells, there is increase in the number of base station transceivers and hence an increase in the network capacity. However, there is a practical limit to cell splitting, often a 1.6km minimum cell radius. The use of the cell splitting technique to increase coverage and capacity clearly increases the cost of the network [1, 2, and 25, 73].

2.6.2 Channel Borrowing and Sharing

Channel borrowing or channel sharing (in 2G only) is a scheme introduced to ease the problem of capacity in mobile telecommunication networks. In the case of the channel borrowing scheme, a busy cell can borrow unused channels from an inactive one using a channel borrowing algorithm. Channel sharing is a scheme where channels are allocated to each cel1 dynamically according to its need by introducing a distributed channel sharing algorithm into the network. By doing this no channel can be locked up in one cell while others cells of the mobile telecommunication network are experiencing blockage [25, 70, and 74].

2.6.3 Cell Overlay Schemes

Mobile telecommunication networks often employ different classes of cells with many small cells within an area covered by large umbrella cells, quite often operating in an alternative frequency band (a 900MHz umbrella cell may cover an area also served by several smaller 1800MHz cells). Although the scheme increases the coverage and network capacity it requires an intelligence network to be applied to manage users and the network resources which leaves the network too complex [28].

2.6.4 Variable Electrical Tilt Antennas

Tilting of base station transceiver (BTS) antennas on macro-sites has long been a tool used by network planners to optimise cell coverage and inter-cell interference. In GSM systems an additional tool for minimising inter-cell interference has been that of frequency spectrum management by cell frequency reuse assignments [1, 2 and 25]. In 3G networks utilising WCDMA, inter-cell interference minimisation by frequency spectrum management is not an option since all cells operate over the same wide bandwidth [16, 25]. Furthermore, owing to greater propagation losses at UMTS frequencies, signal-to-(interference + noise) ratios will be sensitive to the precise elevation of beam down-tilt on a site-by-site basis assuming varying terrain. As such, each cell (and perhaps each sector within a cell) may require a different antenna down-tilt. This can be achieved by variable electrical down-tilt antennas and many 3G networks and some 2G networks are now being equipped with these variable electrical tiling antennas which can be remotely controlled without sending riggers to each mast to change mechanical down-tilts [75, 76]. Furthermore, electrical tilting maintains the same elevation down-tilt at all azimuth angles, while mechanical down-tilt does not. Remote electrical tilting ability has also recently been standardised within 3GPP providing a new interface between the BTS and the Radio Network Controller (RNC) systems within a UMTS network [77].

2.6.5 Dynamic Cell-Size Control

Dynamic cell-size control is an adaptive scheme of controlling cell size according to time-variance of geographical mobile telecommunication user distribution. It is a scheme where several BTS radiation patterns are dynamically controlled according to subscriber geographical distribution to reduce outage probability. This scheme can minimize outage probability of the whole cellular system in order to guarantee the desired quality of service to each user and then lighten the burden imposed on a specific BTS [38].

2.6.6 Microcells and Pico-cells

Many mobile telecommunication networks make use of small cells known as microcells and very small cells known as pico-cells to provide coverage in areas such as traffic hotspots (sport centre) and gaps in mobile telecommunication coverage areas which are not covered by high tower macro-cell base stations [1,2,17,25,65]. These small cells usually employ low-gain antennas mounted at street level or within buildings and other structures to improve their coverage area. It is a fast and easy method for improving service. The advantages of microcell systems include a significant increase in system capacity with low

power at each cell. Microcell systems thus reduce cost and enable the flexible deployment of cells. However, the microcellular network requires a large number of base stations compared to the conventional macro cellular system [1, 2]. The installation and maintenance of the enormous number of base stations is the most serious problem in the deployment of the microcellular networks.

2.7 Summary

A review of the current mobile telecommunication technology has been carried out in this chapter. Key features of GSM mobile telecommunications and UMTS for 3G mobile telecommunication networks have been highlighted. Coverage, capacity and traffic load balancing challenges and various techniques used in resolving it at present and the limitation of the techniques have also been reviewed. The use of the cell splitting technique to increase coverage and capacity clearly increases the mobile telecommunication network cost. Channel borrowing and sharing schemes can help to relieve cell congestion, but requires an intelligent network to be able to manage mobile telecommunication network resources. A remotely tilted antenna can enhance coverage and capacity and also help to reduce the cost of riggers going to cell sites. The technique does not have the ability to reconfigure the antenna beam width to enhance coverage and maintain capacity of a subsector area of a mobile telecommunication network. Hence, there is a need to review smart antenna technology. The next chapter will review smart antenna technology with its benefits as a possible technique to solve the problem of coverage, capacity and traffic load balancing for mobile telecommunication networks.

Chapter 3 - REVIEW OF SMART ANTENNA TECHNOLOGY

3.1 Introduction

An overview of smart antenna technology, types of smart antennas and coverage and capacity increasing capabilities will be discussed in this chapter. Antennas are not smart; it is the antenna plus the signal processing unit that are smart. The major components of multiple switched beam smart antennas will be presented in the later part of this chapter using both academic and commercial product literature. The aim of this review is to establish the state of conceptual understanding/knowledge on the subject of dynamic capacity optimisation using smart antennas for mobile telecommunication networks. The literature review will assist in the comparison between smart antenna concept and existing techniques.

3.2 Fundamentals of Smart Antennas

The concept of using multiple antennas and innovative signal processing to serve cells more intelligently has existed for many years [15, 23]. Smart antenna technology could be dated back to World War II with the Bartlett beam former [15]. In fact, varying degrees of relatively costly smart antenna systems have already been applied in military defence systems and mobile telecommunications [23]. As mobile telecommunications began to materialize, it was evident that interference in wireless networks was limiting the total number of subscribers and quality of service the network could handle before unacceptable call quality and blocking occurred. In the past, cost barriers have prevented the use of smart antenna in commercial mobile communication systems. The advent of powerful, low-cost digital signal processors (DSP), as well as innovative software-based signal-processing techniques (algorithms) has made smart antennas practical for mobile telecommunications networks. Today, when spectrally efficient solutions are increasingly a business imperative, these systems are providing greater coverage area for each cell site, higher rejection of interference, and substantial capacity improvements [15, 16, 23, 78].

3.2.1 Overview of Smart Antenna Technology

A massive increase in the numbers of mobile telecommunication users worldwide has triggered a great interest in the investigation of the use of smart antennas in mobile communication networks.

A viable solution to this increase in the number of subscribers is the use of spatial filtering. Spatial filtering is a major feature of smart antenna systems. It has been suggested that smart antennas and TD-SCDMA access technology are the enabling technologies that will allow efficient use of the limited radio spectrum needed to provide high quality service, good coverage and increased capacity in dense traffic areas [41]. The term smart antenna incorporates all situations in which a system is using an array of antenna elements and a signal processing unit to dynamically adjust the radiation pattern to suit the system requirement [15, 16]. Generally collocated with a base station, a smart antenna system combines an antenna array with a digital signal-processing capability to transmit and receive in an adaptive, spatially sensitive manner [15, 16, 78-80]. In other words, such a system can automatically change the directionality of its radiation patterns in response to its signal environment. This can dramatically increase the performance characteristics (such as capacity) of a mobile communication network [15, 16, and 80]. The type of array antenna elements and information supplied to the signal processing unit depends on the application. Smart antennas are currently used in wireless communication systems to provide interference reduction and enhance user capacity [23]. Capacity here refers to the number of subscribers that can be simultaneously serviced in a system at a specific data rate. This is achieved by focusing the radiation only in the desired direction and adjusting itself to changing traffic conditions or signal environments [81]. The use of smart antennas can produce different benefits. The most important of all the benefits of smart antennas is the ability to serve more users per base station thereby increasing revenues of network providers and also giving network subscribers less probability of blocked or dropped calls [15, 16, and 23]. The transmission quality is also improved by increasing the desired signal power and cancelling interference. A smart antenna is capable of providing multiple narrow beams and/or adaptive beam shapes which increases signal level and suppresses interference compared to “normal” fixed wide-beam sector antennas. This increases signal to interference plus noise ratio (SINR) and, hence, coverage and capacity [16, 81].

3.2.2 Features of Smart Antennas

The following points highlight the features of smart antennas:

- Range improvement

Since smart antennas employ a collection of individual elements in the form of an array, they give rise to a narrow beam with increased gain when compared to conventional antennas using the same power. The increase in gain leads to an increase in range and coverage of the system. Therefore fewer base stations are required to cover a given area. This is why that the TD-SCDMA standard which dictates the use of smart antennas is employed in China.

- Reduction in transmitted power

Conventional antennas radiate energy over a wide angular area leading to a waste of power. Comparatively, smart antennas radiate energy only in the desired direction; hence less power is required for radiation at the base station. Reduction in transmitted power also implies reduction in interference towards other users.

- Mitigation of multipath effects

Multipath is a condition which arises when a transmitted signal undergoes reflection from various structures in the propagation environment. This reflection of a transmitted signal gives rise to multiple signals arriving from different directions to the mobile user. When these signals arrive at the user's mobile receiver, they arrive with different phases because they follow different paths to the receiver. The effect is degradation in signal quality when they combine at the receiver. The most severe impact of the multipath effect is the complete loss of signal. When two signals with the same amplitude from different paths arrive at the same time, the resulting composite signal could be a null if the two signals are out-of-phase. Smart antennas can both reduce the illumination of multipath components on the down link and thus reduce interference, mitigating its effects in terms of fading or on the uplink it can use the multipath components and add them constructively to enhance system performance [15, 16, 23, and 83].

3.2.3 Smart Antenna Impact on Coverage and Capacity

Coverage and capacity are interdependent in the WCDMA access technique. When one is improved the other will be degraded if conventional broad beam sector antennas are employed because interference from other users is received on the beam. Thus the effect of "cell-breathing" occurs, i.e. interference is a function of the number of simultaneous users, dynamically raising and lowering the noise floor; however, with smart antennas coverage and capacity can be improved simultaneously. Any smart antenna system whether fixed multiple beam or fully adaptive that uses arrays of elements can provide greater gains compared to any conventional sector antenna system in a mobile communication network.

The gains provided by smart antennas have two major elements, aperture gain and spatial filtering gain. The aperture gain is proportional to the number of elements used for the array of the antenna and is given by the equation 10log (N), where 'N' is the number of elements. When a signal propagates in a radio channel, the signal is subject to spatial and temporal dispersions (delay). This spatial distribution of signal power is known as power azimuth spread (PAS). The standard deviation of the PAS is commonly referred to as the angular spread (AS). The degree of AS directly impacts the signal strength at the mobile, and is correlated to the signal power from adjacent antenna. As angular spread increases, the effective antenna gains decreases. Spatial filtering limits the interference in a limited AS, therefore the gain is greatest for low AS because the interference is curbed to a small angular region and is decreased as the AS is increased [16, 83-84].

3.2.4 Cost/Performance Trade-offs for Smart Antennas

Although smart antennas have many benefits, they do have a number of disadvantages which can preclude the use of certain types of smart antenna into commercial systems. A fully adaptive smart antenna typically needs separate transceiver chains for each array antenna element and accurate real–time calibration for each of them. Also the antenna beam-forming is computationally rigorous which means that smart antenna base stations must be equipped with very powerful digital signal processors. This leads to a substantial increase in the cost of the system [79] which may be difficult to justify in terms of improved system capacity. Alternatively, a simpler conventional switched beam smart antenna could be implemented, but such a solution can only provide fixed multiple narrow beams which do not provide any beam shape flexibility [15-16]. Another issue with smart antennas is that when the angle of arrival of the interferer signals is very close to the mobile user, the antenna effectiveness becomes less. A number of different types of smart

antennas have been developed and there is no ultimate antenna solution for all wireless environments, optimal solution depends on the environment in which the smart antenna is to operate and the channel characteristics and subscriber behaviour[80-86].

3.3 Type of Smart Antennas

There are basically two types of smart antennas that offer a higher service capacity gain, therefore reducing to less than half the number of base stations required compared to the conventional antennas when trying to establish a new network provider. They are switched beam smart antenna and adaptive smart antenna [15, 16, and 81]. The switched fixed multi-beam smart antennas consist of a finite number of fixed beams with predefined beam patterns and fix pointing directions. In uplink (UL), the antenna elements are used to collect all incoming energy resulting in increased antenna gain, while in downlink (DL), the beam with the largest UL power received from the mobile of interest will be used for transmission. The second type of antenna system is the more advanced steered beam solution [15-16]. That is, the shape of the beams is fixed and the pointing directions are steered towards the mobile of interest both in UL and DL directions within the cell. As a consequence, the pointing errors of the fixed beam solution can be eliminated. The two concepts require different system architectures. For example, in order to translate the angle of arrival into angle of departure, the steered beam solution requires stringent UL and DL calibration (coherency requirement). Furthermore, a dedicated pilot signal is required to be transmitted by the BTS to each user. The dedicated pilot signal should have high enough power such that the channel estimation is sufficiently good to ensure adequate signal-to-noise ratio within the demodulator [84, 87].

3.3.1 Multiple Switched Beam Smart Antennas

Multiple fixed-beam smart antennas consist of an antenna array and a multiple beam-forming network. In this system overlapping fixed beams are generated. Hence, each beam can be treated as an individual sector serving an individual user or a group of users. These antennas typically do not have a uniform gain in all directions, but when compared to a conventional antenna system they have increased gain in preferred directions. It is a system that can select a beam in order to enhance the received signal. When an incoming signal is detected, the base station chooses the appropriate predefined beam that is best aligned to the signal-of-interest direction to communicate with the user. The aim of the multiple fixed-beam system is to increase the gain in the direction of the desired user and to reduce

gain in the direction of other users (interferers). The multiple fixed-beam approach is simpler compared to the fully adaptive approach [59]. However, the multiple fixed beam design is limited when only one transceiver (it is desirable to avoid increasing the number of transceivers from the number required using sector antennas to minimise cost impact) is available because only one narrow beam at a time can be used but it has been shown that it offers more capacity gain compared to the fully adaptive concept at the expense of much higher complexity [15-16, and 79].

3.3.1.1 Interference Rejection Capability of Fixed Multiple Switched Beam

Smart antennas have the capability of rejecting interference when used in mobile communication networks. Assuming four signal sources, $S_1(t)$, $S_2(t)$, $S_3(t)$, $S_4(t)$, are located along the directions of a fixed multiple beams with N interfering signal sources $I_n(t)$, located at arbitrary angles φ_n. Let the transfer functions between the signal sources along the main beams and their corresponding output ports be denoted by F_j and the transfer function between interfering signal n and port j be denoted by F_{nj}. Also assume all signals are uncorrelated (no mutual coupling).

Therefore the total signal appearing at port j is given by the equation

$$y_j(t) = S_j(t)F_j + \sum_{n=1}^{N} I_n(t)F_{nj}\,(\varphi_n) \tag{3-1}$$

The total output power at j will then be given by

$$\left|y_j(t)\right|^2 = \left|S_j(t)F_j + \textstyle\sum_{n=1}^{N} I_n(t)F_{nj}(\varphi_n)\right|^2 \tag{3-2}$$

$$\left|y_j(t)\right|^2 = \left|S_j(t)F_j\right|^2 + \left|\textstyle\sum_{n=1}^{N} I_n(t)F_{nj}(\varphi_n)\right|^2 + 2Re\left|\left(S_j(t)F_j\right)\left(\textstyle\sum_{n=1}^{N} I_n(t)F_{nj}(\varphi_n)\right)\right| \tag{3-3}$$

Since the entire signal is uncorrelated, the total output power reduces to

$$\left|y_j(t)\right|^2 = \left|S_j(t)\right|^2\left|F_j\right|^2 + \left(\textstyle\sum_{n=1}^{N}|I_n(t)|^2\right)\left(\left|F_{nj}(\varphi_n)\right|^2\right) \tag{3-4}$$

The first term on the right side of equation (3-3) is the desired signal power whereas the second term represents the interference that combines with the desired signal [16, 83]. Hence, because a Smart antenna produces multiple narrow beams, the values of $F_{nj}(\varphi_n)$ in

the direction of the interferers is low compared to a conventional sector antenna and interference is reduced. The amount of information (data) that a wireless system can transmit is limited by energy-per-bit and signal to interference plus noise level.

3.3.2 Fully Adaptive

Adaptive antenna technology represents the most advanced smart antenna approach to date. Using a variety of new signal-processing algorithms, the adaptive system takes advantage of its ability to effectively locate and track various types of signals to dynamically minimize interference and maximize intended signal reception. The digital signal processing algorithm is basically an adaptive antenna algorithm and the direction of arrival algorithm. The multiple switched beam and fully adaptive smart antenna systems attempt to increase gain according to the location of the user; however, only the adaptive system provides optimal gain while simultaneously identifying, tracking, and minimizing interfering signals [15].

The adaptive array approach is the smarter of the two methods of implementing smart antennas. This approach continues to track the mobile user by directing the beam towards the user and at the same time forming nulls in the directions of the interfering signals as shown in the Fig.3.2. Like switched beam systems, they also incorporate arrays. Typically, the received signal from each of the spatially distributed antenna elements is multiplied by a weight. The weights are complex in nature and adjust the amplitude and phase. These signals are combined to yield the array output for a single beam. The complex weights are computed by a complicated adaptive algorithm, which is pre-programmed into the digital signal-processing unit that manages the signal radiated by the base station [15-16, 79].

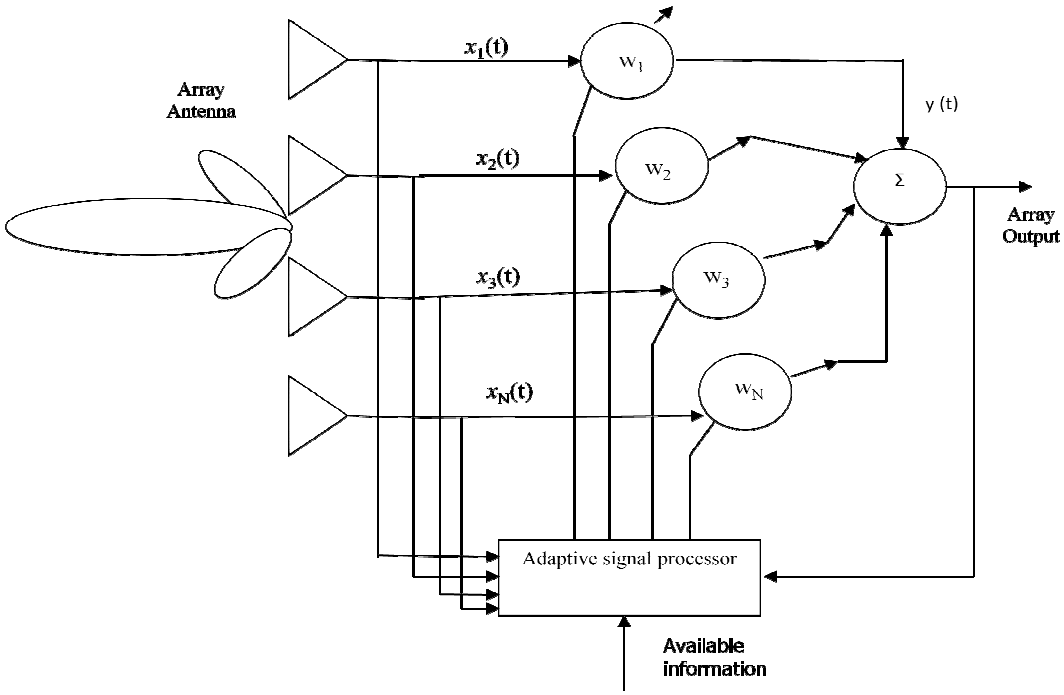

Fig.3.2: An adaptive smart antenna system

3.3.2.1 Interference Rejection Capability of Adaptive Antenna

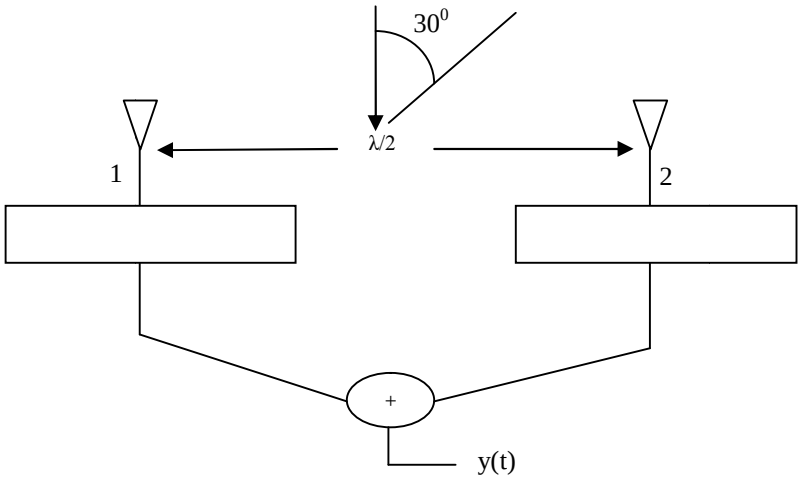

Fig.3.3: Two element array adaptive smart antenna

The information supplied by the direction of arrival algorithm is processed by the adaptive algorithm to steer the antenna beam maximum toward the mobile user and place nulls in the path of interfering signals [15-16, 79]. Fig.3.3 is a simple two element linear array half-wavelength apart adaptive smart antenna to receive a desired signal of certain weight say one at $\varphi_0 = 0^0$ why rejecting interferer at $\varphi_1=30^0$. The array element in Fig.3.3 is assumed to be an isotropic radiator and the signal source is sinusoidal.

The output signal due to the wanted signal is given by [15]:

$$y(t) = Se^{ja_0 t}(a_1 + a_2) \tag{3-5}$$

where *S* is the wanted signal

For *y(t)* to be equal to the desired signal *s(t)*= $Se^{ja_0 t}$,

$$a_1 + a_2 = 1 \tag{3-6}$$

y(t) due to the unwanted signal *n(t)*= $Ne^{ja_0 t}$is given as:

$$y(t) = Ne^{j(a_0 t - \pi/4)}a_1 + Ne^{j(a_o t + \pi/4)}a_2 \tag{3-7}$$

N is noise, -π/4 and +π/4 are phase lag and phase lead when the reference point is the midpoint of the array.

Re-arranging the output of *y(t)* due to interference,

$$y(t) = Ne^{ja_0 t}\left[\frac{\sqrt{2}}{2}(1-j)a_1 + \frac{\sqrt{2}}{2}(1+j)a_2\right] \tag{3-8}$$

For the output *y(t)* due to interference to be zero,

$$\left[\frac{\sqrt{2}}{2}(1-j)a_1 + \frac{\sqrt{2}}{2}(1+j)a_2\right] = 0 \tag{3-9}$$

Solving the two equation simultaneously we have,

$$a_1 = \frac{1}{2} - j\frac{1}{2} = a_1' + j\,a_1'',\ and\ a_2 = \frac{1}{2} + j\frac{1}{2} = a2' + j\,a_2'' \tag{3-10}$$

Hence the values of a_1 and a_2 are the optimum weights that we be computed by the adaptive algorithm to guarantee maximum signal to interference noise ratio for the desired signal at $\varphi_0=0^0$ and interference at $\varphi_1=30^0$. The fully adaptive smart antenna is more complex when compared to fixed multiple switched beam smart antennas and the increase in performance does not typically justify the higher cost and complexity in a real mobile communications network application; therefore the research is concentrated on fixed multiple switched beam smart antenna system. There are two basic subsystems of a multiple switched beam smart antenna, which is comprised of an array antenna and beam forming network [15-16].

3.4 Antenna Array

A smart antenna requires an array of elements in order to form multiple beams with high range or a single controllable beam with high range [15-16, 81 and 84]. An array antenna typically has identical elements, however it is not compulsory for the elements to be identical, but it makes it simple, convenient and practical. The array individual element can be of any type such as: dipole, microstrip slot, patch, horn, wires etc. The total radiation characteristics of the array are determined by the vector sum of all the individual fields radiated by each element. However, element signals are perturbed due to mutual coupling between the elements which will change the radiation and active impedance of the element. This is discussed in chapter seven.

Linear, circular and planar configurations are the most common of array geometries [15-16, and 87]. The linear array configuration is mostly used for multiple switched beam smart antennas. The element signal weights are provided by a feed network (beam-forming network), these can provide a phase weight to each element yielding a fixed beam or can provide variable phase weights to form phased array with an adjustable beam direction. The pattern characteristics such as the beam pointing angle and side lobes levels can be controlled by adjusting the amplitude and phase weight distribution of the array elements. The radiated field of the array antenna may be linearly (vertical, horizontally and vertical/horizontal) or circularly polarised. Although, the industry standard for dual-polar BTS antennas (sometimes called cross-polar antennas) is ± slant 45^{o} dual linear polarisation.

3.4.1 Linear Array

In a linear configuration, the elements are aligned along a straight line (vertically or horizontally) as shown in Fig.3.4, and if the elements are equally spaced this is called a uniform linear array [15, 87]. The uniform linear array is the simplest of all array geometries which allows array-processing techniques to be applied easily. However, in a uniform linear array all elements are not in the same environment especially the end elements. As such, the element radiation patterns for the end elements may differ appreciably compared to the central elements. Uniform linear arrays are commonly used in multiple fixed beam smart antennas [87].

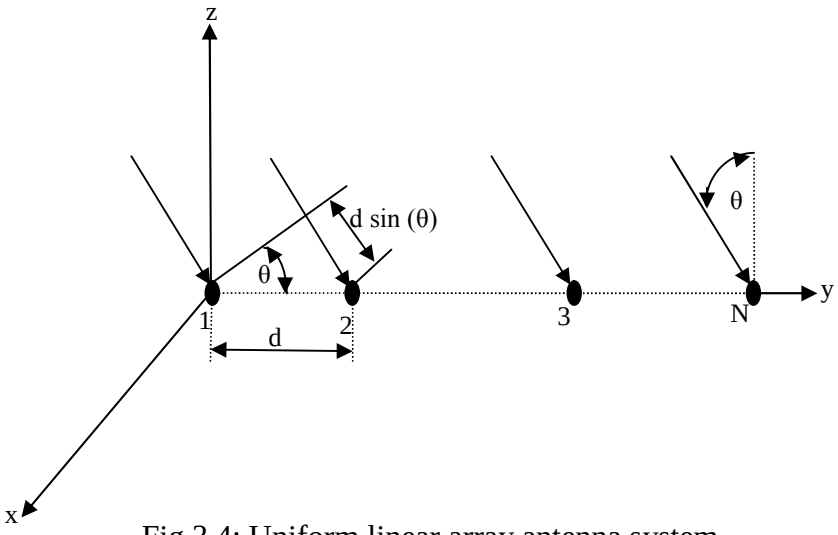

Fig.3.4: Uniform linear array antenna system

Assuming arbitrary complex weights, the total field radiated by a uniform linear array of elements at a far field $E(\theta, \phi)$ in a particular direction is given by [15]:

$$E(\theta,\phi) = EL(\theta,\phi).AF(\theta,\phi), \quad (3\text{-}11)$$

where $EL(\theta, \phi)$ is the radiation pattern of a single element and $AF(\theta, \phi)$ is the array factor.

If the elements are arranged along the y-axis and the reference point is at element one as shown in Fig.3.4 we have:

$$AF(\theta,\phi) = \sum_{n=1}^{N}\left[w_n e^{j(n-1)kdsin(\theta)}\right] \quad (3\text{-}12)$$

w_n= complex weight, N is the total number of elements, d is inter-element spacing and k is the propagation constant.

3.4.2 Polarisation

Antenna polarisation is another important characteristics of base station antennas, it is defined [15,25] as ‘‘that property of an electromagnetic wave describing the time varying direction and relative magnitude of the electric-field vector’’ that is the orientation of its radiated field in a specific direction. Polarisation that applies to antennas is classified as linear (vertical, horizontal and slant $\pm 45^0$), circular (left hand or right hand) or elliptical polarisation. Fig.3.5 shows the three class of polarisation. A linearly polarised antenna means the electric field of the antenna radiated field exists in a direction that is normal to the direction of propagation as shown in Fig.3.5(a), which is usually vertical, horizontal or slant 45^0. Fig.3.5 (a) presents a plane wave travelling in the positive z-direction and the

electric field directed toward the y-direction at all times. The electric field of this wave in terms of time and position is given by:

$$E_y = E_2 \sin(wt - \beta z) \tag{3-13}$$

where βz is the phase shift varying with distance in the z-direction.

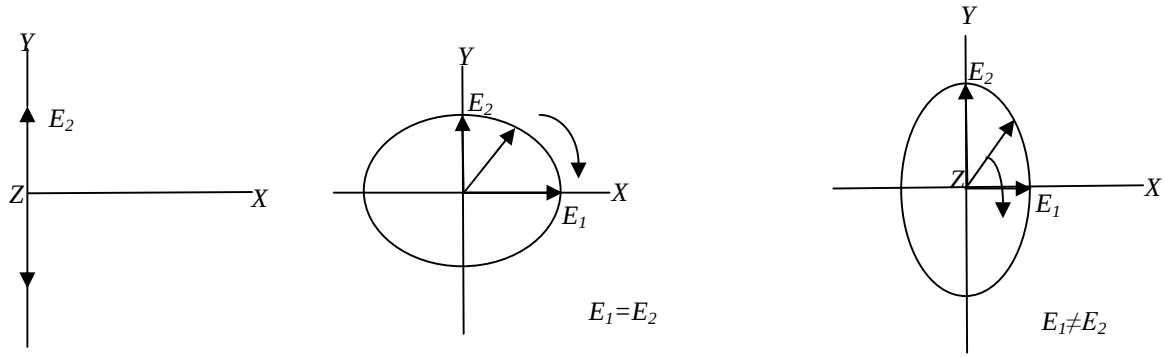

(a) Linear Polarisation (b) Circular Polarisation (c) Elliptical Polarisation

Fig.3.5: Wave polarisation

Circularly or elliptical polarised antennas can be mathematically represented as the sum of a vertical and horizontally polarised field, $\pm 90^0$ out of phase. It has electric field component in x and y-direction as shown in Fig.3.5 (b) and Fig.3.5 (c) above. The linear polarised components in x and y-direction are given by [15, 25]:

$$E_x = E_1 \sin(wt - \beta z) \tag{3-14}$$

$$E_y = E_2 \sin(wt - \beta z + \delta) \tag{3-15}$$

where E_1 and E_2 are the amplitudes of the electric fields in the x and y-directions and δ represents the time-phase difference between E_1 and E_2. When $E_1 = E_2$ and the phase difference between the two components is $\pm 90^0$ then it is circularly polarised. If $E_1 \neq E_2$ the wave is said to be elliptically polarised.

Conventional base station antennas and mobile subscriber antennas are linearly polarised [2, 25]. In many situations the mobile user antenna polarisation is not aligned with that of the base station antenna polarisation and any misalignment between these will lead to polarisation mismatch loss and therefore system efficiency reduction. Objects and barriers in the communication environment also cause polarisation shifts which may further reduce the quality of communication.

The polarisation of the antenna is most important for network efficiency [88]. For best performance the base station antenna polarisation needs to match up with the subscriber antenna polarisation which is not possible because the subscriber in many situations place their mobile receiver angle in alignment with the polarisation of the base station antenna. The mismatch loss between two linearly polarised antennas (transmitting and receiving antenna) can be calculated by [88]:

$$\text{Polarisation mismatch loss (dB)} = 20log\ (cos\theta) \tag{3-16}$$

where θ is the angle of misalignment between the transmitting antenna and the receiving antenna.

3.5 Beam-Forming Network

Array antennas for multi-beam transmit/reception requires a beam-forming network (BFN) to separate signals according to the signal arrival or transmit directions [15-16 and 81, 89]. Several types of *BFN* exist such as digital beam-forming (DBF), Maxon-Blass matrix multiple beam-forming [90], Rotman lens multiple beam-forming [91-92], Butler matrix multiple beam-forming network [89, 93] and Nolen matrix beam former [94-95]. A multi-beam forming network consists of interconnected components that introduce multiple phase shift distributions and weighting on the signals received by antenna array in parallel, thereby producing simultaneous beams. Therefore, it is used to provide the array element weights to form multiple overlapping fixed beams for 120 degree sector coverage [16, 89-95]. The required characteristics of multi beam forming networks are:

- To provide array element weights to form multiple overlapping fixed beams for 120^o sector coverage, by:
- Multiple simultaneous weights set to produce multiple orthogonal beams with ± 60 degree combined coverage from a planar array.
- Low loss (~ $\leq$ 0.5 dB)
- Low *VSWR* (~ $\leq$ 1.3:1)
- High inter-beam-port isolation (~ $\geq$ 30 dB)
- Low passive inter-modulation products (~ $\leq$ -153 dBc) (note: dBc refers to dB relative to the carrier level)

Typical number of beam ports is four or eight (for 3G mobile network) [16], [91].

3.5.1 Types of Multiple Beam Formers

The following are the most well known multiple beam-formers.

- Butler matrix
- Maxon-Blass matrix
- Rotman lens
- Nolen matrix
- Digital beam former.

3.5.1.1 Butler Matrix

Butler matrix multiple beam former is a beam forming network that uses a combination of hybrids (90° or 180^0 hybrids) and phase shifters to form *N* simultaneous independent beams/channels from an *N* element antenna array, where *N* is some power of 2 [16, 89, 95]. A 4x4 Butler matrix is shown in Fig.3.6 [89]. It performs a spatial discrete Fourier transform and provides orthogonal beams. These beams are linearly independent combinations of the array element patterns. When used with a linear array, the Butler matrix produces beams that overlap at about 3.9 dB below the beam maxima. A Butler matrix-fed array can cover a sector of up to 360° (for a circular array) depending on element patterns, array geometry and spacing. Each beam can be used by a dedicated transmitter and/or receiver, or a single transmitter and/or receiver can be used, and the appropriate beam can be selected using an RF switch.

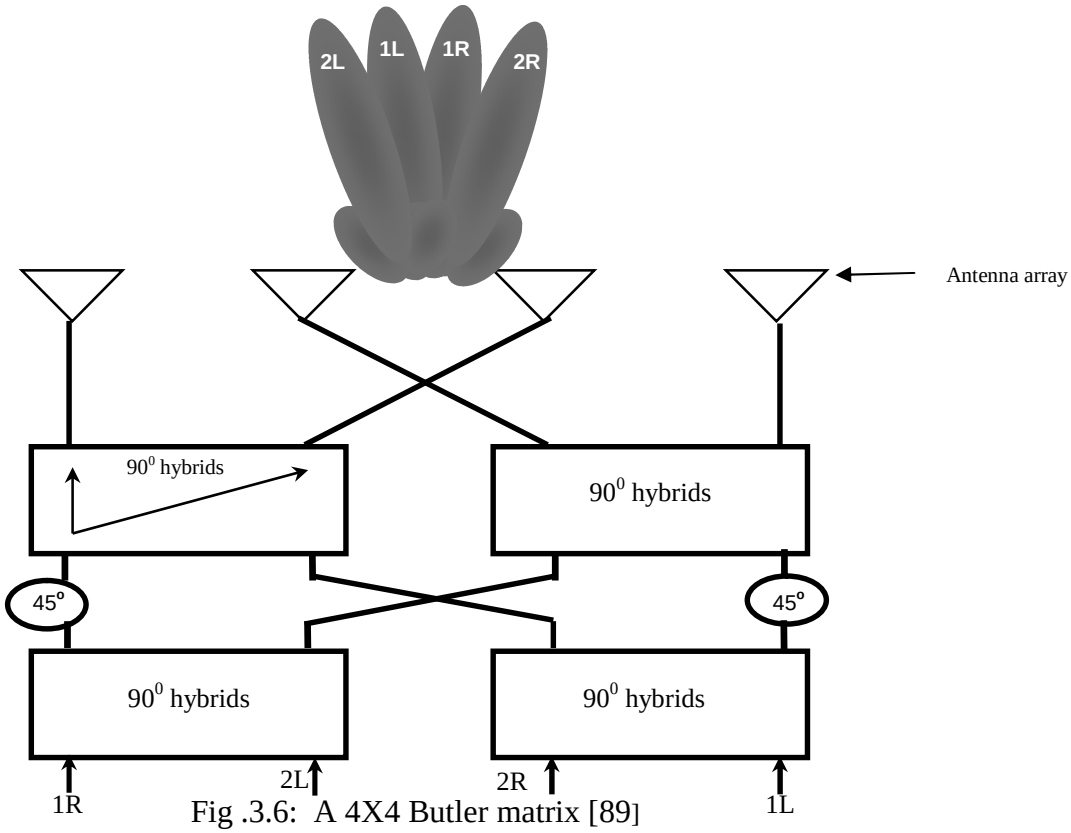

Fig .3.6: A 4X4 Butler matrix [89]

A Butler matrix can also be used to steer the beam of a circular array by exciting the Butler matrix beam ports with amplitude and phase weighted inputs followed by a variable uniform phase taper [97]. According to antenna array theory, the most crucial part of beam-forming task is the relative phase shifts of each of the radiating elements [16]. A conventional Butler matrix realisation has a challenge regarding the relative phase error with respect to the bandwidth because it operates on very narrow bandwidth. This is true because the phase shifts required ideally should be fixed (i.e. invariant with frequency).Since couplers and phase shifters are usually constructed using transmission line circuits (true time delay which yields phase shifts varying linearly with frequency, i.e. not fixed phase), the implementation of a Butler matrix usually has fast degrading relative phase errors as the frequency changes. Several techniques have been proposed to improve the bandwidth, relative phase error, reduce size and losses of the Butler matrix [96-103]. In [96] the authors have demonstrated a procedure for designing and implementing wideband Butler matrix using Schiffman lines to realise the fixed phase shifters. They have been able to show experimentally that using Schiffman lines yields fixed phase shifts for a Butler matrix configuration over a bandwidth of 26%. However, the setback of this technique is that it would require the implementation of long reference lines and couplers with very

precise even and odd mode characteristic impedances on a relatively thick microstrip substrate, which would mean very high complexity and difficulty in its implementation.

In [99] the authors have suggested another configuration which can improve the bandwidth of the relative phase error of the Butler matrix. They used 4x4 Butler matrix feed network and incorporated half-wavelength open stubs to improve the relative phase error performance. The result of the experiment proved that their modified Butler matrix network configuration produces relative phase errors that are not more than 2^0 over the used frequency band (850MHz to 900MHz). The advantage of this configuration is the relative ease with which it was fabricated in a planar configuration.

A 4x4 Butler matrix was designed in [100] using suspended strip line to reduce the losses. The Butler matrix is design to operate within frequency range of 880MHz to 960MHz. The proposed suspended strip line consists of two conducting layers and three dielectric layers sandwiched between two ground planes. The design requires extensive even and odd mode analyses to find the optimum overlap between the conducting lines to produce the desired coupling for the couplers and to minimize the coupling for the crossover between the hybrids. The designs were able to achieve 0.4dB loss, maximum amplitude error of 0.6dB, but a maximum of 10^0 relative phase error. The problem associated with this configuration is the problem of interconnection between the two conducting layers. It required vias to be used as interconnects, which have degrading effects on transmission line circuits, where the crossovers became a problem in the layout of the circuit which sometimes makes the layout very large. The major setback of this configuration is the increase in the design complexity and the fabrication, due to the use of multilayer printed circuit boards (PCB) with different dielectrics used for the non-conducting layers and the extensive even and odd mode analyses required. This configuration would also be more costly since vias are also to be incorporated in the circuits when interconnecting lines are not on the same conducting layer.

Reference [103] has used multilayer strip line to design a reduced size 8x8 Butler matrix. Over a frequency range of 1.6GHz to 2.8GHz they measured 1.1dB insertion loss and overall circuit size was 175mmx135mm which is good compared to the one designed using microstrip transmission lines. The only setback of this design is the increase in the insertion loss. Recently, a multilayer 8x8 Butler matrix was realised in 0.13µm CMOS for

5GHz to 6GHz. Although the design shows great size reduction and performance improvement it is complex and complicated [104].

3.5.1.2 Maxon-Blass Matrix

The Maxon-Blass matrix uses directional couplers and transmission lines to provide the necessary amplitude taper and phase shift for the arrays in order to produce multiple shaped beams. Fig.3.7 shows a 4-element array fed by a Maxon-Blass matrix. Each cross-over network is a directional coupler to cross-connect the transmission lines and to provide the desired amplitude weight. In principle, subject to the directional couplers being realisable for the specific coupling values required, the Maxon-Blass network can provide multiple beams (in excess of the number of elements, if required) of arbitrary shape and direction (within quantisation errors associated with the number of elements). However, the Maxon-Blass matrix has a low performance as a result of the loss attributed to the resistive terminations, also there will be a reduction in efficiency for non-orthogonal beams. The Maxon-Blass matrix has the advantage of real-time beam formation, orthogonal and non-orthogonal beams, low sidelobes, high beam crossover and a non-binary number of beams. However, the Maxon-Blass matrix has a setback in the realisation of directional couplers with inherent crossover and high directivity. It is difficult to realize in a single layer PCB, poor efficiency for non-orthogonal beams and the losses increase with increasing beam number [90].

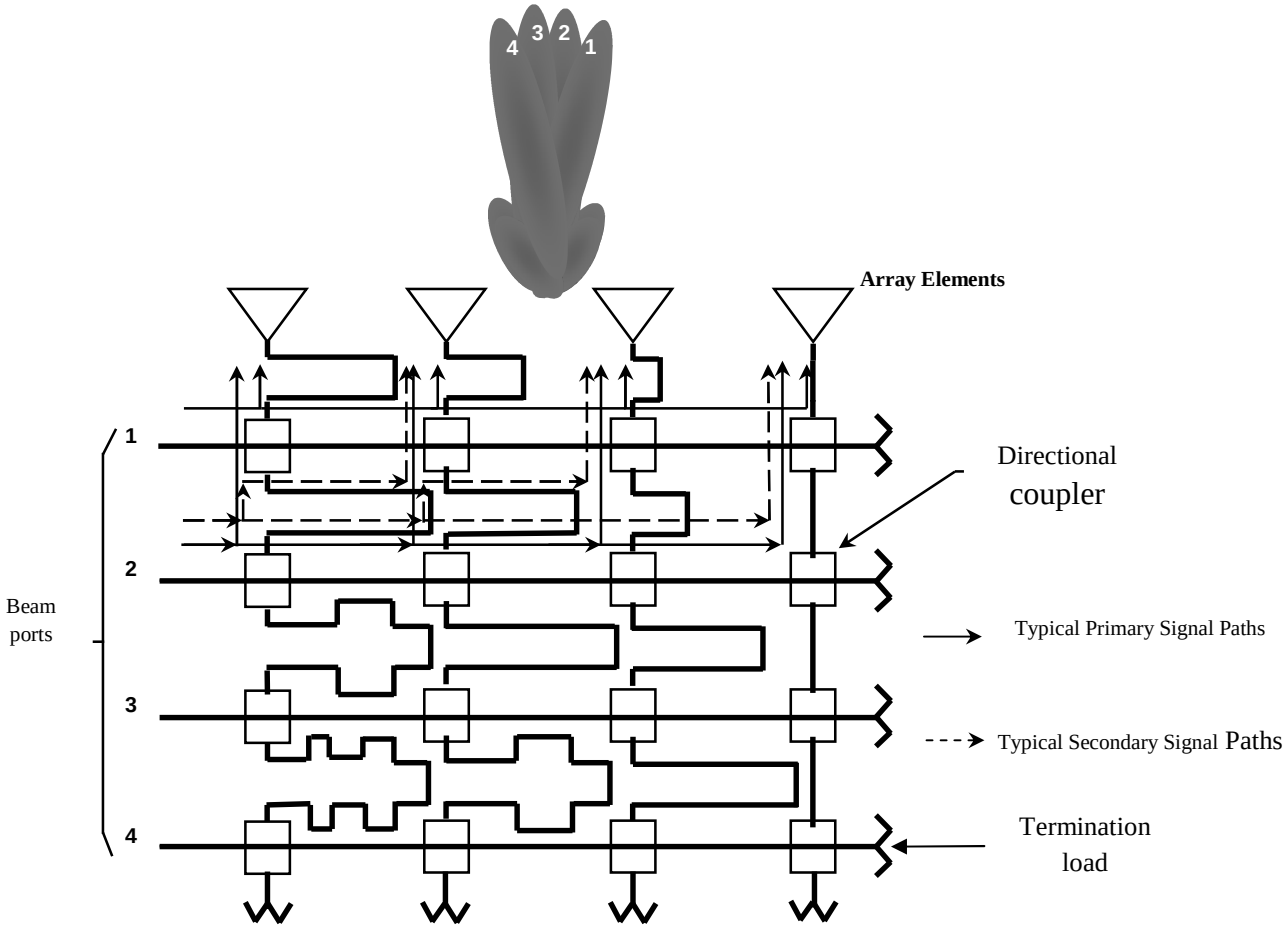

Fig .3.7: A Maxon-Blass matrix beam forming network [90]

3.5.1.3 Nolen matrix

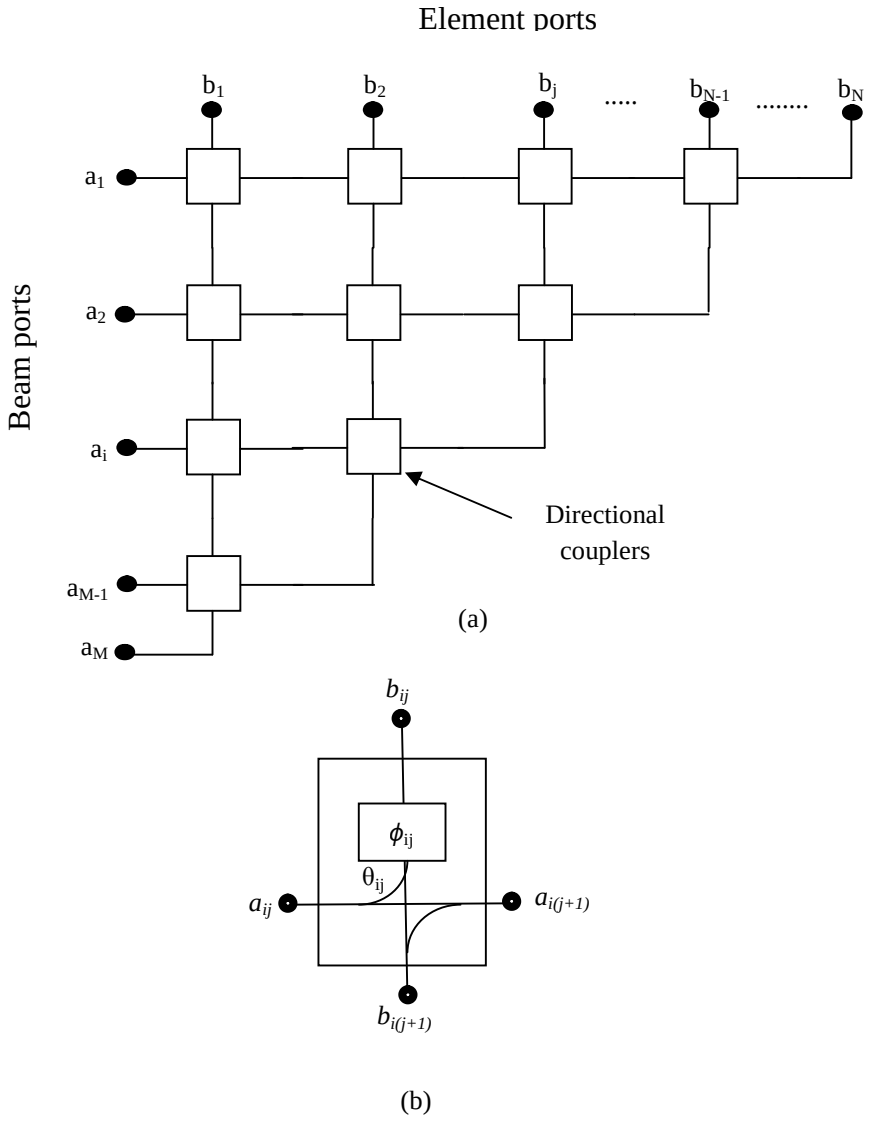

Fig. 3.8: (a) Basic form of a Nolen matrix (b) detail node [94]

The Nolen matrix is another form of beam forming network used with an array antenna to implement smart antenna systems. It is an improved form of Maxon-Blass matrix with less number of branch line couplers. The diagram of Fig.3.8 shows the general form of Nolen matrix network. The drawbacks of the Nolen matrix are that the number of the output ports must be greater or equal to the number of input ports ($N \geq M$,where N is the number of element ports and M is the number of beam ports) [94-95].

3.5.1.4 Rotman Lens

Fixed beams can also be formed using a Rotman lens multiple beam-former. The Lenses are made to focus energy radiated by feed antennas that are less directive [105]. Lenses can be made from dielectric materials or implemented as space-fed arrays.

A Rotman lens is a parallel-plate structure used as the beam forming network for a linear array of radiating antenna elements. One can form a two dimensional beam forming network suitable for use with a planar arrays by stacking multiple lenses.[106]. The advantages of the Rotman lens multiple beam forming network include: broadband (true time delay), real-time beam formation, it could be used to form orthogonal and non-orthogonal beams, it has low side lobes, high beam crossovers and non-binary number of beams. Because Rotman lens multiple beam former is a true time-delay device, the Rotman lens produces frequency-independent beam steering and is therefore capable of extremely wide-band operation.

These characteristics make the Rotman lens an attractive beam former for use in multi-beam satellite-based applications. Fig.3.9 shows a Rotman lens multiple beam-former. However, the Rotman lens beam former suffers a disadvantage when the number of array elements is small (~<20). Then, Rotman lenses have an excessive spill-over loss and the physical size is very large which makes it difficult to realize [92, 105-106].

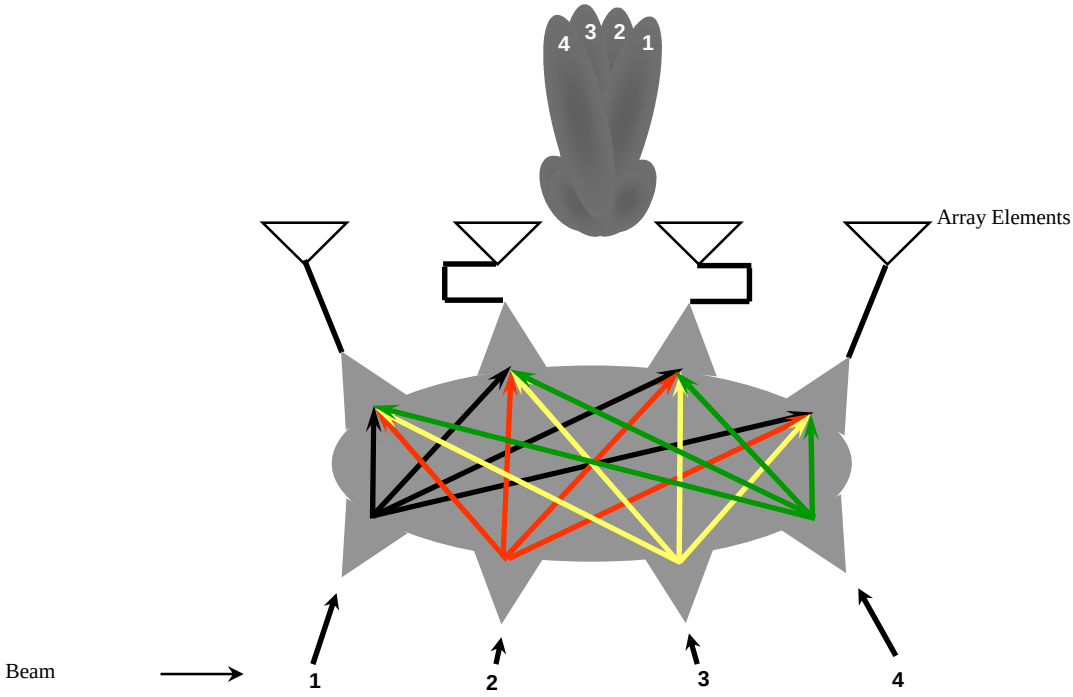

Fig.3.9: A Rotman lens beam former

3.5.1.5 Digital Beam Former

The digital beam former is another type of beam forming network that is being used mostly by adaptive smart antennas. Fig 3.10 shows a generic block diagram of a digital beam former for the uplink *(RX)* mode. A similar network could be implemented for the downlink.

The complex weights, w_n, are adjusted in such a way that in the angle of arrival direction, the waves from the different elements sum coherently in phase, providing directivity gain in the desired direction. Similarly, no energy is radiated towards the directions where the waves cancel each other (i.e. the null directions). If the phase shift between each antenna element is set to zero, the main beam of the antenna pattern would appear in a direction perpendicular to the line array ($\theta = \pi/2$). For a phased array system, the beam-forming algorithm only changes the phase of the weights (w_n), and keeps the amplitude $|w_n|$ fixed. For an adaptive array, both the amplitude and phase of the weights are optimised to get the desired beam pattern. In other words, there is no fixed 'antenna pattern' compared to conventional antennas with fixed radiation patterns. All antenna elements receive all signals at all times without any form of discrimination (except their inherent element

radiation patterns), and it is the processing of that information in the digital signal processing that ‘generates’ the antenna pattern. Since this processing can be done in parallel for several users, it is possible to generate one separate antenna pattern for each user at the same time with the same antenna elements. These are discriminated by their digital codes in 3G WCDMA networks. Digital beam forming networks have the advantage of closely spaced low sidelobe beams and without degradation of signal to interference plus noise ratio [107]. However, for the case of multiple fixed beams (i.e. not fully adaptive) the added complexity of the digital beam former cannot be justified. For simultaneous *Tx* & *Rx, T/R* modules (in the case of fixed multiple beams) are required at each element as well as high speed processing of a suitable algorithm for all the beams to be active. This imposes additional cost penalties on the design of base station.

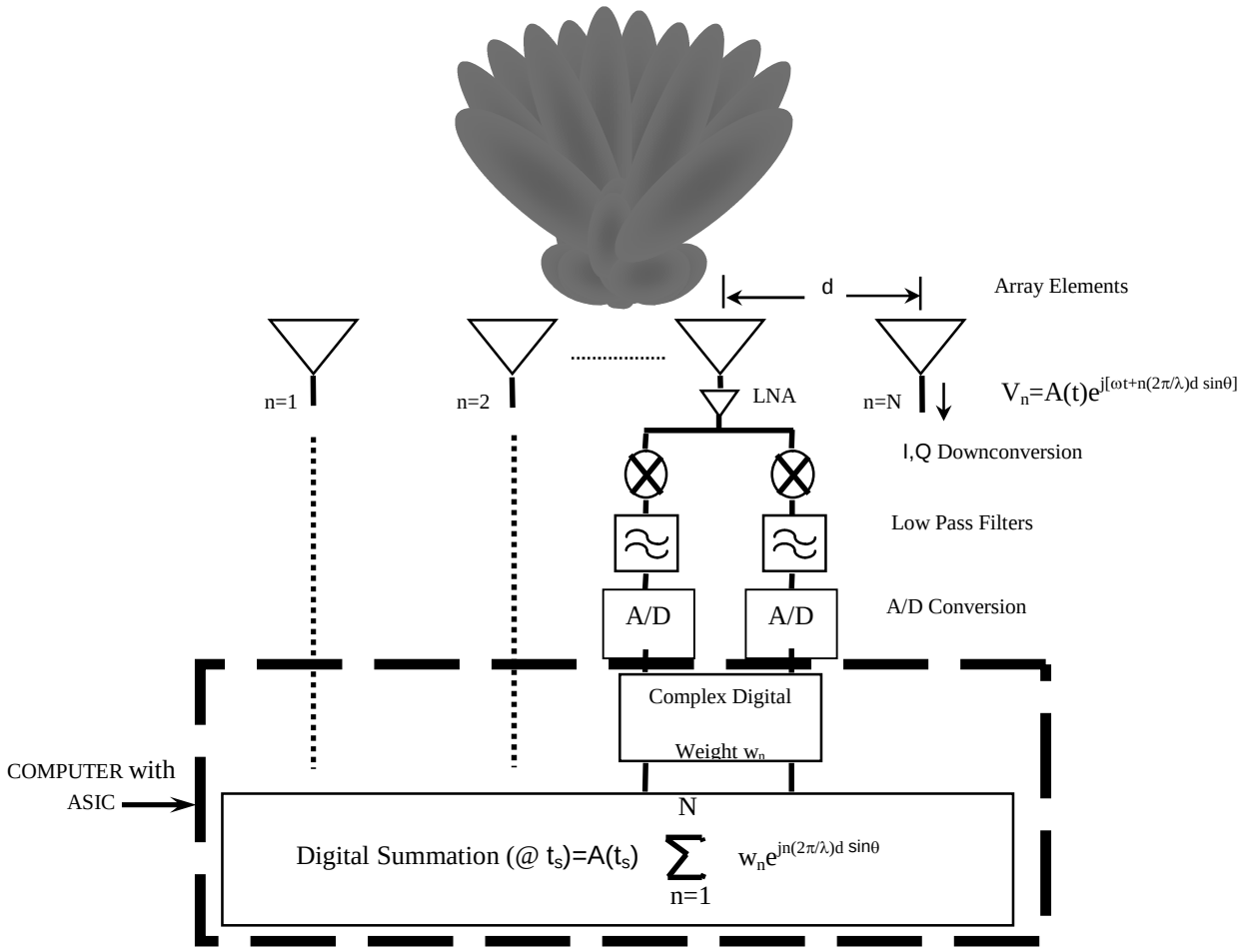

Fig.3.10: Digital beam former for uplink [107]

3.5.2 Multi-Beam Forming Network Component Considerations

The components required to realise many of the multi-beam forming networks discussed above include:

- Branch line couplers
- Phase shifters

These are discussed in the following sections

3.5.2.1 Branch Line Couplers

Branch-line couplers are fundamental and important components for the basic power division element in microwave circuits [108]. Fig.3.11 shows a basic architecture of a branch line coupler. They are used in microwave integrated circuits (MICs) as well as in monolithic microwave integrated circuits (MMICs), such as balanced mixers, multiple beam-forming networks and reflection type phase shifters. Conventional branch line couplers are four port networks, using a minimum of four quarter wavelength transmission

line microwave structures, where power is fed into one of the four ports is coupled into two of the four ports while the fourth one is isolated from the fed port. A two-branch line coupler could be designed for equal power division and unequal power division [108]. The equal power division branch line coupler is known as a hybrid coupler. Hybrid couplers are a special type of a four-port branch line coupler that is designed for a -3dB (equal) power split. Hybrid couplers come in two types, 90 degree or quadrature hybrids, and 180 degree hybrids. The basic advantages of couplers are that they are low loss and 90 degree or 180 degree phase shift can be realised between the coupled ports. The 0dB type of coupler has three branches and is comprised of six quarter wave transmission lines so that the power transmitted from one port to the diagonally opposite port will always be equal to the input signal (minus a small dissipative loss) and delayed by 270 degrees (or equivalently advanced by 90 degrees) phase shift at the centre frequency of operation [108-113].

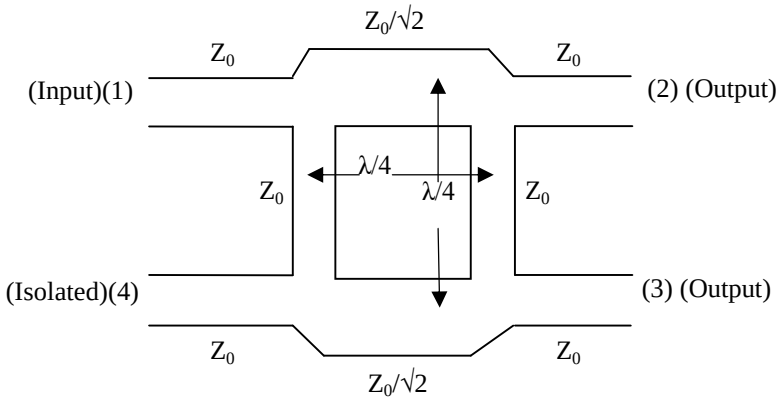

Fig.3.11: Architecture of a branch line coupler (-3dB hybrid shown) [108]

3.5.2.1.1 Coupling Factor

Coupling factor indicates the fraction of the input power that is coupled to the coupled output port of a coupler. A hybrid coupler that has equal power division has the coupling factor of -3dB [108]. The size of a traditional branch line coupler increases as the frequency reduces. Research into methods to reduce the size of branch line couplers and improve the performance is ongoing [111-114]. This two branch-line coupler will be realised with microstrip transmission lines.

3.5.2.1.2 Microstrip Transmission Lines

Microstrip transmission lines are one of the most popular types of planar transmission lines primarily because they can be fabricated by photolithographic processes and are easily integrated with other passive and active microwave devices. They are composed of a thin conducting metal strip of width W_0, thickness t and length L placed on a nonmagnetic dielectric substrate that is in turn placed on a conducting metal ground-plane [15, 108]. The substrate has thickness h and relative permittivity, ε_r. There are mainly three types of losses in microstrip transmission lines and these three losses are related to the quality factor Q. The three losses are

- Conductor losses
- Dielectric losses
- Radiation losses

3.5.2.1.2.1 Conductor Loss

Conductor losses occur due to the finite conductivity of the strip and ground plane. In RF transmission lines the resistance of the conductor is never equal to zero. Whenever current flows through the conductor, some energy is dissipated in the form of heat. Losses could also occur as a result of the skin effect. This loss occurs due to the inductance produced by the magnetic field within the conductor. As frequency is increased the opposition to flow of current in the centre of the conductor increases and the signal in the centre of the microstrip line becomes smaller and most of it will flow on the surface of the microstrip line. It is reported that the conductor losses can be reduced when the thickness of the conductor is $\pi/2$ times the skin depth [108].

3.5.2.1.2.2 Dielectric Losses

Dielectric losses result from the heating effect on the dielectric material between the conductors. The heat produced is dissipated into the surrounding medium. When there is no potential difference between two conductors, the atoms in the dielectric material between them are normal and the orbits of the electrons are elliptical. When there is a potential difference between two conductors, the orbits of the electrons change. The negative charge on one conductor repels electrons on the dielectric toward the positive conductor and thus distorts the orbits of the electrons. A change in the path of the electrons requires more energy, introducing a power loss which is known as dielectric loss [15].

3.5.2.1.2.3 Radiation Loss

The field surrounding the conductor causes radiation losses. These losses occur because some magnetic fields of the signal do not return to the conductor when the cycle alternates and this especially occurs in the vicinity of discontinuities in the microstrip line. These signals are projected into space as radiation and this result in power loss. These radiation losses become important when working with multiples of quarter wave length resonators, but in other cases the losses are small enough to be neglected [108,110].

3.5.2.1.3 Impedance Matching

The impedance match defines how well the load impedance matches the characteristic impedance of the system (typically 50ohms). If a mismatch occurs then a reflected wave is generated and maximum energy transfer is not achieved. A number of techniques can be used to eliminate reflections when the transmission line characteristic impedance and load impedance are mismatched. Impedance matching techniques can be designed to be effective for a specific frequency of operation (narrow band techniques) or for a given frequency spectrum (broadband techniques). One method of impedance matching involves the insertion of an impedance transformer between the transmission line and load [15, 108].

3.6 Performance Comparison of Multi-Beam Forming Network Designs

Alternative multi-beam forming networks which include: Butler matrix, Maxon-Blass matrix, Nolen matrix, Rotman lens and digital beam forming networks have been reviewed above. Table 3.1 below presents the advantages and disadvantages of the multi-beam forming networks. The Butler matrix multiple beam forming network has been selected based upon its overall performance for the specific application of a small array of multiple switched beams smart antenna in a 3G network using the WCDMA air interface [16]. The reasons for this selection are as follows:

- Although the main disadvantage of the Butler matrix is that it is narrowband, this is not relevant for the subject application as separate multi-beam forming networks are used for the uplink and downlink bands. Furthermore, the subject smart antenna would be designed for the specific uplink and downlink **sub-bands** of a specific mobile network operator (Orange UK has been assumed as an example). These sub-bands are extremely narrow. Hence, narrow band performance is not relevant.

- For the subject application, seven beams are required (four narrow beams, a right and left shaped beam and a wide broadcast beam). Clearly, the Butler matrix can only provide the four narrow orthogonal beams; however, the addition of a beam shaping network overcomes this limitation by exciting all four beam ports of the Butler matrix simultaneously with the appropriate adjustable complex weights which then facilitates the production of all seven beam shapes required. The total feed network is then comprised of a Butler matrix augmented by a beam shaping network. This is described in detail on the next chapter.
- The Maxon-Blass and the Nolen networks suffer from poor efficiency and the Nolen network can only produce four beams if only four elements are used. Hence, these are not attractive for this application.
- The Rotman lens is a high efficiency network, but when designed for a small number of elements (4), there would be excessive spill-over loss.
- Lastly, the use of a digital beam forming network would add unnecessary complexity.

Table3.1: Multi-beam forming network design comparison

Design	Advantages	Disadvantages
Butler matrix	• Straightforward design • Low inter-pot coupling • Real-time beam former	• Narrow band (fixed phase shifter required) • Only orthogonal beams • -13.2dB sidelobes • -3.9dB beam crossovers • Network crossover required • Network losses • PIM(many connections, unless single layer microstrip used) • Binary number of beams.
Maxon-Blass matrix	• Real-time beam formation • Orthogonal & non-orthogonal beams • Low sidelobes • High beam crossovers • Non-binary number of beams	• Directional couplers with inherent crossover & high directivity difficult to realise in single layer PCB • Loss in loads • Loss increases with increasing number of beams • PIM(many connections, unless single layer microstrip used)
Nolen matrix	• Same advantages as Maxon -Blass matrix with less number of couplers	• Same disadvantages as Maxon -Blass matrix but with reduced loss. • Number of beam ports must be $\leq$ number of elements
Rotman Lens	• Broadband (true time delay) • Real-time beam former • Orthogonal & non-orthogonal beams • Low sidelobes • High number of beams • Low PIMs	• Spill-over Loss • Physical size large • Difficult design for low number of array elements • Difficult to maintain equal beam shapes high if designed for low beam crossover
Digital beam former	• Closely spaced low sidelobe beams without degradation of signal-to-noise ratio • Array element pattern correction • Array self-calibration • Improved adaptive pattern nulling	• Complexity • T /R modules required for simultaneous Tx &Rx • High speed processing required

3.7 Summary

This chapter has discussed smart antenna technology, including: the two major types of smart antenna systems, their advantages over conventional sector antennas and the drawbacks of the smart antenna system. The fixed multiple switched beam approach is simpler compared to the fully adaptive approach. Its design is limited when only one transceiver is available because only one narrow beam can be used at a time, but it has been shown that it offers more capacity gain in mobile telecommunication networks compared to the fully adaptive concept at the expense of much higher complexity [109]. Hence this research is to develop a smart antenna concept that represents a "half-way" house between multiple switched beam smart antenna system and the fully adaptive smart antenna system to overcome the drawbacks of fully adaptive and multiple switched beam smart antenna systems. The novel smart antenna is a multiple switched beam smart antenna excited with an adjustable beam shaping network. Major components of a switched beam smart antenna system which include multi-beam forming networks and array antenna have been highlighted in this chapter. The next chapter will detail the modelling and analysis of the novel smart antenna concept.

Chapter 4 - MODELING AND ANALYSIS

4.1 Introduction

In this chapter, modelling and analysis of the new smart antenna concept is described. The chapter outlines the rational for the development of a dynamically reconfigurable smart antenna system without greatly increasing the complexity of the system. The subject smart antenna system is developed to offer good coverage and capacity using multiple beams throughout a cell sector and to be able to reconfigure the beam to provide enhanced coverage and maintain capacity in certain areas at reduced, but acceptable coverage throughout the rest of the cell sector of a mobile telecommunication network. First, the motivation behind the architecture and the methodology used is discussed and then modelling and analysis of the antenna system is presented.

4.2 Antenna System Motivation and Definition

Many different technologies and protocols are used around the world to provide mobile telecommunication coverage, capacity and traffic load balancing. The mobile telecommunication base station transceiver configuration depends on the network operator and currently the majority of mobile telecommunication networks using WCDMA access techniques use 3 sector antennas each covering 120^0. These exhibit modest gain (typically 17.5 dBi), good coverage and modest capacity, but do not suppress interference from other users. The demand for increased capacity is growing (video, TV on the move, etc.); hence, there is a need for higher antenna gain, narrow multiple beams to reduce interference and to track high user demand. Smart antennas already exist with multiple fixed beams, but as a separate transceiver on each beam port is typically required, there is increased complexity and cost.

In 3G systems there is also a need for constant monitoring and continuous optimisation for coverage and capacity because of the dynamic variations of subscriber locations in the sector and traffic behaviour [65]. The behaviour of the traffic demand affects the network signal quality of the mobile network provider [25]. To avoid coverage holes, cell overlaps have been used as a remedy [25], but waste power when the traffic demand moves to another sector. Therefore, there is a desire for antenna system features including: high gain, narrow beams, tracking capability and, most importantly, shaped beams for optimum capacity distribution within a sector. The latter is needed because it is desirable to accommodate a subsector with high capacity demand (for example, during a football

match) while still maintaining coverage over the remainder of the sector with reduced capacity demand using a single transceiver per polarisation. To achieve these antenna system features, a new and novel antenna system concept has been developed. This antenna system is a multiple switched beam smart antenna which uses a dynamic beam shaping network to feed a multiple beam forming network to "blend" the beams in order to enhance subsector coverage and maintain capacity. Such a smart antenna system that can dynamically select appropriate beam shapes as traffic load requirements change will be of great interest since traffic demands change much slower than individual signals of subscribers. The time available to change the radiation pattern of the smart antenna system is much longer compared to that of individual signal changes [65].

In order to adapt to an unequal user distribution between beams it is a great advantage to share the power that is available to serve a sector dynamically between the beams of the sector providing more coverage to areas that have more users and/or higher capacity demands (that is why it requires two shaped beams). The advantage of this dynamic sharing is to reduce dropped calls in a sector. The antenna system's radiation patterns can be dynamically shaped to enhance the right or left hand side of the sector to accommodate the traffic load imbalances within a sector. The desired beams are called the right-hand shaped beam, left-hand shaped beam and a broad shaped beam for the broadcast channel to avoid the use of a separate integrated sector antenna for the broadcast channel. These are in addition to the four narrow overlapping beams. The salient features of the required antenna system that would distinguish the design to be novel include:

- Four narrow beams, two shaped and a broadcast channel beam
- Increased gain (relative to typical sector antenna) and small array width ($< 4\lambda$)
- Low complexity and robustness
- Low cost
- Compact size and light weight
- Minimal maintenance requirements

4.2.1 Broadcast Channel

In a wide-band code-division multiple-access (WCDMA) system, a common pilot channel is broadcast throughout a sector continuously to provide for cell identification, channel estimation and handover decisions [25]. Most networks use an independent, but integrated sector antenna to provide the broad beam for this broadcasting. It has been argued that if a common pilot is used for a sector using fixed multiple narrow beams for traffic signal transmission, the phase of the pilot signal and the traffic signal received at the mobile unit will be different because of multipath effects [84]. Therefore it is advisable to transmit the pilot signal and the traffic signal through the same channel (on the same beams) when using a fixed multiple beam antenna for wireless communication (using auxiliary pilots) [16, 84]. However, if the network provider does not have the facility to use the auxiliary pilots there is a need to make provision for the sector broadcast channel beam as this design could be integrated into an existing mobile communication network.

4.3 Standard Switched Beam Smart Antenna System Using Butler Matrix Modelling

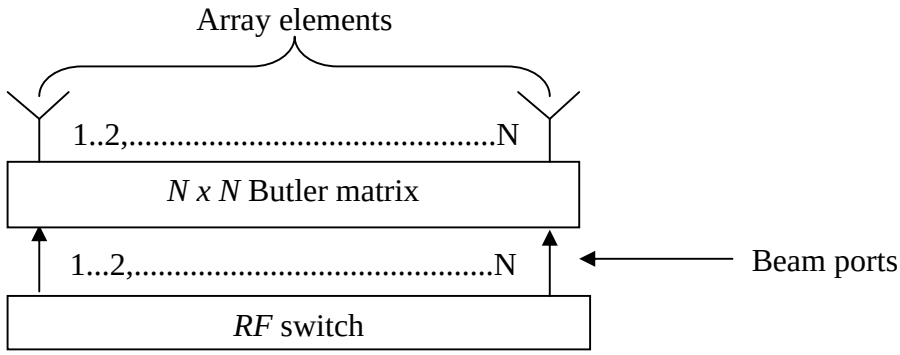

Fig. 4.1: Standard multiple switched smart beam antenna using Butler matrix

The fundamental components of a basic multiple switched beam smart antenna system are: the antenna array, multiple beam forming network and a switching network responsible for switching the individual beams for communication. The beam shapes produced by the antenna array are dependent upon the complex weights (magnitude and phase) applied to each array antenna element ports through the beam forming network [46, 81, 87, 103, 115-116].

A basic multiple switched beam smart antenna system using a uniform linear array antenna of *N* elements and a *N x N* Butler matrix shown in Fig.4.1 with *N* beam port weights $A_m e^{j\phi m}$ (*m*=1,2,3,...*N*), will provide array element complex weights, w_n, given by [16, 81and 89]:

$$w_n = \sum_{m=1}^{N} \left\{ \frac{A_m}{\sqrt{N}} e^{j\emptyset_m} e^{-j(n-1)\Delta\emptyset} \right\} \qquad (4\text{-}1)$$

Where: $\Delta\emptyset = \pm(2p-1)\frac{\pi}{N}$, *p*= (1,....N/2) and *n* is integer (*n* = 1,2,3.....N).

Note that if **only a single beam port is excited**, then the complex weights of the array would be **equal in amplitude** and **linear in phase** producing a narrow beam with -13.2 dB sidelobes (assuming isotropic radiating elements). Hence, equation 4-1 above represents the complex weights that would occur if all beam ports are simultaneously excited. The resultant amplitudes will not, in general, be uniform and the phases will not be a linear distribution. This means that by proper selection of the beam port excitations, arbitrary (within limits) beam shapes can be provided.

The total array factor is given by:

$$AF(\theta) = \sum_{n=1}^{N} w_n e^{jkd(n-1)\sin\theta} \qquad (4\text{-}2)$$

If *N* is equal to four, the Butler matrix will provide four sets of excitation weights to form a set of four fixed multiple beams for a cell sector of a wireless communication network as shown in Fig.4.2. In order to obtain the additional shaped beams and broadcast beam, a beam shaping network must also be introduced capable of producing the required seven different beams using one transceiver per polarisation.

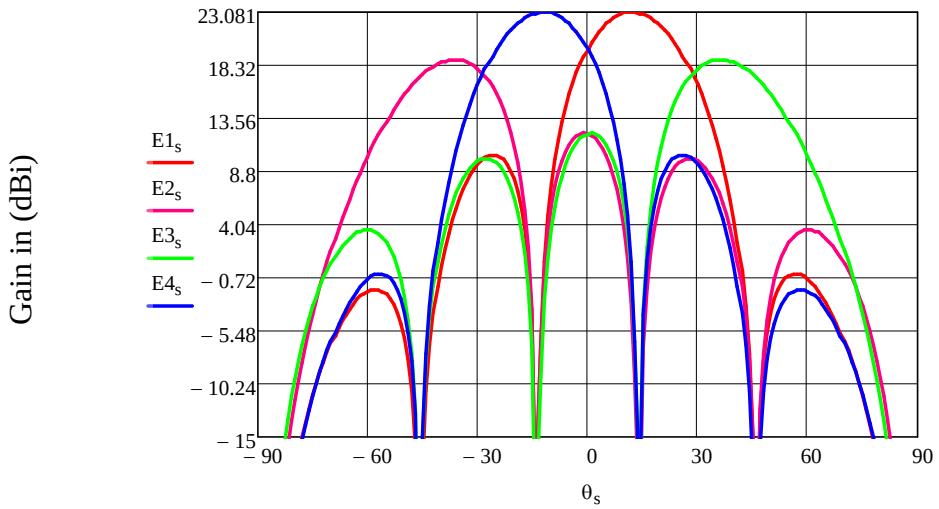

Fig.4.2: Multiple beams formed by using only Butler matrix as beam former

Alternative beam forming networks include: Maxon-Blass matrix with a seven way switch and Nolen matrix [91-94]. A Maxon-Blass matrix with a seven way switch can provide arbitrary complex weights to excite a 4-column linear array antenna to produce the seven required beams but is lossy and complicated. The Nolen matrix although less lossy cannot provide seven beams with 4 array elements because the number of element ports must be greater or equal to the number of beam ports. The Butler matrix multiple beam forming network provides the best overall performance for the specific application of a small number of smart antenna switched beams for mobile telecommunication networks. The Butler matrix is a network without any active circuit elements (passive feeding network) and it works the same way either in the transmit (*Tx)* mode or received *(Rx)* mode. Among other reasons to select the Butler matrix is that it is easy to realise in microstrip PCB (low cost), design simulation and optimisation can be done on in house microwave office software and the PCB can be produced for experimental testing and verification of performance [16].

In isolation, the Butler matrix can only provide four narrow beams. However, the Butler matrix plus a dynamic beam shaping network can produce the required seven beams. By producing a weighted combination of these four narrow beams we can get the extra two shaped and broadcast beams. Hence, the addition of the beam shaping network to excite the multiple beam ports of the Butler matrix simultaneously to combine the narrow beams in space. The proposed design system aims to do this in a simple and efficient manner.

4.4 Novel Smart Antenna System Modelling

The block diagram of the proposed smart antenna system is shown in Fig.4.3. The fundamental components of the system are: the antenna array, multiple beam forming network (4x4 Butler matrix) and the beam shaping network. Each of the array columns has a gain of 17.5dBi (as a conventional sector antenna). The horizontal beam shape produced by the antenna array is dependent upon the complex weights (magnitude and phase) applied to each array column. The aim of this proposed design is to provide an antenna which offers the required features given in section 4.2. These include the ability to offer good coverage throughout a cell sector to be able to reconfigure the beam to provide enhanced coverage in certain areas at reduced, but acceptable coverage throughout the rest of the cell sector.

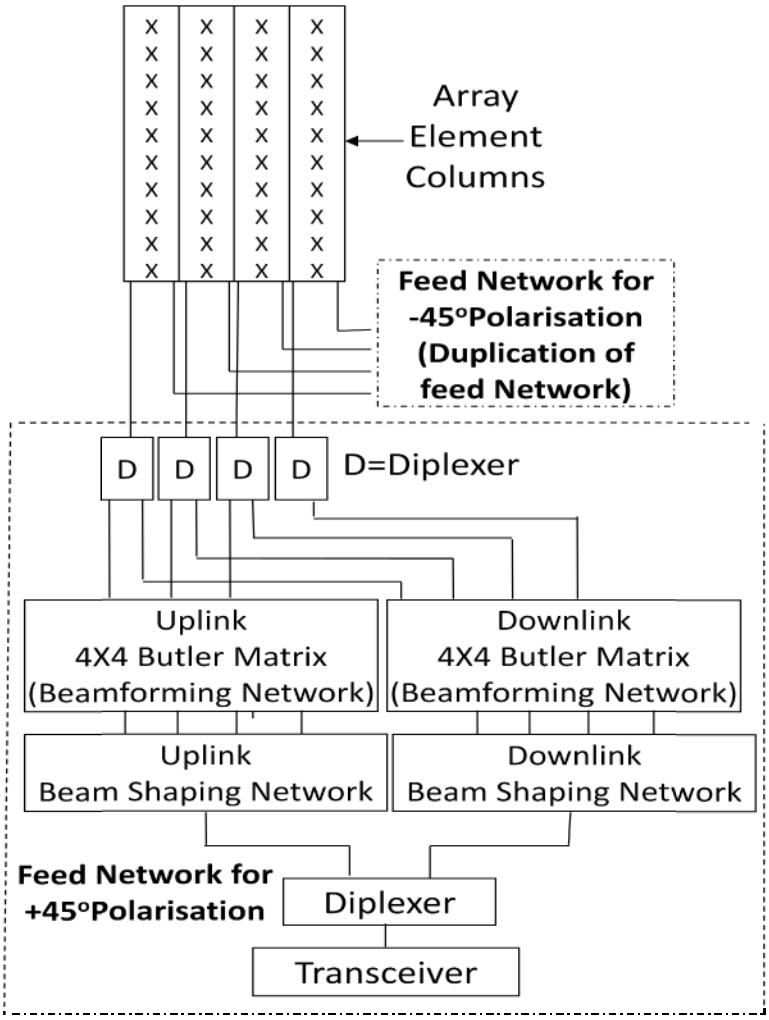

Fig.4.3: A smart antenna using Butler matrix and beam shaping network

A significant improvement over conventional switched beam antennas can be provided by the use of a combined beam forming network and beam shaping network as shown in Fig.4.3. The level of this improvement will be demonstrated by simulations. Such a system enables shaped beams to be dynamically directed to the left or right directions in addition to the original multi-beam patterns. An advantage of this approach is that the shaped beam has a footprint without nulls providing reduced, but adequate, coverage over the remainder of the cell sector. This approach allows for “soft optimisation” of coverage within the cell as power can be directed on a dynamically based real customer demand basis. Examples of this occur at large public gatherings at sports and music facilities. It should be noted that a single Butler matrix and a single beam shaping network could have been utilised, but these would have been required to operate over the separated up & down-link frequency sub-bands. As such, performance would not be optimum for both bands. Hence, it was decided to incorporate separate Butler matrix and beam shaping networks each operating over their

respective up & down-link bands and therefore could be easily optimised because each sub-band is extremely narrow. This also required the inclusion of diplexers before and after the feed networks. At present this situation can be resolved by costly measures such as the introduction of mobile masts to accept large increases in calls on a temporary basis. The novel technique here overcomes these limitations whilst minimising additional complexity. It does this by using the architecture outlined in Fig.4.3 with separate beam forming and beam shaping networks to cover uplink and downlink bands. This slight increase in complexity is more than offset by the ability to produce shaped beams to cover uplink and downlink with minimum radiation pattern variation over each frequency band and with the ability to dynamically alter the antenna performance in a simple manner.

4.4.1 Beam Shaping

The azimuth radiation pattern is controlled by the amplitude and phase of the excitation weight distribution. The amplitude of the excitation weight distribution has a controlling effect on the gain and sidelobe levels of array antenna radiation pattern. The greater the tapering of the amplitude distribution toward the ends of the array, the greater the achievable sidelobe suppression; however, the greater the tapering, the lower the aperture efficiency and the lower the antenna gain. Hence, there is a trade-off between sidelobe supression and array antenna gain.

The angle of the azimuth radiation pattern of an array antenna is primarily controlled by the phase of the excitation weight distribution. A linear phase progression component between the array antenna elements affects the scan angle of the antenna radiation and nonlinear phase progression component will facilitate a further shaping of the azimuth pattern. In fact, a nonlinear phase progression component can be used to provide null-filling between the main beam and the first sidelobe below the main beam antenna radiation pattern which maintains coverage in the null region [15]. The nonlinear phase progression component can also be used in conjuntion with a modest amplitude taper to achieve sidelobe suppression. By using this technique, a better optimum combination of sidelobe suppression and gain can be achieved at the small sacrifice of slightly higher sidelobes at wider angles. This does not normally affect network performance. Applying this technique the multiple beams can be blended to form one wide beam and also can be shaped to provide enhanced coverage over either the right or left of the base station sector of mobile telecommunication networks.

For the power to be appropriately ‘’blended’’ using four narrow beams of the Butler matrix, the technique introduced by Woodward-Lawson can be used [15]. The beam shaping is achieved by sampling the desired radiation pattern at various discrete locations. The technique is simple, straight forward and it provides insight into the process of shaping antenna beams.

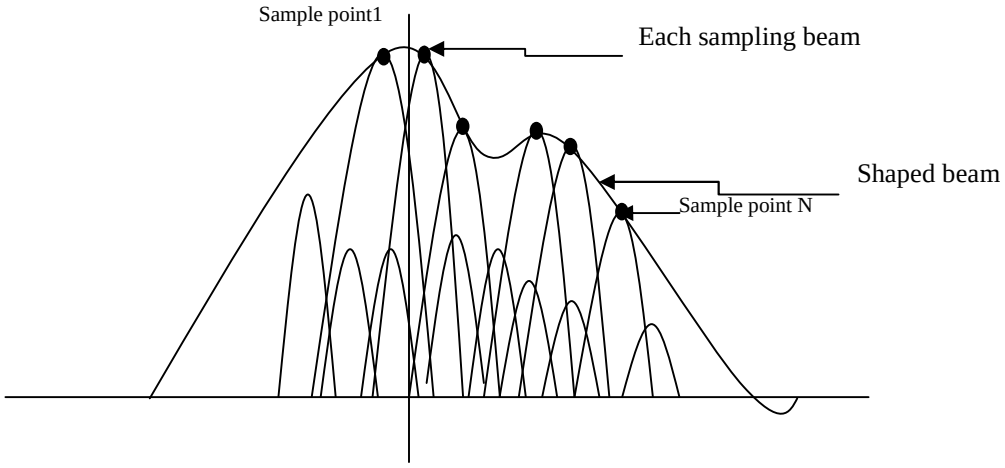

Fig.4.4: Woodward Lawson pattern synthesis

4.4.2 Description of the Beam Shaping Technique

This is a beam shaping technique which uses equal amplitude weights and a linear phase progression. The sampling beam as shown in Fig.4.4 is scanned to sample angle then each set of sampling beam excitation (weights) are added together.

Example:

Assuming sample point 1

$a_1{}^{[1]} = a_2{}^{[1]} = a_3{}^{[1]} = a_4{}^{[1]} = a$

$\Delta\emptyset^{[1]} = \emptyset_0$

$\emptyset_1{}^{[1]} = 0, \quad \emptyset_2{}^{[1]} = \emptyset_0, \quad \emptyset_3{}^{[1]} = 2\emptyset_0, \quad \emptyset_4{}^{[1]} = 3\emptyset_0$

Sample point 2

$a_1{}^{[2]} = a_2{}^{[2]} = a_3{}^{[2]} = a_4{}^{[2]} = ka$

$\Delta\emptyset^{[2]} = g\emptyset_0$

$$\emptyset_1{}^{[2]} = 0, \quad \emptyset_2{}^{[2]} = g\emptyset_0, \quad \emptyset_3{}^{[2]} = 2g\emptyset_0, \quad \emptyset_4{}^{[2]} = 3g\emptyset_0$$

where *a* is the sample amplitude and *Ø'* is the sampling progressive phase.

The total complex weights needed to form the shaped beam is given by [15]:

$$w_n e^{j\psi_n} = \sum_{s=1}^{N} a_n{}^{[s]}\, e^{j\emptyset_n{}^{[s]}} \qquad (4\text{-}3)$$

The above considerations facilitate the determination of the beam weights through interactive simulation. The study have determined that combining four narrow fixed beams, with the two left-hand narrow beams 12dB down compared to the two right-hand narrow beams, the total radiation pattern will be shaped to the right of the sector and vice versa (see the MathCAD program in the appendix A).

This right shaped beam will enhance subsector coverage and maintain high capacity on the right-hand side of the sector while maintaining low coverage and capacity on the left side of the same cell sector. The left shaped beam is produced when the excitation is the mirror image of the right shaped beam (see Fig.4.5 for the shaped beams). Table 4.1 present the required relative amplitude and phase of the Butler matrix beam ports

Table 4.1: Relative signal amplitude and phase of Butler matrix beam ports

Beam state	Beam Port1		Beam Port2		Beam Port3		Beam Port4	
	Amp(dB)	Phase (deg)	Amp(dB)	Phase (deg)	Amp(dB)	Phase (deg)	Amp(dB)	Phase (deg)
Beam1 only	0	0	-∞	N/A	-∞	N/A	-∞	N/A
Beam2 only	-∞	N/A	0	-135	-∞	N/A	-∞	N/A
Beam3only	-∞	N/A	-∞	N/A	0	-135	-∞	N/A
Beam4 only	-∞	N/A	-∞	N/A	-∞	N/A	0	0
Broadcast beam	0	0	0	-135	0	-135	0	0
Right-hand shaped beam	0	0	-12	-135	0	-135	-12	0
Left-hand shaped beam	-12	0	0	-135	-12	-135	0	0

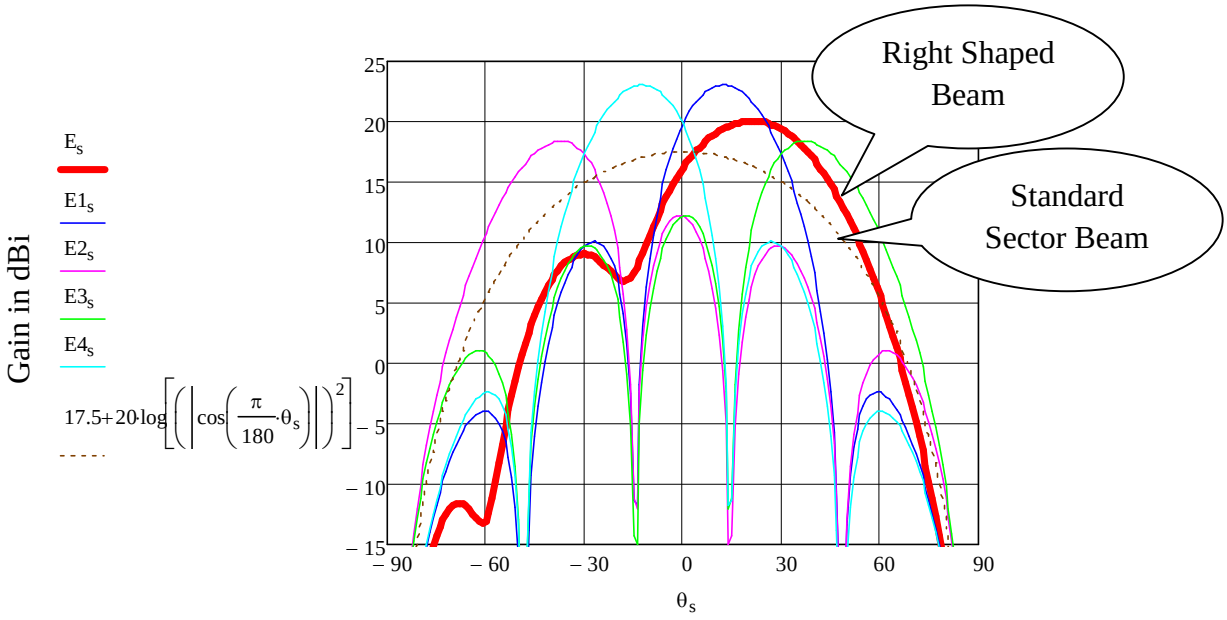

Fig.4.5: Plot showing right shaped beam, fixed multiple beams & standard sector beam

4.5 Summary

In this chapter, the modelling and analysis of a novel smart antenna system has been presented. This chapter has outlined the coverage limitation, which exist within a cell sector restricted to four high gain narrow beams. This research has proposed a technique to optimise coverage in advantageous manner by including the provision of a right and left shaped beam together with a broadcast beam. The chapter has examined relative merit of a number of techniques which could be employed to produce this combination of seven beams in an efficient manner and has selected a combination of Butler matrix and beam shaping network as the most efficient solution. The beam shaping network was introduced to excite the Butler matrix in order to ‘‘blend’’ beams. For this combination it has also determine the required excitation weight to be applied to the antenna beam ports in order to achieve the desired seven beams. The next chapter will detail the design procedure for producing this novel smart antenna system.

Chapter 5 - DESIGN OF THE SMART ANTENNA SYSTEM

5.1 Introduction

This chapter presents the design processes of the smart antenna with dynamic beam shaping capability. The antenna design process consists of several steps. The first step is to design a suitable antenna element for the antenna array and then array the elements to form array antenna for the smart antenna system. The next step is to design a feeder network which consists of 4x4 Butler matrix and a beam shaping network. The Butler matrix and the beam shaping network are comprised of hybrids and phase shifters. Hence to have a good Butler matrix and beam shaping network, there is need for well designed hybrids which will be coupled together to form the Butler matrix and beam shaping networks. Both the variable phase shifters (required in the beam shaping network) and the hybrids have been designed using microstrip PCBs. The antenna element, antenna array, transmission lines, microstrip hybrids, 0dB cross-over network (to replace the connecting crossing lines of the Butler matrix), the 4x4 Butler matrix beam forming network and beam shaping network have been simulated using in-house microwave software (Genesys network analysis and CST electromagnetic simulation software)[117-118].

5.2 Array Element Design

Antenna elements that are low profile are mostly used in the design of modern base station antennas for operation in mobile telecommunication networks. Microstrip patch antennas represent one family of low profile antennas that are very simple and not expensive to fabricate using modern printed-circuit technology. Microstrip patch antennas can take different shapes and are excited in different ways but all have a basic element that consists of a patch of conductor on the upper surface of grounded dielectric substrate [15] as shown in Fig. 5.1.

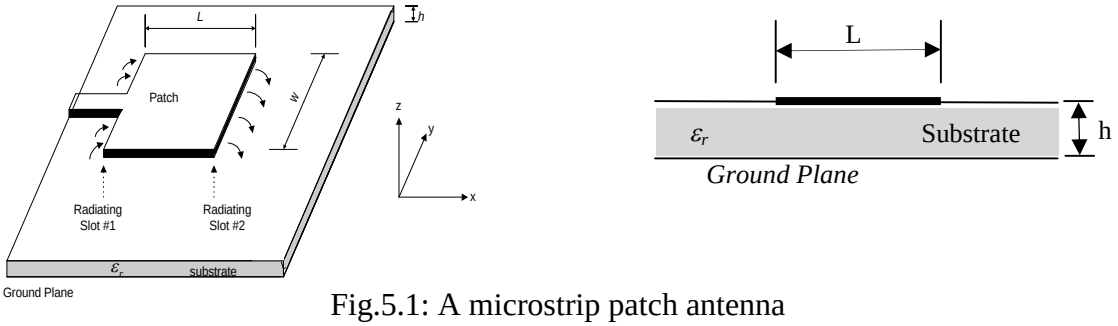

Fig.5.1: A microstrip patch antenna

It is simple because the patch is easy to design and analyse using both cavity and transmission-line models which are most accurate for thin substrates and it has very attractive radiation characteristics and low cross-polarisation radiation. The full details of design and analysis of microstrip patch antennas can been found in [15,119]. The major and serious drawback of a conventional microstrip patch antenna is its narrow bandwidth; a lot work has been done to enhance the bandwidth of microstrip patch radiators for the past decades. In [119] the straight forward way to increase a microstrip patch antenna bandwidth is to use a stacked coupled element to produce a double tuned resonance. The top patch is electrically coupled to the bottom patch thereby increasing bandwidth.

The array element for this smart antenna concept is a two port slant $\pm 45^0$ dual-polarised microstrip stacked patch antenna. Currently, base station antennas make use of two port slant $\pm 45^0$ dual-polarisation for simultaneous transmit/receive [121] and for diversity.

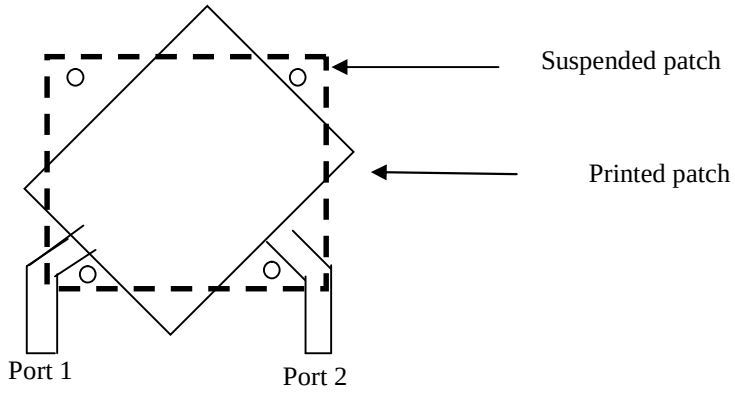

Fig.5.2: Dual –polarised slant $\pm 45^0$ microstrip stacked patch antenna

Fig.5.2 shows the slant $\pm 45^0$ dual-polarised patch antenna where port 1 is $+45^0$ polarisation and port 2 is -45^0 polarisation. Linear polarisation antennas are described with their radiation pattern both for a co-polarised and cross-polarised response. For port 1 which is nominally +45 degree polarised (co-polar), there will be a small amount of -45 degree polarisation which represents the cross-polar component. Similarly, for port 2, the -45 degree polarisation is the co-polar and the +45 degree polarisation is the cross-polar component.

Note that the use of dual-polar $\pm 45^0$ polarisations facilitates polarisation diversity gain and this is a much more compact solution than the use of spatial diversity which required two single polarised antennas separated by typically 10 wavelengths. The two port slant $\pm 45^0$

dual-polarised antenna not only acts as radiating element with orthogonal polarisations but helps to isolate the transmit signal from the received signal. Another advantage of a slant $\pm 45^0$ dual-polarised antenna element is that the two polarisations will provide identical azimuth radiation patterns while vertical and horizontal polarisations would provide different beam widths [122]. The dimension of the printed patch, suspended patch, substrate and conductor of the stacked patch is shown in Table5.1below.

Table 5.1: antenna element dimension

Parameters	values
Operating frequency in GHz	Uplink(1.9697-1.9797) Downlink(2.1597 -2.1697) (These are the Orange UK licensed bands)
Substrate	RT/duriod5870
Substrate dielectric constant	2.33
Substrate height	1.575 mm
Conductor thickness	0.035 mm
Length/width of the printed patch	46.79 mm
Length/width of the suspended patch	59.02 mm
Spacing between the printed and suspended patch	10 mm

5.3 Array Design

The single slant $\pm 45^0$ dual-polarised antenna element design discussed above was used to form array antenna for the smart antenna system. Fig.5.3 shows the antenna array with dimensions of 797.5 x 362.5 x 12.1mm. It consists of four identical columns for frequency band of (uplink 1.9697GHz to 1.9797GHz and downlink 2.1597GHz to 2.1697GHz) Orange UK, forming an array along the horizontal y- axis. Each of the four identical columns consists of ten identical elements array along the z-axis. The column spacing is 72.5mm ($0.5\lambda_0$ at the centre frequency of 2.069GHz).

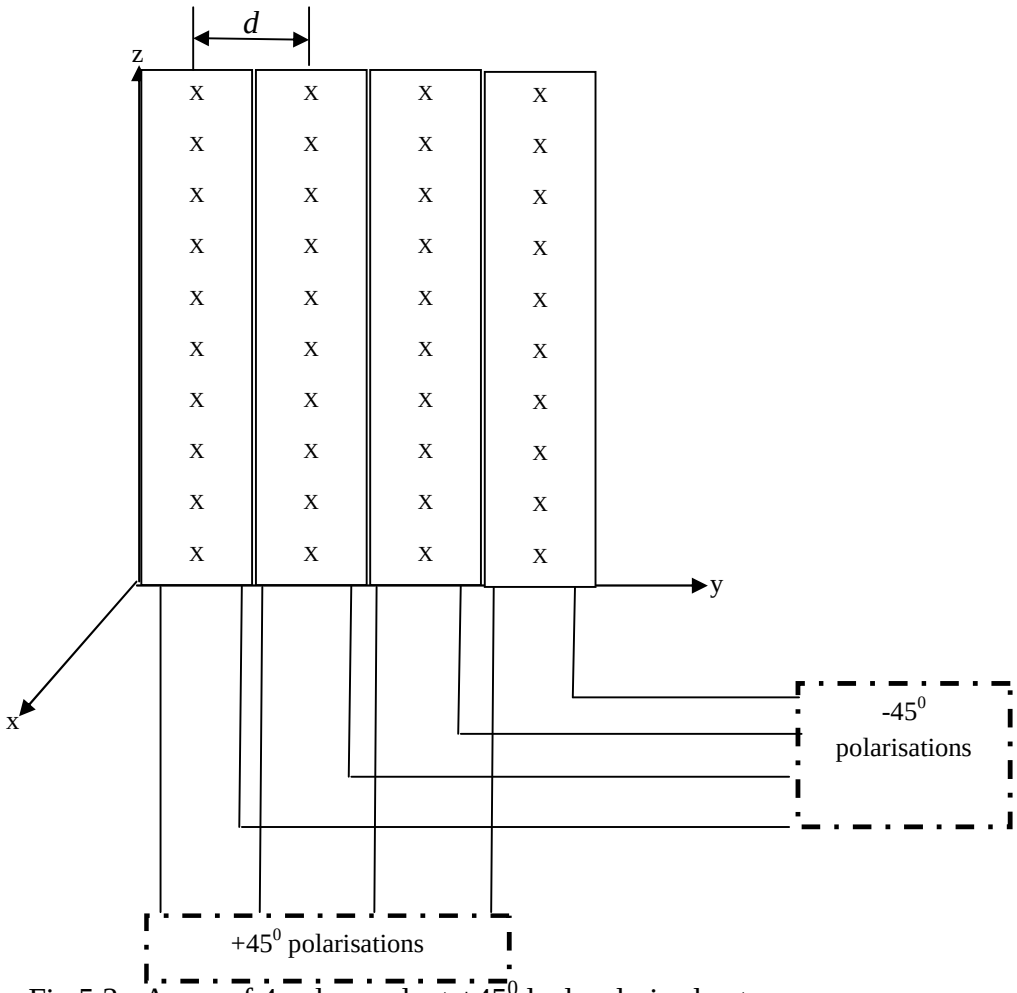

Fig.5.3: Array of 4 column slant $\pm 45^0$ dual-polarised antenna

The horizontal element spacing, *d* has a significant impact on the shape of the far-field azimuth radiation pattern of the antenna array. It has been shown that the larger the array gets, the better the characteristics of the radiation pattern as far as its shape and degree of freedom and one way of getting a larger array is by increasing *d*. The drawback of this approach is the appearance of the replicas of the main lobe in unwanted directions which are referred to as grating lobes. In practice, the optimum element spacing for beam-forming and adaptive interference cancellation applications is $\lambda/2$. For the purpose of this design the element spacing of $\lambda/2$ (at the mid frequency between the uplink & downlink bands) has been chosen to avoid unwanted grating lobes [15].

The number of elements in an antenna array is another important antenna array parameter. Increasing the number of linear array elements is an advantage for smart antenna performance as it yields better interference reduction capabilities due to narrower beams and higher gain. However, the consequence is larger arrays which are more costly and present a more obtrusive appearance in installations. Four columns and ten elements in

each column have been identified as a good compromise array antenna. The antenna is designed for dual-linear polarisation and each column has two ports, one for slant $+45^0$ polarisations and the other for slant - 45^0 polarisations.

Given a linear array of equally spaced identical elements, it can be shown that the total horizontal (azimuth) radiation pattern of the antenna array *E (∅)* in the far field, is given by [15]:

$$E(\emptyset) = Ee(\emptyset) * AF(\emptyset) \quad (5\text{-}4)$$

where *Ee(∅)* is the horizontal pattern of the column element and *AF(∅)* is the horizontal array factor.

$$E(\emptyset)dBi = Ee(\emptyset)dBi + 20log_{10}[AF(\emptyset)] \quad (5\text{-}5)$$

For the proposed design which comprises a set of columns of ten elements *Ee(Ø)* is given by

$$Ee(\emptyset)dBi = 17.5dBi + 20log_{10}[cos^2(\emptyset)] \quad (5\text{-}6)$$

Note: Each array column has an identical elevation pattern and the above azimuth pattern is valid at the peak of the elevation pattern. Equation (5-6) approximately accounts for the effect of finite ground plane of the patch element as published during this research work [124-125].

The total array factor ($AF(\emptyset)$) is given by [15]

$$AF(\emptyset) = \sum_{n=1}^{N} \left[w_n e^{j(N-1)\frac{2\pi}{\lambda} d \sin\emptyset} \right] \quad (5\text{-}7)$$

and *d* is the inter-element spacing (horizontal) (*d* = 72.474 mm)

w_n are the complex weights, *Ø* is the azimuth angle (zero at centre of the sector) and *N* is the total number of elements which is four for this design.

5.4 Butler Matrix Design

A Butler matrix consists of a multiplicity branch line couplers (hybrids) and fixed phase shifters.

A Butler matrix beam-forming network that will feed *N* element array antenna would require [97]:

$\frac{N}{2}\log_2 N$ of 90^0 hybrids (5-8)

and $\frac{N}{2}(\log_2(N)-1)$ fixed phase shifters to form an *N* beam patterns

For a 4x4 Butler matrix, the number of the 90^0 hybrids is calculated by substituting 4 for '*N*' in the above equation

$\frac{4}{2}\log_2 4 = \frac{4}{2}\left(\frac{\log_{10} 4}{\log_{10} 2}\right) = 4$ 90^0 hybrids

The number of fixed phase shifters required for a 4x4 Butler matrix is given by [98]:

$\left(\frac{4}{2}\right)(\log_2(4)-1) = 2$ Fixed phase shifters of 45^0

The 4x4 Butler matrix requires four hybrids and two fixed phase shifters which will be configured to form the network of Fig.5.4 below [90].

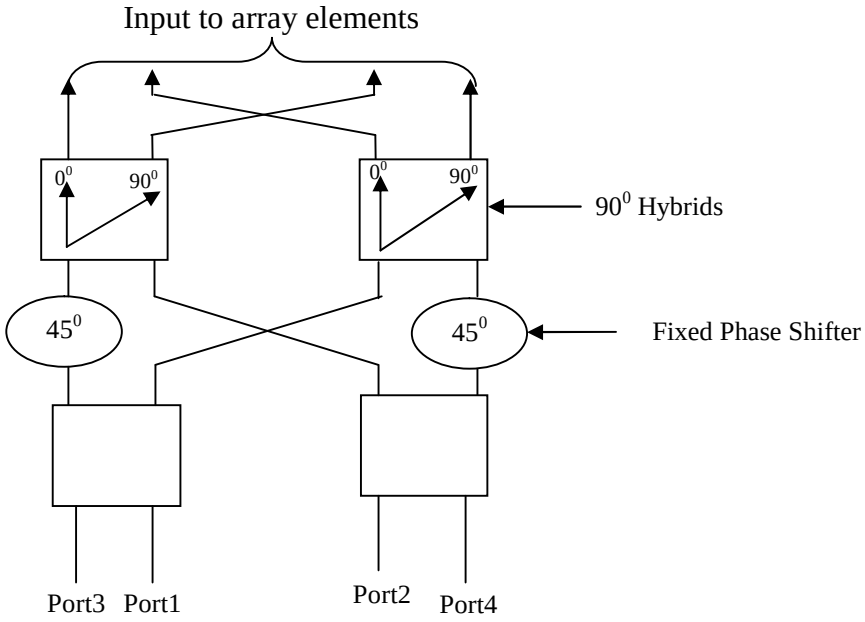

Fig.5.4: 4x4 Butler matrix beam-former

When a signal is sent into an input port of the Butler matrix, it produces different inter-element phase shifts between the output ports. The set of the different inter-element phase shifts is given by [16, 97]:

$$\Delta\varphi = \pm(2p-1)\frac{\pi}{N} \qquad (5\text{-}9)$$

Where *p* is the number of beam ports and $p = \left(1, \cdots \frac{N}{2}\right)$

When *N* is equal to four and p takes number from one to two, the set of different inter-element phase shift are $+45^0$, $+135^0$, -45^0 and -135^0. If one of the input ports is excited by an RF signal, all the output ports will produce a progressive phase shift between the ports.

The amplitude and phase of a 4x4 Butler matrix with unity beam port excitation are given in the table5.2 below.

Table 5.2: 4x4 Butler matrix element weights for unity beam port excitations

Beam direction	P	$\Delta\phi$	Element weights			
			1	2	3	4
1L	1	$+45^0$	$1/2\angle 45^0$	$1/2\angle 90^0$	$1/2\angle 135^0$	$1/2\angle 180^0$
1R	1	-45^0	$1/2\angle 180^0$	$1/2\angle 135^0$	$1/2\angle 90^0$	$1/2\angle 45^0$
2L	2	$+135^0$	$1/2\angle 90^0$	$1/2\angle 225^0$	$1/2\angle 0^0$	$1/2\angle 135^0$
2R	2	-135^0	$1/2\angle 135^0$	$1/2\angle 0^0$	$1/2\angle 225^0$	$1/2\angle 90^0$

Where *1R, 2R* are the right narrow beams and *1L, 2L* are the left narrow beams of the 4x4 Butler matrix.

5.4.1 Fixed Phase Shifter Design

Phase shifters are used to change the transmission phase angle of a network. The phase shifters will be implemented using transmission lines whose lengths introduce the required phase shift. The phase shifters will be implemented in microstrip transmission line. The phase shift φ associated to a transmission line of length l is given by [16, 97] the equation:

$$\varphi = \frac{-2\pi}{\lambda_g} l \qquad (5\text{-}11)$$

Where l is in meters, φ is in radians and λ_g is the wavelength in the transmission line medium. For microstrip transmission lines, the wavelength is given by $\frac{\lambda_0}{\sqrt{\varepsilon_{reff}}}$, where λ_0 is the wavelength in free-space and ε_{reff} is the effective dielectric constant of the microstrip substrate.

The required lengths of microstrip line to produce -45^o phase shift at the centre of the uplink and downlink bands are as given below in table 5.3.

Table 5.3: Fixed phase shifter dimension

Phase shift	Uplink centre frequency 1.9747GHz		Downlink centre frequency 2.165GHz	
	Width W(mm)	Length (mm)	Width W(mm)	Length (mm)
-45^0	4.63	12.31	4.63	13.50

5.4.2 Branch-line Coupler Hybrid

The geometry of the hybrid branch-line coupler is shown in Fig.5.5a [108]. This coupler has equal length and different characteristic impedances for the adjacent arms. The lines are assumed to be lossless and the characteristic impedance at the ports is taken as Z_0, Z_1 is the through line impedance and Z_2 is the branch lines impedance, θ_1 and θ_2 being their respective electrical lengths. Port 1 is the input port and port 4 is the isolated port. Port 2 and 3 are the output ports.

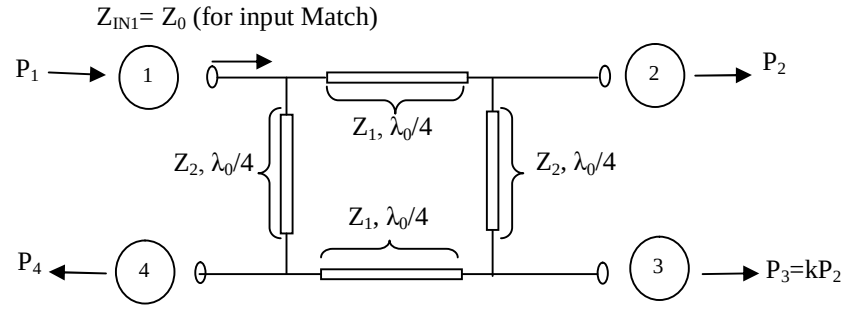

(a)

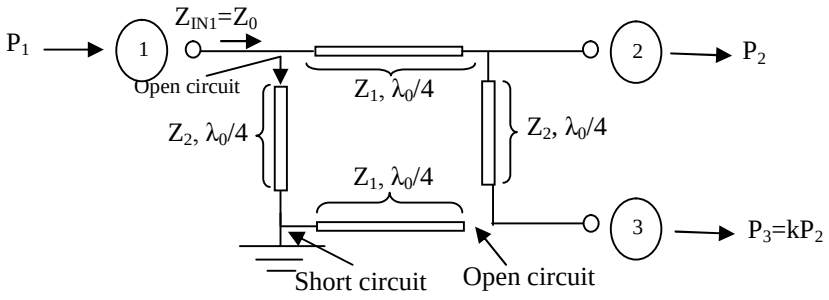

(b)

Fig.5.5a: hybrid branch line coupler

(b): hybrid branch line coupler with open circuit

For a desired power ratio of $P_3 = KP_2$, the task is to find the values of Z_1 and Z_2 such that the input impedance at port 1 will be equal to Z_0 and power at port 4 will be zero ($P_4 = 0$) at the desired centre frequency f_c.

For power at port 4 (P_4) is equal to zero and the voltage is also equal to zero, port 4 is short circuited between port 1 and port 4and also open circuited between port 3 and port 4, hence the network looks like this:

After removing the open circuit transmission line at the centre frequency f_c, the circuit looks like Fig.5.6 below,

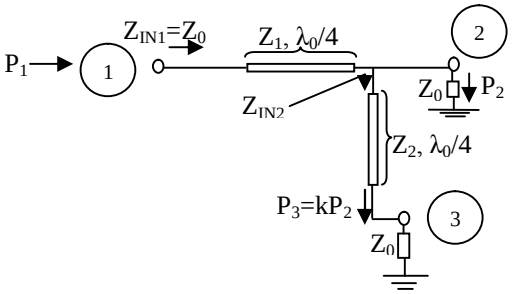

Fig.5.6: Two branch line coupler with only three ports

$$P_2 = \frac{|V_2|^2}{Z_0} \quad (5\text{-}12)$$

$$P_3 = \frac{|V_3|^2}{Z_0} \ , \quad (5\text{-}13)$$

$$P_3 = KP_2 \quad (5\text{-}14)$$

$$P_3 = \frac{|V_2|^2}{Z_{IN2}} \quad (5\text{-}15)$$

Substituting equation (5-12) into (5-14) we have,

$$P_3 = K\frac{|V_2|^2}{Z_0} \quad (5\text{-}16)$$

Equating equation (5-15) and (5-16) we have,

$$P_3 = \frac{|V_2|^2}{Z_{IN2}} = K\frac{|V_2|^2}{Z_0} \quad (5\text{-}17)$$

Hence, $Z_2 = \frac{Z_0}{\sqrt{K}}$ (5-18)

Also from Fig 5.6,

If $Z_L = Z_{IN2} \parallel Z_0$ and

$Y_L = KY_0 + Y_0$

$$Z_0 = \frac{{Z_1}^2}{Z_L} = \left(\frac{{Z_1}^2}{Z_0}\right)(1+K)$$

$$Z_1 = \frac{Z_0}{(1+K)^{\frac{1}{2}}} \quad (5\text{-}19)$$

Therefore equation (5-18) and (5-19) are used to find the value of the impedance of the through arms and the branch lines of the coupler. For an ideal two branch line coupler, at the centre frequency *fc K=1*, where *K* is the power ratio and Z_0=50 ohms.

Hence the value of Z_1 = 35.35 ohms and $Z_2 = Z_0$= 50ohms.

The *S*-parameters provide the values of the return loss, isolation and insertion loss.

For a coupler of four ports the *S*-parameter matrix at the centre frequency f_c is given by [108]:

$$[S] = \begin{bmatrix} S_{11} & S_{12} & S_{13} & S_{14} \\ S_{21} & S_{22} & S_{23} & S_{24} \\ S_{31} & S_{32} & S_{33} & S_{34} \\ S_{41} & S_{42} & S_{43} & S_{44} \end{bmatrix}$$

Assuming an impedance match at all four ports: $S_{11} = S_{22} = S_{33} = S_{44} = 0$

Since the network is reciprocal: $S_{ij} = S_{ji}$, where $i \neq j$

By symmetry: $S_{41} = S_{23} = 0$

Hence, the S-parameter matrix looks like this

$$[S] = \begin{bmatrix} 0 & S_{12} & S_{13} & 0 \\ S_{21} & 0 & 0 & S_{24} \\ S_{31} & 0 & 0 & S_{34} \\ 0 & S_{42} & S_{43} & 0 \end{bmatrix}$$

The power at port two of Fig.5.6 will be:

$$P_2 = |S_{21}|^2 P_1 \quad (5\text{-}20)$$

$$P_1 = P_2 + P_3 \quad (5\text{-}21)$$

$$P_1 = (1+K)P_2$$

$$|S_{21}| = \left(P_2/P_3\right)^{1/2} \quad (5\text{-}22)$$

$$|S_{21}| = (1+K)^{-1/2} \quad (5\text{-}23)$$

Similarly

$$|S_{31}| = \left(K/(1+K)\right)^{1/2}$$

When *K*=1 we have,

$S_{21} = 0.7071$, which is -3.01dB and also the coupling factor is -3.01dB

5.4.3 0dB Branch line Coupler

0dB branch line directional couplers are an efficient means of crossing two transmission lines with minimal coupling between them. There are many versions of 0dB branch line directional couplers [110], but for the purpose of this design the three- branch line directional coupler with quarter-wavelength for each branch have be used. It has been reported in [97, 110] that when three branch directional coupler with quarter-wavelength at each branch as shown in Fig.5.7 and excited at one of its ports the diagonal output magnitude will be 0dB at the central frequency of its operation. This will be used to replace the crossover line in the microstrip 4x4 Butler matrices. Note, the network shown in Fig.5.7 consists of ideal transmission lines, all of which have a characteristic impedance of Z_o and are a quarter wavelength at the centre frequency. In the next chapter, it will be shown that the realisation of this network in microstrip will require small alterations of the characteristic impedances in order to compensate for discontinuity effects in the microstrip realisation.

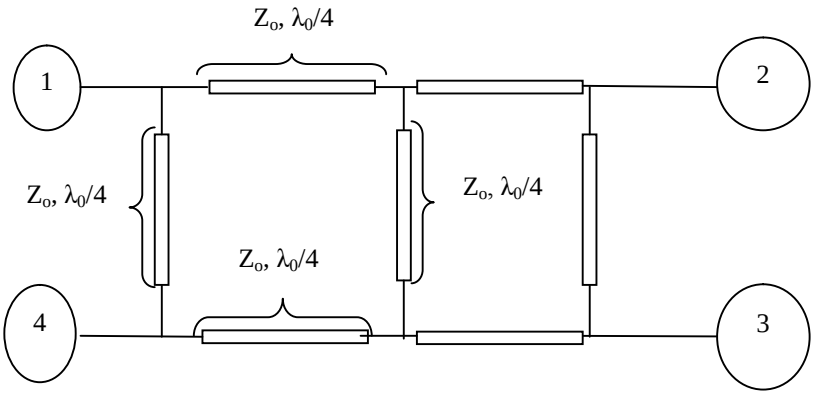

Fig.5.7:0dB branch line coupler [98]

5.5 Beam Shaping Network

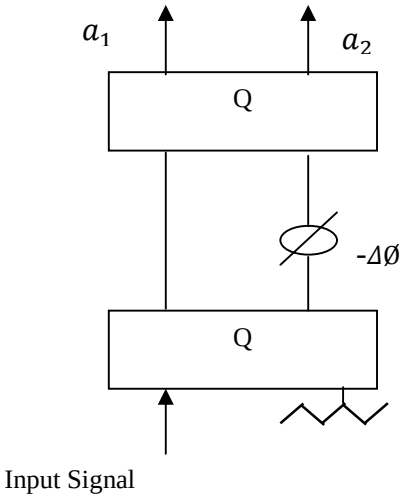

Fig.5.8: 2-way variable power divider/combiner controlled by one phase shifter

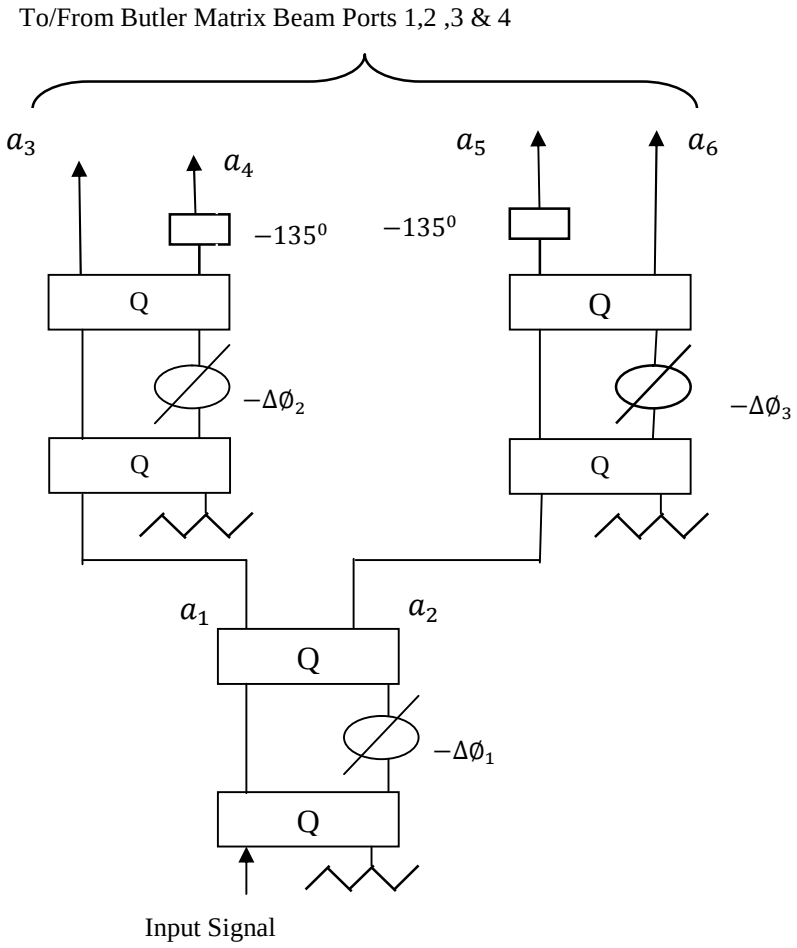

Fig.5.9: Beam shaping network

In order to provide non-uniform amplitude and non-uniform phase weights to produce the shaped beams we need to have a network to connect to the Butler matrix to "blend the narrow beams of the Butler matrix" and this is called the beam shaping network.

The beam shaping network is essentially a variable 4-way power divider/combiner that utilizes a 2-way variable power divider/combiner which drives two 2-way variable power dividers/combiners as shown in Fig.5.9. Each 2-way variable power divider/combiner is realised as shown in the network of Fig.5.8. When two 3dB hybrids are arranged as shown in Fig5.8 above, the output signals a_1 and $a_2 are$ given by the equation [108]

$$a_1 = \frac{1}{2} + \frac{1}{2}e^{-j(180^0+\Delta\emptyset_1)} \quad (5\text{-}24)$$

$$a_2 = \frac{1}{2}e^{-j(90^0)} + \frac{1}{2}e^{-j(90^0+\Delta\emptyset_1)} \quad (5\text{-}25)$$

Also when the network is arranged as shown in Fig.5.9 above the outputs of a_3, a_4 a_5 and a_6 are given by the equations

$$a_3 = a_1[\frac{1}{2} + \frac{1}{2}e^{-j(180^0+\Delta\emptyset_2)}] \quad (5\text{-}26)$$

$$a_4 = a_1[\frac{1}{2}e^{-j(90^0)} + \frac{1}{2}e^{-j(225^0+\Delta\emptyset_2)}] \quad (5\text{-}27)$$

$$a_5 = a_2[\frac{1}{2} + \frac{1}{2}e^{-j(315^0+\Delta\emptyset_3)}] \quad (5.28)$$

$$a_6 = a_2[\frac{1}{2}e^{-j(90^0)} + \frac{1}{2}e^{-j(90^0+\Delta\emptyset_3)}] \quad (5\text{-}29)$$

For equal amplitude and phase outputs from the 2-way power divider/combiner,

$|a_1| = |a_2|$

$\Delta\emptyset = 270^0$

For routing the entire signal to port 1, i.e. zero at port 2,

$\Delta\emptyset = 180^0$

Table 5.4.0 below summarises the operation of the variable 2-way power divider of Fig 5.8.

Table 5.4: 2-way Power divider/Combiner states

ΔØ	$\|a_1\|$	Phase (a_1)	$\|a_2\|$	Phase (a_2)
0^0	0	N/A	1	-90^0
180^0	1	0^0	0	N/A
208^0	0.97	-14^0	0.242	-14^0
270^0	0.707	-45^0	0.707	-45^0
332^0	0.242	-14^0	0.97	-14^0

Three two-way power dividers/combiners are connected to form the beam shaping network of Fig.5.9. Depending upon the communications traffic demand, a control algorithm based on the parameters of table 5.4 can adjust the relative power divider/combiner ratio to blend all the beams, or do beam switching or beam broadening for optimum service i.e. control of the three phase shifters within the beam shaping network dynamically provides the required complex weights for the desired beam shapes. Table 5.5 shows the Butler matrix beam ports weights and phase shifter values.

Table 5.5: Butler Matrix Beam Ports Signal Amplitudes & Phases and Phase Shifter Values @ f_c (Downlink & Uplink the same)

Relative Signal Amplitude & Phase of Butler Matrix Beam Ports									Phase Shifter Settings		
Beam state	Beam Port 1		Beam Port 2		Beam Port 3		Beam Port 4				
	Amp (dB)	Phase (deg)	Amp (dB)	Phase (deg)	Amp (dB)	Phase (deg)	Amp (dB)	Phase (deg)	$\Delta\phi 1$	$\Delta\phi 2$	$\Delta\phi 3$
B1L	0	0	−∞	N/A	−∞	N/A	−∞	N/A	180	180	Any
B1R	−∞	N/A	−∞	N/A	−∞	N/A	0	0	0	Any	0
B2L	−∞	N/A	−∞	N/A	0	-135	−∞	N/A	0	Any	180
B2R	−∞	N/A	0	-135	−∞	N/A	−∞	N/A	180	0	Any
BCB	0	0	0	-135	0	-135	0	0	270	270	270
RSB	0	0	-12	-135	0	-135	-12	0	270	208	208
LSB	-12	0	0	-135	-12	-135	0	0	270	332	332

5.5.1 Variable Phase Shifter

Coaxial, microstrip and coplanar waveguide are types of transmission line that could be used to form variable phase shifters. Although microstrip lines have the disadvantage of dispersion (not relevant in this application because both the uplink and downlink bands are very narrow band) and significant insertion loss they still remain the preferred approach which can easily be integrated with other passive and active microwave devices. The structure of a microstrip line variable phase shifter is shown in Fig.5.10. It consists of two parallel microstrip lines printed on a fixed dielectric substrate and covered with thin Teflon

tape (1/4 mm thick) of dielectric constant 2.1 and a chamfered edge U-shaped microstrip line printed on a movable dielectric substrate which is directly above the two parallel microstrip lines. The chamfered edge U-shaped microstrip line slides over the two parallel microstrip lines and is configured such that the movable microstrip line can slide along the fixed lines, which ensures a continual change of the physical length of the line so as to realise continuous phase shifting [126-127].

The relationship between transmission line length *l* and phase delay is given by:

$\theta = \frac{-l}{\lambda_g} 360^0$, where λ_g is the wavelength in the dielectric substrate.

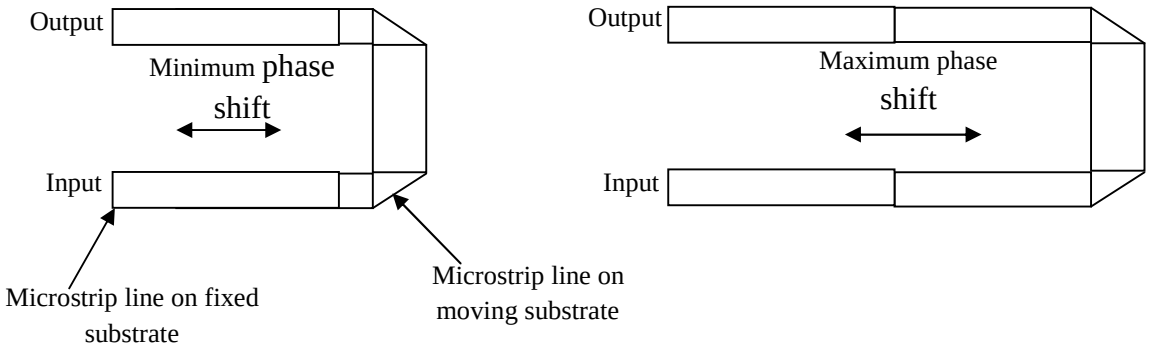

Fig.5.10: A "Trombone" microstrip line phase shifter

5.6 Summary

The design of the major components of the novel multiple switched beam smart antenna system with beam shaping capability has been presented in this chapter. These include: array elements, array antenna, Butler matrix beam forming network and a beam shaping network. The Butler matrix consists of multiple branch line couplers. The beam shaping network also consists of multiple branch line couplers and variable phase shifters. The quality of the Butler matrix and the beam shaping network depends on the branch line coupler. The design of a branch line coupler is also presented in this chapter. In this chapter all components have been assumed ideal, i.e. comprised of ideal transmission lines. The next chapter will present simulation results for all components using both ideal transmission lines and using microstrip transmission lines. It will be shown that for the latter case, the components will need to be modified in order to compensate for the discontinuity effects in the microstrip networks.

Chapter 6 - SIMULATION OF THE ANTENNA SYSTEM

6.1 Introduction

The previous chapter has dealt with the design of antenna elements and a suitable combined feed network for the proposed smart antenna system. To verify the concept of the proposed smart antenna system over the up and downlink sub-bands for a specific UK 3G network operator (Orange, UK), the array element, antenna array and the feed network (beam shaping network and Butler matrix) has been simulated using Genesys software and CST 3D electromagnetic simulation software [117-118]. Two designs of the feed network were simulated; one for the downlink frequency band and another for the uplink frequency band. The array antenna was simulated first by modelling one single slant $\pm 45^0$ dual-polarised stacked microstrip patch antenna element and then a column array of ten elements of slant $\pm 45^0$ dual-polarised stacked patches was formed. Thereafter, four column arrays were employed to form the smart antenna system. The orange UK sub-bands have been assumed as a practical example (downlink frequency band of 2.1597GHz to 2.1697GHz and uplink frequency band 1.9697GHz to 1.9797GHz). The smart antenna system feeder network was configured initially using ideal transmission lines and then using microstrip transmission lines to enable comparison.

6.2 Array Antenna Element Simulation

The array antenna element model used for the numerical simulation in CST microwave studio is as shown in Fig.6.1. The slant $\pm 45^0$ dual-polarised stacked patch antenna is designed to simultaneously operate over the Orange UK sub-bands (downlink frequency band of 2.1597GHz to 2.1697GHz and uplink frequency band 1.9697GHz to 1.9797GHz) on a substrate (Rogers Corp. 5870) with 2.33 permittivity and 1.575 mm thickness. Both the suspended patch and the printed patch are square to obtain a symmetric radiation pattern and identical performance for both polarisations. However, the suspended patch is rotated 45 degrees to improve the impedance match. The printed patch and the suspended patch are located at the centre of the square ground plane of dimensions $0.5\lambda_0$ x $0.5\lambda_0$ ('λ_0' is the wavelength in free space). The printed patch size is 46.83mm square and the suspended patch size is 56.8mm square with a spacing of 10.5mm from the printed patch to increase the bandwidth of the antenna (this bandwidth broadening occurs because the volume of the radiating structure is increased when a suspended patch is added).

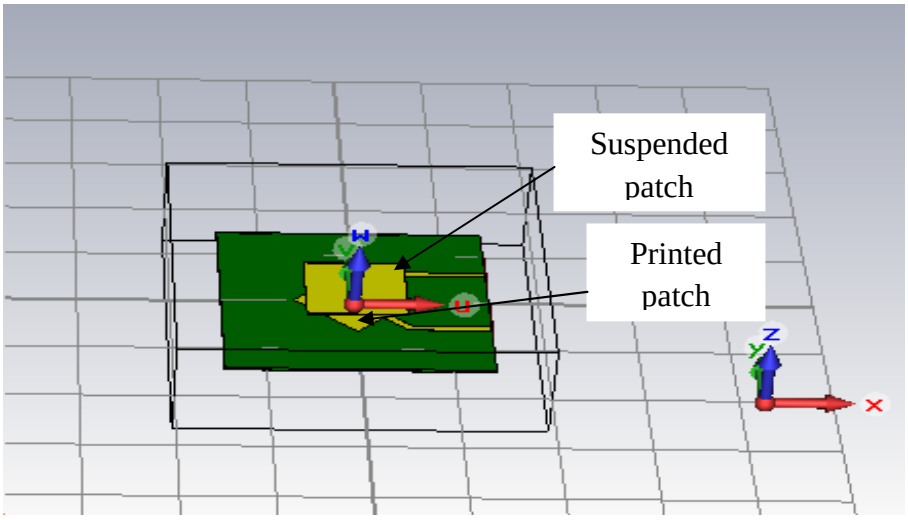

Fig.6.1: Slant $\pm 45^0$ dual-polarised stacked patch antenna model in CST

6.2.1 Radiation Pattern of the Single Element

The slant $\pm 45^0$ dual-polarised sacked patch antenna was simulated in CST microwave studio by exciting the $+45^0$ port and then by exciting the -45^0 port. Two sets of radiation patterns were obtained for each port at a frequency of 1.975GHz (the result presented in this report is for the chosen uplink centre frequency and a similar result was also obtained for the chosen downlink centre frequency). Dual-polarised antennas are described in terms of the isolation between the two ports and co-polarisation and cross-polarisation of the antenna patterns for each port. Fig. 6.2 shows the radiation patterns of slant $+45^0$ polarisation (co-polar and cross-polar) and Fig.6.3 shows radiation patterns for slant -45^0 polarisation (co-polar and cross-polar). Dual ± slant 45^0 linear polarisation is necessary so that polarisation diversity can be achieved on the uplink and so that on the downlink the broadcast channel can be transmitted on one polarisation and another beam can be transmitted on the other polarisation on the downlink. The element's 3dB beam width is 63.9^0, the element gain is 9.3dBi and the VSWR is 1.45:1 maximum. The ratio of co-polar to cross-polar radiation pattern of slant $+45^0$polarisation and slant -45^0 polarisations is 25dB on axis at a frequency of 1.975GHz, which agrees with the report in [120] that a properly designed microstrip element will usually have a cross-polar of 20dB or more below the co-polarisation level on axis. The simulated radiation pattern at both ports ($+45^0$polarisation and -45^0polarisation) and at frequency of 1.975GHz, are very similar and they are mirror images of each other which agrees with [122-123] that a slant $\pm 45^0$ dual-polarised antenna will provide identical azimuth beam width and performance.

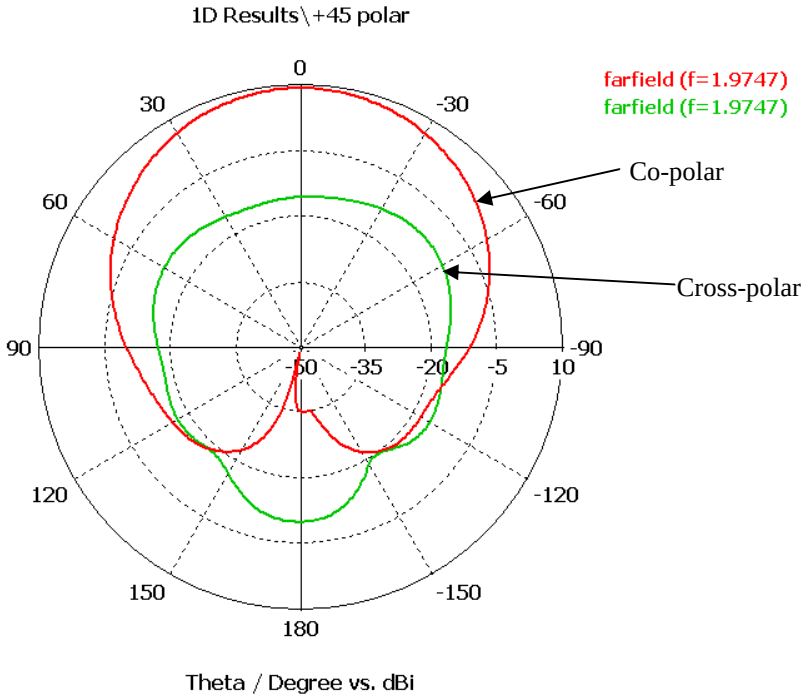

Fig.6.2: Azimuth Pattern of the $+45^0$ polarisation port of stacked patch

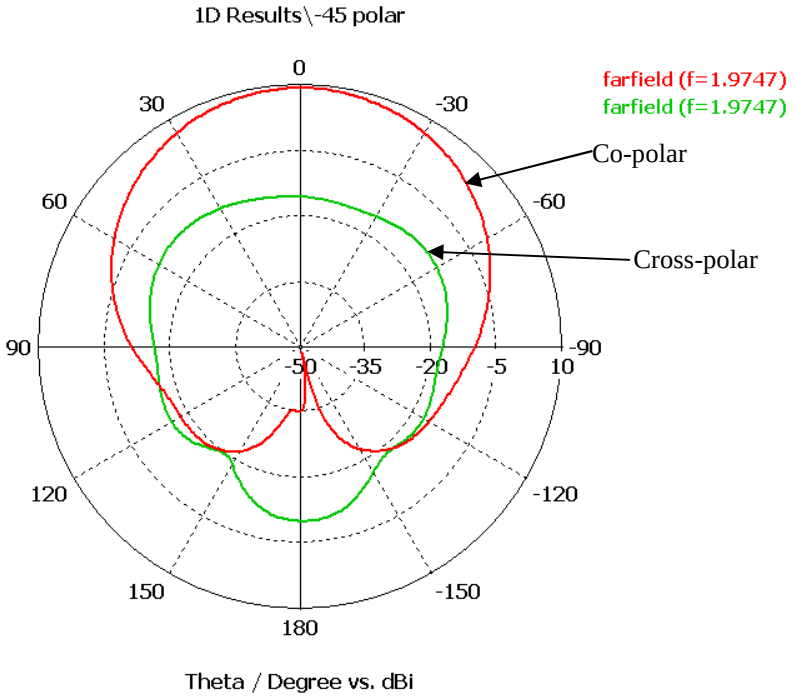

Fig.6.3: Azimuth pattern of the -45^0 polarisation port of stacked patch

6.2.2 Return loss and Isolation of the Single Element

The return loss is a measure of the amount of power that is reflected back to input port of the antenna. For a well matched antenna, the return loss is greater than 15 dB [108]. Fig.6.4 and Fig.6.5 show the return loss of the slant $\pm 45^0$ dual-polarised stacked patch antenna at each port respectively. Over the uplink band, the worst cast return loss is 19 dB and over the downlink band the worst case return loss is 15dB. Fig.6.6 shows the isolation between the two ports which is approximately 21dB. The standard mobile telecom network specification for isolation is 30 dB minimum. Hence, for a practical product, the isolation of the subject design would need to be increased. This can be done by the inclusion of a coupling cancellation network. However, this was deemed not to be necessary since the essence of the research relates to the ability to provide dynamically changeable radiation patterns and this is not affected by the isolation performance.

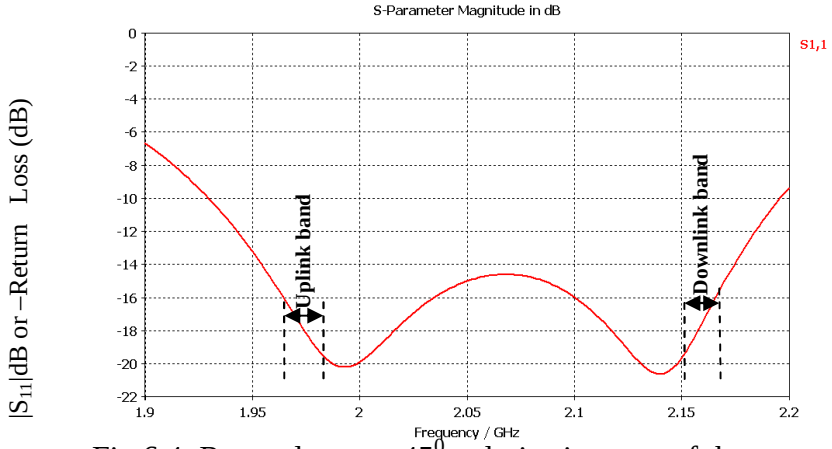

Fig.6.4: Return loss at $+45^0$ polarisation port of the array

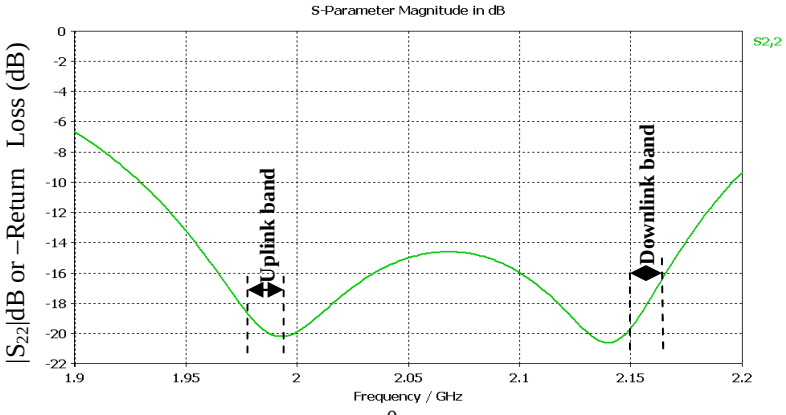

Fig.6.5: Return Loss at -45^0 polarisation port of the array

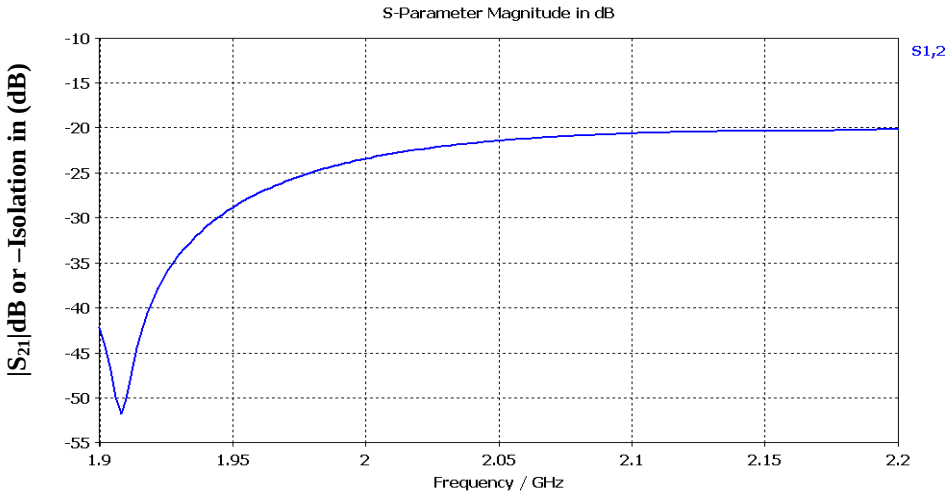

Fig.6.6: Isolation between the two ports of the array

6.3 Antenna Array Simulation

The slant $\pm 45^0$ dual-polarisation stacked patch antenna modelled above was configured into a linear column array of ten elements each, and these were then configured into four side-by-side column arrays to provide for the smart antenna array with a horizontal element spacing (centre-to-centre) of 72.5mm and the elements within the column arrays are excited with equal amplitude and phase and simulated in CST. The radiation patterns and gain of the linear column array and the linear four column smart antenna array were then studied.

6.3.1 Radiation Pattern of Column Array Antenna Simulation

Fig6.7 presents the elevation pattern of the slant $+45^0$ polarisation (co- polar and cross-polar) radiation pattern and Fig.6.8 presents the elevation pattern of the slant -45^0 polarisation (co-polar and cross-polar) radiation pattern of the ten element column array at the centre uplink frequency of 1.975GHz. The output radiation pattern is an array multiplication of the single element far-field pattern and the array factor. As all the elements in the array are identical, the cross polar pattern of the array product will be the same as that of the element. The slant $+45^0$ polarised patterns and the slant -45^0 polarised patterns are mirror images of each other. The column array gain is 17.1dBi which is close to the figure of 17.5 dBi assumed during the initial modelling of the antenna

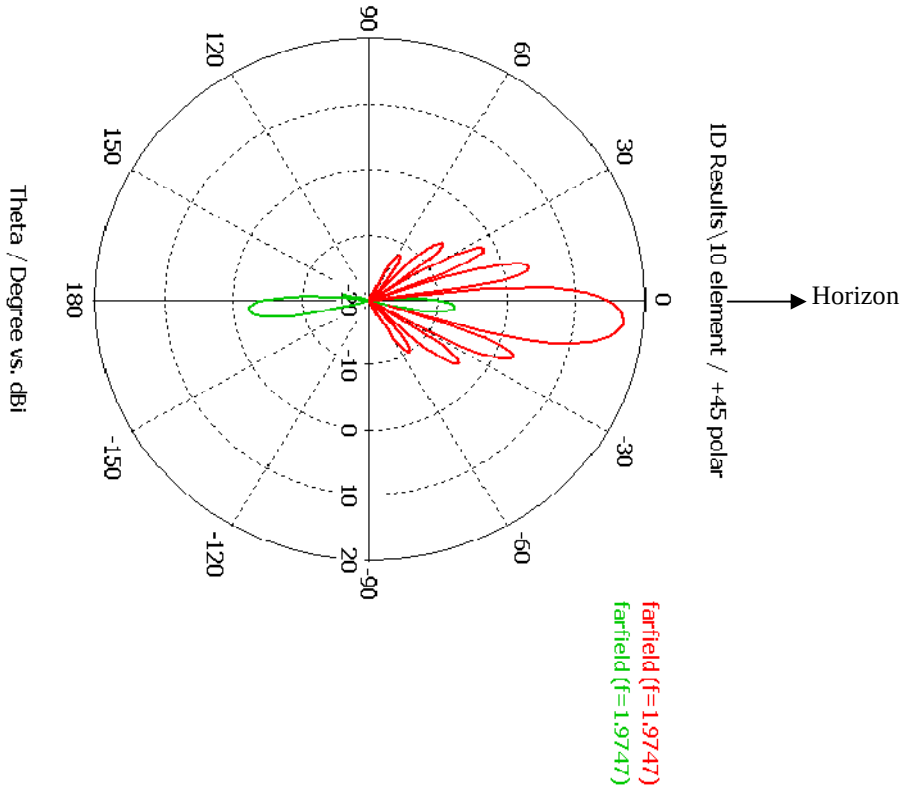

Fig.6.7: Elevation pattern of column array of $+45^0$polarisation port

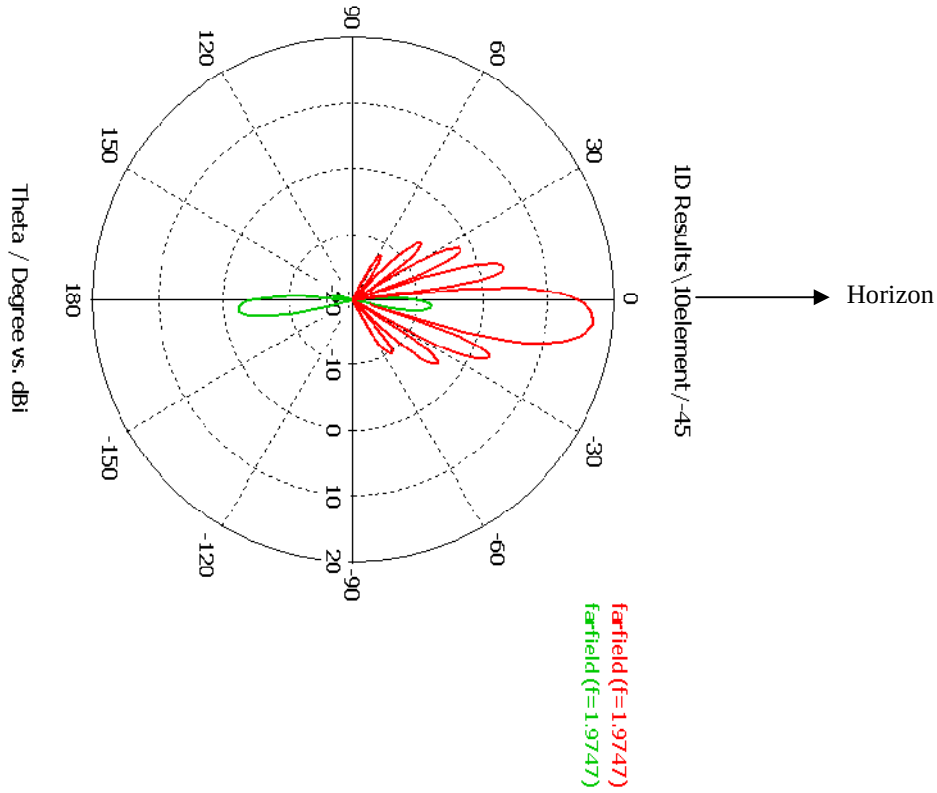

Fig.6.8: Elevation pattern of column array of -45^0polarisation port

6.3.2 Radiation Pattern of Four Column Array Simulation

The slant $\pm 45^0$ dual-polarised 10 element column array was configured into a horizontal array of four columns. Fig.6.9 is the azimuth pattern of the slant $+45^0$ polarised (co- polar and cross-polar) radiation pattern and Fig.6.10 is the azimuth pattern of the slant -45^0 polarised (co- polar and cross-polar) radiation pattern of the 4 column x 10 element linear array at 1.975GHz frequency excited with equal amplitude and equal phase. Again the radiation pattern at port slant $+45^0$ polarisation is the mirror image of the port slant -45^0 polarisation radiation pattern.

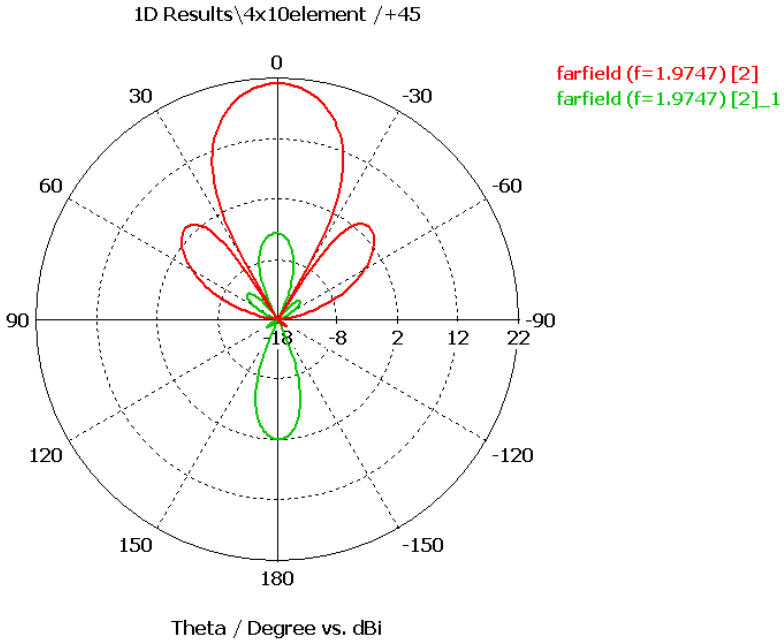

Fig.6.9: Azimuth pattern of four column array of $+45^0$polarisation port

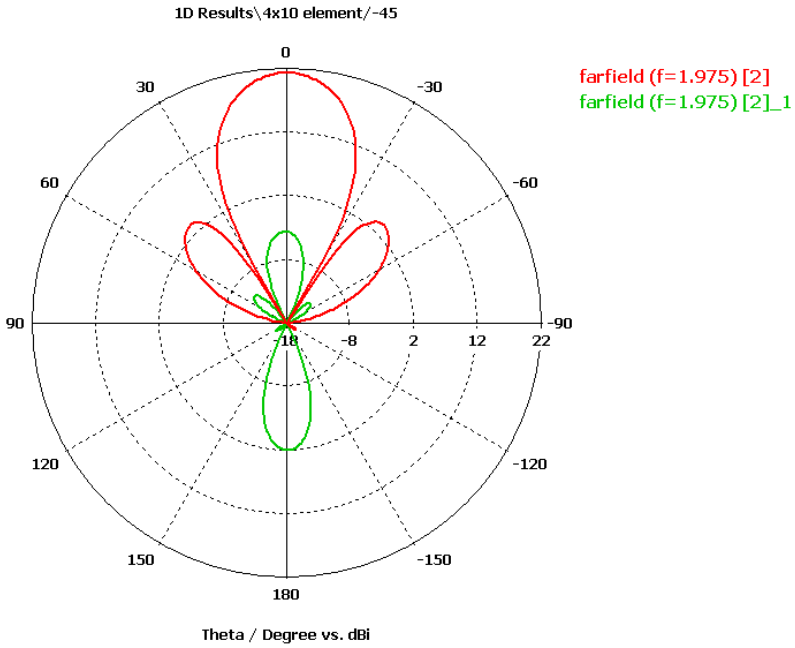

Fig.6.10: Azimuth pattern of four column array -45^0 polarisation port

6.4 Butler Matrix Simulation

A Butler matrix multiple beam former uses a combination of branch line coupler hybrids, phase shifters and 0dB couplers (to realise cross-overs on a single layer) to form *N* simultaneous independent beams from an *N* element antenna array. The performance of the microstrip Butler matrix depends on the performance of the hybrid coupler and the 0dB coupler. Therefore the hybrid branch line coupler was modelled, simulated and analysed first using ideal transmission lines and then using microstrip transmission lines in Genesys microwave network analysis software for comparison.

6.4.1 Ideal Transmission line Hybrid Branch line Coupler Simulation

The performance of the ideal 3dB branch line coupler over the uplink and downlink bands was simulated. Fig.6.11, 6.12 & 6.13 below presents the return loss, isolation at port 4, coupling from port 1 to port 2 and port3 and phase shift between port2 and port3(only results for uplinkf_L, f_C, f_H = 1.9697GHz, 1.9747GHz and 1.9797GHz are presented here). The 3dB branch-line coupler demonstrates the expected characteristics and it is seen that the branch line coupler characteristics are virtually invariant over the band based upon the ideal network model and the narrow uplink band. The isolation (-S_{14}dB) and return loss (-S_{11}dB) at the centre frequency is 76dB, the coupling factors between port 1 and port 2 (S_{12}) and between port 1 and port 3 (S_{13}) are -3dB and the phase difference between port2 and port 3 (arg[S_{12}]- arg[S_{13}]) is 90^0.

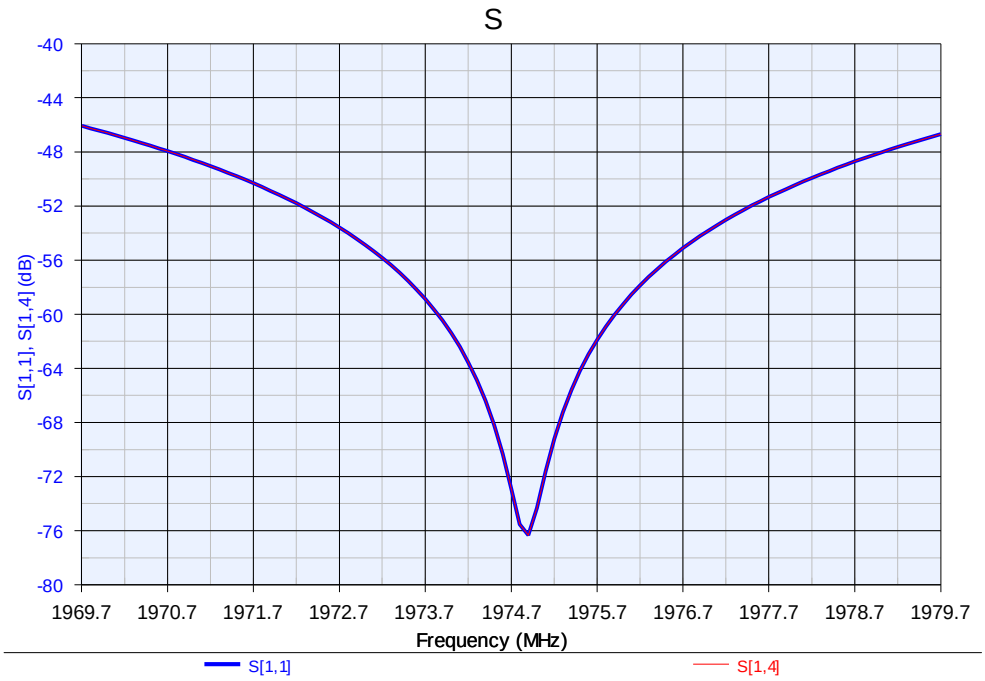

Fig. 6.11: Return loss (-S_{11}dB) and Isolation (-S_{14}dB) of ideal branch line coupler

Fig .6.12: coupling between port 1 and 2(S_{12}) and between port1 and 3(S_{13})

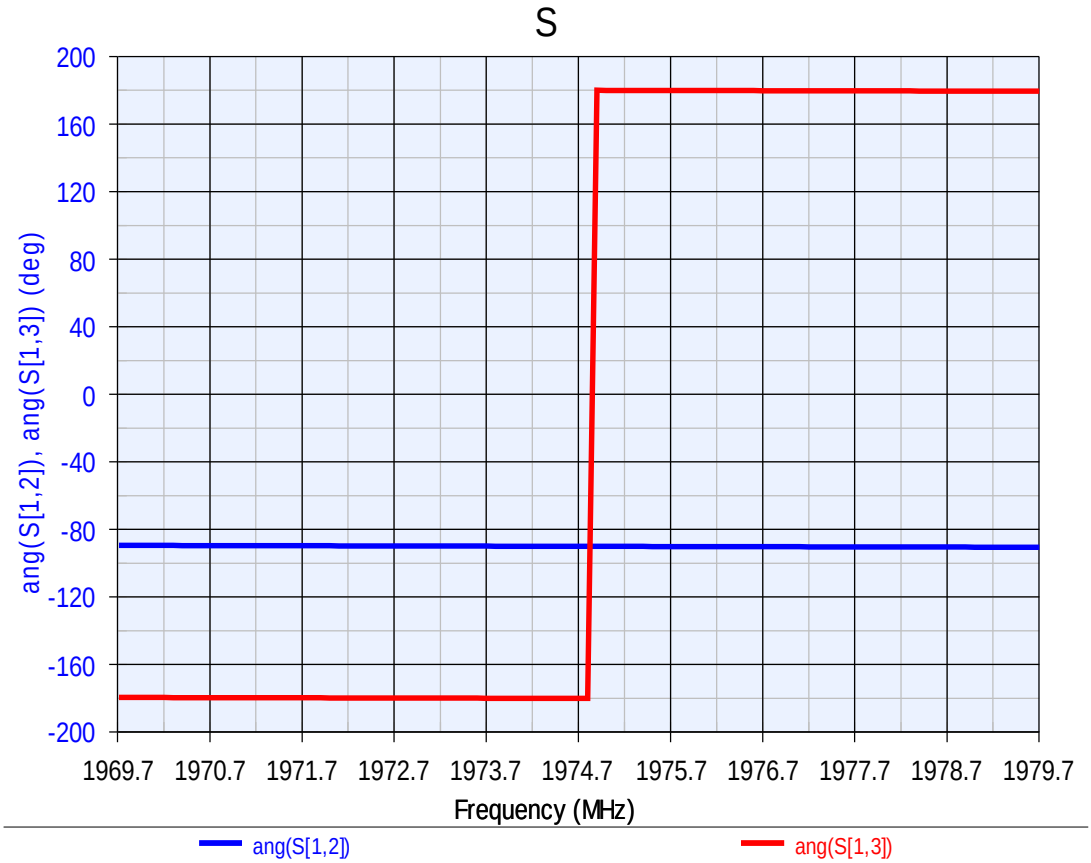

Fig .6.13: Phase different between port2 and 3 (arg[S_{12}]- arg[S_{13}]) of ideal branch line coupler

6.4.2 Microstrip Branch Line Coupler Simulation

The branch line coupler designed in chapter five was modelled in Genesys using microstrip lines with an RT/duroid 5870 substrate of relative permittivity of 2.33, height (H) of 1.575mm and copper thickness (t) of 0.035mm. Fig.6.14, 6.15 & 6.16 show the performance of the branch line coupler for the uplink frequency band. The coupler shows a worst case return loss ($-S_{11}$dB) and isolation ($-S_{14}$dB) of better than 29 dB which represents an excellent result. At the centre frequency the 90^0 hybrid constructed with microstrip lines shows a good return loss ($-S_{11}$dB) and high isolation ($-S_{14}$dB) of 30.78dB and 31.08dB respectively which again is excellent performance. The coupling factor between port1 and port 2 (S_{12}) and between port1 and port3 (S_{13}) is virtually unchanged from the ideal model at the centre frequencies of the band. The results confirm that every time the EM wave propagation is changed in a transmission line circuit, some disturbance is created by RF current crowding that behaves inductively, and by the electric field fringing that has a capacitive nature. When two or more transmission lines of different geometries are connected, we experience transmission line discontinuities and the most commonly occurring transmission line discontinuities are change in track widths, Tees and bends. Current crowding occurs in the lines as they approach the discontinuities. The presence of the T-junction results in an excess capacitance to ground. The principle effect is a significant shift in the resonant frequency compared to the ideal model and this effect has been compensated by changing the microstrip transmission line lengths.

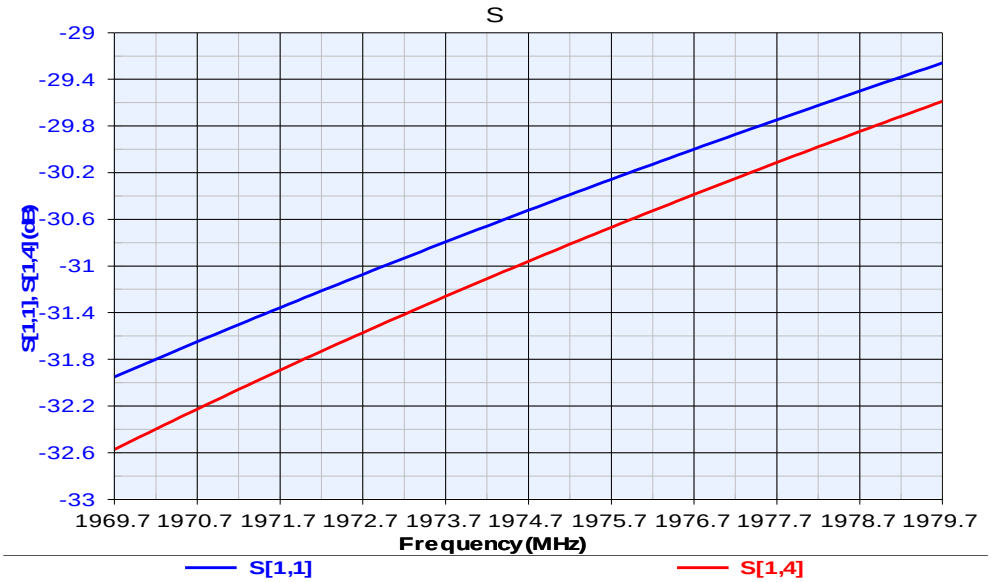

Fig.6.14: Return loss ($-S_{11}$dB) and Isolation ($-S_{14}$dB) of microstrip branch line coupler

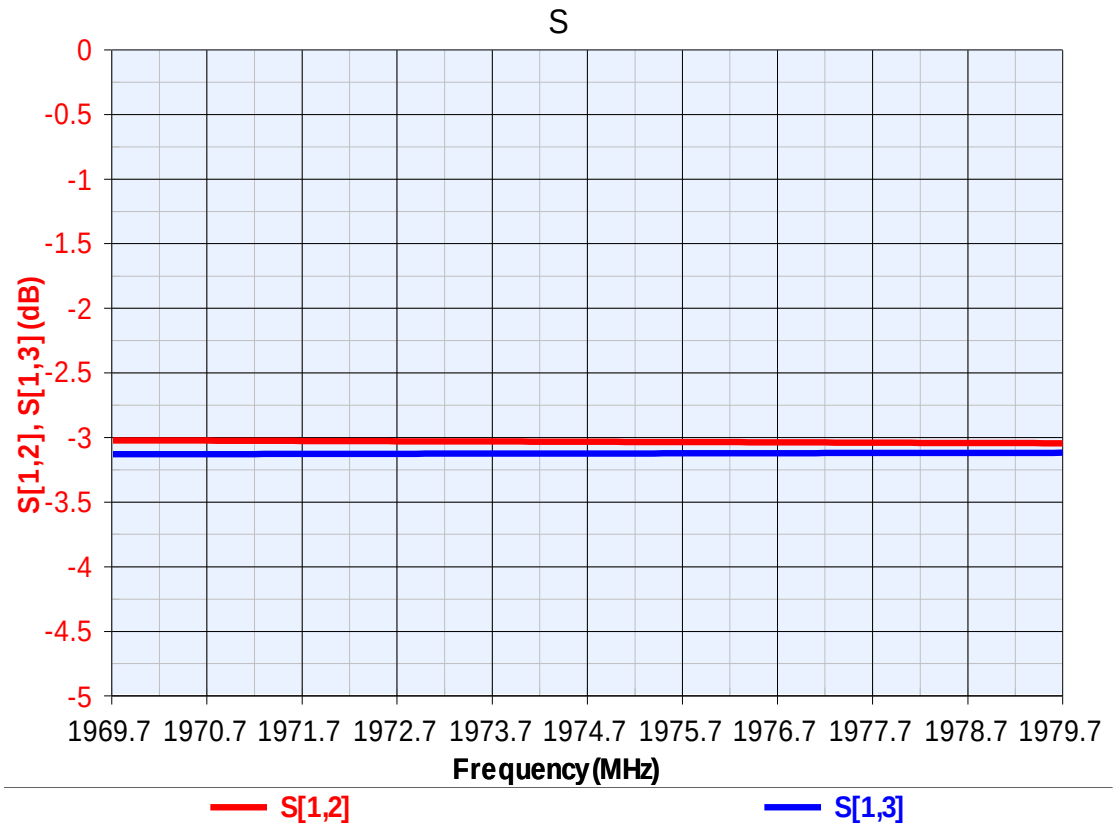

Fig .6.15: coupling between port 1 and 2(S_{12}) and between port1 and 3(S_{13}) of microstrip branch line coupler

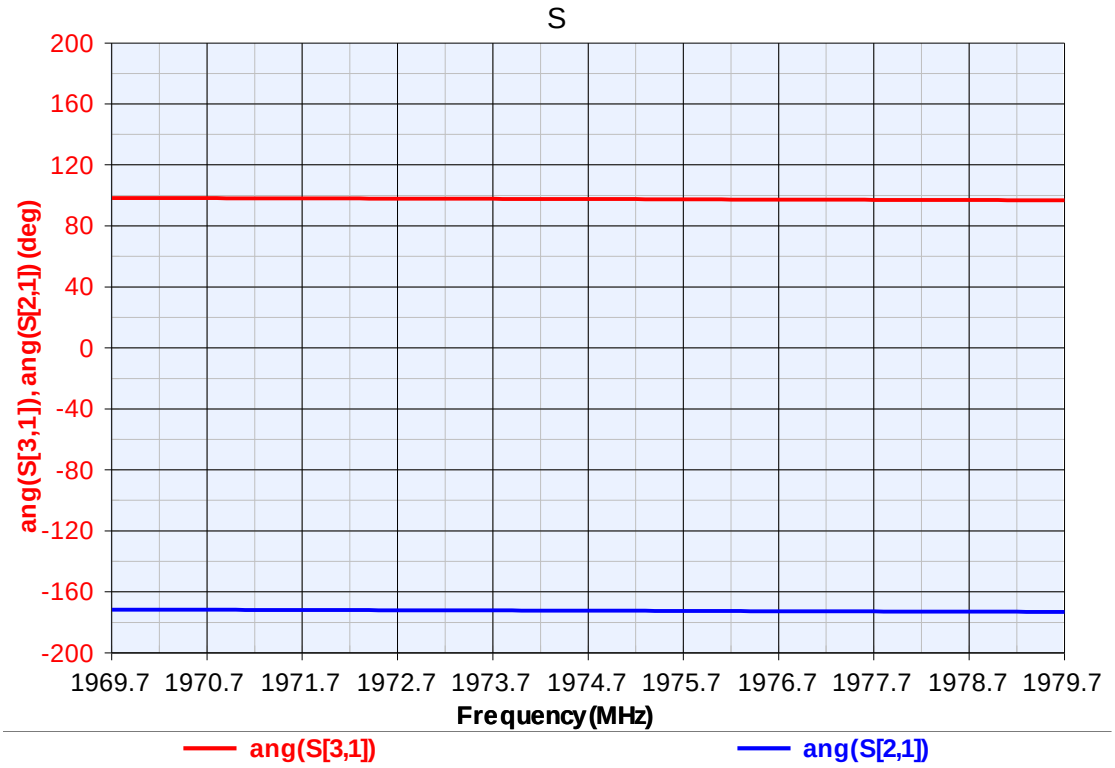

Fig. 6.16: Phase different between port2 and 3 (arg[S_{12}]- arg[S_{13}]) of microstrip branch line coupler

6.4.3 0dB Coupler Simulation

The 0dB branch line directional coupler was modelled in Genesys, using three branch lines with equal track widths and equal track lengths but slight modification to centre line length of the coupler to compensate for discontinuity effects and simulated. Fig.6.17 below shows the microstrip 0dB coupler model and Fig.6.18 shows the loss between diagonal ports of the coupler. This is seen to be virtually 0dB as desired, i.e. coupling between port1 and port3 (S_{13}) port4 and port2 (S_{42}) is 0dB.

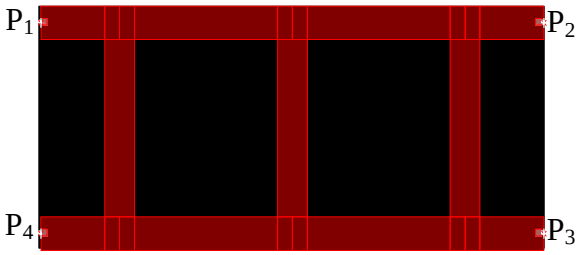

Fig.6.17: Microstrip 0dB coupler

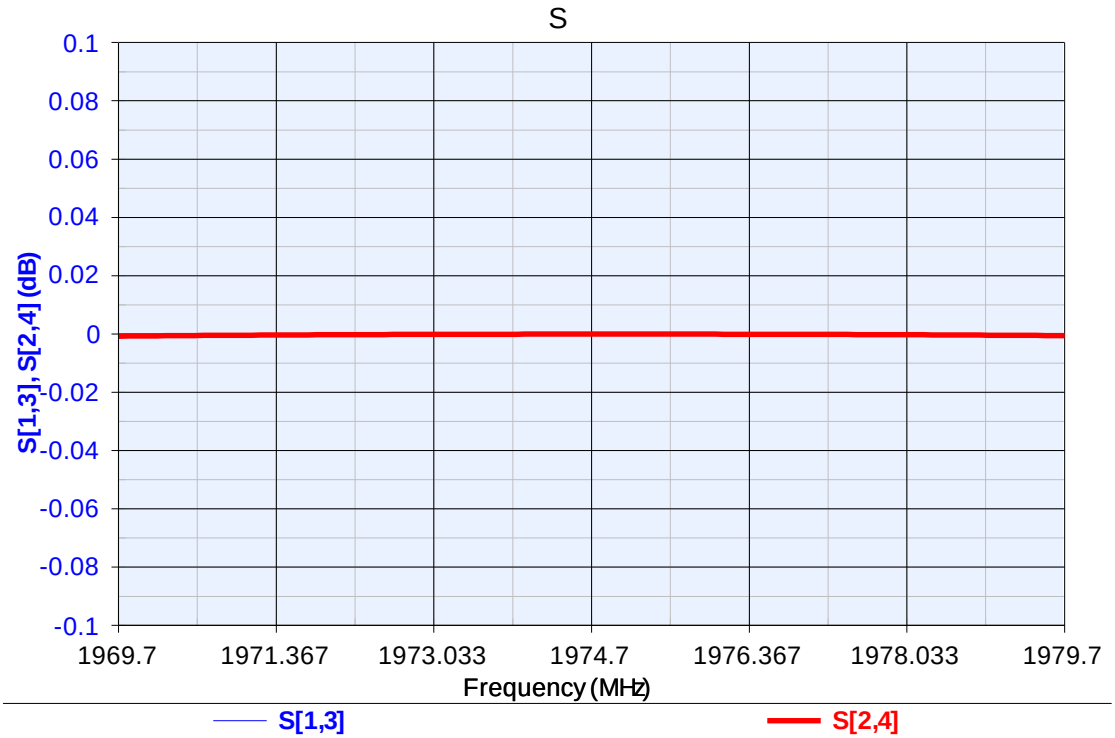

Fig.6.18: Diagonal port-to-port coupling plot

6.4.4 Ideal Butler Matrix Configuration Simulation

Four ideal transmission line branch line couplers were configured to form 4x4 Butler matrix in Genesys network analysis software. The required phase shifts, two 45^0 phase shifters, are implemented using transmission lines that introduce the required phase shift at the centre frequency of the uplink frequency band. The concept of Butler matrix for beam-forming and the use of branch line couplers to form it have been well established in chapter three. A signal (amplitude and phase) at any of the input ports (port 1, 2, 3, and 4) produces equal amplitude and progressive phase difference across the frequency band at all of the output ports (Port 5, 6, 7 and 8) as shown in Fig.5.5

Fig.6.19 and 6.20 shows the output results when a signal is input at beam port1 (using ideal transmission lines). Fig.6.19 shows the magnitude graph while Fig.6.20 shows the linear progression phase shift at the element ports. The theoretical value for the amplitude distribution is -6.02dB at the centre frequency. The simulated amplitude value of the Butler matrix design with ideal transmission (S_{15}) is -6.02dB, which agreed with the theoretical value. The phase difference also agreed with the theoretical calculation (see table 5.1 for the various values of amplitude and phase progression when each beam port is excited). It is seen that the Butler matrix characteristics (amplitude and phase progression) are virtually invariant over the bands based upon the ideal network and the narrow band width.

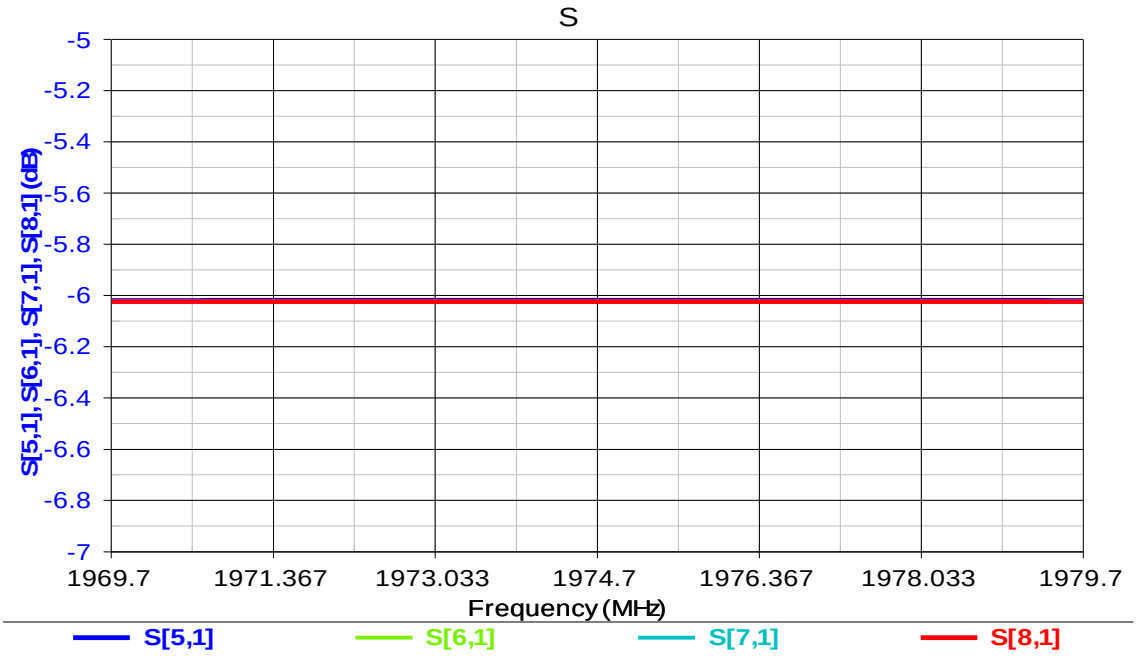

Fig. 6.19: The output magnitude in (dB) when signal is in put into port1 of an ideal Butler matrix

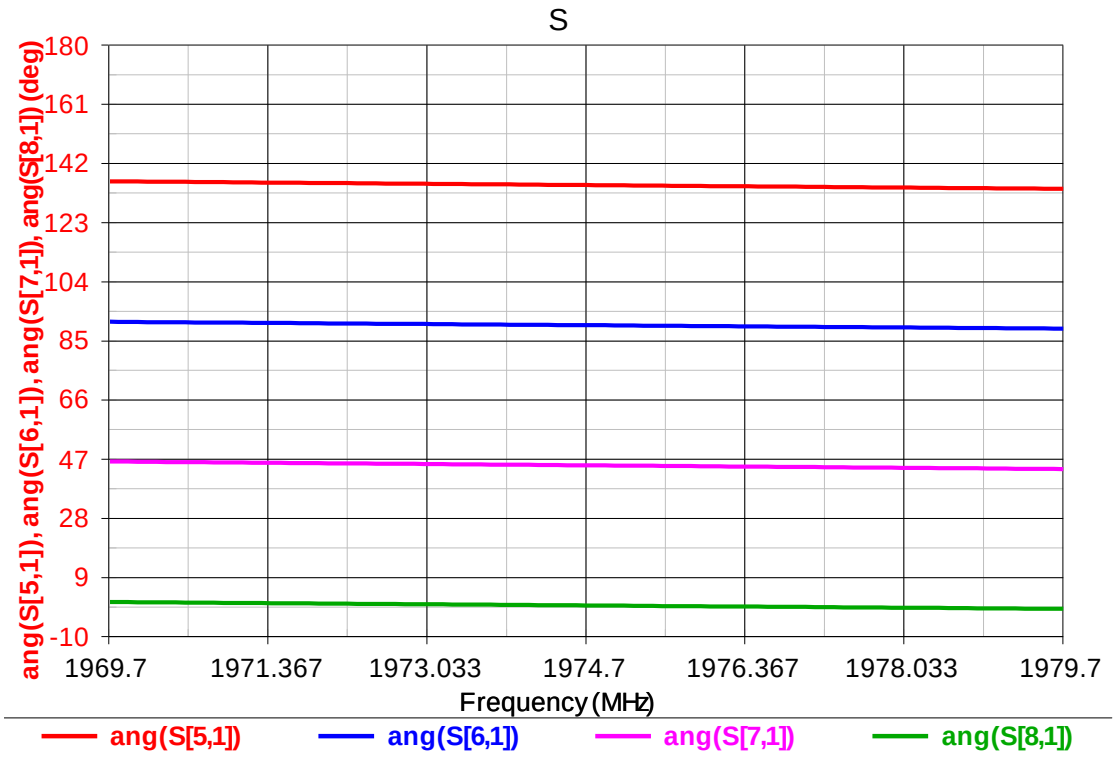

Fig. 6.20: Phase progression graph when signal is input into port1 of an ideal Butler matrix

6.4.5 Microstrip Butler Matrix Simulation

The microstrip branch line coupler was configured with crossover lines replaced with a 0dB coupler for easy layout to form a 4x4 microstrip line Butler matrix to operate in the uplink frequency band. A signal at any of the input beam ports (port 1, 2, 3 and 4) it is expected to produces equal amplitude at the centre frequency at all of the output ports (Port 5, 6, 7 and 8). Fig.6.21and 6.22 shows the plots for the amplitude and phase progression at the four output ports with reference to port 1. The reflection at each input beam port (that is port1 ($-S_{11}$), port two ($-S_{22}$) etc) varies from 33dB to 44dB across the uplink frequency band (Fig.6.23 shows the plot). The amplitude of the output signals is not equal across the uplink frequency band, which are the problems alighted in chapter two about microstrip Butler matrix. The presence of bends and Tee-joints causes some discontinuities in the design which now shift the amplitude from 6.02dB for ideal transmission line to 6.56dB for the microstrip line at the centre frequency. There is also variation in the phase shift of the 4x4 microstrip Butler matrix. The final layout of the microstrip Butler matrix is presented in Fig.6.23.

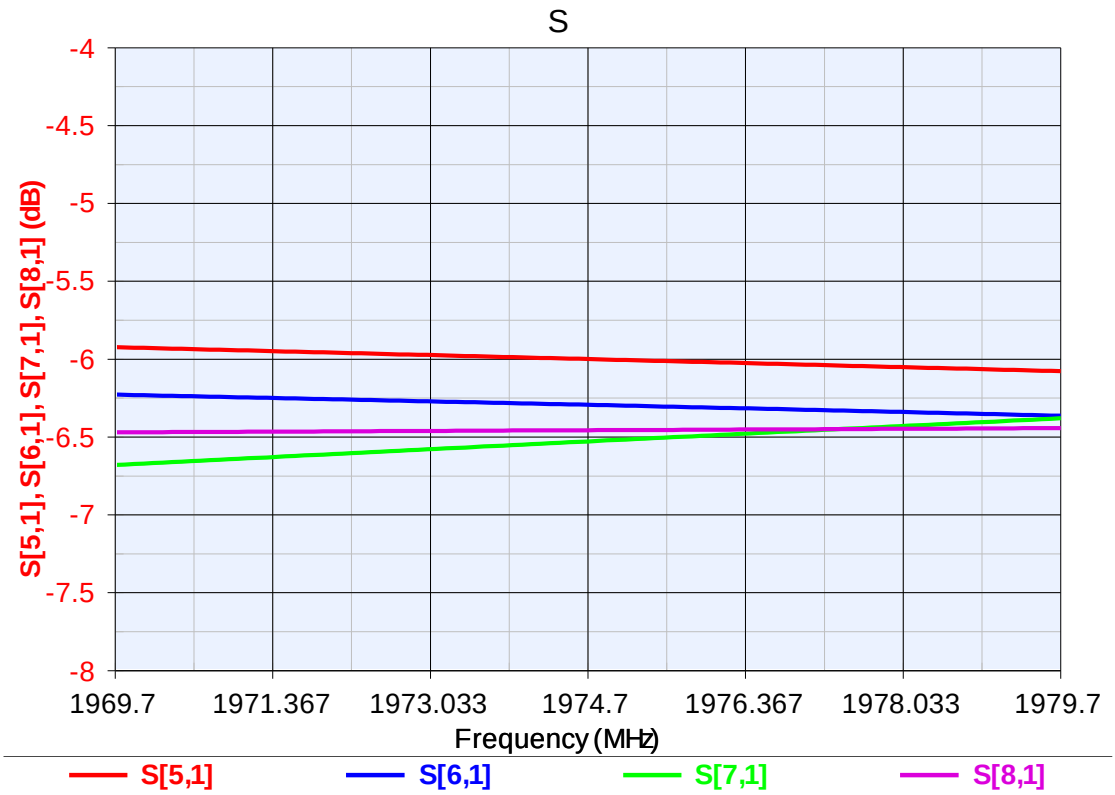

Fig. 6.21: The output magnitude in (dB) when signal is in put into port1 of the microstrip Butler matrix

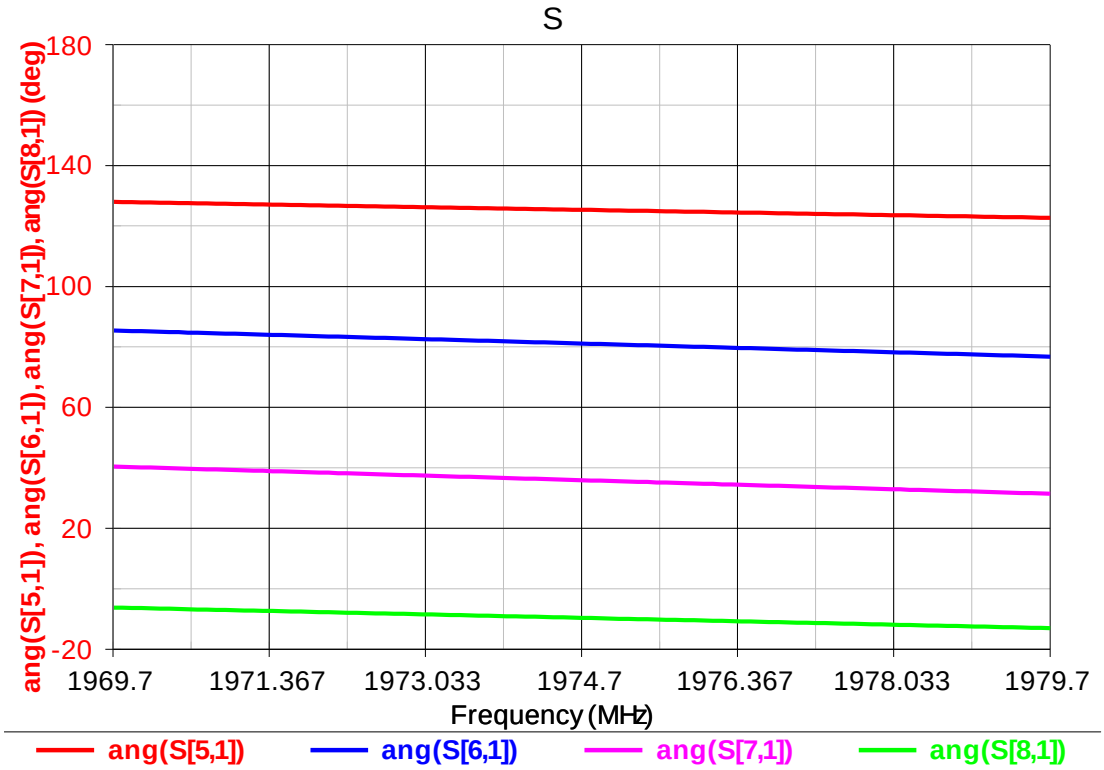

Fig. 6.22: Phase progression graph when signal is input into port1 of the microstrip Butler matrix

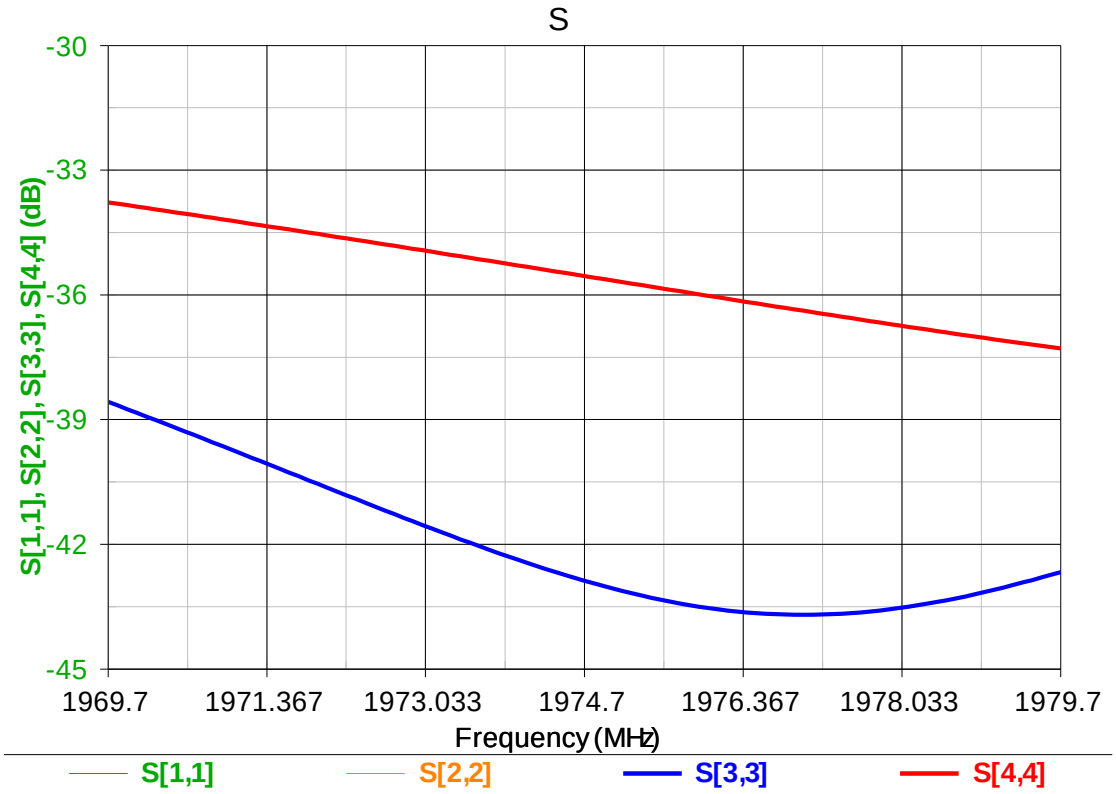

Fig.6.23: Microstrip Butler matrix returns loss

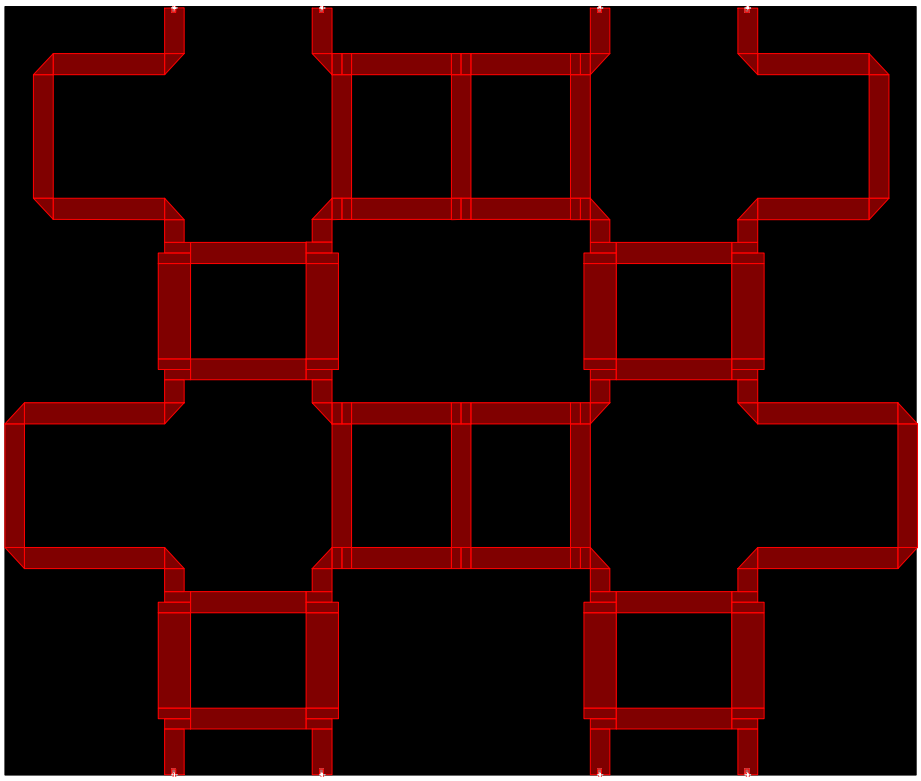

Fig.6.24: 4x4 microstrip Butler matrix layout

6.5 Beam Shaping Network Simulation

The beam shaping network was constructed and modelled in Genesys using ideal transmission lines first to verify the concept of the beam shaping network and then microstrip transmission lines for the implementation. Six branch line couplers and three variable phase shifters was used to construct the beam shaping network. The three variable phase shifters are implemented using transmission line lengths that can be varied to introduce the required phase shift (true time delay) at the centre frequency of interest. When the three variable phase shifters are set at $\Delta\emptyset_1=270^0$, $\Delta\emptyset_2=332^0$ $\Delta\emptyset_3=332^0$(condition for the left hand shaped beam), Fig.6.25 and 6.26 below present the non-uniform amplitude and phase outputs of the microstrip beam shaping network. A close examination of the amplitude plot shows that the amplitude of port 2 and port 4 are -12dB down compared to port3 and port4, which is the condition to excite the Butler matrix to blend the four narrow beams to the left hand side of a cell sector. The required phase delay at port3 and port4 was also shown in the plot (-135^0 at the two ports). The required amplitude and phase delay at the four output ports of the beam shaping network both for ideal transmission lines and microstrip lines are quite uniform across the uplink frequency band. Fig.6.27 shows the beam shaping network implemented with microstrip lines.

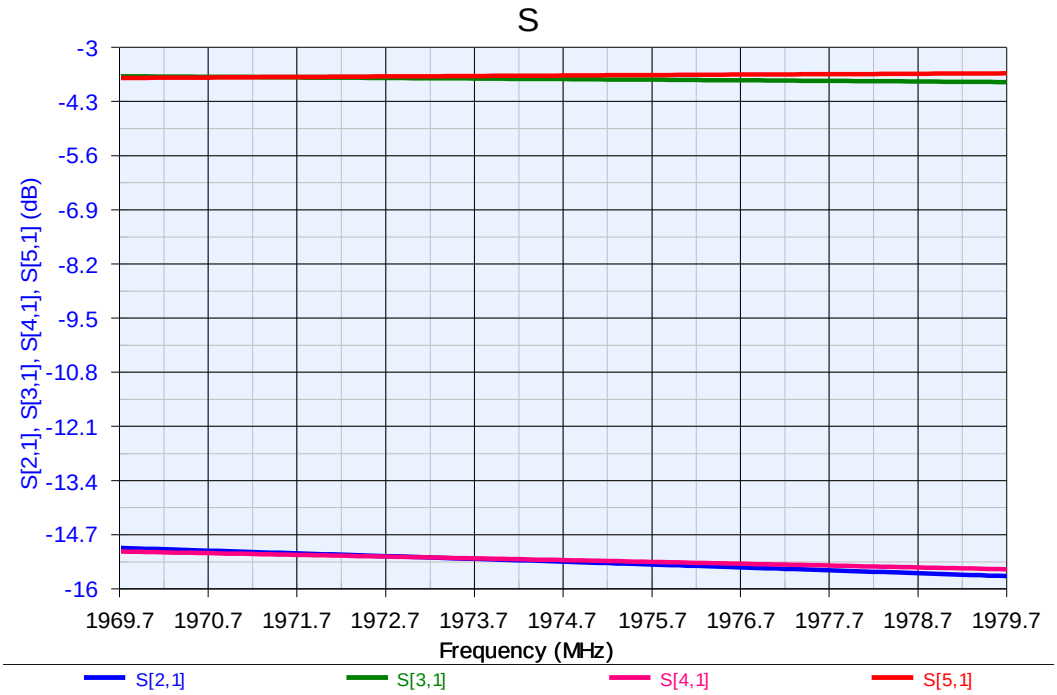

Fig .6.25: The output magnitudes in (dB) when a signal is input into port1 of the microstrip beam shaping network

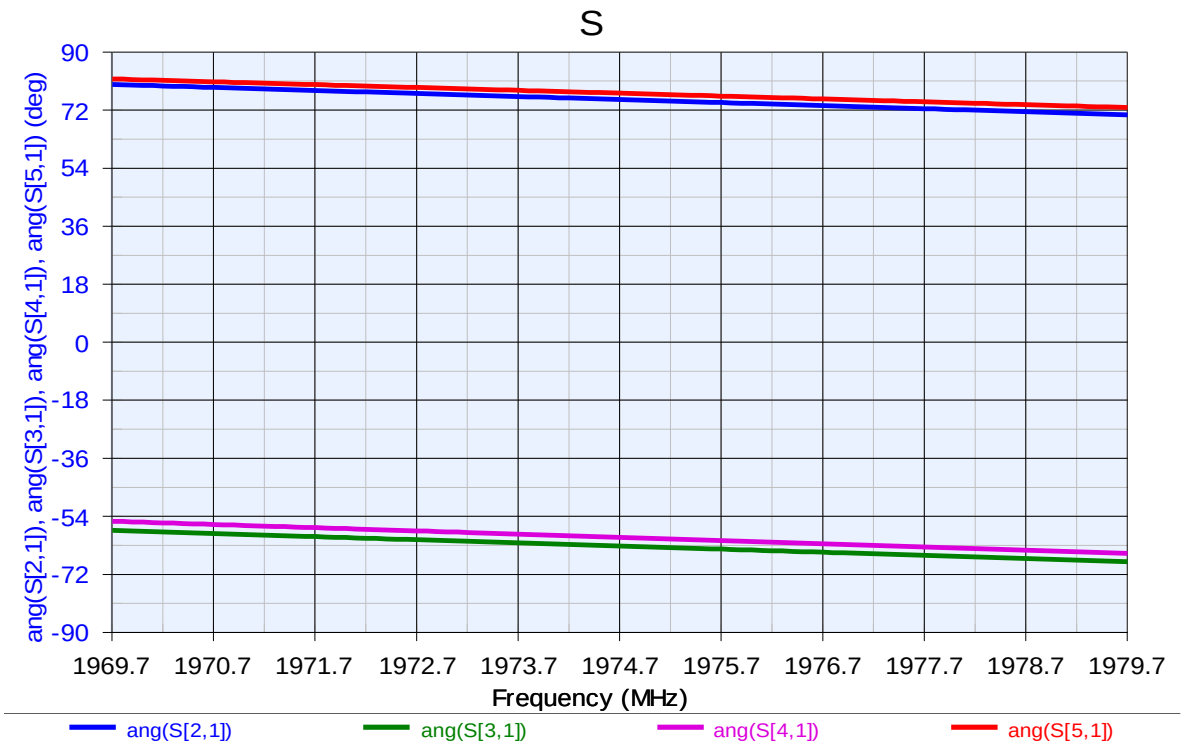

Fig .6.26 Phase progression graph when a signal is input into port1 of the microstrip beam shaping network

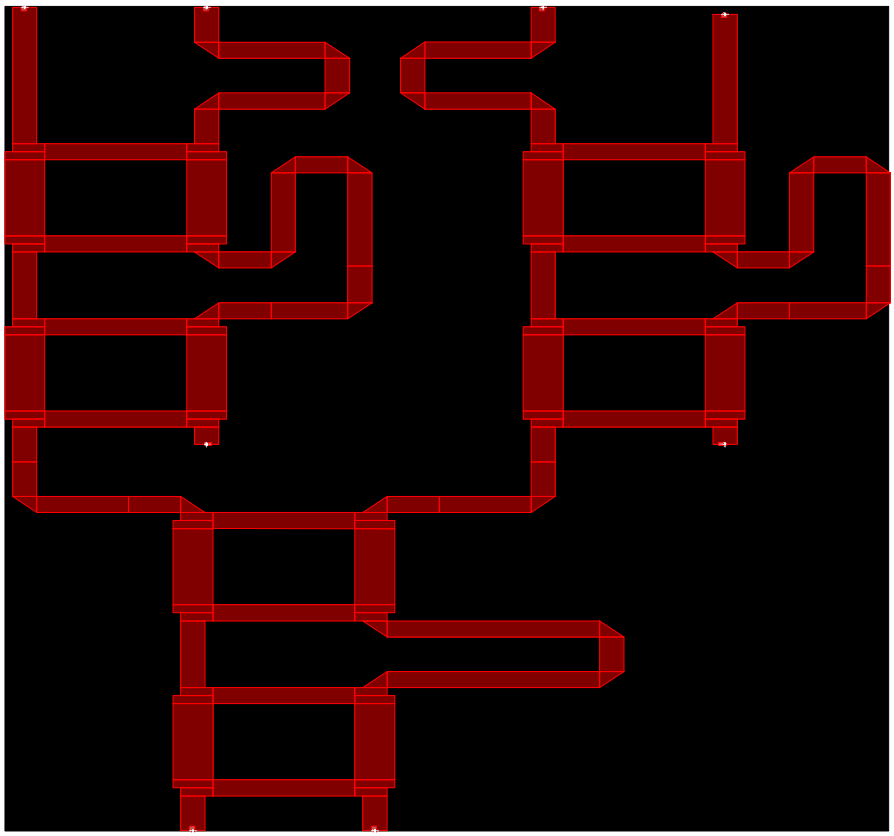

Fig.6.27 Microstrip beam shaping network layout

6.6 Feeder Network Configuration

The feeder network which is comprised of the beam shaping network plus the Butler matrix was modelled and simulated in Genesys using ideal and microstrip transmission line couplers. Fig.6.28 and Fig 6.29 shows the amplitude and phase distribution output of the feeder network implemented in microstrip lines when the variable phase shifters of the beam shaping network are set at $\Delta\emptyset_1=270^0$, $\Delta\emptyset_2=332^0$ $\Delta\emptyset_3=332^0$. The output results correspond to the synthesised results presented in chapter four. The non-uniform amplitude and phase distribution to produce the left shaped beam was almost invariant across the frequency band.

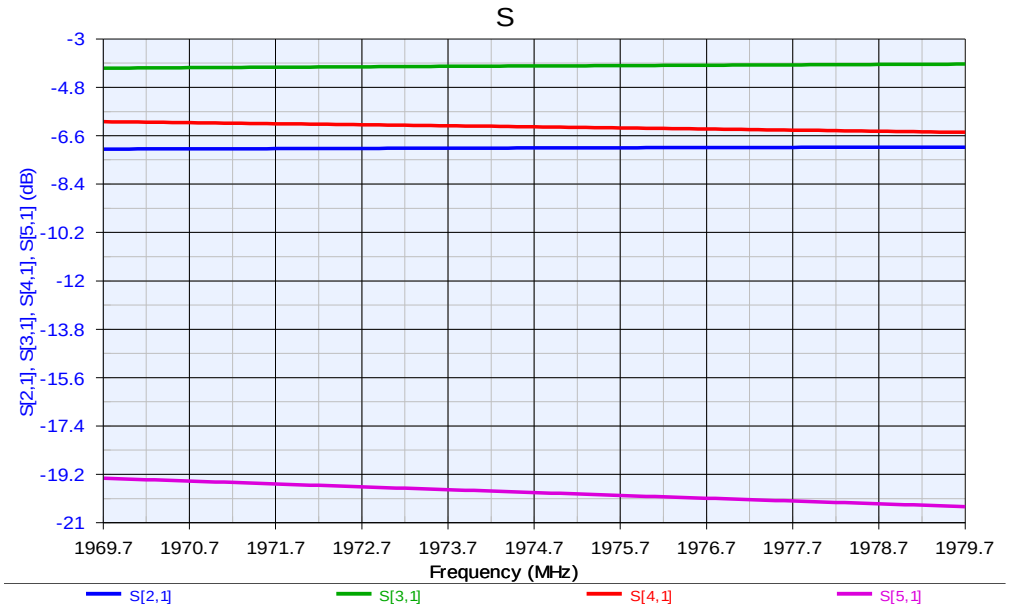

Fig. 6.28: The output magnitudes in (dB) for the left shaped beam

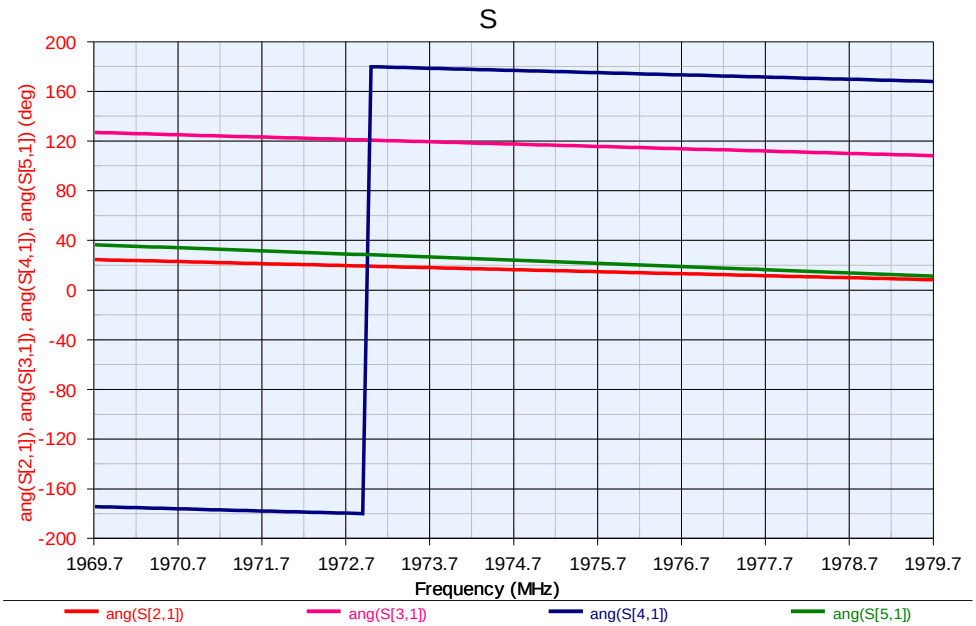

Fig. 6.29 Phase progression graph for the left shaped beam

6.7 Smart antenna System Simulation (ideal)

The results (complex weights) of the ideal feeder network modelled in Genesys was put into a four column array with inter-element spacing of 72.47mm (d) in CST electromagnetic simulation software program and simulated. Table 6.1 below shows the complex weights applied for each beam state and the conditions (phase shifter settings) at which each beam is formed.

Table 6.1: Complex Weights @ Array Element Columns @ f_C (Downlink & Uplink)

Beam State	**Complex weights: Values are for Downlink with corresponding values for Uplink in ()**								**Phase Shifter Settings**		
	W_1		W_2		W_3		W_4		$\Delta\phi_1$	$\Delta\phi_2$	$\Delta\phi_3$
	Amp (dB)	**Phase (deg)**	**Amp (dB)**	**Phase (deg)**	**Amp (dB)**	**Phase (deg)**	**Amp (dB)**	**Phase (deg)**	**Phase (deg)**	**Phase (deg)**	**Phase (deg)**
B1L only	-6.02 (-6.07)	135 (138.8)	-6.02 (-6.01)	90 (93.8)	-6.02 (-6.02)	45 (49.23)	-6.02 (-6.07)	0 (4.15)	-180	-180	Any
B2 R only	-6.02 (-6.09)	180 (-176.1)	-6.02 (-6.06)	-45 (-40.83)	-6.02 (-5.99)	90 (94.02)	-6.02 (-6.02)	-135 (-131.2)	-180	0	Any
B2L only	-6.02 (-6.07)	-135 (-130.8)	-6.02 (-6.02)	90 (94.18)	-6.02 (-6.0)	-45 (-41.18)	-6.02 (-6.07)	-180 (-176.2)	0	Any	-180
B1R only	-6.02 (-6.08)	-180 (-176)	-6.02 (-6.04)	-135 (-131.3)	-6.02 (-6.00)	-90 (-56)	-6.02 (-6.04)	-45 (-40.79)	0	Any	0
BCB	-9.03 (-9.099)	-135 (-130.7)	-4.26 (-4.292)	-9.7 (-5.64)	-4.26 (-4.26)	-9.7 (-5.64)	-9.03 (-9.01)	-135 (-130.7)	-270	-270	-270
RHSB	-18.36 (-18.43)	-104 (-98.53)	-5.77 (-5.83)	56.59 (60.44)	-3.14 (-3.16)	-3.9 (-0.025)	-6.29 (-6.26)	-104 (-100.1)	-270	-208	-208
LHSB	-6.28 (-6.35)	-165.9 (-162)	-3.14 (-3.16)	-65.98 (-62.07)	-5.77 (-5.76)	-5.44 (-1.35)	-18.36 (-18.32)	-165.9 (-163.4)	-270	-332	-332

6.7.1 Multiple Beam Radiation Patterns

The performance of the proposed smart antenna over the uplink and downlink bands was simulated (downlink f_L, f_C, f_H , = 2.1597GHz, 2.1647GHz, and 2.1697GHz and uplink f_L, f_C, f_H, = 1.9697GHz, 1.9747GHz and 1.9797GHz). Fig.6.30, 6.31 & 6.32, below presents the azimuth plots of the radiation patterns of the smart antenna system in the multiple beam modes (only uplink frequency band radiation patterns are presented in this report). It is seen that the beams are virtually invariant over each of the bands based upon the ideal network model and the narrow uplink and downlink bands. The four narrow beams formed by the antenna array agrees with theory that when a Butler matrix multiple beam-forming network is connected with a linear antenna array, the network will produce beams that overlap at about 3.9dB below the beam maxima. For this design, the beams overlap at -3.3dB and the beams are multiple simultaneous orthogonal beams. One important thing to

notice with these beams is that as the beams move away from zero degree azimuth, the sidelobs get higher and higher and the beamwidth gets broader and broader.

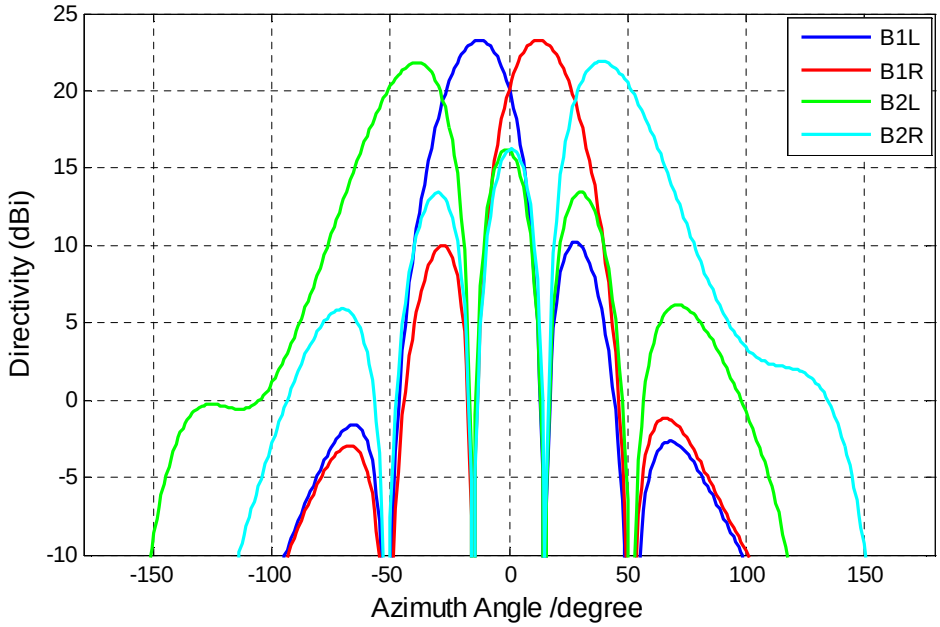

Fig.6.30: Uplink multiple beams @fL

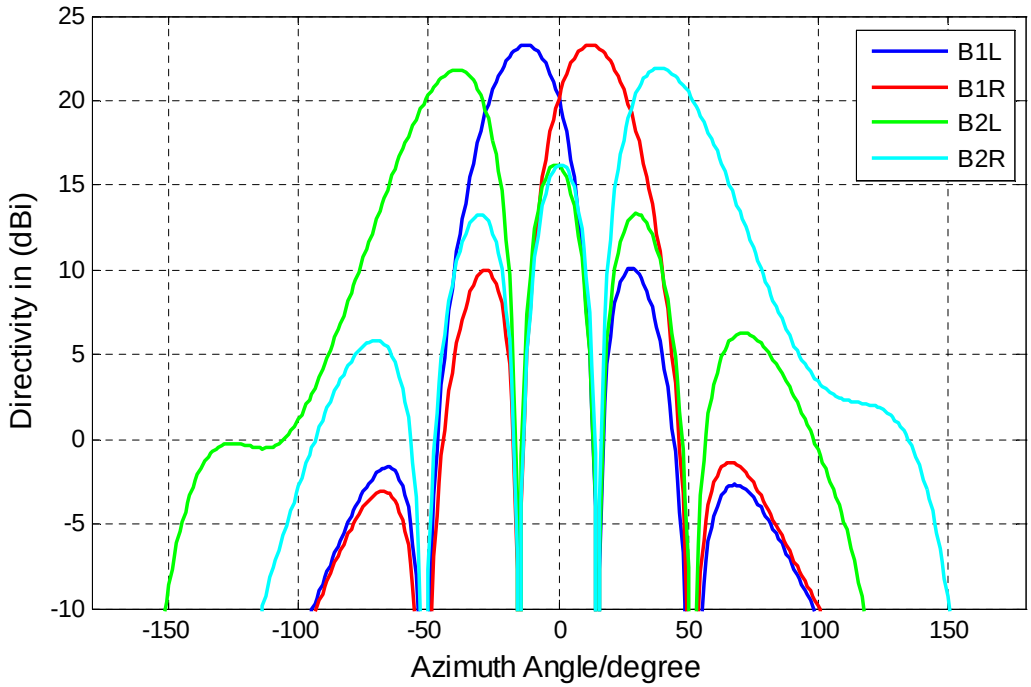

Fig.6.31: Uplink multiple beams @fc

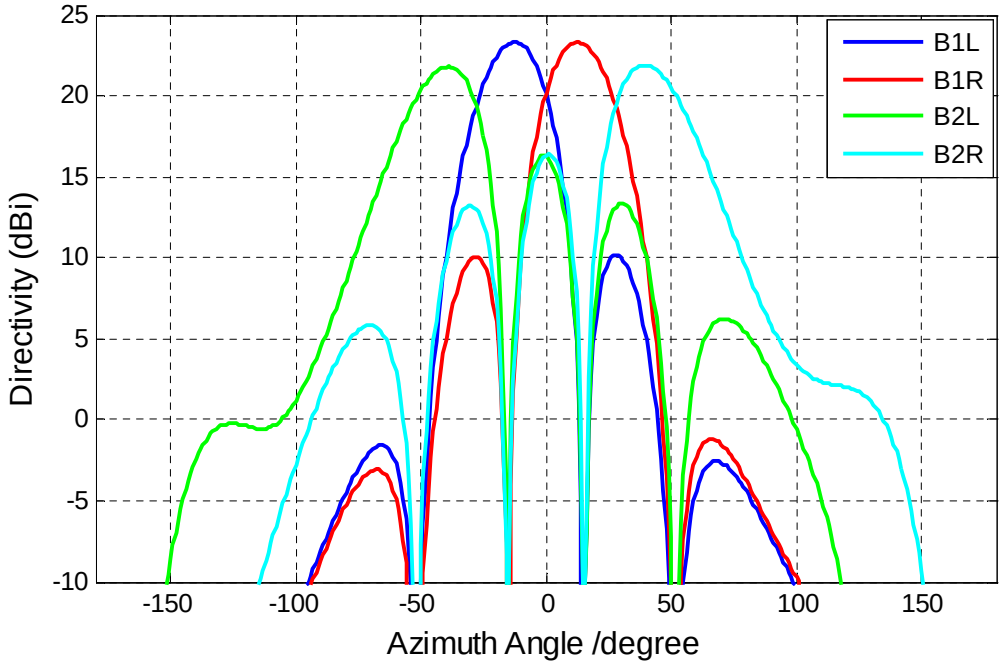

Fig.6.32: Uplink multiple beams @fH

6.7.2 Shaped Beams Radiation Patterns

Fig. 6.33, 6.34 & 6.35 present the right, left and broadcast channel shaped beams for the uplink frequency band of the chosen frequency band. The dynamic operating states used to form these beams were also displayed in Table 6.1. Again these beam shapes are virtually frequency invariant over their respective bands based upon the ideal network model and the narrow uplink and downlink bands.

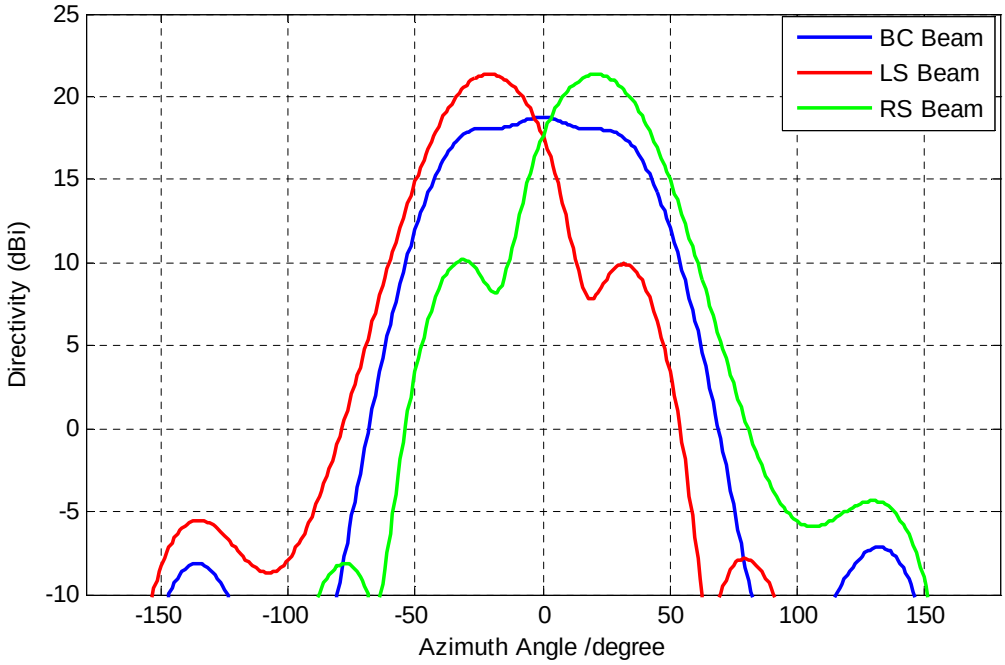

Fig.6.33: Uplink shaped beam @fL

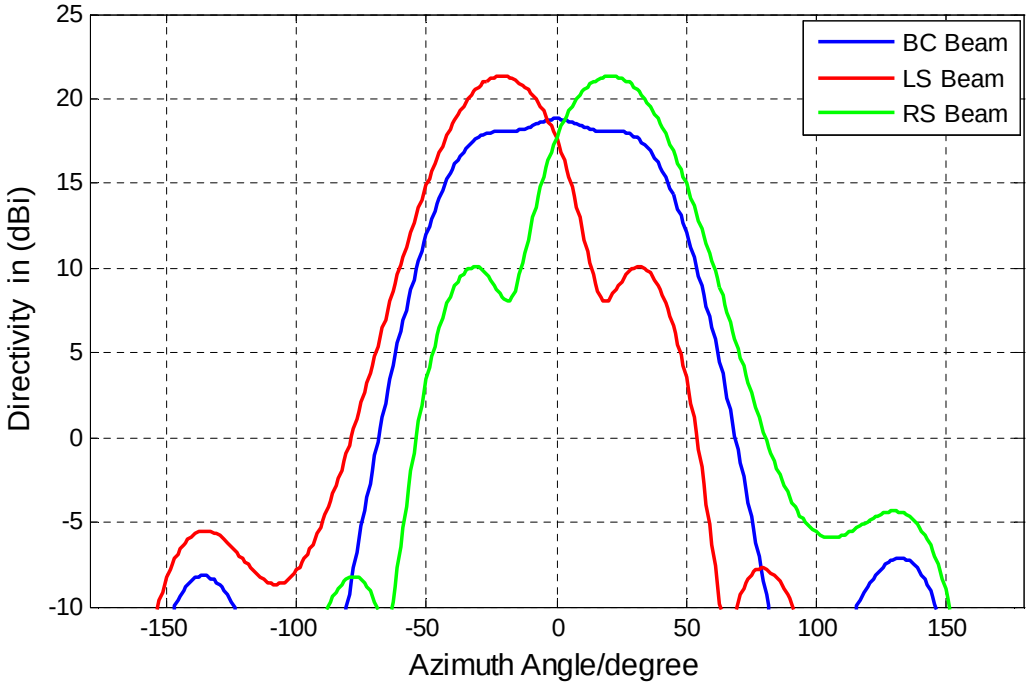

Fig.6.34: Uplink shaped beam @fc

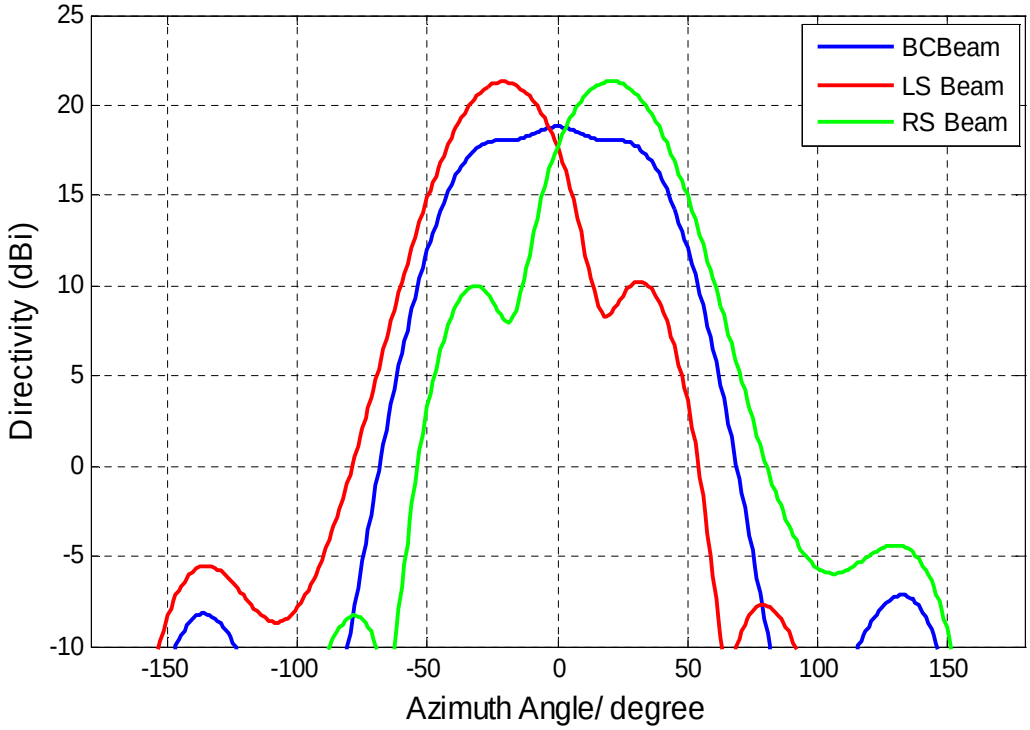

Fig.6.35: Uplink shaped beam @fH

6.8 Summary

The simulation data for the individual major components of the smart antenna system which include: array elements, branch line couplers, Butler matrix network and beam shaping network have been shown to be close to the theoretical values with relatively small errors in phase progressions (typically < 3degrees). The final layout of the Butler matrix and beam shaping network realised in microstrip was simulated with little difference to the ideal case. The small error in phase shift did not affect performance of the far-field beams noticeably. Hence, the simulated performance presented is very close to ideal.

If this design is integrated with a control system, it will provide a considerable increase in network capacity, range and reduce interference when compared to traditional omnidirectional antennas or sectorised antennas. The beams will be directed towards the desired user only and hence the user will have a signal with reduced interference. When a sub-sector of the cell sector is experiencing high traffic of mobile users the three phase shifters in the beam shaping network can be varied to blend the four narrow beams to shape the beams to the left or right part of the sector depending on the area that is experiencing high traffic. Since the four narrow beams are spatially orthogonal this allows reuse of codes (SDMA) and increases capacity (if additional transceivers are included). Note that this antenna, in the multiple beam mode does not have a uniform gain in all directions. As the beams scan (switch) from the zero degrees azimuth, the beam becomes broader with an increase in the size of the sidelobes. This shows that interference suppression will be less effective at wide azimuth angles.

Chapter 7 - MUTUAL COUPLING ANALYSIS AND COMPENSATION TECHNIQUES

7.1 Introduction

In chapter six, the simulation of a smart antenna for mobile applications, incorporating an array of slant $\pm 45^0$ dual-polarised stacked patch elements four columns wide excited by a multi-beam forming and beam shaping network, has been described. Four narrow overlapping beams, one wide "broadcast channel" beam and right and left shaped beams can be provided. The shaped beams are to provide high capacity coverage in a specific narrow angular sector, while low capacity coverage is maintained over the remainder of a 120^0 sector. Results (assuming the array elements are in isolation, that is no mutual coupling) are presented for this smart antenna using CST EM simulation software. However when these antenna elements are arranged in an array, it is possible that some radiation from each of the elements could couple to one another.

The existence of mutual coupling between array elements in an array antenna causes two performance degrading effects. These are radiation pattern distortion (relative to the radiation pattern that would exist without mutual coupling) and variation of the active reflection coefficients at each array element port. Furthermore, the radiation pattern performance is affected by the truncation of the finite ground plane. Accurate determination of this mutual coupling between the array elements is an important factor which needs to be considered when implementing smart antenna systems to fully realise the benefits of the smart antenna.

This chapter will present a brief description of the effects of mutual coupling on smart antenna systems and discuses the analysis of mutual coupling in array antenna. Compensating techniques, results achieved with compensated excitation weights and wide angle impedance matching technique will be presented. The final section of this chapter will describe an improved design technique (together with simulation results) that has been developed for compensating the performance degrading effects of mutual coupling and finite ground plane dimensions in microstrip antenna arrays.

7.2 Mutual Coupling and Smart Antenna Systems

Mutual coupling (MC) can alter the scan angle which in turn results in gain and pattern degradation [15-16, 128-129]. The majority of effort in current studies of MC on smart antennas has been directed towards adaptive smart antennas, direction of arrival estimation and beam forming algorithms [130-136]. It is clear that MC effects are more significant in adaptive smart antennas than in other types of smart antennas because of their ability to automatically place null to unknown interference and direct their signals to desired users [130, 133]. In [130] the authors show that mutual coupling distorts the adaptive matrices and the array pattern beam formed. The effects of mutual coupling on adaptive smart antennas were also investigated in [133]. Using an array of half wavelength dipole antennas it was concluded that mutual coupling between array elements of an adaptive smart antenna distorts the radiation pattern of the antenna. References [132, 134-136] reported on the use of an array of half wavelength dipoles to investigate the performance of an adaptive smart antenna in the presence of mutual coupling. In [135] it was shown that MC affects the antenna gain and does not affect the adaptive processing of the antenna. The effects of MC on a multiple switched beam smart antenna using a slant $\pm 45^0$ dual-polarisation stacked patch array excited with a beam shaping network have not been investigated to the best of my knowledge hence this investigation.

7.3 Analysis of Mutual Coupling in Array Antennas

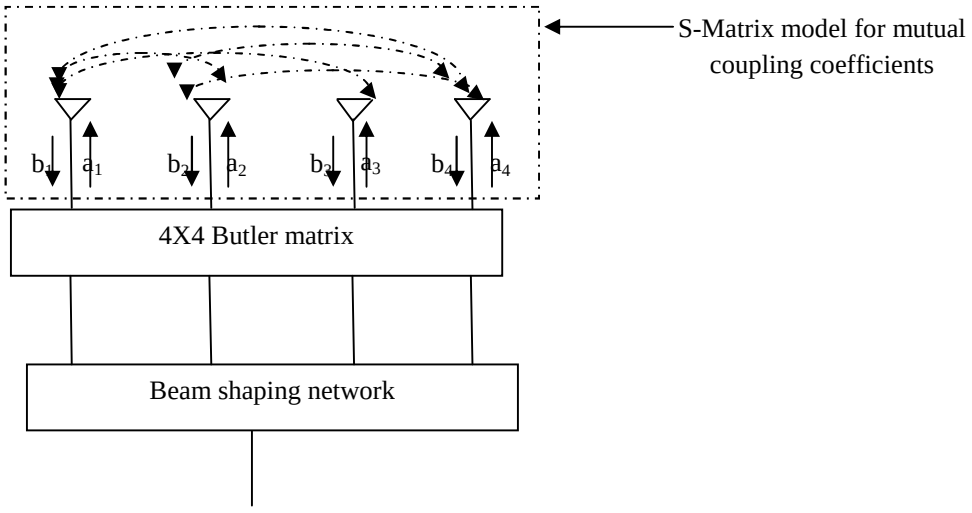

Fig.7.1: S-matrix model of mutual coupling with feed network

In multiple switched beam smart antenna systems the aperture of the antenna is increased by placing several antenna elements in an array. When these elements are arranged in an array and fed by a feeder network, as shown in Fig.7.1 above, the element excitation voltage [v_i] is define by [139]:

$$[v_i] = [a_i]+[b_i] \quad (7\text{-}1)$$

Where [a_i] is the complex incident voltage wave at array element *i* (these are the outputs of the array feed network) and [b_i] is the complex reflected voltage wave at array element *i*.

For the case of an ideal antenna with no mutual coupling

$$[v_i] = [a_i] \text{ when } [b_i] = 0 \quad (7\text{-}2)$$

However for a practical antenna where mutual coupling is present $[b_i] = [S_{ij}][a_i]$, where $[S_{ij}]$ are the S-parameters. S_{ij}, $i \neq j$ are the mutual coupling coefficients which will depend upon the specific radiating elements used and the array geometry. The effect of the mutual coupling on the antenna is pattern degradation, loss of gain and a shift in antenna scan angle.

The performance of the proposed smart antenna in the presence of mutual coupling was simulated using four array elements (to demonstrate concept, see Fig.7.2 for the CST four array geometry) modelled in an electromagnetic simulator over chosen uplink and downlink frequency bands, as shown in Fig.7.3 and Fig.7.4 below (only the uplink result is presented in this report). An examination of these results shows that the mutual coupling has little effect upon the shape or side lobe levels of the four individual narrow beams but leads to a substantial dip, ~5dB, in the shaped beam patterns and a poorly shaped central section of the broadcast beam. Additionally examination of the active reflection coefficients for the antenna elements, as given in table 7.1, indicates a high degree of impedance mismatch with return loss higher than -4dB. This will result in an unacceptable reduction in antenna gain and hence, compensation is desired. This chapter provides details of a number of different compensation techniques which have been examined.

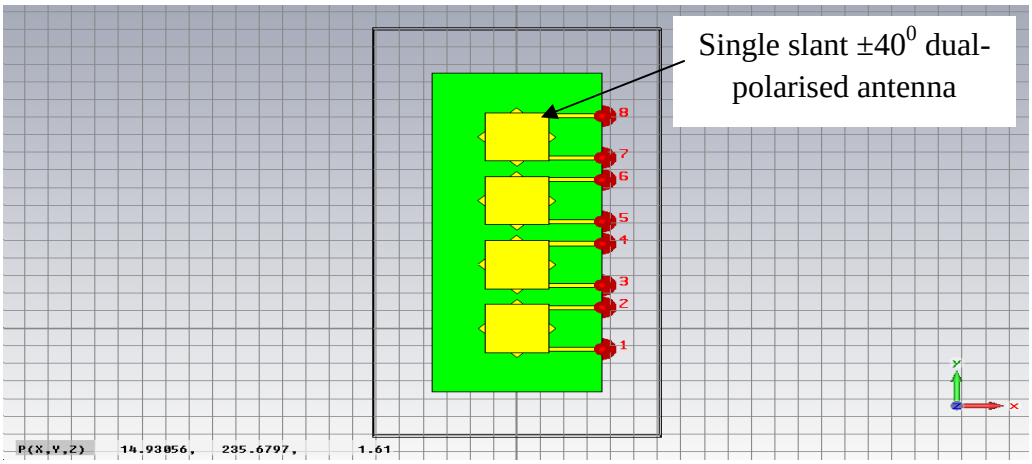

Fig.7.2: CST model of four array element

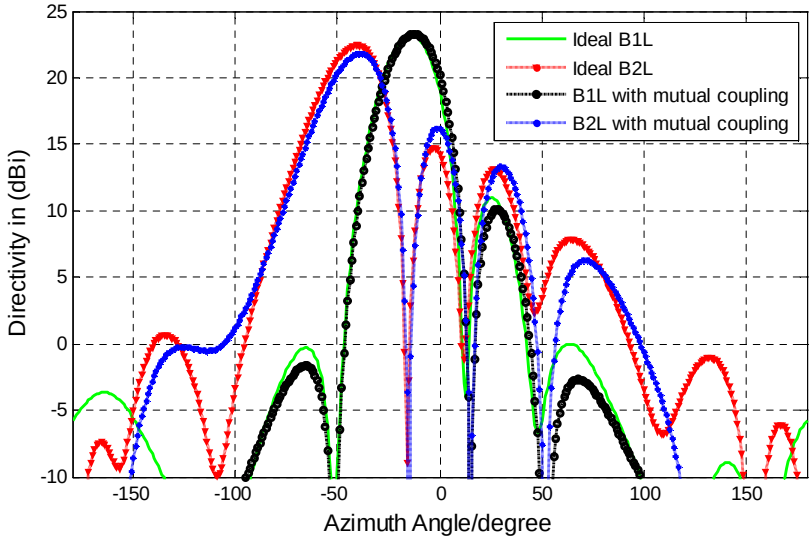

Fig. 7.3: Azimuth plots of multiple beams pattern with and without mutual coupling included

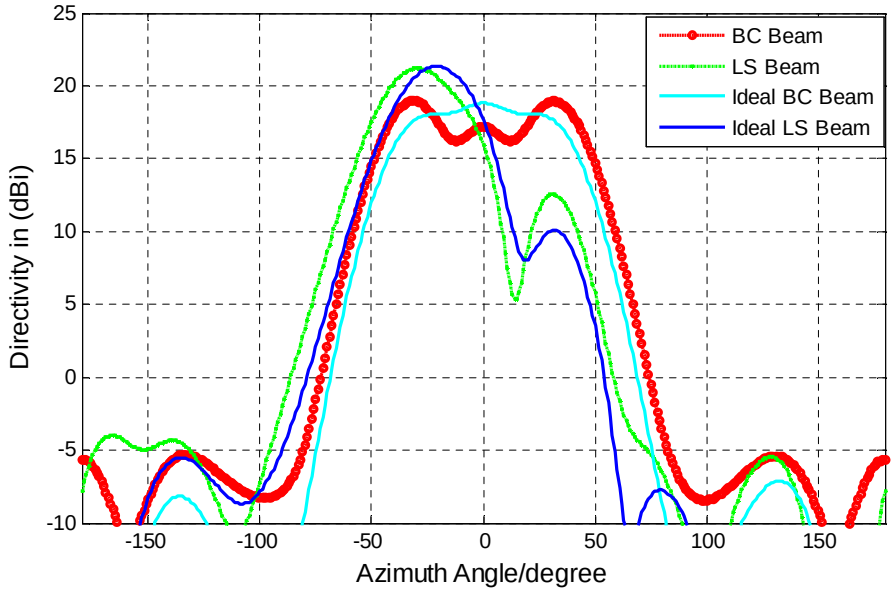

Fig.7.4: Azimuth plots of shaped beam patterns with and without mutual coupling included

Table 7.1: Element reflection coefficients with MC

Reflection coefficient with mutual coupling without compensation				
	S11dB	S22dB	S33dB	S44dB
B1L	-14.25	**-9.90**	-11.99	-16.76
B1R	-16.99	-12.01	**-9.95**	-14.20
B2L	**-7.61**	**-5.96**	**-7.96**	-11.37
B2R	-11.15	**-7.91**	**-6.04**	**-7.84**
BC-Beam	**-8.64**	-18.77	-18.66	**-8.85**
LS-Beam	**-7.73**	-29.04	-11.14	**-3.84**
RS-Beam	**-3.58**	-11.04	-29.35	**-7.95**

7.4 Compensation Techniques

A number of different techniques can be used to mitigate or compensate mutual coupling effects in smart antenna arrays. One technique is to place dummy columns between the array elements to prevent coupling between elements. This is at the expense of increased size and is not acceptable for smart antennas in base stations. Also, this would increase the spacing between elements causing grating lobes. A second technique is the use of decoupling networks [138] placed between the feed network and array elements. The technique can give some improvement in the array characteristics, but it would greatly increase the complexity of the network. Furthermore, unless the decoupling networks are adjustable, then mutual coupling can only be cancelled for a specific scan angle condition. It has been reported in [139] that the best way to compensate in a shaped beam antenna is by modifying the excitation input from the beam forming network. This is discussed below in the scattering matrix compensation technique. Additionally, for wide angle scanning, one of the easiest methods is to use a high dielectric thin sheet in front of the array elements called wide angle impedance matching (WAIM) sheet [140-141]. The following sections investigate the use of these techniques. The sections will examine how the use of each technique in isolation affects both the antenna beam shapes and the input impedance match. The limitations of each technique will be described, together with a proposed solution which is a combination of both techniques to produce final design with desired beam shapes and a good impedance match.

7.4.1 Compensation of Complex Weights Based Upon the Scattering Matrix

It has been established in section 7.3 that for a practical antenna the complex incident voltage wave at array element 'i' is given by [139]:

$$[v_i] = [a_i] + [b_i], \text{ i = 1,2,3,4}$$

But what is desired is $[v_i] = [a_i]$ because $[a_i]$ gives the desired shaped beams, hence we need to change$[a_i]$ to $[a_i']$ where $[a_i']$is the compensated excitation.

$$[a_i] = [a_i'] + [b_i]$$

$$[b_i] = [s][a_i]$$

$$[a_i] = [a_i'] + [s][a_i']$$

$$[a_i] = [u][a_i'] + [s][a_i']$$

where

$$[u] = \begin{bmatrix} 1 & 0 & 0 & 0 \\ 0 & 1 & 0 & 0 \\ 0 & 0 & 1 & 0 \\ 0 & 0 & 0 & 1 \end{bmatrix}$$

$$[a_i] = [a_i']\big[[u] + [s]\big]$$

Therefore

$$[a_i'] = \big[[u] + [s]\big]^{-1}[a_i] \text{ [138]} \qquad (7\text{-}3)$$

Where $[a_i']$ are the compensated excitation weights, 'u' is the unit matrix, 's' are the S-parameters (mutual coupling coefficients) which depends upon the specific radiating elements used and the array geometry and $[a_i]$ is the excitation that would have been required if there was no mutual coupling. The s-matrix can be determined from CST by inputting known $[a_i]$ in the array antenna and then determining$[a_i']$. Applying the technique directly does not compensate for pattern distortion caused by the scattering between array elements however, modification of the excitation weights gives a closer pattern to the ideal one. The complex weights are provided by the array feed network. The excitation weight without mutual coupling and modified compensated excitation weights for the broadcast beam and the shaped beams are shown in table7. 2.

Table7. 2: Excitation weight without mutual coupling and compensated excitation weights for shaped beams

Beams	excitation weights without mutual coupling		Modified excitation weights	
	Mag.(dB)	Phase (dg)	Mag.(dB)	Phase (dg)
BC Beam	-9.10	-131	-9.0	-132
	-4.29	-5.64	-3.0	-20
	-4.29	-5.64	-3.0	-20
	-9.010	-131	-9.0	-132
Left shaped Beam	-6.35	-162	-5.0	-160
	-3.16	-62	0.0	-62
	-5.76	-1.35	-4.0	-8
	-18.32	-163.4	-18.0	-160
Right shaped Beam	-18.43	-98.53	-18.0	-78
	-5.83	60.44	-4.0	52
	-3.16	0.025	0.0	0.78
	-6.26	-100.1	-5.0	-88

Fig.7.5 presents the simulation result for the multiple narrow beams (only beams B1L and B2L are presented in this report. B1R and B2R are flipping over of beams B1L and B2L) Fig.7.6 below shows the simulation results for shaped beam patterns using the modified complex excitation weights given in table 7.2. The use of compensated excitation weights has resulted in improved beam patterns for both shaped beams and the broadcast beam but an examination of the antenna active element reflection coefficients, as shown in table7.3, still indicates a high degree of impedance mismatch with corresponding loss of gain, hence additional techniques are required to compensate for the poor reflection coefficient of the antenna. One method of additional compensation is the use of wide angle impedance matching.

Table 7.3: Active reflection coefficients after excitation compensation

Reflection coefficient of weight modified compensation				
	S11dB	S22dB	S33dB	S44dB
B1L	-12.58	-10.96	-13.02	-14.97
B1R	-15.14	-13.89	-11.65	-12.05
B2L	-6.544	-7.37	-9.63	-10.47
B2R	-10.28	-9.61	-7.46	-6.75
BC-Beam	-7.69	-17.06	-16.99	-7.87
LS-Beam	-5.36	-35.15	-9.52	-3.70
RS-Beam	-3.36	-9.47	-40.82	-5.68

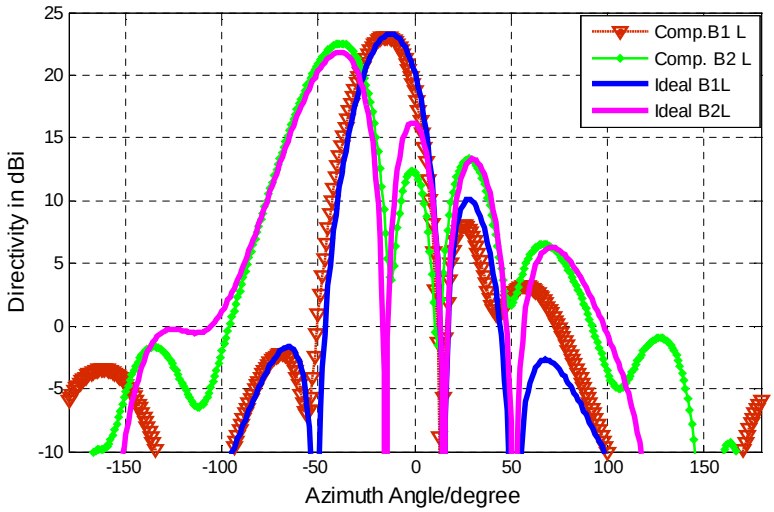

Fig.7.5: Azimuth plots of multiple beams pattern using compensated complex weights based upon the scattering matrix

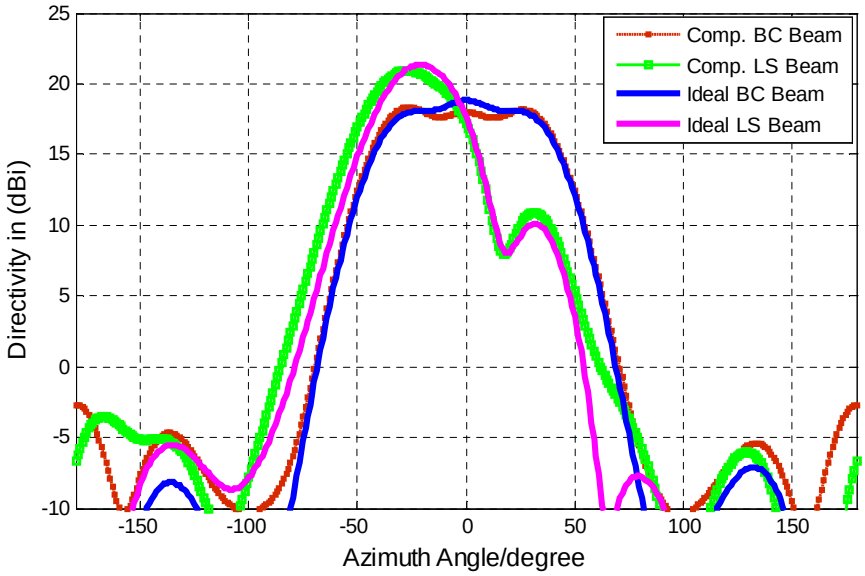

Fig. 7.6: Azimuth patterns of shaped beam patterns using compensated complex weights based upon the scattering matrix

7.4.2 WAIM Sheet Technique

In the Wide Angle Impedance Matching technique use is made of a thin sheet of high dielectric constant material placed just above the radiating elements as shown in Fig.7.7 [140,141] Magill and Wheeler describe how the reflection due to the antenna aperture in an array can be cancelled over wide angles by the introduction of an additional susceptance provided by the dielectric sheet located at an appropriate distance from the antenna aperture. This is possible because the sheet susceptance varies differently in the E and H planes [140,141]. The reflection of the antenna element at the aperture plane can be determined by measurement or in our case by simulation. This can be translated to provide the reflection coefficients in the E and H planes at the position of the thin dielectric sheet. These can be cancelled by the addition of the reflection provided by the dielectric sheet resulting in a decrease in the overall reflection and an improved match. For the case of Magill and Wheeler which used a circular waveguide element in a triangular array the optimal distance of the sheet was 0.11λ above the antenna array. For the geometry used in this work the optimum distance has been determined as 0.125λ where 'λ' is the mean wavelength between up and downlink wavelengths. The thin sheet is as large as the array, placed in front, parallel to the array face. The sheet wave-reflection properties depend on polarization and scan angle [140].

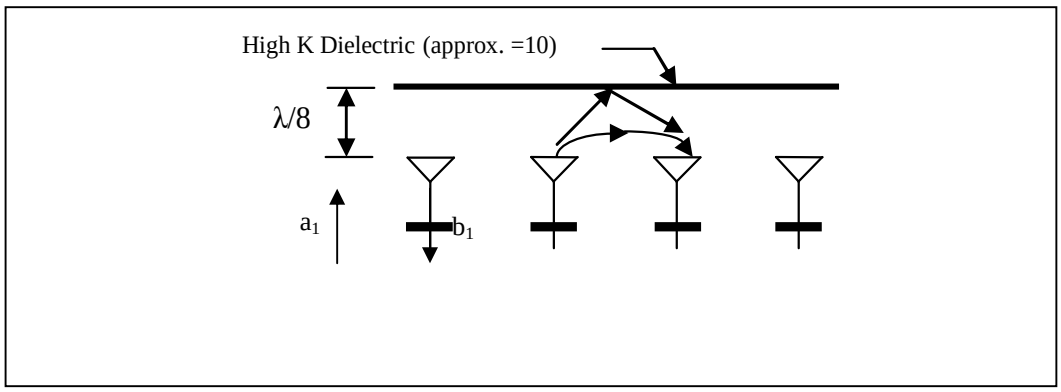

Fig.7.7: Wide angle impedance matching (WAIM) structure geometry

A brief outline of how the techniques work is as follows.

Total power into the array is defined as [110, 142]:

$$P_{in} = \sum_{n=1}^{N} |a_n|^2 \tag{7-4}$$

The total reflected power is defined as [110,142]:

$$P_{rflected} = \sum_{n=1}^{N} |b_n|^2 \tag{7-5}$$

The active reflection coefficient Γ_{active} is given by:

$\Gamma_{n\text{-active}} = b_n/a_n$ where n = 1, 2.....4 (7-6)

where,

$$\begin{bmatrix} b_1 \\ b_2 \\ \vdots \\ b_N \end{bmatrix} = \begin{bmatrix} S_{11} & S_{21} & S_{31} & \dots & S_{N1} \\ S_{21} & S_{22} & 0 & 0 & \vdots \\ S_{31} & 0 & \ddots & 0 & \vdots \\ \vdots & 0 & 0 & \ddots & \vdots \\ S_{N1} & \dots & \dots & \dots & S_{NN} \end{bmatrix} \begin{bmatrix} a_1 \\ a_2 \\ \vdots \\ a_N \end{bmatrix}$$

$$b_1 = S_{11}a_1 + S_{21}a_2 + S_{31}a_3 + \cdots + S_{NN}a_N \tag{7-7}$$

$\Gamma_{1\text{-active}} = b_1/a_1 = S_{11} + S_{21}\, a_2/\, a_1 + S_{31}\, a_3/\, a_1 + S_{41}\, a_4/\, a_1$ (7-8)

The WAIM sheet attempts to cancel the second, third and fourth term in equation (7-8) thereby reducing the effects of mutual coupling. Full EM simulations have been carried out, using CST, for the case of a WAIM sheet with dielectric constant ε_r = 10, thickness, t = 1.5 mm, located at a height, h = 18.12 mm, above the antenna.

Results shown in table7.4, Fig.7.8 and Fig.7.9 indicate, as expected, an improvement in the impedance matching but at the expense of a degradation of beam patterns, in particular this has resulted in a pronounced reduction dip in the central section of the control beam and the return of a pronounced local minimum for the shaped beams.

Table7. 4: Active reflection coefficients with WAIM sheet

Reflection coefficient with WAIM sheet				
	S11dB	S22dB	S33dB	S44dB
B1L	-12.25	**-7.66**	**-9.00**	-10.95
B1R	-11.12	**-8.94**	**-7.72**	-11.98
B2L	-13.79	-15.58	-14.46	-10.72
B2R	-10.62	-14.33	-15.82	-14.13
BC-Beam	-15.9	-10.98	-10.95	-15.33
LS-Beam	-11.26	-15.43	-8.69	-11.47
RS-Beam	-10.78	**-8.65**	-15.39	-11.23

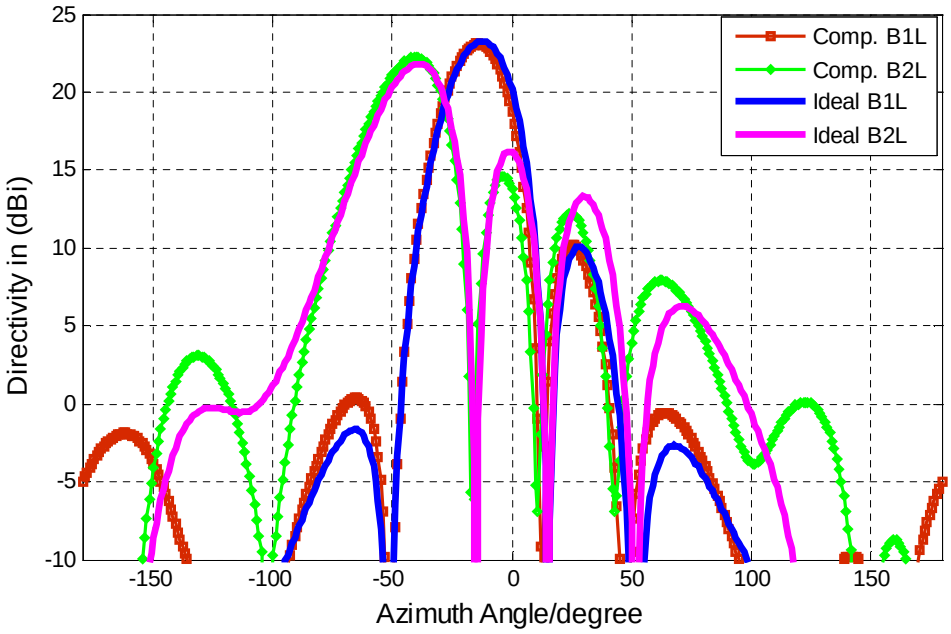

Fig. 7.8: Azimuth plots of multiple beams pattern compensated with WAIM

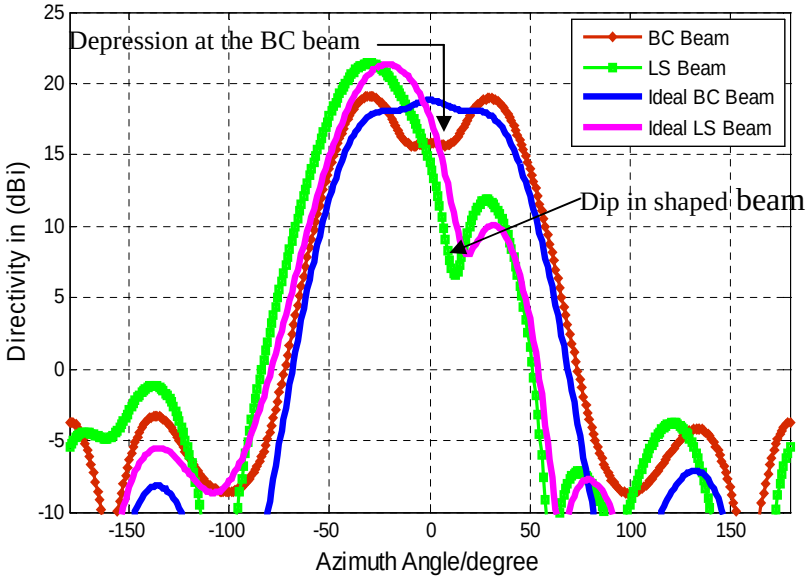

Fig.7.9: Azimuth plots of shaped beam patterns compensated with WAIM

7.4.3 Combined Technique

Section 7.4.1 has demonstrated that mutual coupling effects in multiple switched beam smart antennas with beam shaping capability can be compensated for by using modified complex excitation weights to excite the array elements. The resultant beam patterns are close to the ideal case, however this results in unacceptable impedance mismatch at the antenna input ports leading to significant reduction in antenna gain. Section 7.4.2 has shown that by incorporating a Wide Angle Impedance Matching Technique (WAIM sheet) the impedance matching can be improved but at the expense of degrading antenna beam patterns. By appropriately combining both techniques it has been shown that it is possible to achieve good beam shape close to the ideal and good impedance matching resulting in improved antenna efficiency. This has been achieved by adding complex excitation weights, compensation by inversion of the array mutual coupling scattering matrix and the incorporation of a WAIM (wide angle impedance matching) sheet. When these are implemented, an iterative optimisation of performance is required as each affects the compensating effects of the other. CST simulation results for antenna beam patterns using the combined techniques are given in Fig.7.10 and Fig.7.11. This approach produces a significantly improved pattern for the broadcast beam together with improved shaped beams, closely matching the patterns for the ideal case. Table7.5 indicates that this arrangement also results in active reflection coefficient values for all beam excitations of less than 10 dB.

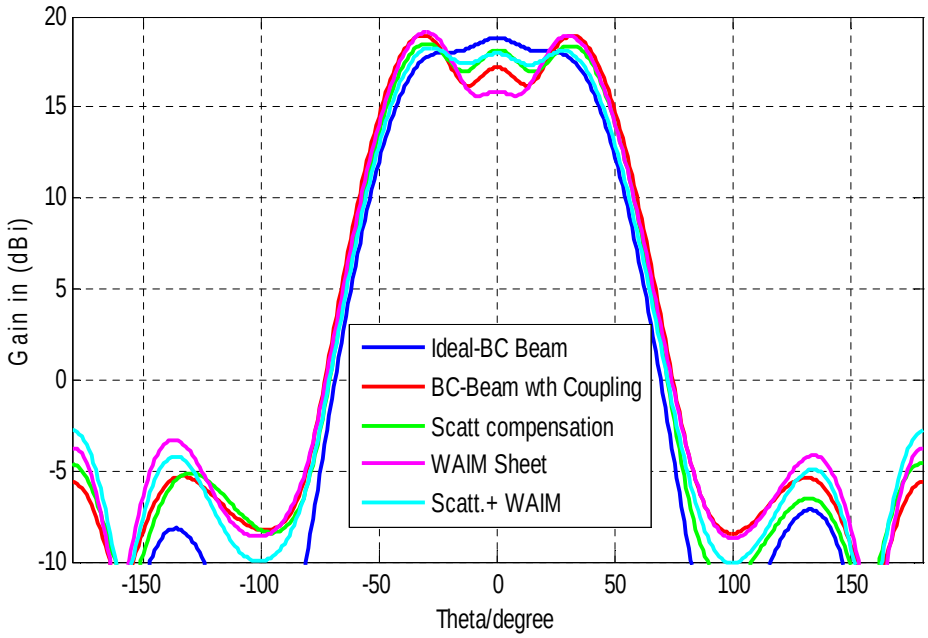

Fig.7.10: Azimuth plot of broadcast beam patterns compensated weight. +WAIM sheet

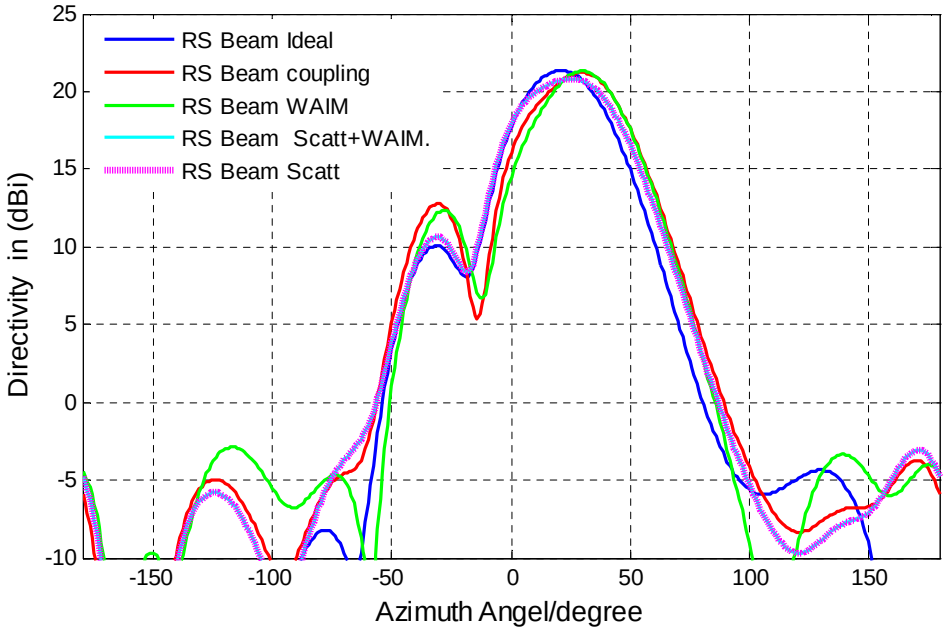

Fig.7.11: Azimuth plot of RS beam patterns compensated weight. +WAIM sheet

Table 7.5: Active reflection coefficient after compensation and WAIM sheet

Reflection coefficient of modified weight compensation + WAIM				
	S11dB	S22dB	S33dB	S44dB
B1L	-12.25	-10.02	-11.22	-11.23
B1R	-11.23	-11.22	-10.02	-12.25
B2L	-11.67	-11.11	-11.35	-10.47
B2R	-10.48	-11.35	-11.11	-11.67
BC-Beam	-13.37	-12.34	-12.32	-13.30
LS-Beam	-13.819	-17.43	-10.43	-10.27
RS-Beam	-10.27	-10.43	-17.43	-13.819

7.5 Summary

An investigation has been carried out into a four element array smart antenna suitable for mobile base station use. Full electromagnetic simulation has shown that the performance of a practical antenna departs significantly from the ideal case due to mutual coupling. The use of compensated excitation coefficients has been shown to restore acceptable beam patterns but introduces significant impedance mismatch at the input ports of the antenna elements. The inclusion of a high dielectric constant WAIM sheet has been shown to improve the impedance match but degrades the beam patterns. By using a suitable combination of both techniques it has been shown that it is possible to achieve good beam patterns and good impedance matching resulting in improved antenna efficiency. Note that all simulation results presented were for the uplink band. Very similar results have also

been obtained for the downlink band. Table7.6 presents detailed comparison of the smart antenna reflection coefficients using the two different techniques.

Table 7.6: Reflection coefficient of weight modification and weight modification + WAIM technique

Reflection coefficient of weight modified compensation				
	S11dB	S22dB	S33dB	S44dB
B1L	-12.58	-10.96	-13.02	-14.97
B1R	-15.14	-13.89	-11.65	-12.05
B2L	**-6.54**	**-7.37**	-9.63	-10.47
B2R	-10.28	**-9.61**	**-7.46**	**-6.75**
BC-Beam	**-7.69**	-17.06	-16.99	**-7.87**
LS-Beam	**-5.36**	-35.15	**-9.52**	**-3.70**
RS-Beam	**-3.36**	**-9.47**	-40.82	**-5.68**
Reflection coefficient of modified weight compensation + WAIM				
	S11dB	S22dB	S33dB	S44dB
B1L	-12.25	-10.02	-11.22	-11.23
B1R	-11.23	-11.22	-10.02	-12.25
B2L	-11.67	-11.11	-11.35	-10.47
B2R	-10.48	-11.35	-11.11	-11.67
BC-Beam	-13.37	-12.34	-12.32	-13.30
LS-Beam	-13.82	-17.43	-10.43	-10.27
RS-Beam	-10.27	-10.43	-17.43	-13.82

Chapter 8 - EXPERIMENTAL VERIFICATION

8.1 Introduction

The design of a multiple switched beam smart antenna with dynamic beam shaping to operate at an uplink frequency of 1.9697GHz to 1.9797GHz and a downlink frequency of 2.1597 to 2.1697GHz has been discussed in chapter five. The simulation of all the smart antenna system major components which consist of an array of four slant $\pm 45^0$ dual-polarised stacked patch elements, a Butler matrix beam forming network and a beam shaping network with variable phase shifters, have been presented in chapter six. Depending on the state of the phase shifters in the beam shaping network, which provide phase and amplitude control of the array element weights, seven different shaped beams can be formed. The effects of mutual coupling on the smart antenna system and a novel technique to compensate for mutual coupling have also been discussed in chapter seven.

In this chapter, an experimental demonstration of a multiple switched beam smart antenna with dynamic beam shaping to operate at an uplink frequency of 1.9697GHz to 1.9797GHz will be discussed. The actual complete smart antenna would incorporate vertical array columns of ten elements high, but as a feasibility demonstration, only single elements have been used for each column. As such, all azimuth radiation patterns measured are representative of the complete smart antenna system. All measured results of the smart antenna system major components which include: array element, array antenna, Butler matrix beam forming network and the novel beam shaping network, will be presented in this chapter.

8.2 Slant $\pm 45^0$ Dual-Polarised Stacked Microstrip Patch Antenna Measurement

The main slant $\pm 45^0$ dual-polarised stacked patch antenna characteristic measured is its return loss (S_{11}& S_{22}) at each port and coupling (S_{12}) between the two ports. Fig.8.1 shows the experimental setup to measure the return loss (S_{11}& S_{22}) and coupling (S_{12}) between the two ports of the dual-polarised stacked patch antenna. The performance of the single element will determine the performance of the array of four elements. The instrument used to measure the S-parameters of this antenna is a network analyzer which has two measurement ports and a frequency range of 10MHz to 40GHz. The network analyzer (N5230A PNA-L Agilent technology) was calibrated using an electronic cal-kit. This calibration removed the effects of the connecting cables from subsequent measurements. A single antenna element was attached to the network analyzer as shown in Fig.8.1 with

port1 of the analyzer connected to one input and port2 connected to the second input. Fig.8.2 presents the measured and simulated return loss ($-S_{11}$ & $-S_{22}$) of the single dual-polarised stacked patch antenna. The dual-polarised antenna has a return loss of about -18dB at the desired frequencies. The isolation (S_{12}) between the two ports of the antenna was also measured using the same setup. The measured and simulated isolation between the two ports of the dual-polarised patch is shown in Fig.8.3. At the desired frequencies the measured coupling between the two ports of the antenna is 28dB at the uplink frequency band and 21dB at the downlink frequency band.

Fig.8.1: Experiment to determine return loss and isolation of single element

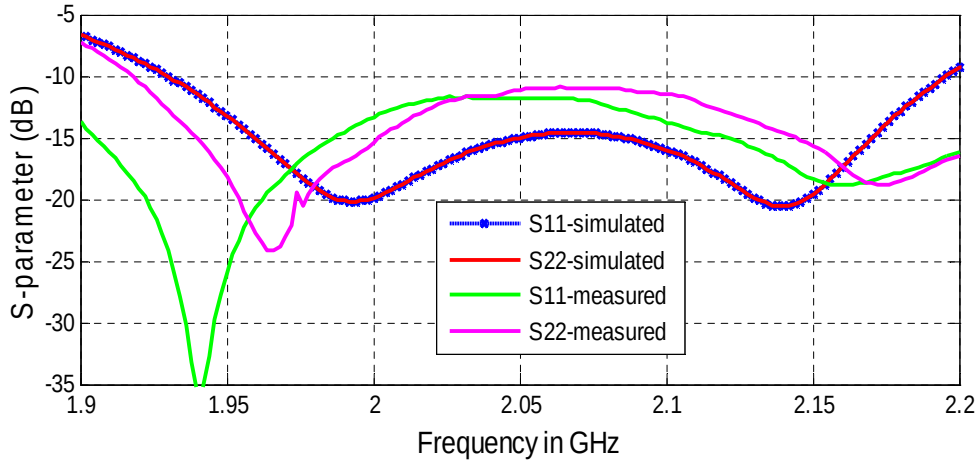

Fig.8.2: Measured and simulated return loss of single element

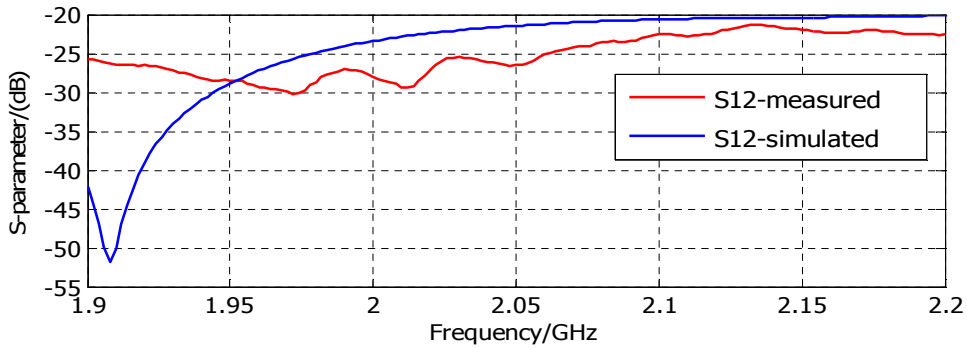

Fig.8.3: Measured and simulated isolation (S_{12}) between two ports of single element

8.3 Array of 4 Slant ±45^0 Dual-Polarised Stacked Patch Antenna Measurement

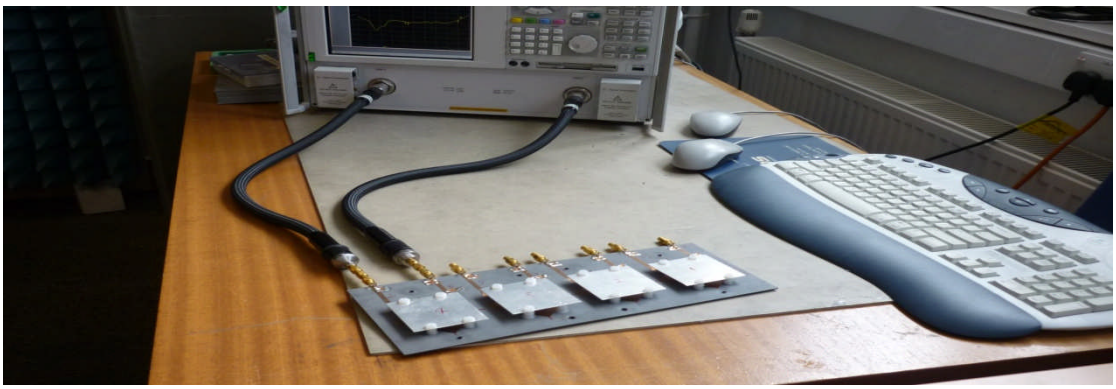

Fig.8.4: Experiment to determine return loss and isolation of 4 array antenna

The single dual-polarised antenna element measured in section 8.2 was then configured and implemented into a four element array. Measurement was then performed on the four element array as shown in Fig.8.4. Measurements were performed on each of the four elements in turn. For all measurements all other antenna ports were terminated in matched loads. Fig.8.5 shows the input reflection coefficient (i.e. S_{11}, S_{22}, S_{33} and S_{44}) for each element without WAIM sheet and Fig.8.6 shows the input reflection coefficient with WAIM sheet $\lambda/8$ above the four element array antenna. Fig.8.7 presents the isolation between ports (S_{12}, S_{23} and S_{34}) of the array antenna +45^0 polarisation without WAIM sheet above the top of the array antenna and Fig.8.8 shows the isolation between ports with WAIM sheet. A similar result was also achieved for -45^0 polarisation ports. The antenna array has a return loss of 18dB at the desired frequencies (1.9697GHz to 1.9797GHz at the uplink frequency band and 2.1597GHz to 2.1697GHz at the downlink frequency band). Fig.8.8 shows the isolation of the antenna array with general level is below -15dB. While this is not acceptable for a commercial product, -30dB required, this level of isolation is sufficient for proof of concept of the antenna. The effect of connecting cables from subsequent measurements affects the measured isolation between the four element array ports with WAIM sheet.

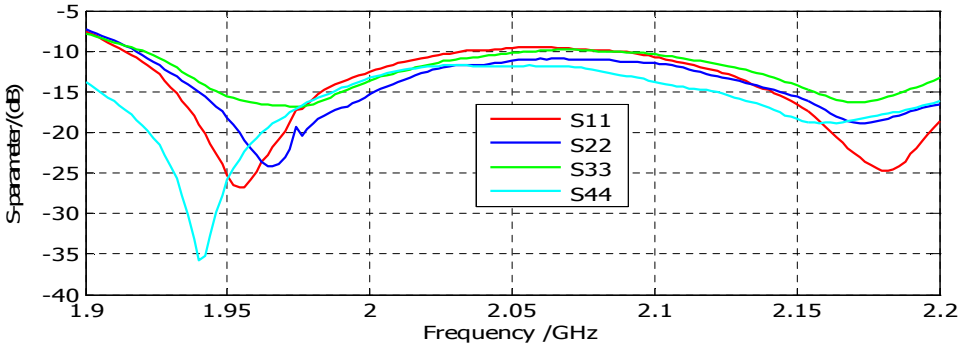

Fig.8.5: Measured return loss of 4 array elements without WAIM sheet

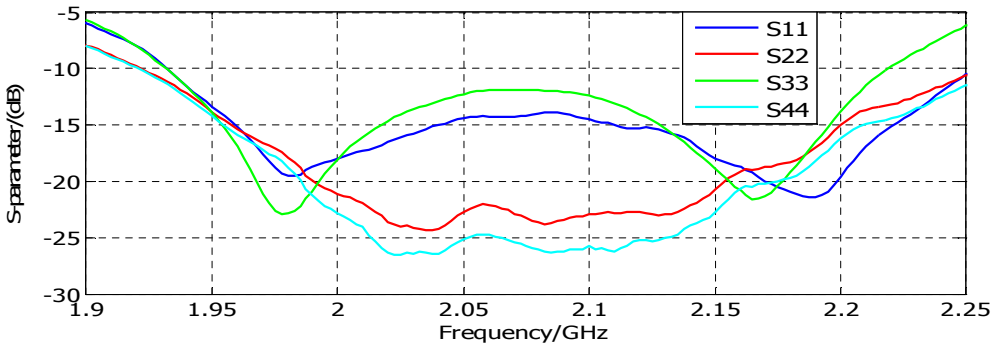

Fig.8.6: Measured return loss of 4 elements array with WAIM sheet

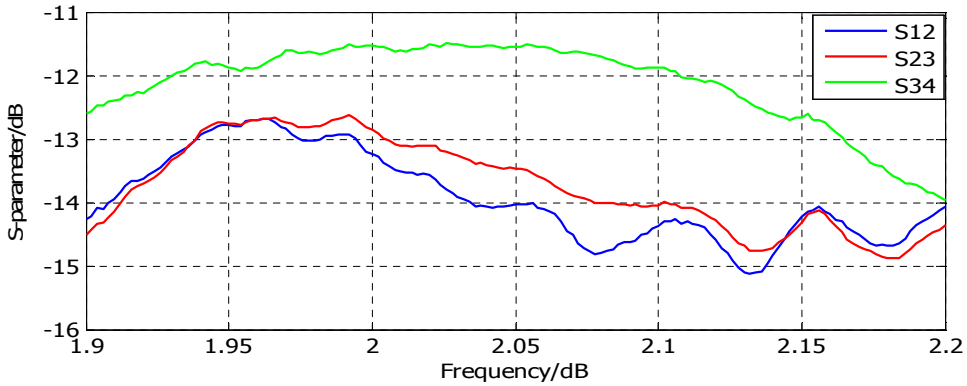

Fig.8.7: Measured isolation between 4 elements array ports without WAIM sheet

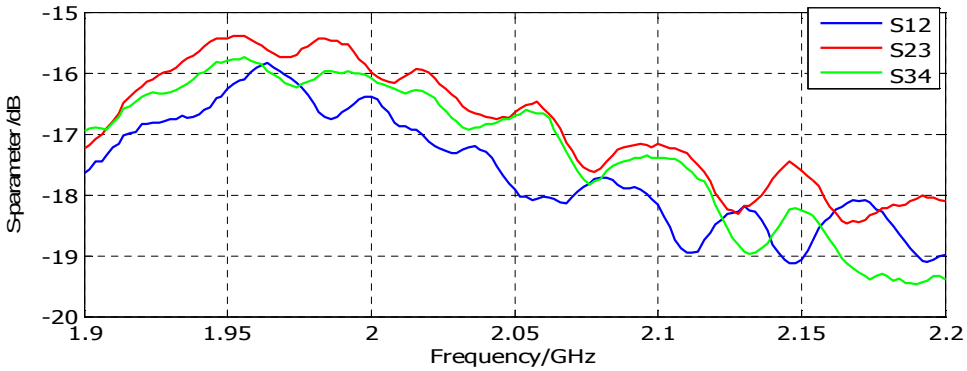

Fig.8.8: Measured isolation between 4 elements array ports with WAIM sheet

8.4 Feeder Network Measurement

The feeder network consists of a Butler matrix and a beam shaping network shown in Fig.8.9 and Fig.8.10. The performance of each of these networks has been determined over the frequency range of interest using the N5230A 10MHz to 40GHz network analyzer. The Butler matrix consists of four inputs and four outputs. The full 8x8 scattering matrix was determine by measuring each S-parameter in turn with all remaining ports terminated in matched loads. Similar results were obtained on the beam shaping network. Table 8.1 shows the measured and simulated S-parameters of the Butler matrix output ports at the uplink centre frequency.

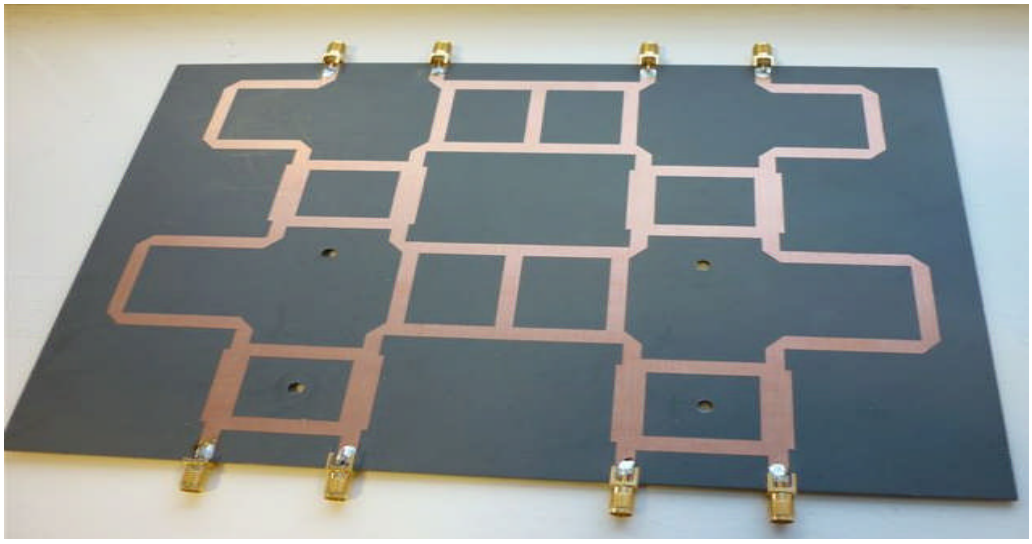

Fig.8.9: PCB microstrip 4X4 Butler matrix @uplink frequency band

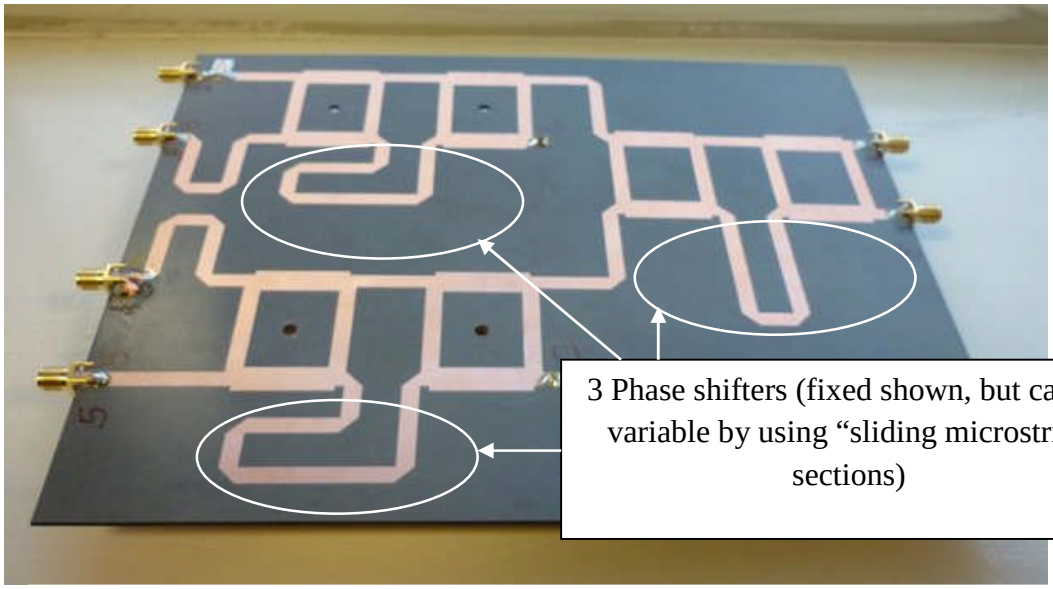

Fig.8.10: PCB microstrip beam shaping network @uplink frequency band

Table.8.1: Simulated and measured Butler matrix output S-parameters @ uplink

Beam 1R	Simulation Results		Measured Results	
	Magnitude(dB)	Phase in degree	Magnitude(dB)	Phase in degree
S5,1	-5.99	125.38	-6.08	7.0
S6,1	-6.29	81.15	-6.08	-35.5
S7,1	-6.52	35.93	-7.4	-74.5
S8,1	-6.45	-9.62	-6.35	-128.50
Beam 2R	Simulation Results		Measured Results	
	Magnitude(dB)	Phase in degree	Magnitude(dB)	Phase in degree
S5,3	-6.29	80.46	-6.42	-40
S6,3	-6.23	-54.98	-5.85	-179.5
S7,3	-6.19	169.81	-7.0	45.1
S8,3	-6.38	35.75	-7.18	-90.8
Beam 1L	Simulation Results		Measured Results	
	Magnitude(dB)	Phase in degree	Magnitude(dB)	Phase in degree
S5,4	-6.45	-9.62	-6.30	-128.00
S6,4	-6.52	35.93	-7.3	-75.00
S7,4	-6.29	81.15	-6.14	-37.00
S8,4	-5.99	125.38	-6.00	5.70
Beam 2R	Simulation Results		Measured Results	
	Magnitude(dB)	Phase in degree	Magnitude(dB)	Phase in degree
S5,2	-6.38	35.75	-7.00	-78.1
S6,2	-6.19	169.81	-7.00	46.3
S7,2	-6.23	-54.98	-5.85	-179.40
S8,2	-6.29	80.46	-6.23	-39.39

The results in table8.1 for the Butler matrix show that the measured and simulated results are in close agreement based on the chosen narrow bandwidth. The measured beam shaping network performance is presented in table 8.2. On inspection, Table 8.2 shows close agreement between theory and experiment.

Table.8.2: simulation and measured S-parameters of beam shaping network @uplink f_c

Beam 1L	Simulation Results		Measured Results		Phase shifter settings		
	Magnitude- dB	Phase in degree	Magnitude-dB	Phase in degree	$\Delta\emptyset_1$	$\Delta\emptyset_1$	$\Delta\emptyset_1$
S2,1	N/A	N/A	-51.02	N/A	-180	-180	Any
S3,1	-70	135	-31.25	-112.0			
S4,1	-70	135	-38.01	-112.8			
S5,1	N/A	N/A	N/A	67.5			
Beam 2L	Simulation Results		Measured Results				
	Magnitude- dB	Phase in degree	Magnitude-dB	Phase in degree	$\Delta\emptyset_1$	$\Delta\emptyset_1$	$\Delta\emptyset_1$
S2,1	-69.18	0.174	-43	0.25	0	Any	-180
S3,1	N/A	135.16	-50	133.5			
S4,1	-72.45	45.18	-39	43.16			
S5,1	N/A	N/A	-48	0.17			
Beam 1R	Simulation Results		Measured Results				
	Magnitude-dB	Phase in degree	Magnitude- dB	Phase in degree	$\Delta\emptyset_1$	$\Delta\emptyset_1$	$\Delta\emptyset_1$
S2,1	N/A	0.159	-0.52	67.50	0	Any	0
S3,1	-72.4	45	-38.01	-112.8			
S4,1	-72.4	45	-31.25	-112.0			
S5,1	N/A	N/A	N/A	N/A			
Beam 2R	Simulation Results		Measured Results				
	Magnitude-dB	Phase in degree	Magnitude-dB	Phase in degree	$\Delta\emptyset_1$	$\Delta\emptyset_1$	$\Delta\emptyset_1$
S2,1	N/A	0.193	-48	0.17	-180	0	Any
S3,1	-70	135	-39	43.65			
S4,1	N/A	135	-50	133.8			
S5,1	-72	90	-43	0.19			
BC Beam	Simulation Results		Measured Results				
	Magnitude- dB	Phase in degree	Magnitude- dB	Phase in degree	$\Delta\emptyset_1$	$\Delta\emptyset_1$	$\Delta\emptyset_1$
S2,1	-6.33	103.50	-6.83	-18.90	-270	-285	-285
S3,1	-6.57	-32.53	-6.79	-155.60			
S4,1	-6.29	-32.11	-6.40	-152.82			
S5,1	-6.48	108.10	-6.32	-20.17			
LS Beam	Simulation Results		Measured Results				
	Magnitude- dB	Phase in degree	Magnitude-dB	Phase in degree	$\Delta\emptyset_1$	$\Delta\emptyset_1$	$\Delta\emptyset_1$
S2,1	-15.34	75.31	-17.2	-41	-270	-346	-346
S3,1	-3.76	-63.18	-4.5	-175			
S4,1	-15.30	-60.48	-16.70	-172			
S5,1	-3.67	77.27	-3.9	-39			
RS Beam	Simulation Results		Measured Results				
	Magnitude-dB	Phase in degree	Magnitude-dB	Phase in degree	$\Delta\emptyset_1$	$\Delta\emptyset_1$	$\Delta\emptyset_1$
S2,1	-3.67	77.27	-3.9	-39	-270	-222	-222
S3,1	-15.30	-60.48	-16.70	-172			
S4,1	-3.76	-63.18	-4.5	-175			
S5,1	-15.34	75.31	-17.2	-41			

The beam shaping network and the Butler matrix were connected together to form the feeder network of Fig.8.11 and the overall S-parameters were also measured using the network analyzer. Table 8.3 presents the simulated and measured S-parameter of each beam state (B1L B2L, B1R B2R and LS beam RS beam and BC beam). These S-parameters are measured by varying the three phase shifters in the beam shaping network. From the Table8.3 it is seen that the simulated feeder network S-parameters and measured results are in close agreement.

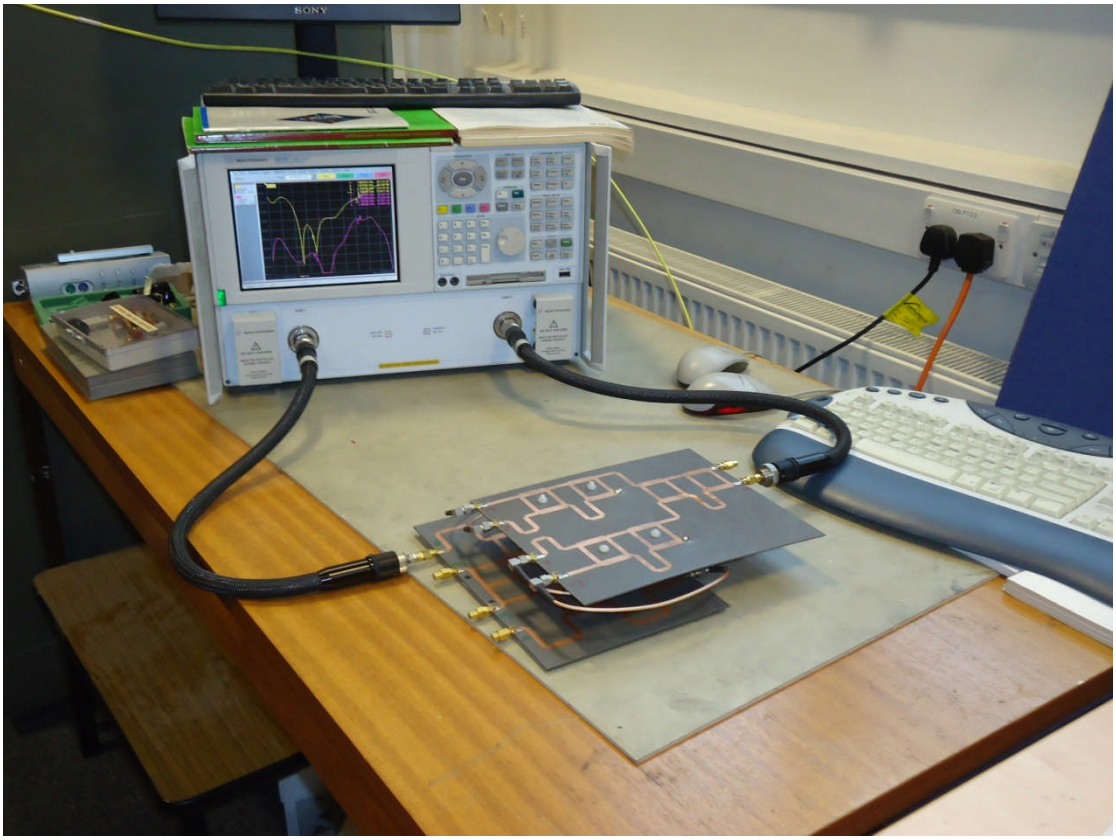

Fig.8.11: Feeder network S-parameter measurement @ uplink frequency band

Table.8.3: Simulated and measured output S-parameter of feeder network @uplink f_c

Beam 1L	Simulation Results		Measured Results		Phase shifter setting		
	Magnitude- dB	Phase in degree	Magnitude-dB	Phase in degree	$\Delta\emptyset_1$	$\Delta\emptyset_2$	$\Delta\emptyset_3$
S2,1	-6.63	179.58	-6.43	-177	-180	-180	Any
S3,1	-7.02	-132.79	-7.43	-134			
S4,1	-6.44	-89.99	-6.7	-89			
S5,1	-6.43	-43.29	-6.11	-45			
Beam 2L	Simulation Results		Measured Results				
	Magnitude-dB	Phase in degree	Magnitude- dB	Phase in degree	$\Delta\emptyset_1$	$\Delta\emptyset_2$	$\Delta\emptyset_3$
S2,1	-6.53	6.67	-7.43	-134	0	Any	-180
S3,1	-6.80	137.58	-6.43	-3			
S4,1	-6.22	-83.99	-6.11	-225			
S5,1	-6.89	46.83	-6.7	-89			
Beam 1R	Simulation Results		Measured Results				
	Magnitude-dB	Phase in degree	Magnitude- dB	Phase in degree	$\Delta\emptyset_1$	$\Delta\emptyset_2$	$\Delta\emptyset_3$
S2,1	-6.43	-43.29	-6.11	-45	0	Any	0
S3,1	-6.44	-89.99	-6.7	-89			
S4,1	-7.02	-132.79	-7.43	-134			
S5,1	-6.63	179.58	-6.43	177			
Beam 2R	Simulation Results		Measured Results				
	Magnitude- dB	Phase in degree	Magnitude- dB	Phase in degree	$\Delta\emptyset_1$	$\Delta\emptyset_2$	$\Delta\emptyset_3$
S2,1	-6.89	46.83	-6.7	-89	-180	0	Any
S3,1	-6.22	-83.99	-6.11	-225			
S4,1	-6.80	137.58	-6.43	-3.00			
S5,1	-6.53	6.67	-7.43	-1.34			
BC Beam	Simulation Results		Measured Results				
	Magnitude- dB	Phase in degree	Magnitude- dB	Phase in degree	$\Delta\emptyset_1$	$\Delta\emptyset_2$	$\Delta\emptyset_3$
S2,1	-10.02	46.7	-9.25	60.9	-270	-285	-285
S3,1	-4.87	174.72	-5.24	-172			
S4,1	-5.04	172.95	-4.7	-172.2			
S5,1	-10.05	49.13	-9.40	59.0			
LS Beam	Simulation Results		Measured Results				
	Magnitude-dB	Phase in degree	Magnitude-dB	Phase in degree	$\Delta\emptyset_1$	$\Delta\emptyset_2$	$\Delta\emptyset_3$
S2,1	-7.03	17.16	-6.34	39.4	-270	-346	-346
S3,1	-4.0	118.61	-5.93	135.00			
S4,1	-6.18	177.02	-6.64	-163.8			
S5,1	-19.31	18.50	-19.1	59.02			
RS Beam	Simulation Results		Measured Results				
	Magnitude- dB	Phase in degree	Magnitude- dB	Phase in degree	$\Delta\emptyset_1$	$\Delta\emptyset_2$	$\Delta\emptyset_3$
S2,1	-19.31	18.50	-19.1	59.02	-270	-222	-222
S3,1	-6.18	177.02	-5.64	-163.8			
S4,1	-4.0	118.61	-4.93	135.00			
S5,1	-7.03	17.16	-6.34	39.4			

8.5 Smart Antenna System Measurement

A full design demonstrator model of the smart antenna has been implemented and this includes: a four element slant $\pm 45^0$ dual-polarised stacked patch array complete with beam forming (Butler matrix) and beam shaping networks. This antenna is shown in Fig.8.12 which consists of an array of four slant $\pm 45^0$ dual-polarised stacked patch elements, a 4x4 Butler matrix beam-forming network and a beam shaping network and Fig.8.13 which illustrate the antenna system with WAIM sheet covering the array antenna.

The array antenna, the beam-forming network and the beam shaping network are coupled together to form the smart antenna system. The implemented smart antenna system is manufactured on 1.575mm thick (5870 RT/duriod) substrate material, which has permittivity of 2.33 and a loss tangent of 0.0012. The array elements have been designed to be double tuned with good return loss performance in the Orange UK 3G uplink frequency band (1.9697GHz to 1.9797GHz) and downlink frequency band (2.1597GHz to 2.1697GHz). The multi-beam forming and beam shaping networks can be specifically tuned for either the uplink or downlink band. In this case the uplink frequency band 1.9697GHz to 1.9797GHz was used. Control of the three phase shifters within the beam shaping network dynamically provides the required complex weights for the desired beam shapes. Ideally, the array with feeding networks should be etched on one PCB, however, owing to practical limitations in etching facilities available within the school, this design has been constructed on three separate PCBs. This has necessitated considerable re-design and the acquisition of phased matched inter-connecting cables to realise the demonstrator model. The phase matched cables are required to ensure that the correct phase relation is maintained between Butler matrix, beam shaping network and the antenna array.

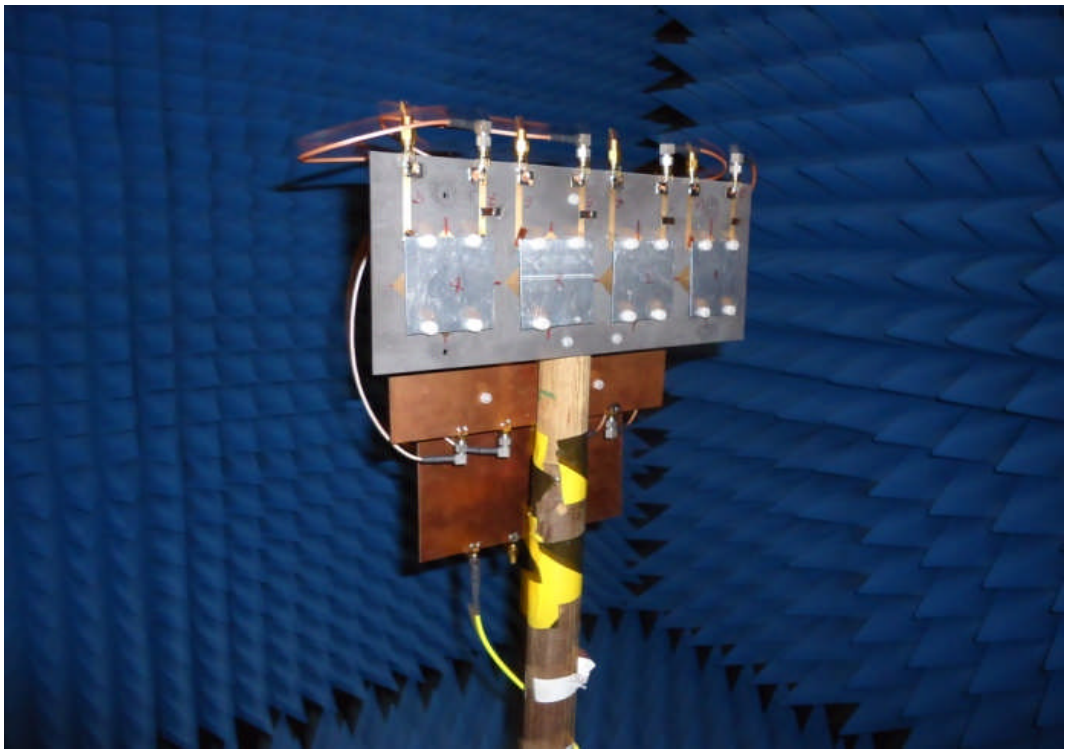

Fig.8.12: multiple switched beams smart with beam shaping capability in anechoic chamber under test

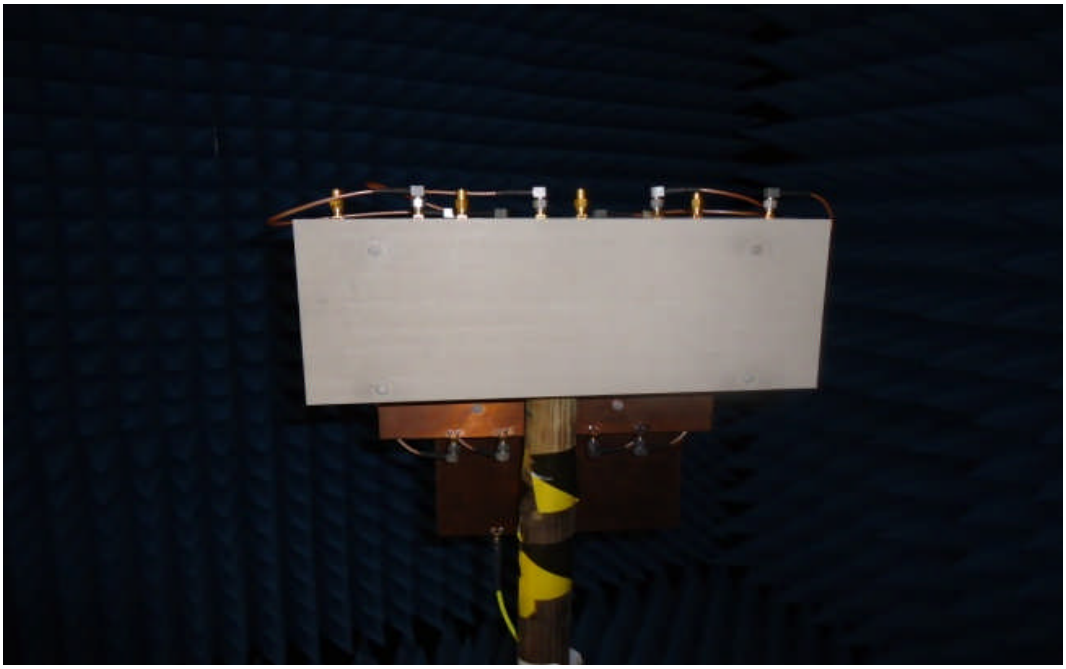

Fig.8.13: multiple switched beams smart with beam shaping and WAIM sheet covering top of the array antenna capability in anechoic chamber under test

8.5.1 Active reflection coefficient measurement

The basic properties used to describe the performance of an antenna include: active reflection coefficients and 3dB radiation pattern. Active reflection coefficient Γ_{An} is defined by [110, 142]:

$$\Gamma_{An} = \frac{b_n}{a_n} \tag{8-1}$$

Γ_{An} = active reflection coefficient at the n^{th} element.

$$b_n = a_n[S]$$

where

$$S = \begin{bmatrix} S_{11} & S_{21} & S_{31} & S_{41} \\ S_{21} & S_{22} & S_{23} & S_{24} \\ S_{31} & S_{23} & S_{33} & S_{34} \\ S_{41} & S_{24} & S_{34} & S_{44} \end{bmatrix}$$

$$b_1 = S_{11}a_1 + S_{21}a_2 + S_{31}a_3 + S_{41}a_4$$

$$b_2 = S_{21}a_1 + S_{22}a_2 + S_{23}a_3 + S_{24}a_4$$

$$b_3 = S_{31}a_1 + S_{23}a_2 + S_{33}a_3 + S_{34}a_4$$

$$b_4 = S_{41}a_1 + S_{24}a_2 + S_{34}a_3 + S_{44}a_4$$

now,

$\Gamma_{A1} = \frac{b_1}{a_1}$, $\Gamma_{A2} = \frac{b_2}{a_2}$, $\Gamma_{A3} = \frac{b_3}{a_3}$ and $\Gamma_{A4} = \frac{b_4}{a_4}$

Hence Γ_{A1}, Γ_{A2}, Γ_{A3} and Γ_{A4} are the active reflection coefficients at each input port of the array antenna.

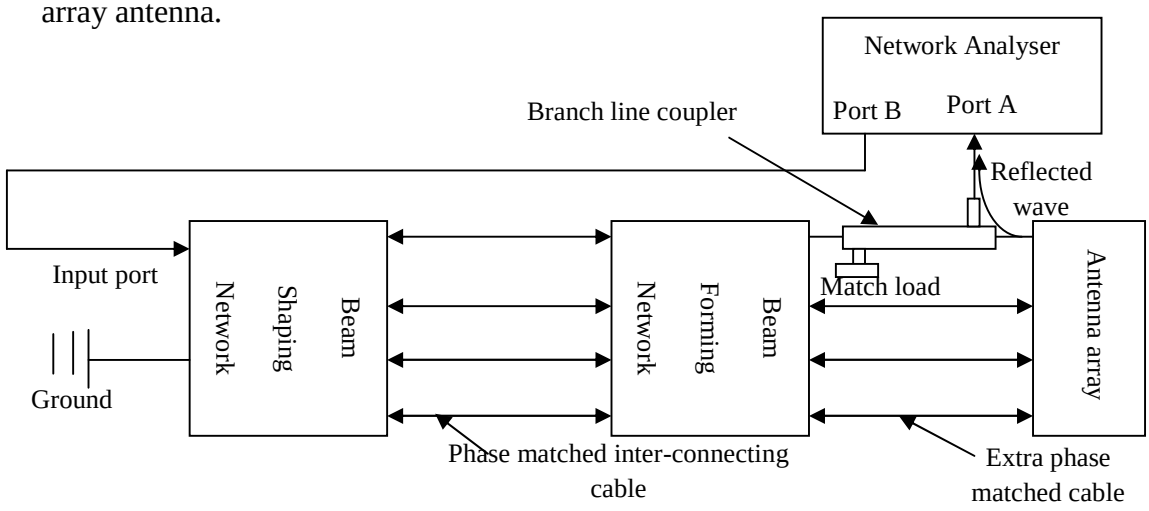

Fig.8.14: Active reflection coefficient measurement arrangement with the smart antenna system

An experiment to determine the active reflection coefficient of the smart antenna system was setup as shown in the Fig.8.14 below. A directional coupler was inserted between line connecting one output port of the feeder network (Butler matrix and beam shaping network) to one input port of the four element array antenna while extra phase matched cables of equal phase and amplitude to the directional coupler (network analyser to measure the phase of the directional coupler "thru-arm") were used to connect the other remaining three output ports of the feeder network to the remaining input ports of the array antenna. The input port of the feeder network was connected to port ‘A’ of a network analyzer and the couple port of the coupler was connected to port ‘B’ of the network analyzer while the other port of the coupler was matched to 50ohm load as shown in Fig.8.15. Two sets of readings was taken, one with the WAIM sheet covering the face of the array antenna and another without the WAIM covering the array antenna. Table 8.4 and table 8.5 present the measured active reflection coefficient with and without WAIM sheet. The results presented in table 8.5 show the smart antenna demonstrator with active reflection coefficient better than -10dB.

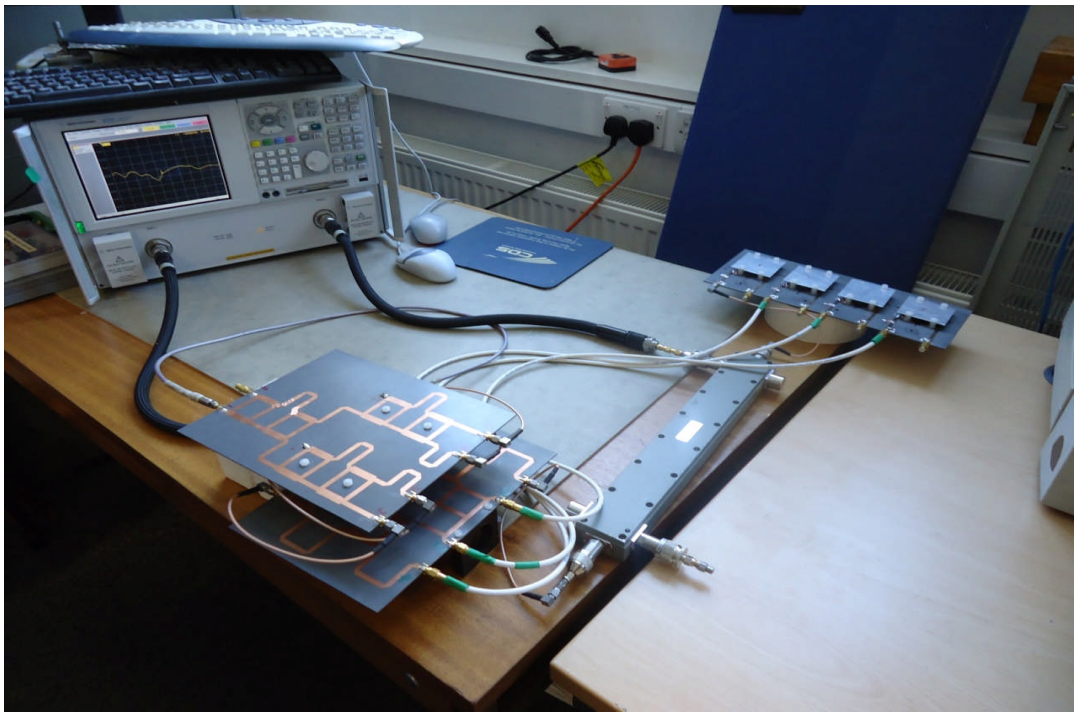

Fig .8.15: Active reflection coefficient measurement Experiment

Table 8.4: Antenna Active Reflection coefficient without WAIM (dB)

	Measured reflection coefficient without WAIM			
Beam Number	Γ_{A1}dB	Γ_{A2}dB	Γ_{A3}dB	Γ_{A4}dB
Beam1 R	-15.73	-5.30	-9.45	-13.02
Beam 2R	-14.80	-10.39	-18.50	-9.70
BC Beam	-17.10	-12.03	-9.53	-13.10
LS Beam	-14.21	-12.8	-11	-2.46

Table 8.5: Antenna Active reflection coefficients with WAIM sheet on top (dB)

Number	Measured reflection coefficient with WAIM sheet			
Beam Number	Γ_{A1}dB	Γ_{A2}dB	Γ_{A3}dB	Γ_{A4}dB
Beam1 R	-19.19	-10.33	-10.43	-10.64
Beam 2R	-10.20	-13.4	-15.07	-10.50
BC Beam	-19.03	-10.03	-11.22	-10.16
LS Beam	-12.69	-11.40	-10.05	-10.11

8.5.2 Insertion loss of the Smart Antenna System with Matched Loads

Insertion loss is the net unrecoverable power loss in dB dissipated within the beam forming network and the beam shaping network at the uplink centre frequency (1.9747GHz). The input to output couplings of the feeder network are S1 (dB), S2 (dB), S3 (dB) and S4 (dB).

If $\alpha_i = 10^{S}{}_i$(dB)/20 where i = 1, 2, 3, and 4.

The total insertion loss in dB for a particular beam state is give as:

Insertion (dB) = $10Log_{10} \sum (\alpha_i)^2$.

Table 8.6 presents the calculated insertion loss of this antenna feeder network for various beam states.

Table.8.6: Insertion loss of uplink band feeder network for all beam state

Beam state	coupling	Magnitude in dB	Insertion loss in dB
Beam1L	S2,1	-6.43	0.62
	S3,1	-7.43	
	S4,1	-6.70	
	S5,1	-6.11	
Beam2L	S2,1	-7.43	0.62
	S3,1	-6.43	
	S4,1	-6.11	
	S5,1	-6.70	
Beam1R	S2,1	-6.11	0.62
	S3,1	-6.70	
	S4,1	-7.43	
	S5,1	-6.43	
Beam2R	S2,1	-6.70	0.62
	S3,1	-6.11	
	S4,1	-6.43	
	S5,1	-7.43	
BC Beam	S2,1	-9.25	0.608
	S3,1	-5.24	
	S4,1	-4.70	
	S5,1	-9.40	
LS Beam	S2,1	-6.34	0.763
	S3,1	-4.93	
	S4,1	-5.64	
	S5,1	-19.10	
RS Beam	S2,1	-19.10	0.763
	S3,1	-5.64	
	S4,1	-4.93	
	S5,1	-6.34	

8.5.3 Radiation Pattern Measurement

The smart antenna radiation patterns were measured in an anechoic chamber. The anechoic chamber has a dimension of 3m wide and 5m long. Fig.8.16 shows the multiple switched beams smart system with beam shaping capability in the anechoic chamber under test. To measure the far-field radiation patterns of this antenna system, the distance between the standard gain antenna and the antenna under test (R) must be:

$$R > \frac{2D^2}{\lambda}$$

where '*D*' is the aperture of the antenna under test and λ is the wavelength.

For this antenna system under test, D=0.363m and λ = 0.145m.

$\frac{2D^2}{\lambda} = 1.81m$ and R is 3m.

Fig.8.17 through to Fig.8.19 show simulated and measured normalized radiation patterns of the smart antenna system. The radiation pattern for each polarisation was measured at 1.975GHz (centre frequency of the uplink frequency band) in both $+45^0$ polarisation and -45^0 polarisation ports. The measured and simulated multiple narrow beams at 1.975GHz

are shown in Fig.8.17. The experimental results for the measured multiple narrow beams patterns are very close to the simulated multiple beams. The shaped beams are shown in Fig.8.18 and Fig.8.19 (Fig.8.18 is the left shaped beam and Fig.8.19 is the broadcast channel beam). The measured left shaped beam has a 2.5dB dip difference at 15^0 compared to the compensated simulated left shaped beam pattern. This dip is caused by the effects of mutual coupling within the array elements. The broadcast channel beam pattern measured is in close agreement with the compensated simulated pattern.

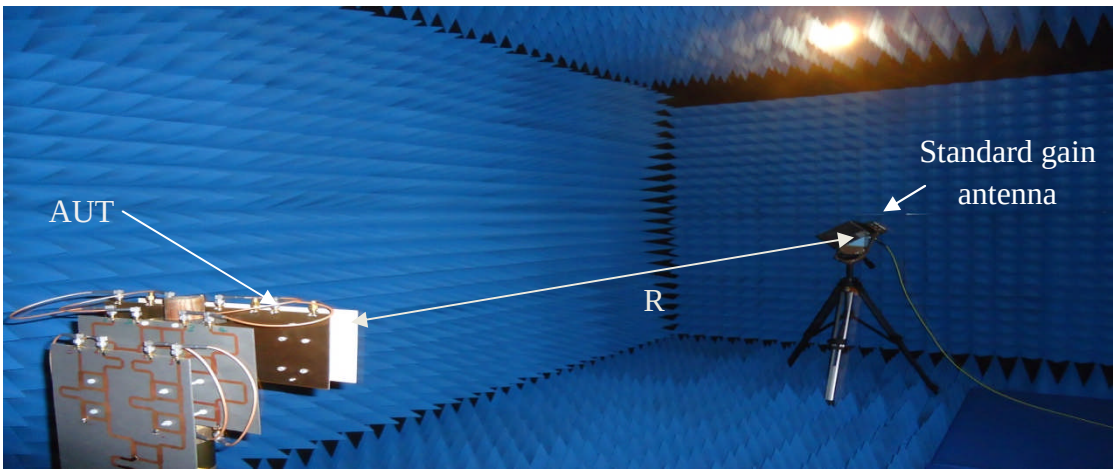

Fig.8.16: Smart antenna gain and radiation pattern measurement

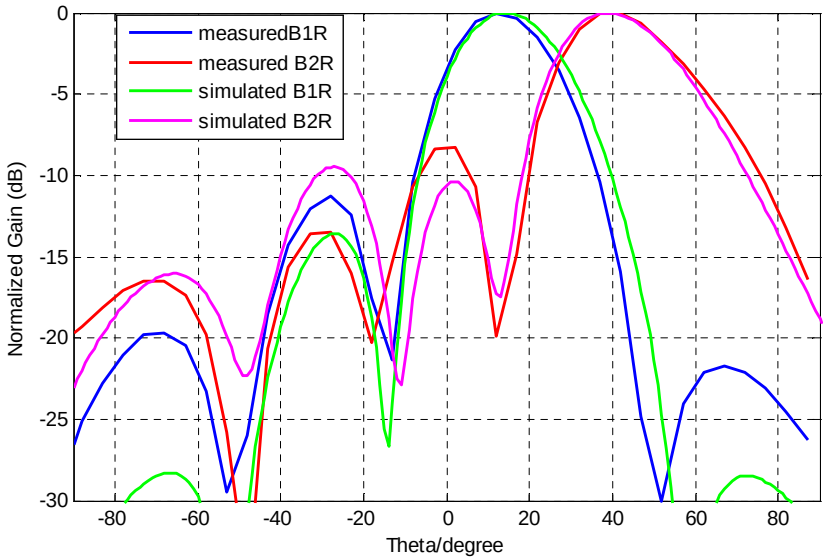

Fig.8.17: Measured and simulated multiple beams @uplink f_c

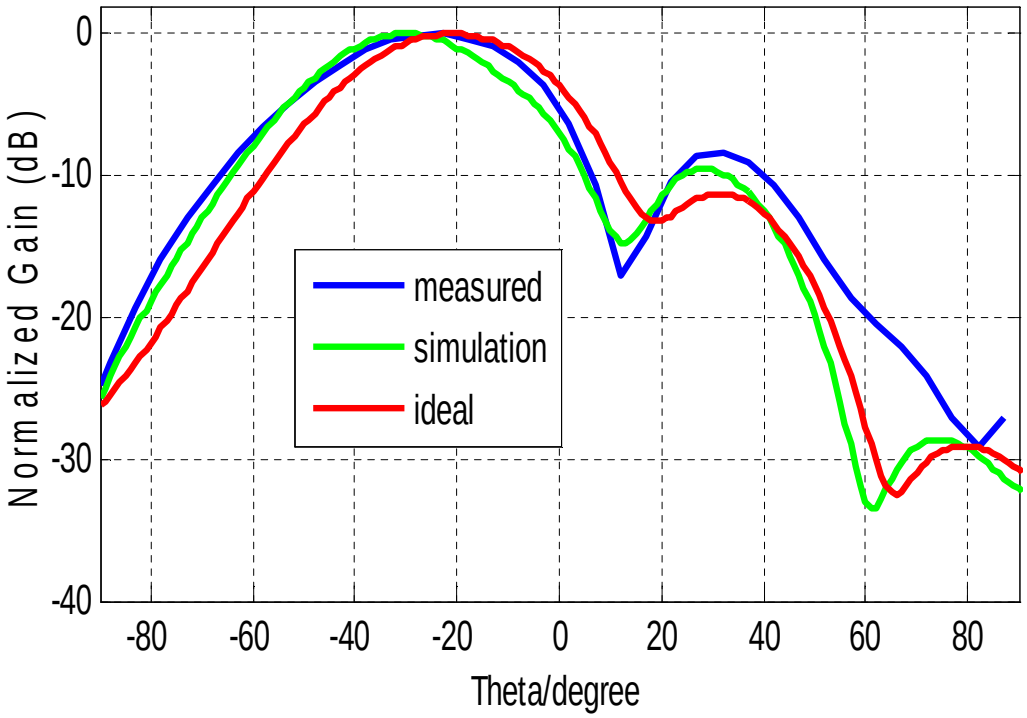

Fig.8.18: Measured, simulated and ideal Left hand shaped beam @uplink f_c

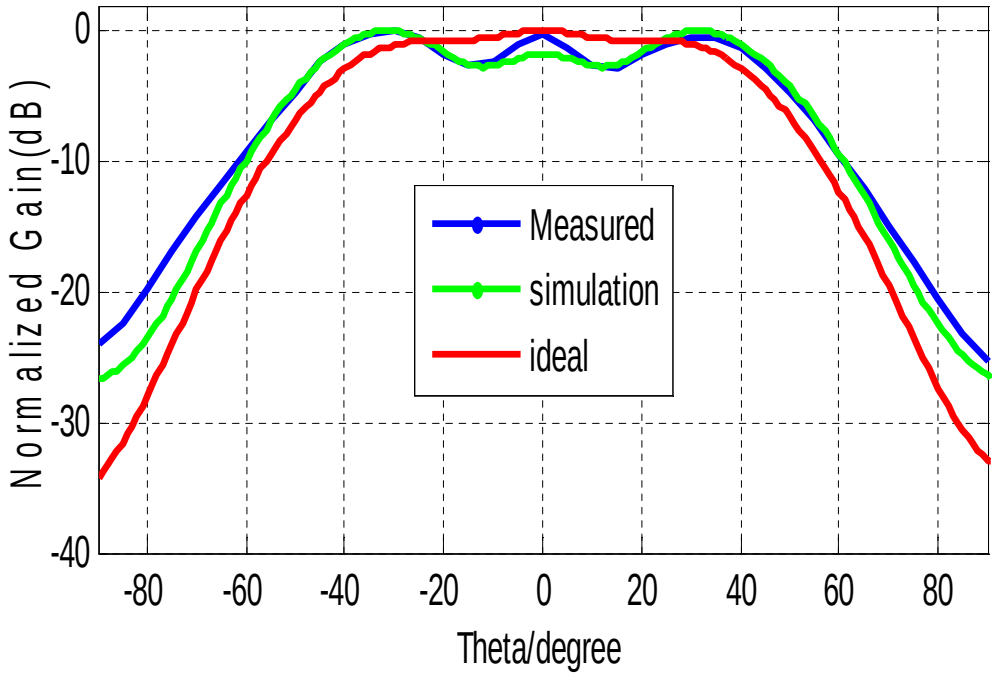

Fig.8.19: Measured and simulated and ideal Broadcast channel beam @uplink f_c

8.5.4 Antenna Gain Measurement

One of most important characteristics that describe the performance of antennas is the gain of the antenna. There are various methods and antenna ranges that are used to measure the gain and the choice of any particular method depends mainly on the frequency of operation and the design of the antenna under measurement. Traditionally free-space ranges have been used to measure the gain of antenna with any operating frequency of 1 GHz and above. Absolute-gain and gain comparison techniques are the two conventional techniques usually used to measure the gain of an antenna [15].

The absolute-gain technique is used to calibrate antennas which can then be used as standards to determine the gain of other antennas and it does not require a priori knowledge of the gains of the antennas [15]. Gain-comparison or transfer methods can be used in conjunction with standard gain antennas to determine the absolute gain of the antenna under measurement. The two antennas that are commonly used as standard gain antennas are the *λ/2* dipole with a gain of about 2.1dB and the standard gain pyramidal horn antenna with a gain ranging from 12–25dB. In this antenna gain measurement, the gain comparison method is used [15].

The experiment (gain comparison method) to measure the gain of the smart antenna system is set up as shown in Fig. 8.16 above in the anechoic chamber. In this case the required polarisations are $\pm 45^0$. The result can be obtained by positioning the antenna under test (*AUT*) as shown in Fig.8.15 and arrange the standard gain antenna to be aligned with the selected polarisation. Following the Friis transmission equation, the ratio of the available power at the input of the antenna under test to output power of the transmitting antenna is given by:

$$P_r(dBm) = P_t G_{SGH} G_{AUT} \left(\frac{\lambda}{4\pi R}\right)^2$$

$$P_r(dBm) - P_t(dBm) = G_{SGH}(dBi) + G_{AUT}(dBi) + 20log\left(\frac{\lambda}{4\pi R}\right)$$

$$G_{AUT}(dBi) = -G_{SGH}(dBi) - (P_r(dBm) - P_t(dBm) - 20log\left(\frac{\lambda}{4\pi R}\right)$$

Where R is the distance between the antenna under test and the standard antenna, P_r is the received power at the antenna under test; P_t is the input into the standard gain antenna,

G_{SGH} is the gain of the standard horn antenna and G_{AUT} is the gain of the antenna under test. Table8.7 presents the maximum power received at each beam state, the transmitted power, the distance between the standard gain antenna and the antenna under test and the calculated gain for each of the smart antenna beams.

Table 8.7: Simulated and measured gain in (dBi) of the smart antenna demonstrator

Beam state	Maximum received power	Transmitted power	Cable Loss(dB)	Distance (R)	Simulated Gain dBi	Measured Gain dBi
B1R	-13.15 dBm	20 dBm	7.80	3 m	13.2	12.95
B2R	-14.82 dBm	20 dBm	7.80	3 m	12.4	11.28
BC Beam	-17.36 dBm	20 dBm	7.80	3 m	9.0	8.74
LS Beam	-15.52 dBm	20 dBm	7.80	3 m	10.9	10.58

8.6 Summary

A multiple switched beam smart antenna demonstrator with beam shaping capability has been successfully designed, analysed, simulated, implemented and tested to provide good coverage and increase capacity throughout a cell sector and to dynamically reconfigure the beams to provide enhanced capacity in certain areas with reduced, but acceptable coverage and capacity, throughout the rest of the cell sector using only one transceiver per polarisation. The simulated building blocks of the smart antenna demonstrator which include a slant $\pm 45^0$ dual-polarised stacked patch, Butler matrix and a beam shaping network have been implemented and tested successfully. The simulated characteristics of all the smart antenna building blocks and the full demonstrator smart antenna system are very close to the measured values. The next chapter will analyse the varying capacity with coverage of the smart antenna system.

Chapter 9 - COVERAGE AND CAPACITY

9.1 Introduction

Dynamic concentration of the users within a part of a cell sector has placed pressure on network operators to find ways to dynamically optimise the sector to increase capacity and quality of service while maintaining coverage. Smart antenna systems have been identified as being capable of dynamically optimising mobile telecommunication networks. Therefore, there is need to estimate the actual performance gain that can be achieved with this smart antenna system and a comprehensive knowledge of radio propagation effects is an important factor for the development and performance evaluation of smart antenna systems in mobile telecommunication networks. This chapter presents a performance evaluation of the smart antenna concept within a realistic radio environment in terms of coverage and capacity relationship (only the downlink frequency band is considered). First a brief overview of the relationship between coverage and capacity in 3G using WCDMA air interface is presented and thereafter the mobile telecommunication propagation environment is described followed by propagation prediction models. Then the received power footprint contours of the proposed smart antenna system are presented and then finally the smart antenna system coverage versus capacity using the Shannon channel equation is presented.

9.2 Coverage and Capacity Relationship in 3G

Coverage in a mobile communication network is defined as the maximum distance that a given user of interest can be from a base station (BTS) and still have reliable received signal strength at the mobile user station while capacity of a single 3G cell is a function of the type of users (data rate) services within it. The capacity of 3G systems is itself soft; more users can be added, provided there are sufficient codes to service the additional users. However, this will increase the overall interference level within the cell and that will become apparent to users. It is a well known fact that in a WCDMA air interface for 3G mobile communication systems the coverage area has a direct relationship with the user capacity; an increase in the number of active users in the cell area causes the total interference seen at the receiver to increase [16,25]. This causes an increase in required received power (power at the base station is fixed hence it cannot increase transmit power) for each user to maintain a certain signal to interference plus noise ratio at the receiver for satisfactory communication.

Conventionally those users furthest from the base station will suffer the greatest interference effects and will be forced below the required signal to interference plus noise ratio (SINR) to maintain continuous communication service and at this stage the mobile user may then be handed over to a more lightly loaded cell. The SINR is actually the energy per bit divided by the noise per hertz (E_b/N_0) and as this decreases the capacity of the cell increases, but bit error rate gets worse (a minimum of 10^{-3} of BER is required for voice communication and 10^{-6} for data communication) [65]. Therefore, capacity is a balance between energy per bit divided by the noise per Hz and the bit error rate which can be mitigated by error correction coding. An accurate estimate of a base station antenna coverage as a function of user capacity is essential in WCDMA network design and deployment, and therefore of great interest in this research [57, 65, 68].

Presently, the majority of mobile telecommunication network operators make use of omni-directional or directional fixed beam sectorised antennas which cannot dynamically optimise the network if there is a sudden concentration of users in part of a cell sector [16, 25, and 65]. Smart antenna systems have been identified as being capable of dynamically optimising the network cell sector to enhance coverage in a subsector cell to maintain capacity and provide the higher quality of service demanded by mobile telecommunication users; but, they have not been exploited to dynamically optimise the network cell sector to my knowledge.

In chapter four a novel smart antenna system have been introduced that could optimise a mobile telecommunication cell sector dynamically. And in chapter eight a demonstrator model of the smart antenna system has been implemented. To evaluate the performance of this smart antenna concept, it is very important to model the system within a realistic radio environment to analyse the received power footprint contours and the relationship between the antenna coverage and the capacity it can offer using Shannon channel capacity equation. Though the smart antenna concept has been extensively studied, most of the research activities have been dedicated to algorithm development, direction of arrival, beam-forming algorithms and angle of departure [84, 143]. Not nearly as much effort has been made on implementing and validating the smart antenna system performance by finding the received power footprint contour within the real environmental characteristics of mobile telecommunication networks. This chapter focuses on the performance and evaluation of the smart antenna concept introduced in chapter four, simulated in chapter six and implemented in chapter eight in a real radio environment by finding the footprint

received power contours over the ground surface and estimating the coverage capacity relationship using Shannon channel capacity equation when the antenna is deployed in mobile telecommunication macro cell sectors.

9.3 Mobile Telecommunication Propagation Environment

The energy radiated by a mobile telecommunication base station antenna often encounters multiple obstructions such as buildings, trees and vehicles etc... before reaching a mobile receiver, possibly a moving one. The radiated electromagnetic field from the base station antenna is reflected, diffracted, and multiply scattered by these various obstructions which result in multiples of waves impinging on the mobile receiver. These mobile receivers are predominately located among these obstacles which therefore have the greatest influence on the propagation of electromagnetic waves over short distances [144].

The radio propagation environment plays a critical role in the operation of mobile telecommunication systems. The environment determines the performance of the systems whether used to transmit real-time voice messages, data or other types of communication traffic [145]. Every day the environment is changing, new types of materials for building and increasing numbers of obstacles for signal propagation (the effects is multipath, angular spread, noise, and delay spread interference, etc.). It is a well known fact that the delay spread and resulting inter-symbol interference (ISI) due to multiple signal paths arriving at the receiver at different times have a critical impact on communication link quality [84]. Therefore, to evaluate the performance of this smart antenna concept, it is very important to model the system within this realistic radio environment.

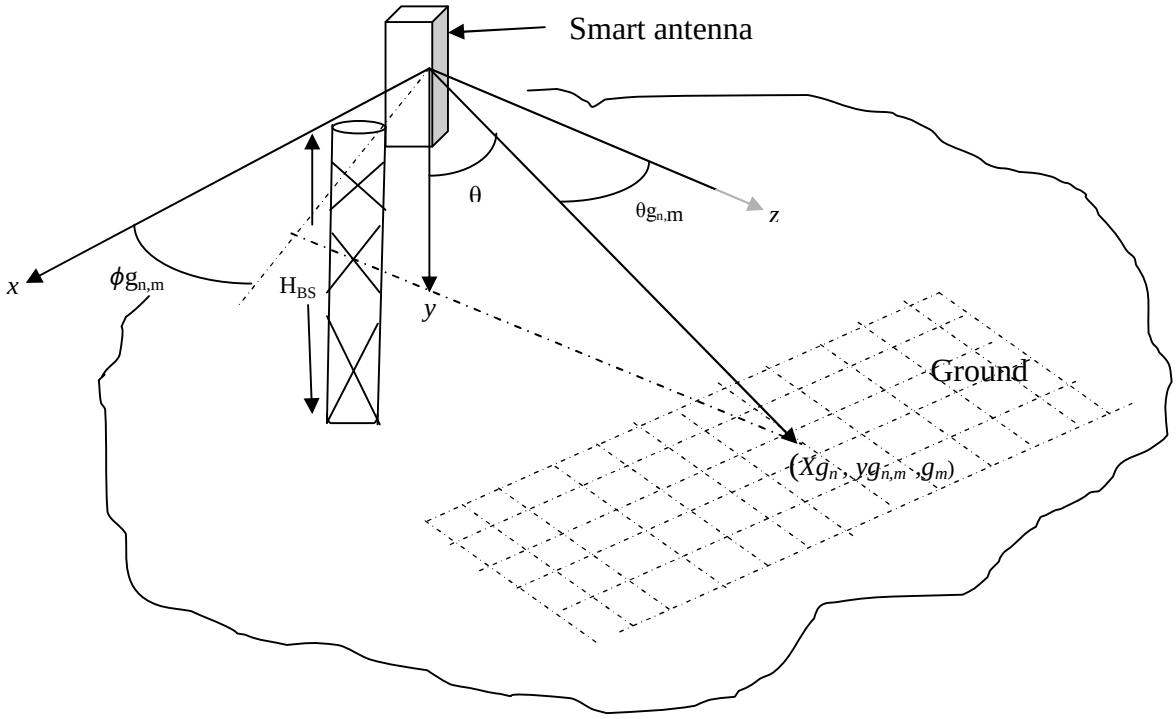

Fig.9.1: Geometry of free space propagation

Fig.9.1 above shows the geometry used to develop the program to predict the 'beams footprint' of the received power contours for the subject smart antenna. Different radio frequency propagation models for different wireless communication services that specifically address varying propagation environments and operating frequency ranges are generally known [145]. A large number of propagation prediction models for various terrain irregularities, like tunnels, urban areas, suburban areas, buildings materials, earth curvature, etc... have been developed [145]. In this simulation [146], free-space propagation model and COST259 propagation model which has the capacity to model several different radio propagation environments have been used [52] to enabling comparison.

9.3.1.1 Free Space Propagation

A program has being developed using a free space propagation model base on Fig.9.1 to analyse the fundamental performance, i.e. without multiple reflection effects of the proposed smart antenna system. The calculated received power on the ground for a free-space propagation environment is given by equation (9-1):

$$P_r = P_t G(\theta, \emptyset) \left(\frac{\lambda}{4\pi R}\right)^2 \qquad (9\text{-}1)$$

where Pr is the received power, P_t is the transmitted power, $G(\theta, \emptyset)$ is the gain of the transmitter antenna in the direction of the receiving antenna, λ is the wavelength at 2165MHz and R is the straight line distance between the transmitter and receiver located at each grid point on the ground.Fig.9.2 shows the propagation loss versus distance in a free space propagation environment.

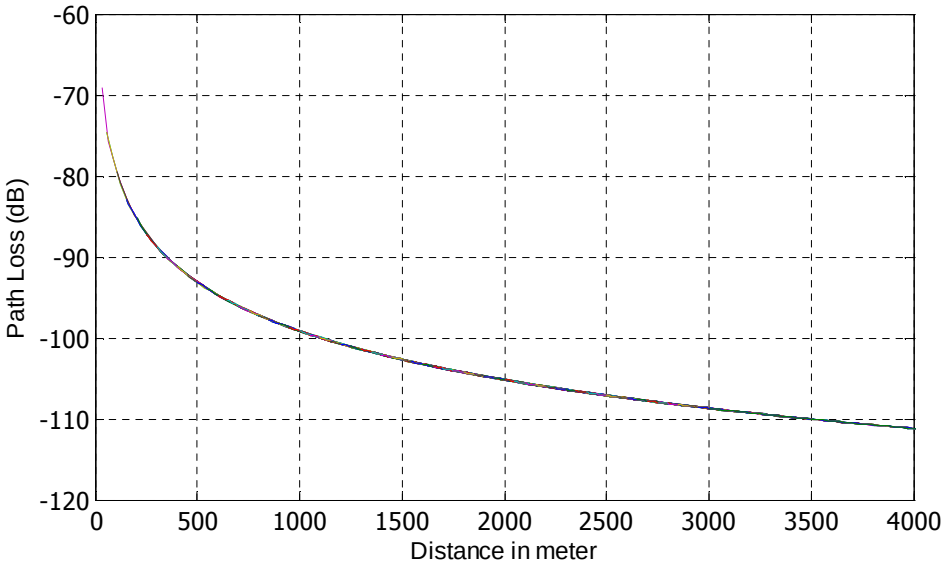

Fig.9.2: Free space propagation path Loss

Fig.9.3 through Fig.9.6 below show representative results from a full study that has been carried out using a free space propagation model. The contour plots have been derived from simulated radiation patterns of the smart antenna system in the downlink frequency band. The radiation patterns of seven different beams (narrow beams are *B1L*, *B2L*, *B1R*, *B2R* and the shaped beams are *LS* Beam, RS Beam and broadcast beam) from the smart antenna system are shown in Fig.9.6 & Fig.9.7 and Table9.1below shows the antenna specification.

Table9.1: Antenna specification @ downlink f_c

	Gain (dBi)	3dB Beam width(deg.)
B1L	23.30	26
B1R	23.30	26
B2L	21.80	29
B2R	21.80	29
BC Beam	17.20	80.7
LS Beam	21.30	39
RS Beam	21.30	39

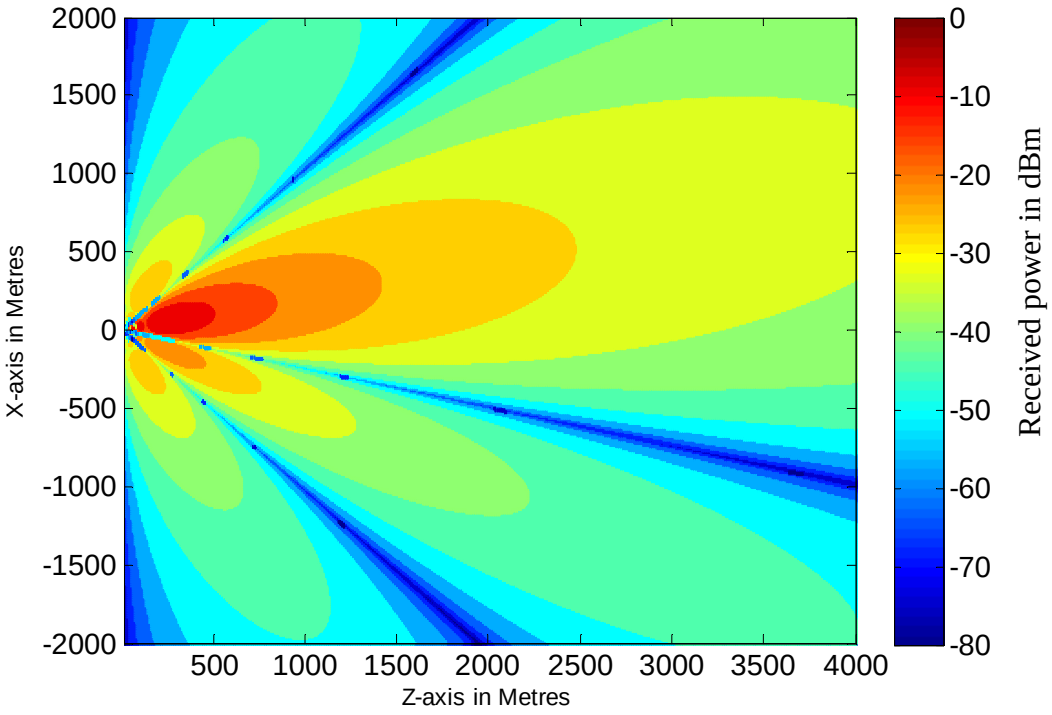

Fig.9.3:Beam1L footprint using free space propagation model

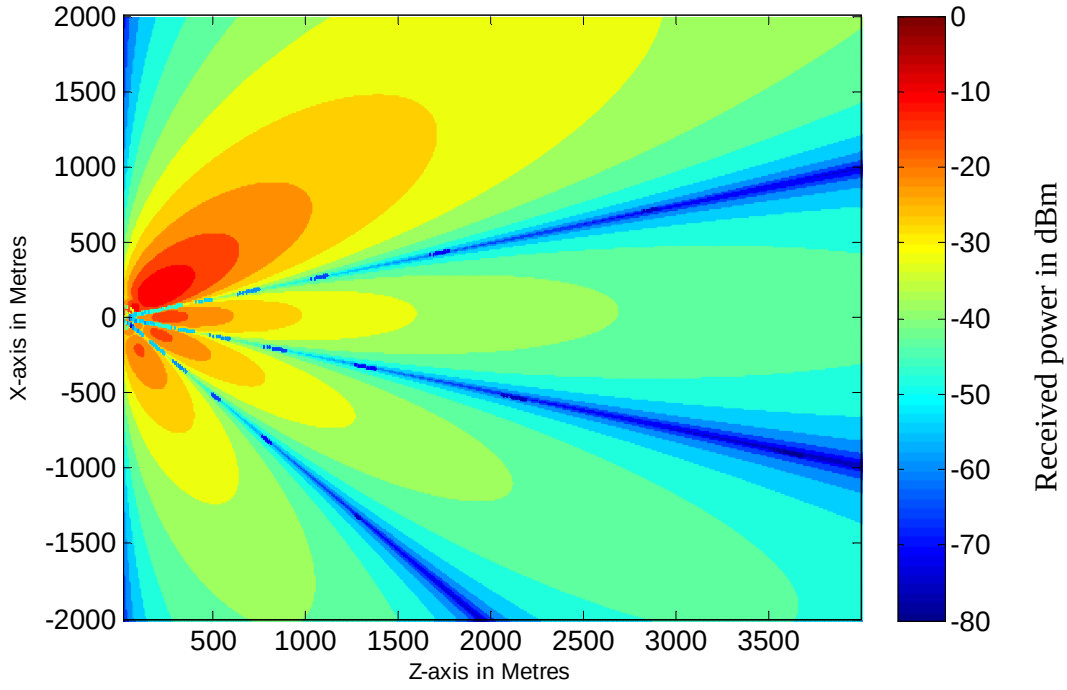

Fig.9.4:Beam2L “footprint” using free space propagation model

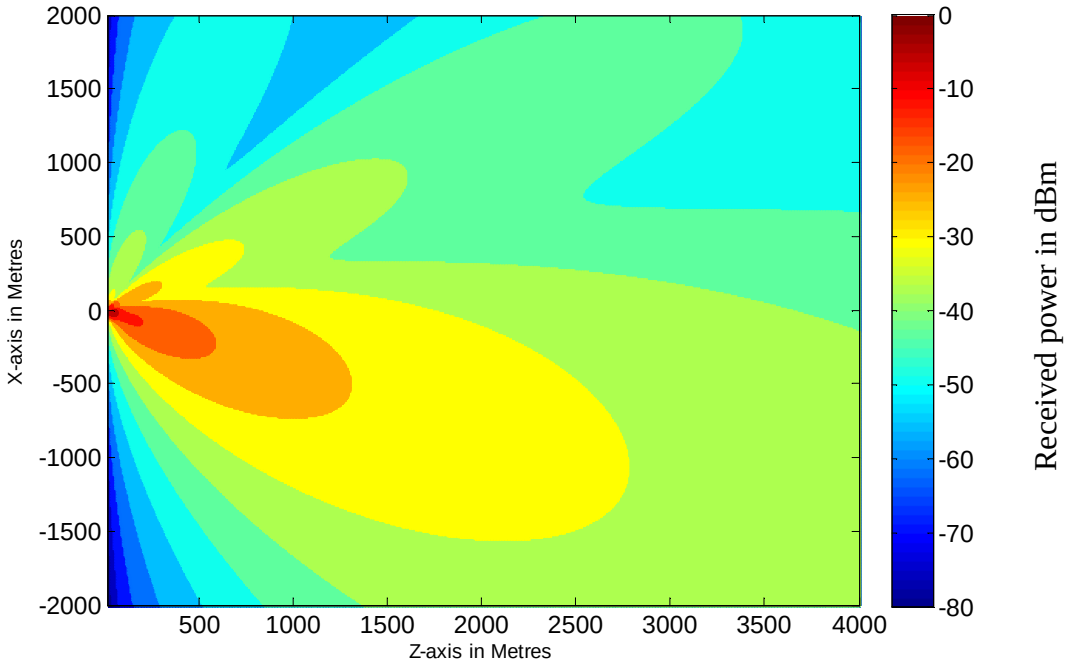

Fig.9.5: Right shaped beam footprint using free space propagation model

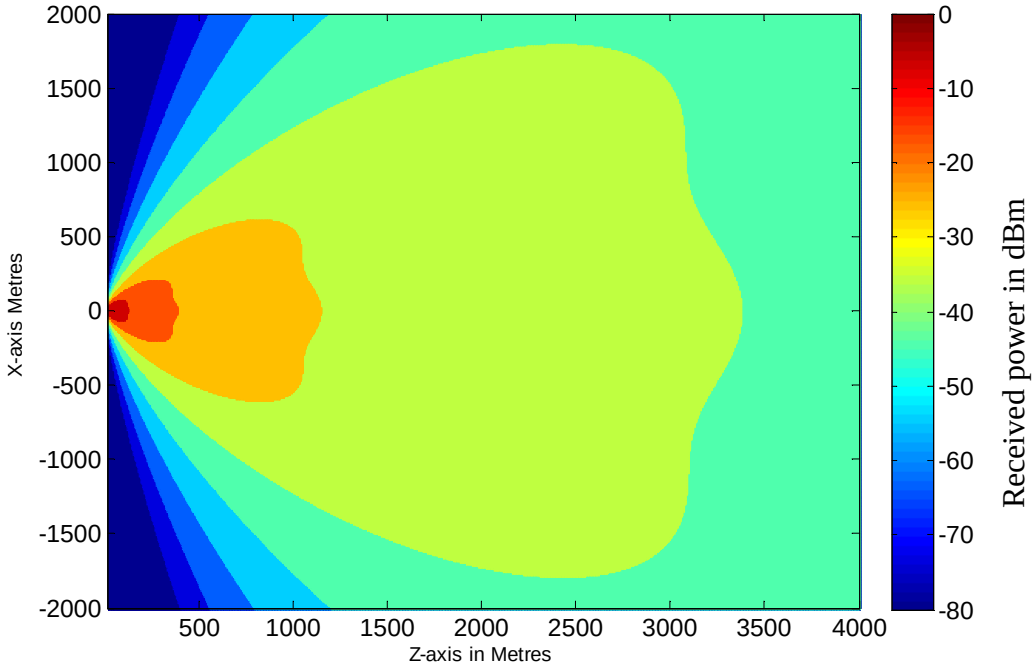

Fig.9.6: Broadcast channel beam footprint using free space propagation model

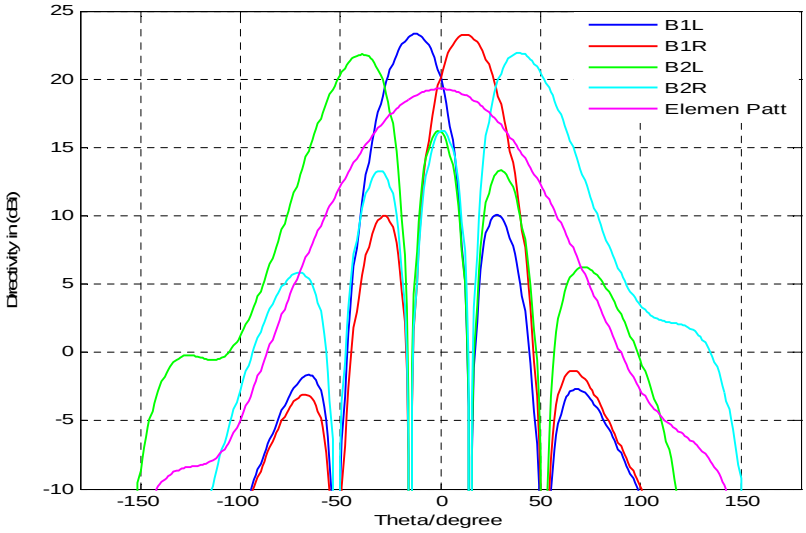

Fig.9.7: Narrow multiple beams @ downlink f_c

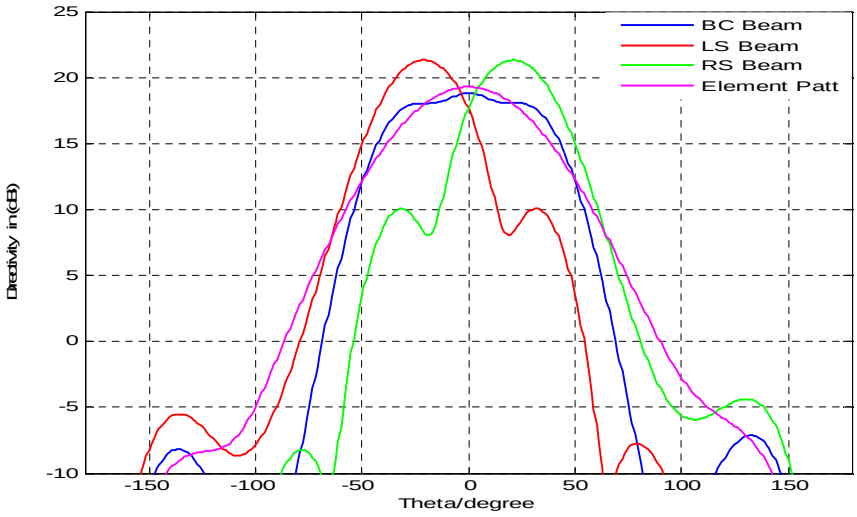

Fig.9.8: Shaped beams @ downlink f_c

The plots of Fig.9.3 through Fig.9.6 show received power footprint contours in the downlink UK orange frequency band when a +40dBm power is input into the antenna placed 30meters above the ground with an area size of 4km x 4km. Note that polarisation effects have been ignored and a total power radiation pattern has been used. It is observed that for the multiple beams Fig.9.3 (B1L), the -20dBm and the -30dBm contours are quite concentrated "spots" on the middle of the ground while the -40dBm contours is spread over a wide area. Conversely, Fig.9.6 shows the broadcast channel beam (BC beam), which spreads its power over the defined ground area while Fig. 9.5 for the shaped beams shows that the -30dBm, -40dBm and the -50dBm contours give a good coverage on the whole of the right hand side while still maintaining some coverage on the remaining part of

the sector. The contour plots show the overall coverage produced by each beam in the field of view. The colour of each pixel corresponds to the signal level on the ground. These plots are useful for identifying overall coverage extent of an antenna system. The shaped beams give enhance coverage in the subsector of the sector while still giving some amount of coverage at the other part of the sector.

9.3.1.2 Urban- Propagation Models

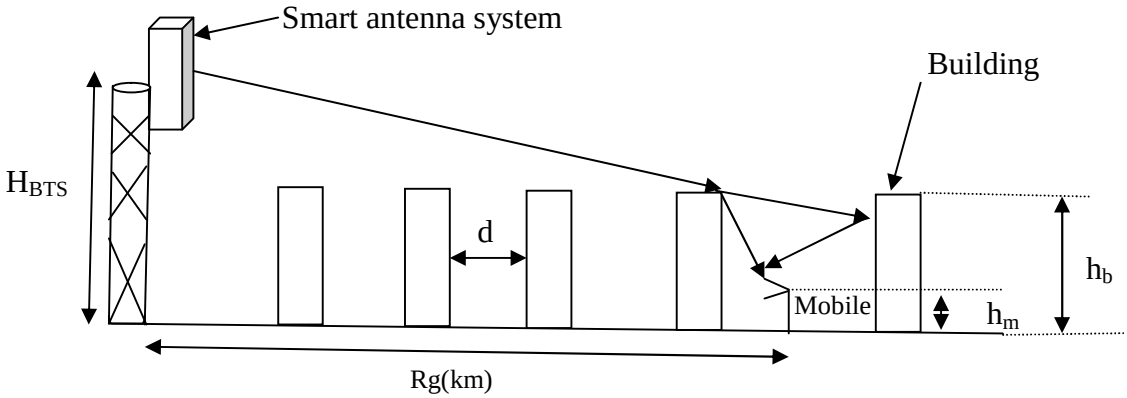

Fig.9.9: Urban propagation environment

To predict the received power footprint contours that can be provided by this antenna system for an urban environment the following assumptions have been made: the buildings in the environment are in a row and the building are separated by the equal distances, the buildings are the same height (average building height of 15meters and average building separation distance of 50meters), the base station is 30meters high, the mobile user antenna height is 1.5meters, and the COST259 model was used to predict the total transmission loss of the system [52]. The propagation model for a typical macro-cell urban environment is defined by [52, 147]:

$$PL[dB] = L_d dB + L_{slow} dB + L_{fast}\ dB \quad (9\text{-}2)$$

Where PL is the total path loss, L_d is the distance dependent loss in a built environment, L_{slow} is slow fading and L_{fast} is the fast fading.

$$L_d = L_{fs} + L_{msd} + L_{rts} \quad (9\text{-}3)$$

Where L_{fs} is free space propagation loss, L_{msd} is multiple screen diffraction loss and L_{rts} is rooftop to street loss.

$$L_{rts} = 10log\left(\frac{\lambda}{2\pi^2 r}\left(\frac{1}{\theta} - \frac{1}{2\pi+\theta}\right)^2\right) \quad (9\text{-}4)$$

$$\theta = tan^{-1}\left(\frac{\Delta h_m}{x}\right)$$

$$r = \sqrt{(\Delta h_m)^2 + x^2}$$

Δh_m is the difference between the height of the building and the mobile antenna height and x is the horizontal distance between the mobile and diffracting edges.

$$L_{msd} = 10log\left({Q_m}^2\right) \quad (9\text{-}5)$$

Where Q_m is a factor which dependents on the relative height of the base station antenna. For a base station antenna height above rooftop level,

$$Q_m = 2.35\left(\frac{\Delta h_b}{R}\sqrt{\frac{d}{\lambda}}\right)^{0.9} \quad (9\text{-}6)$$

Δh_b is the difference in height between base station antenna height and the building height and d is average separation between buildings.

Slow fading is caused by shadowing from buildings, mountains, hills and other obstacles in the front of the direction of signal propagation. The modelling of the effects of slow fading in wireless communication is very important as it causes the received SINR to change drastically over a large time scale. Slow fading is modelled as a log-normal distribution (additive white Gaussian) with 10dB (σ) standard deviation and a mean (μ) of zero. Additive white Gaussian is assumed to have followed a log-normal distribution as a Gaussian random variable [25].

Fast fading is due to multipath propagation of the transmitted signal (scattered electromagnetic wave) and it is modelled using a Rayleigh distribution with a random component. The total fading which is due to fast fading and slow fading is assumed to be 10dB for the investigation [25]. Fig.9.9 shows the propagation path loss versus distance for an urban environment.

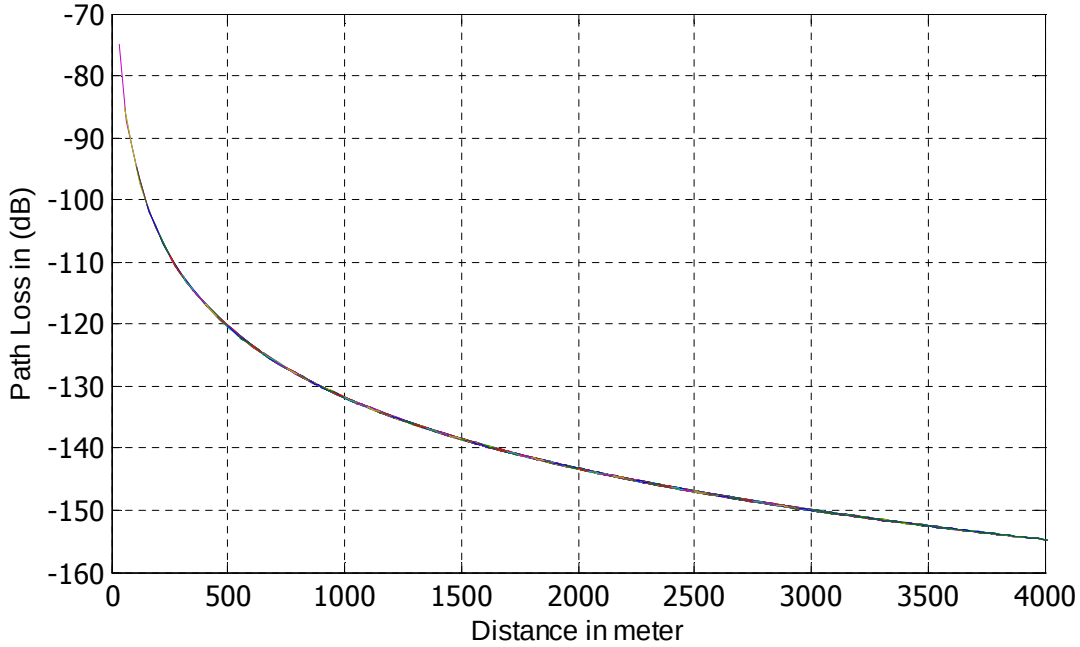

Fig.9.10: Urban propagation path loss versus distance

Fig.9.11, through Fig.9.14 depict the received power footprint contours for two narrow beams, a shaped beam and the broadcast channel beam that occur when the antenna is mounted 30meters high above the ground in an urban macro-cell area of 4 km x 4 km for a mobile telecommunication network. The plot shows that as the electromagnetic waves propagate through urban areas with multiple buildings arranged along the signal path the propagation path loss is greater than in free-space (see Fig9.10 shows the propagation loss versus distance using a macro cell propagation model). The received power footprint contour plot for shaped beams (right shaped) using a macro cell propagation model shows that it provides subsector coverage enhancement while still providing lower, but acceptable coverage for the remainder of the cell sector.

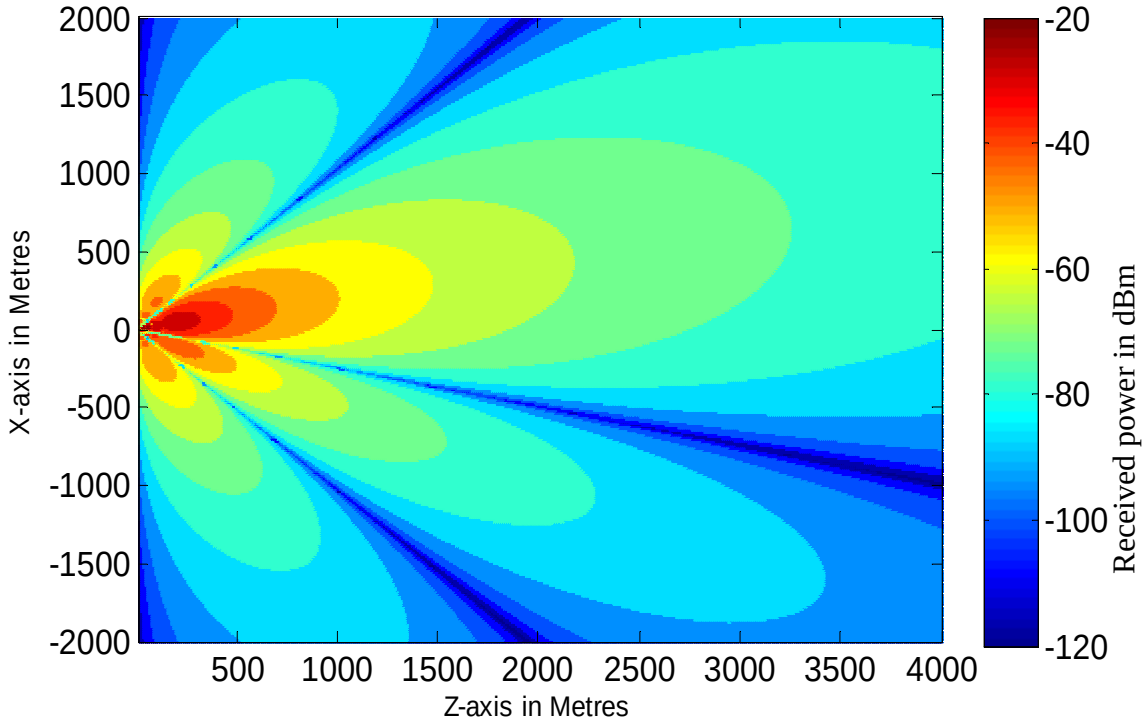

Fig.9.11: Beam1L footprint using urban propagation

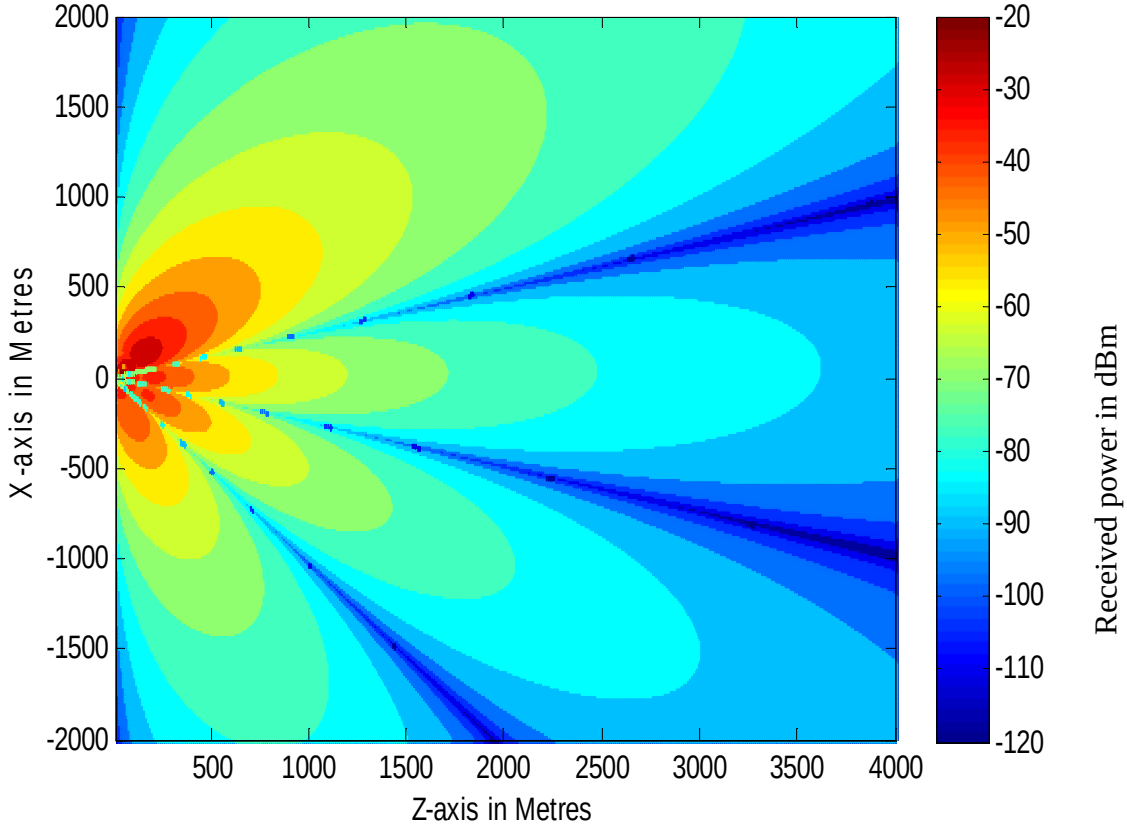

Fig.9.12: Beam2L footprint using urban propagation model

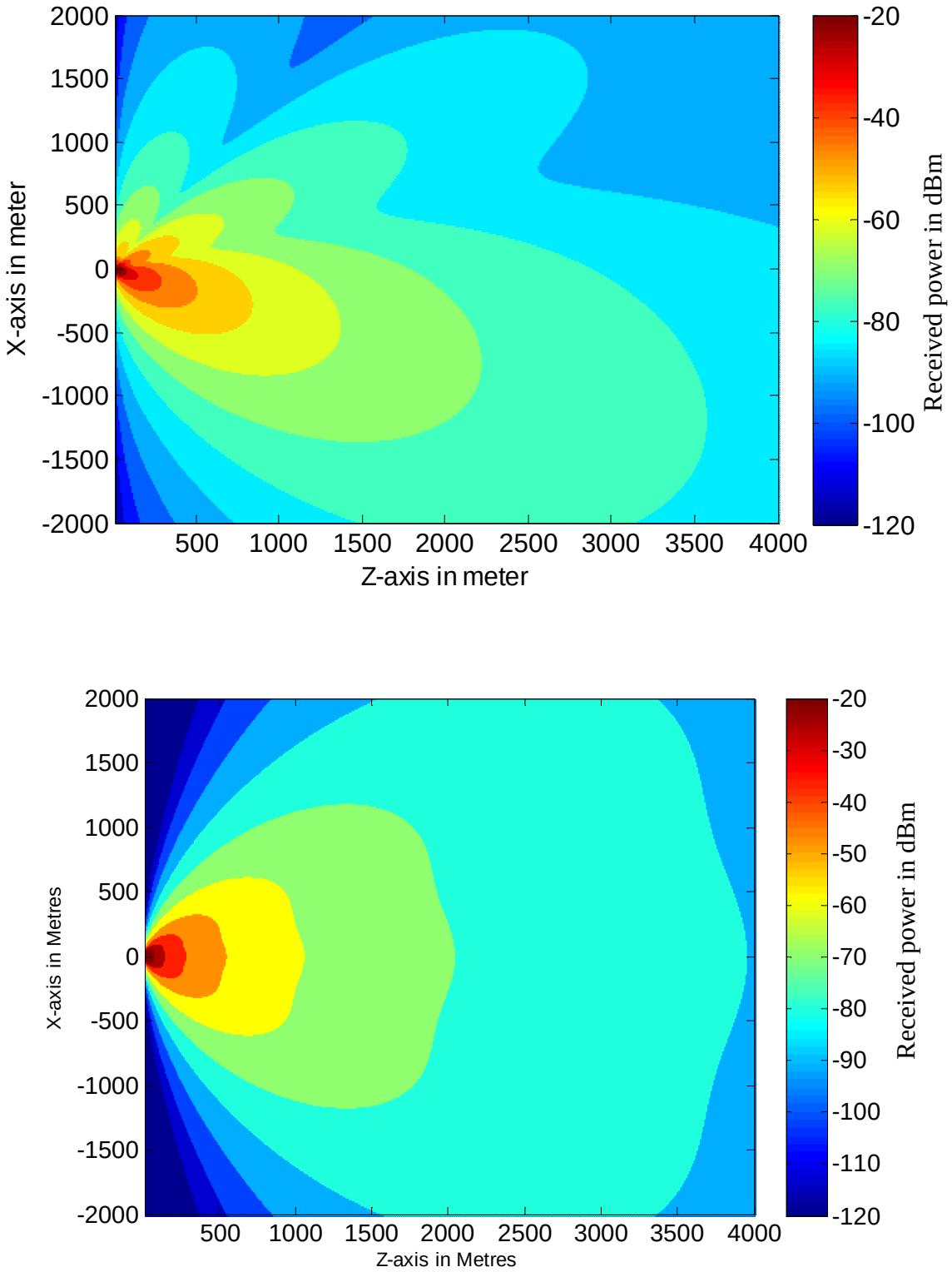

Fig.9.14: Broadcast channel beam footprint contour using urban propagation

9.3.2 Smart Antenna System Coverage versus Capacity Estimation

Spectral efficiency or bandwidth efficiency measured in bit/s/Hz is an important performance figure of merit for characterizing a communication system. Shannon's channel capacity theorem reveals that there is a maximum spectral efficiency or bandwidth efficiency which is called the channel capacity, at which any communication system can operate reliably [148-149]. In other words radio capacity is a parameter which measures spectral efficiency of a wireless system. This parameter is determined by the required signal-to-noise-ratio and the channel bandwidth [25]. The antenna is an important component in a radio communication system and it dominates the overall radio frequency system performance. It is therefore very important to examine the information capacity that an antenna system can consistently transmit in relation to its coverage distance which constitutes the main issue of this research. The capacity of a transmitting antenna based on the Shannon channel information capacity theory is given by [148-150]:

$$C = BLog_2[1 + \frac{S}{N}] \quad (9\text{-}7)$$

Where C is the capacity in bits per second, *B* is the channel bandwidth in Hertz and S/N is the signal-to-noise-ratio.

Applying this Shannon channel capacity equation together with urban propagation model, and assuming the channel bandwidth to be 5MHz, thermal noise density to be -174dBm/Hz, antenna height of 30meters, antenna input power of +40dBm and coverage area of 4km x 4km the channel capacity was computed. Fig 9.15 below shows the capacity in Mbits/s footprint contour for the right hand shaped beam (RS beam) of the smart antenna system and Fig.9.16 is the plot that shows the RS beam capacity in Mbits/s variation with coverage when taken through the beam diagonal. Fig.9.17 shows capacity in Mbits/s footprint contour of a conventional sector antenna with a gain of 17.5dBi and Fig.9.18 is the capacity variation with coverage of conventional sector antenna when taken through the diagonal of the beam. The capacity of the RS beam is concentrated on the right hand side of the specified area while the capacity of the conventional sector antenna is spread all over the specified area.

The capacity footprint contour of the shaped beam again confirms that with this smart antenna system, coverage and capacity can be enhanced in a sub-sector where there is high demand while still maintaining some capacity in the remaining area of the sector.

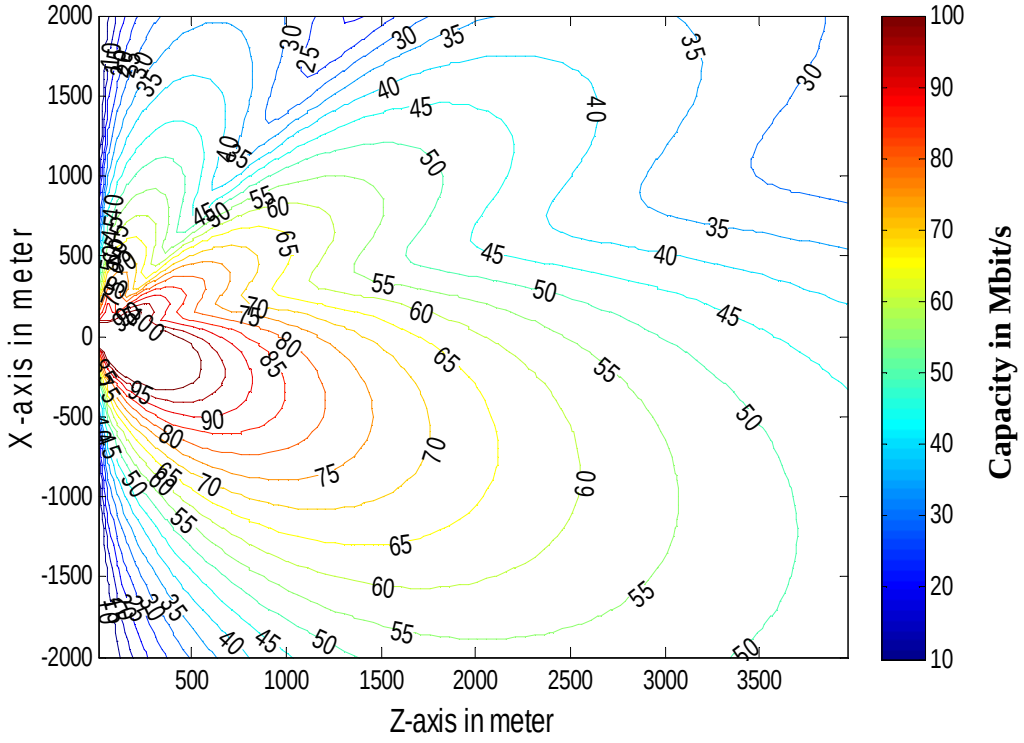

Fig.9.15: RS beam capacity footprint contour using urban propagation model

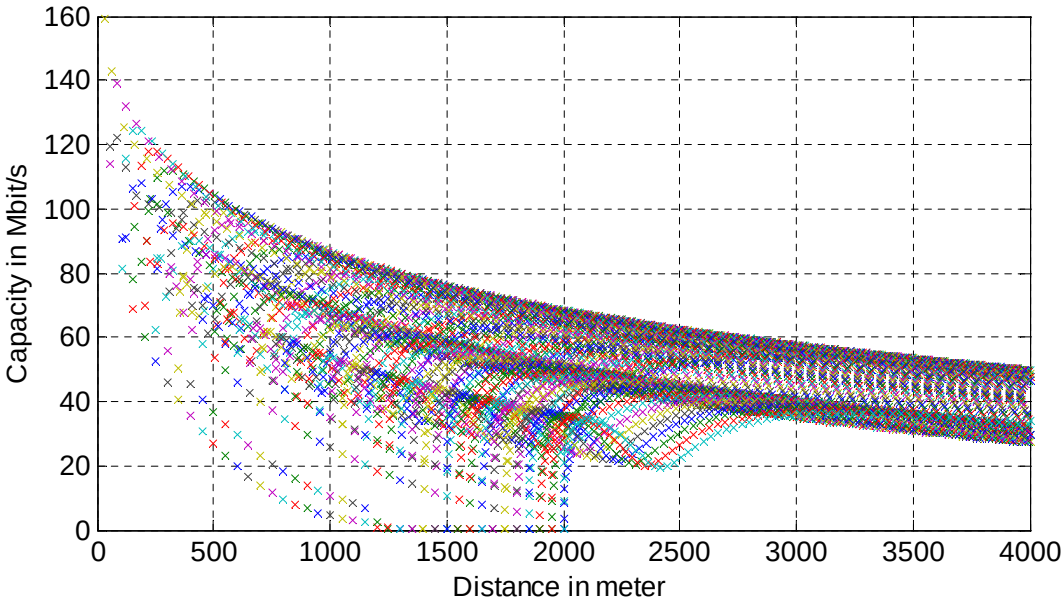

Fig.9.16: RS beam capacity variation with distance using urban propagation model

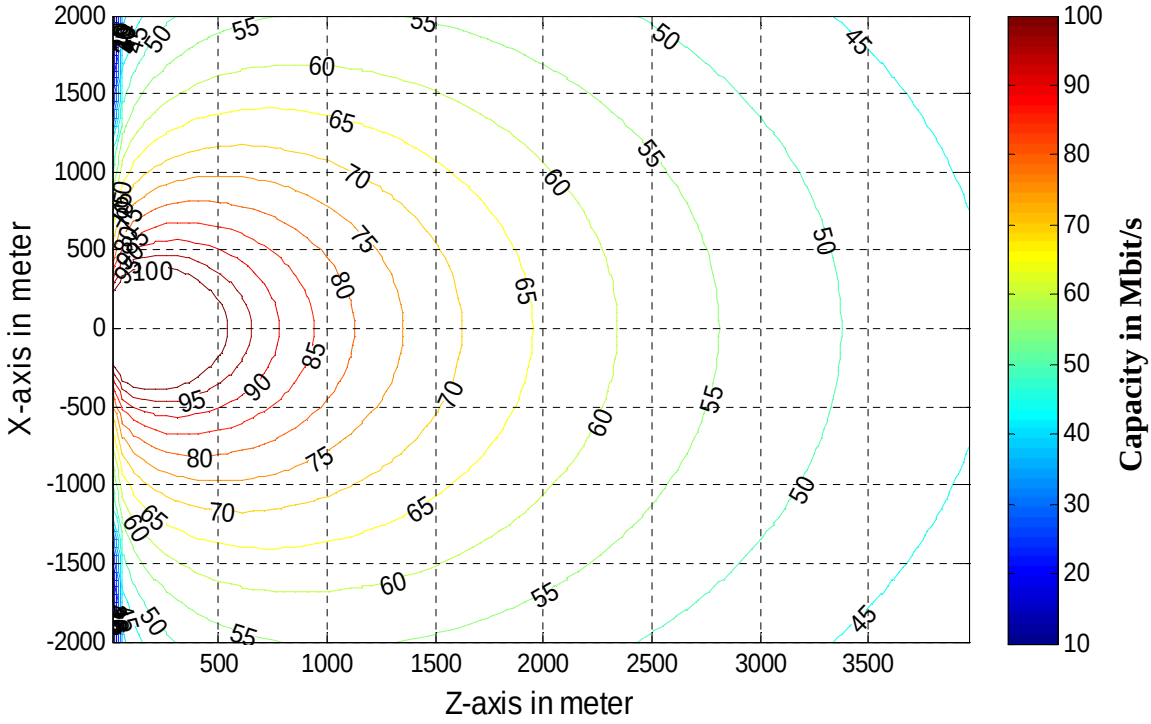

Fig.9.17: Conventional sector antenna beam capacity footprint contour using urban propagation model

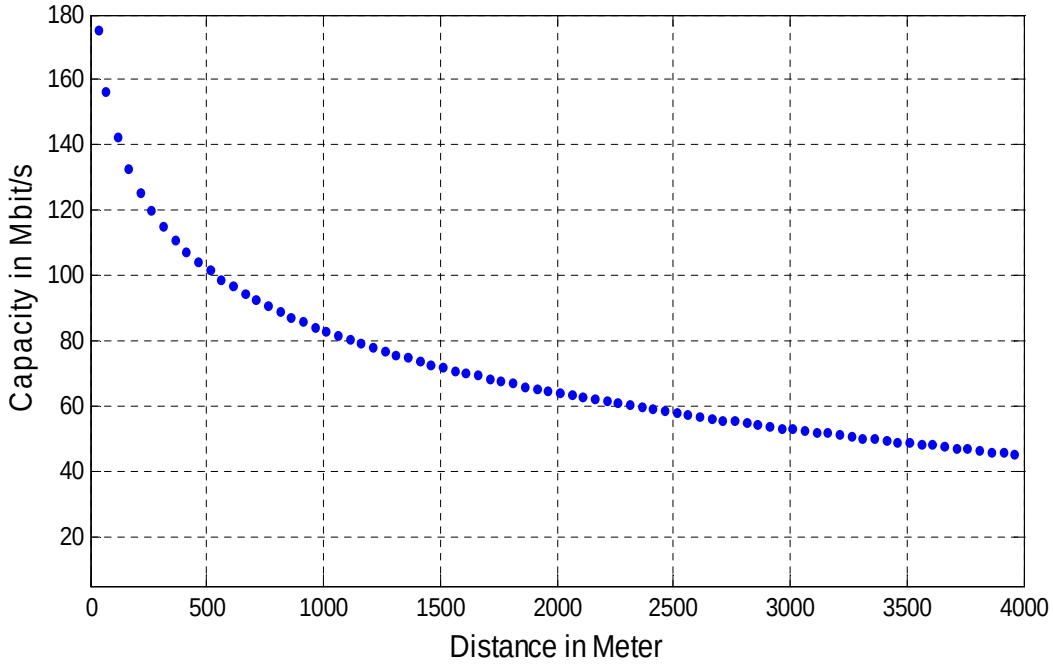

Fig.9.18: Conventional sector antenna beam capacity variation with distance using urban propagation model

9.4 Summary

This chapter have detailed the predicted coverage and capacity in terms of received power footprint contours the smart antenna system offers when used in free space and an urban propagation environment. When the buildings in an urban environment are uniformly spaced 50meters apart with an average height of 15meters, the propagation loss compared to that of free space is much greater. The multiple buildings environment has significant effects on the beams' received power footprint contours modelled by the COST259 propagation model. The shaped beams received power footprint contours demonstrate the advantages that a mobile telecommunication network provider would obtain by dynamic selection of the various beams of the smart antenna system to provide dynamic sub-sector capacity enhancements. This chapter has demonstrated the importance of the subject smart antenna system to dynamically enhance capacity of a sub-sector and thereby maintain capacity and traffic load balancing especially in hotspots of wireless communication networks. The research has also shown the relationship of coverage and capacity of antenna. The next chapter will detail how this smart antenna system can be strategically used in mobile telecommunication network.

Chapter 10 - NETWORK PLANNING STRATEGY

10.1 Introduction

The aims of network planning and optimisation for a 3G network system are to provide connections anywhere anytime and support a high data rate demanded by subscribers. However, 3G network planning and optimisation is more complex compared to 2G radio network planning and optimisation because of a new air interface, new technologies (e.g., MIMO and smart antennas), mixed services (voice, video and data traffic), co-existence of different radio access technologies, growing importance of indoor coverage and multi-dimensional interdependent optimisation problems. Previous chapters have provided details of the design, construction and testing of a dynamically reconfigurable novel smart antenna system. This chapter provides a review of current network planning strategies and basic network planning procedures in 3G network systems and investigates how the deployment of the subject novel smart antenna system can be used to improve 3G radio network system performances.

10.2 Current 3G Radio Network Planning Strategy

The existing UMTS (3G) radio network planning and optimisation strategy starts by first analysing the radio network configuration and then defines the needs of a UMTS network for a certain geographical area before actual planning is started. In this planning strategy work the overall layout of the radio network, the BTS, that is the antenna heights, site density and the traffic growth path are decided upon in order to reach the optimal network configuration for coverage, capacity, and service quality [152]. The next stage of the strategy is to define the UMTS network major topology or layout (macro, micro and pico) in order to define the radio propagation environment and to fix network planning principles. The major technical definitions of the radio network can be made after defining the propagation environment of the radio network. These include the conventional cellular concept and new technologies such as Multiple Input Multiple Output (MIMO) concepts and the smart antenna concept [152]. The following section will present an overview of the 3G radio network planning process.

10.3 Overview of Radio Network Planning Process in 3G

The overall objective of radio network planning and optimisation is to provide the required coverage, capacity and quality of service with minimum equipment. Radio network planning procedures include dimensioning, detailed planning and optimisation. However, detailed planning in GSM which includes configuration planning, coverage planning, capacity planning, frequency planning, and parameter planning and their content must be adjusted for 3G. The 3G radio network has been developed mainly to support new data services including higher and variable data rates (multiple services like speech and internet and high data rate interactive services). All subscribers operate on the same frequency and coverage and capacity are interdependent. This is a clear difference to GSM mobile telecommunication networks where coverage prediction and network capacity are independent. Therefore, the rules and algorithms for dimensioning and optimising 3G networks are typically based on the interference characteristics [65, 152-153]. Fig10.1 shows the 3G radio network planning and optimisation process. The following sections will give brief details of each stage of the radio network planning and optimisation process.

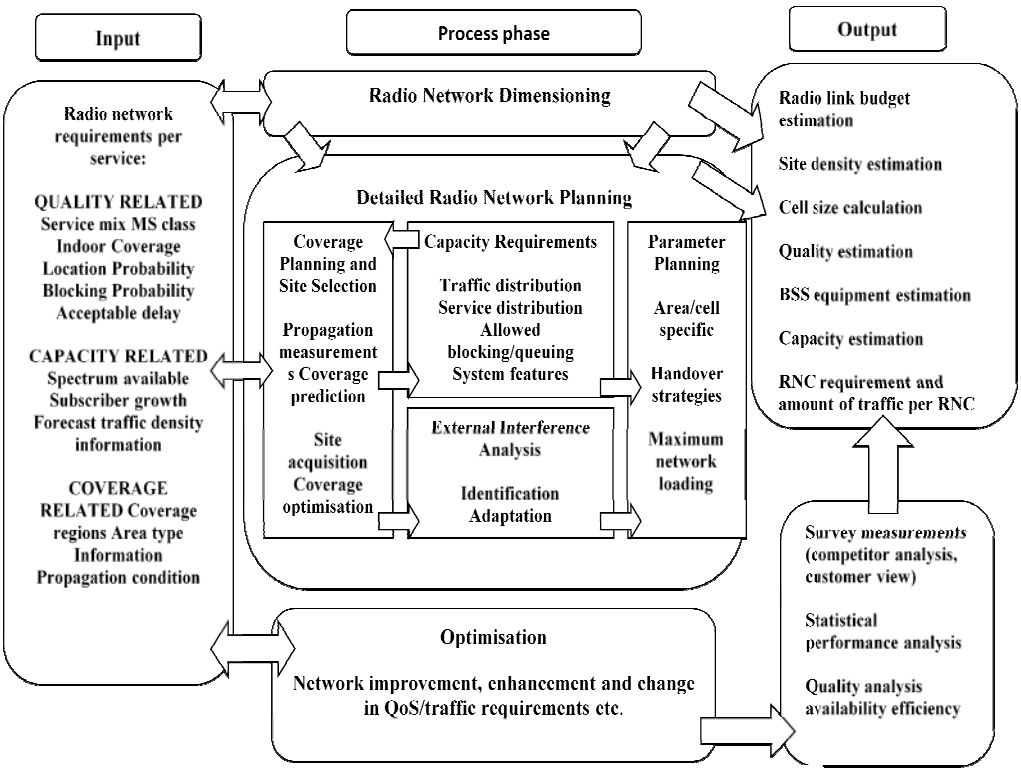

Fig.10.1: Radio network planning and optimisation process [160]

10.3.1 Dimensioning

Dimensioning, which is also known as initial planning, provides an estimation of the equipment needed to provide coverage, capacity, and quality of service required to initiate operation of the network. The aim of the initial planning phase is to calculate the required site density and configuration type for the area of interest. Dimensioning activities can include coverage analysis, capacity evaluation, an estimate of the number of base station transceivers on the site, radio network controller equipment requirements, service distribution definition, traffic density estimates, traffic growth estimates and quality of service (Q0S) requirements in terms of blocking and coverage probability. The capacity requirements of different cell sites during the initial planning phase can be determined by utilizing the standard load equation for link budgets [65]. The link budget takes into account the base transceiver station antenna gain, diversity gain, the cable losses and fading margins when evaluating the uplink and downlink of the radio network. The radio link budget output is the maximum allowable propagation path loss calculation (dependent upon capacity) which in turn determines the cell range and the number of sites needed for the radio network. Interference margin, fast fading margin, transmit power and soft handover are some of the specific parameters in the radio link budget of the WCDMA air interface [65, 152-153].

10.3.2 Detailed Planning

Radio network detailed planning can be divided into configuration planning, topology planning, code planning, and parameter planning. The network is practically ready once the radio network detailed planning process is completed. The aim of configuration planning is to find the optimum configuration of the BTS in each site in the planning area. There are several factors to be considered when doing configuration planning which include: propagation environment (macro, micro, pico and indoor cell), site characteristics, required coverage and capacity and the impact of BTS antenna configuration on interference and network capacity. The output of the configuration planning is a detailed BTS configuration and a list of the base station and corresponding antenna line equipment being specified and maximum uplink and downlink path loss information for coverage prediction. The final configuration phase of the radio network elements is the topology planning or network layout phase. The BTS site configuration includes definition of the site locations, antenna sectoring, antenna orientations, and antenna heights [65, 152-153].

The scrambling codes and parameters planning is a very important stage of detailed planning in the radio network planning process. The major reason for planning parameters

is to optimise the usage of the radio network and to fully utilise the planned coverage and capacity. The parameters that are planned can include admission, load, power, handover control and packet scheduling etc. In the case of scrambling codes, the main work for network planning is allocation of scrambling codes for each BTS downlink direction in order to separate them. The code planning is straightforward as a planning tool typically allocates the scrambling codes automatically to each base transceiver station [65, 152-153].

10.3.3 Optimization and Monitoring

Detailed planning of the radio network requires careful performance verification before launching the network for commercial use. Detailed planning is based on system-level simulations including a number of assumptions and approximations. The optimisation and monitoring is to verify that the planned coverage, capacity and quality of service has been reached with efficient resource usage and whether the key performance indicators (KPI) are met. These KPIs are parameters that need to be checked closely while the network monitoring process is going on. Radio network performance is usually verified using KPI monitoring and radio interface measurements provided by the network management subsystem. Generally, after the WCDMA network is fully launched for commercial use, the network is still constantly optimised and monitored because of subscriber location and traffic behaviour which vary dynamically[65, 152].

10.4 Topology Layout

In order to outline how a smart antenna deployment can systematically increase capacity on a dynamic basis it is useful to provide details of the network topology for 2G and 3G systems because 3G may be deployed in areas where 2G service is already provided. The different base station layer structures such as the one shown in Fig.10.2 and the radio propagation environments must be defined first for the UMTS radio interface before the final site selection can be done. The required size of each base station coverage area must also be determined. In addition to the base station layout, the average base station antenna height for the network must be decided. In the early stage of the radio network development the network requires large coverage areas primarily just to cover areas which are known as macro cellular typical size of macro cell is 30km network topology where base station antennas are above the average building heights in urban areas. If there is a need to increase capacity for a dense urban area, most network providers use several micro cells typical size of micro cell is 500m. In this topology the base station antennas are implemented below the rooftop levels in order to avoid interference because the macro cell

topology is prone to interference from high buildings. The micro cell provides enough capacity for office blocks and shopping centres where special indoor systems are needed. Due to existing 2G networks, being available together, UMTS networks are typically implemented with the macro cellular approach [152, 154-155].

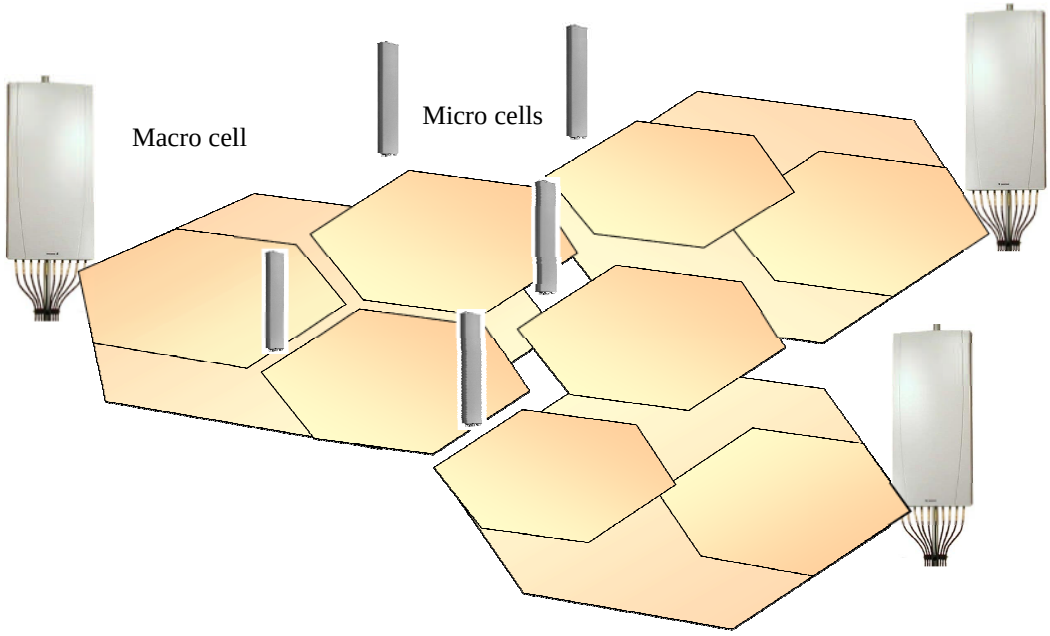

Fig.10.2: Macro and micro cells of mobile telecommunication network

The base station antenna configuration is another important issue in radio network planning. The most conventional layouts for cellular network topology are formed by equally spaced hexagons with the base stations placed in corners of an imaginary hexagon with fixed antenna directions [156]. Three-sectored configurations are preferred in the first stage of UMTS network planning in order to minimise antenna costs; but, later on during the operation of the network six-sectored antenna configurations can be used because they offer significantly higher capacity. It is essential to have a planning strategy, site locations and antenna configurations for changing the network from a three-sectored to a six-sectored configuration with a minimum change in radio network functionality as in soft handover areas.

10.4.1 Radio Network Planning with Conventional Antennas

A variety of antennas are available to be used on UMTS base station sites. Ideally, antennas are selected based upon planned site divisions into sectors as the sector overlapping needs to be kept at optimal level for best possible performance [156]. Generally, antennas that are used in a UMTS network are either dual-polar if polarisation diversity is employed or plane polar if spatial diversity is employed and dual-band (typically 2G & 3G) unless they are wideband in which case they cover both 2G and 3G. The antenna beam width that is commonly employed is 85 or 65 degrees with mechanical or variable electrical elevation down-tilt (VET). The antennas with variable electrical tilting are more expensive compared to other conventional antennas. Although they are more expensive, VET antennas give the greatest flexibility, allowing remote tilting of the sector antenna to enhance coverage in 3G mobile telecommunication networks. The use of directional antennas in a sectored base station configuration are shown to be an efficient method for increasing coverage and capacity of a cellular network system because of a reduction in interference in current 3G mobile telecommunication networks [65, 153 and 158].

10.5 Radio Network Planning with New Technology and Smart Antenna

Conventional radio network planning strategy for UMTS using a WCDMA air interface with conventional antennas must be modified if new technologies like standard smart antennas systems, Space Division Multiple Access techniques (SDMA) and Multiple Input Multiple Output (MIMO) systems are utilised in UMTS networks in the future. Smart antenna systems for mobile telecommunication networks [151] have different grades of complexity in terms of digital signal processing (DSP) and hardware implementation. When complexity is increased, system intelligence and performance are also expected to increase. All of these factors present new challenges for network planning in 3G. Identifying and overcoming the challenges of network planning for smart antennas will help to enhance coverage and maintain capacity in 3G mobile telecommunication networks. Fig.10.3 shows two basic smart antenna systems, fixed multiple beams and adaptive beam forming smart antenna solutions, for a mobile telecommunication network layout.

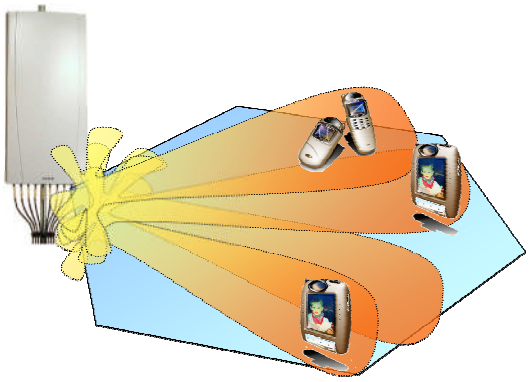

Multiple fixed beams smart antenna for a radio network layout

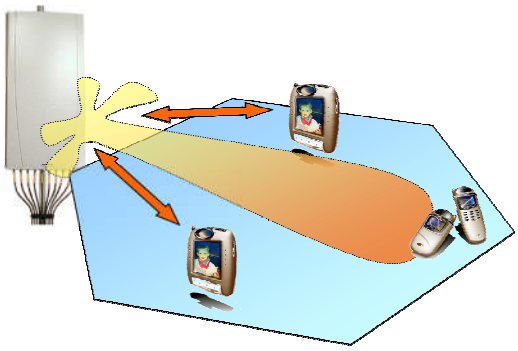

Fully Adaptive beam smart antenna for a radio network layout

Fig. 10.3: Smart antenna system in a macro cell of a mobile telecommunication

The fixed multiple beams system is less complex easier to implement and does not require major changes to the existing BTS or to radio network planning strategy although an increase in the number of transceivers is required. The impact on the system in terms of its ability to dynamically shape the coverage to follow the radio network user is also limited [15-16]. Fully adaptive beam forming systems require major changes to receiver structure in BTS implementation and also an increase in DSP intelligence. Although major changes are required to implement fully adaptive smart antenna systems in mobile telecommunication systems, system performance is significantly increased as the antenna beam can be directed separately for each network user, thereby reducing interference and maintaining a good SINR. Also, there is a need to change radio network planning and optimisation procedures because coverage area, capacity and handover are dynamic. However, this research has introduced a novel smart antenna system that can be used with the existing 3G radio network system with minimal changes to base station transceiver requirements. The next section will investigate the system performance using this novel smart antenna system over a conventional antenna system.

10.6 Investigation of the Novel Smart Antenna System Performance in an Existing 3G Mobile Network

To investigate the strategic deployment of this smart antenna system into mobile telecommunication networks to the optimum techno-economic advantage of mobile network providers, i.e. to identify the best locations for smart antennas in the radio network in the most cost-effective deployment, there is a need for a radio network planning and optimisation tool. A radio network planning and optimisation tool is the main tool used by network operators in planning and optimising their network daily. It consists of a digital map with properties such as projection and ellipsoid, target planning area, selected radio access techniques, input parameters for calculations and antenna models. For 3G mobile telecommunication networks, some mobile network vendors have suggested a stepwise strategy for deploying smart antennas for optimum techno-economic advantage. The vendors first step strategy is coverage driven which is used for the initial network deployment. They suggested that smart antennas should be used only in the network uplink to reduce the number of base station sites. The reason is that, for a lightly loaded radio network, the cell range is mainly limited in the network uplink by the mobile terminal's power. In this strategy, the cost of smart antennas can be easily compensated for by savings in the base station equipment and site leasing cost and the cost of fighting protests from people living nearby who do not want a mobile tower installed close to their homes. In the second step of the vendor strategy, smart antennas should be introduced in the downlink when the traffic load in the network becomes heavy and the downlink power becomes the capacity blockage [67]. However, the network vendor strategy does not cover the situation when the network cell is experiencing unexpected high concentrations of mobile users, i.e. a situation where the network is experiencing traffic imbalance in both uplink and downlink of the radio network.

Orange UK is one of the leading providers of mobile telecommunication networks. The company's spectrum sub-bands have been used as a practical example to design, simulate and implement this smart antenna concept. Its network parameters and Glasgow city centre map have been used for this radio network planning and optimisation tool to investigate the best location of the subject novel smart antenna in the radio network for optimum techno-economic advantage.

10.6.1 Simulation Results

In this project, work has been undertaken in conjunction with Orange UK to demonstrate how the antenna design described here can be used to enhance capacity and improve coverage. As a benchmark result, shown in Fig.10.4 is the coverage plot of a standard sector antenna of 115^0 10dB beam width placed in a macro cell sector of 120^0 downlink in Glasgow city centre and excited with 40watts of power. This antenna is mostly used to cover busy areas of the mobile telecommunication network especially hotspots of the network. Fig.10.5 and Fig.10.6 are the coverage plots of the subject smart antenna beam 1R and beam 2R, also placed in a macro cell sector of 120^0 downlink in Glasgow city centre and excited with 40watts of power. The received power levels are set at default, -58dBm is the highest level and -110dBm is the lowest level. The pink colour indicates the highest received power level on the ground, followed by red, yellow, light green, and light purple is the lowest power level. Also shown on Fig10.4 is an illustration of the sectors within the cell. It can be seen that with a conventional sector antenna there is a significant overlap with adjacent sectors and interference suppression is only through perfect orthogonality of digital codes.

This can be compared with the use of the proposed antenna which can be switched to individual high gain beams. Results shown in Fig10.5 and 10.6 demonstrate the reduced overlap between sectors while providing desirable coverage over the full sector. Additionally, as all subscribers within a sector utilise the whole frequency spectrum, the SINR will be reduced for standard antennas. This can be illustrated with reference to Fig.10.4 where it can be seen that for a conventional antenna the coverage pattern will mean that a strong signal will be received from widely separated interfering subscribers in addition to the wanted signal from the desired user. This will result in an overall lowering of SINR.

This situation can be compared to the situation with the proposed antenna as shown in Fig10.5 and 10.6 where the use of dynamically reconfigurable narrow beams leads to a much reduced level of interference from unwanted subscribers and an increase in SINR. Hence, the subject smart antenna will suppress interference both through orthogonality of digital codes and spatial suppression offered by the narrow beams. The four narrow beams of the subject smart antenna can be reconfigured to produce a shaped beam shown in the plot of Fig.10.7 thereby enhancing sub-sector coverage and maintaining capacity for high

data users in that sector area at the expense of slightly reduced gain compared to the narrow beam mode of operation.

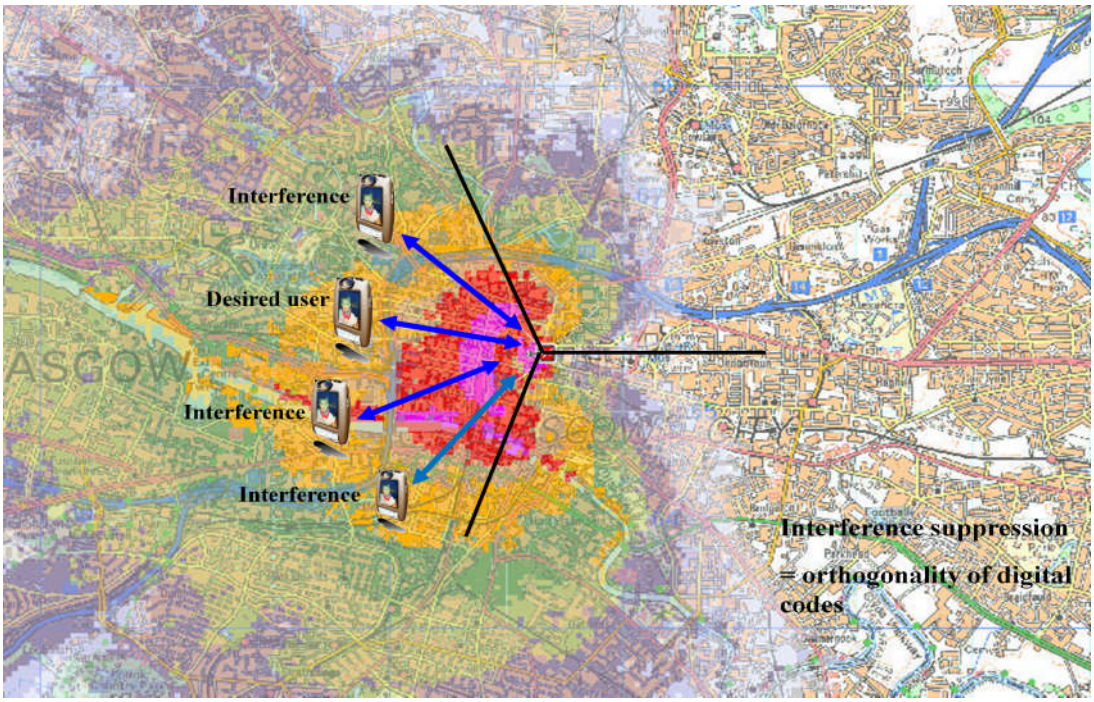

Fig.10.4: standard sector antenna coverage plot

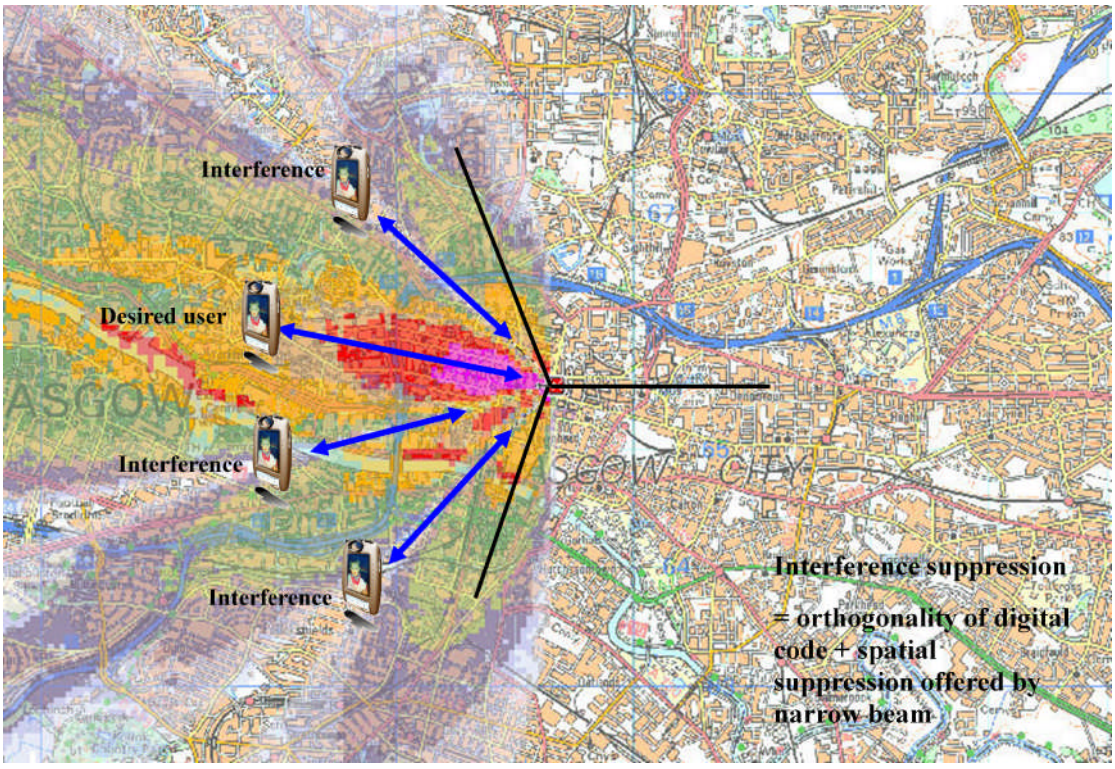

Fig.10.5: Subject smart antenna coverage plot typical beam1R

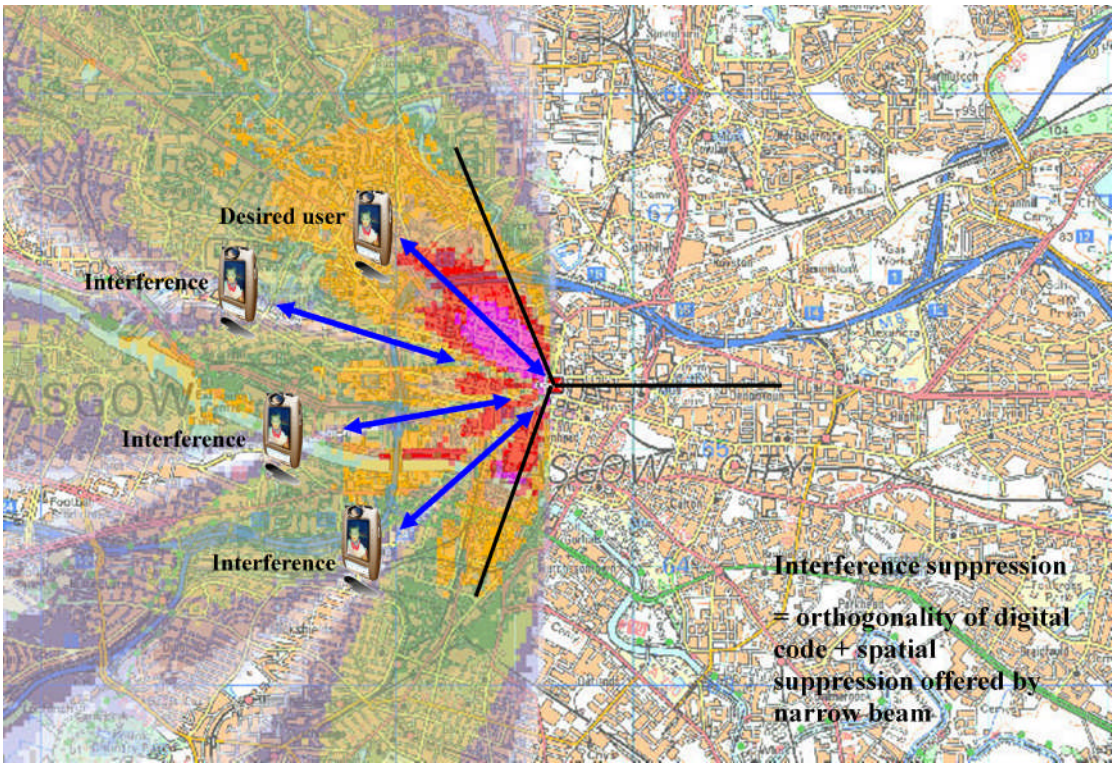

Fig.10. 6: Subject smart antenna coverage plot typical beam2R

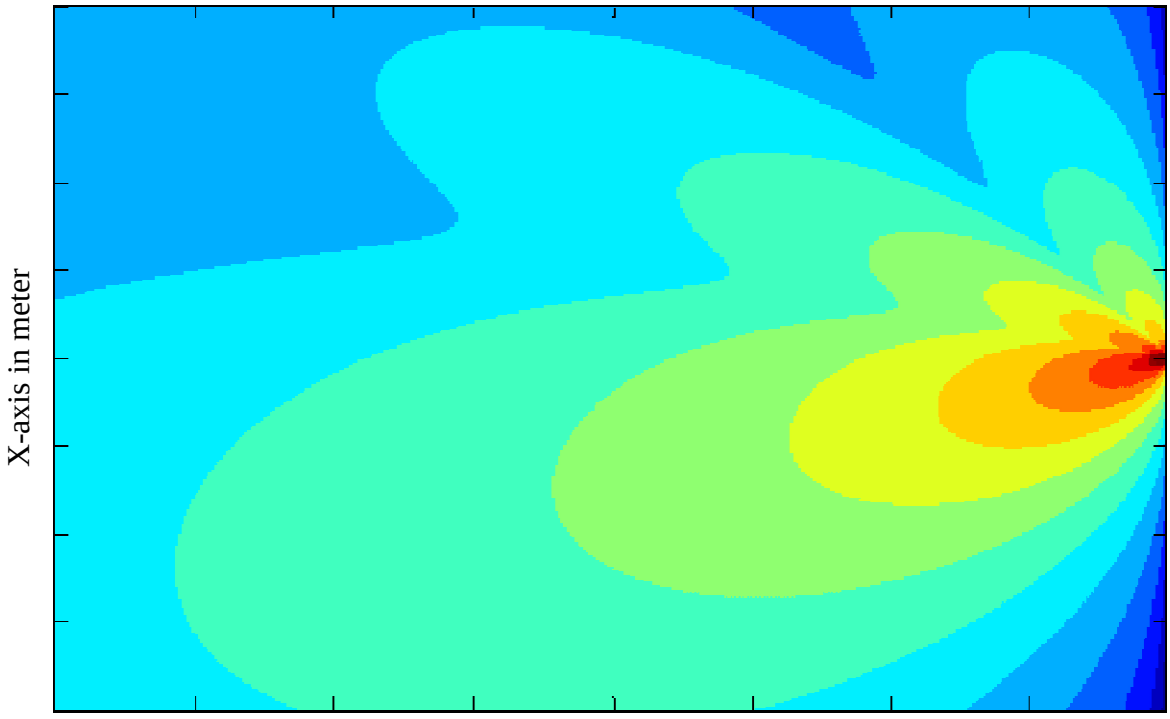

Fig.10.7: Subject smart antenna left hand shaped beam coverage plot

10.7 Summary

The key problems of mobile telecommunication networks and the conventional techniques to minimise the problems have been highlighted in this thesis. Smart antennas have also been reviewed as a promising technology that can mitigate the current problems of mobile telecommunication networks which include: interference impairment and traffic load imbalance especially in hotspot areas of mobile networks. The importance of smart antenna deployment in the overall mobile telecommunication cell plan has also been highlighted. This chapter has reviewed 3G radio network planning strategy and planning procedure. Challenges of cell planning for smart antennas have been identified, including size and receiver structure. These drawbacks have been the major reason why most mobile telecommunication network providers have not installed smart antennas into their networks. A novel smart antenna system has been introduced that can be used with the existing resources, base station electronics without increasing the number of transceivers of mobile telecommunication networks and is cost-effective when shaped beams are utilised.

Using a commercial radio network planning tool, coverage plots of the novel smart antenna system have been shown in this chapter. The result shows that better range and focus can be achieved using this smart antenna system. Since coverage and capacity in 3G are interdependent due to interference when employing standard sector antennas it can be deduced that the smart antenna system employing either multiple narrow beams or shaped beams thus reducing interference will offer better benefits to network providers compared to conventional directional sector antennas.

Chapter 11 - CONCLUSIONS AND FUTURE WORK

11.1 Conclusions

Over the last few years, mobile telecommunications has experienced rapid growth in the number of subscribers for voice services, high data rate mobile multimedia services and traffic load imbalance. To accommodate the current demand for services from mobile communication users and traffic load imbalance, research into new intelligent or self-optimized and highly efficient systems is on-going. Smart or adaptive antennas have emerged as the promising technology to enhance the spectrum efficiency and solve the problem of imbalance in traffic load of present and future mobile telecommunications systems by dynamically exploiting the spatial domain.

Therefore, the main objective for studying the subject smart antenna system for use in mobile telecommunication networks is to exploit its potential in addressing the coverage, capacity and traffic load balancing in cost effective ways. The research reported in this thesis supports this fundamental objective by investigating and analysing the use of a smart antenna system in a mobile telecommunication network as an improved performance alternative to the current conventional antenna systems and traditional techniques of increasing coverage and capacity and traffic load balancing. This work describes an investigation into the performance of antennas for mobile base station applications and techniques for improving the coverage and capacity within a base station cell sector.

The motivation behind this research is to overcome the performance limitations of conventional antenna systems and techniques for solving the problems of coverage and capacity in hotspots of mobile telecommunication networks. The smart antenna has been proven to overcome the limitations of conventional antenna systems and techniques to enhance coverage, capacity and traffic load balancing, but not without its own shortcomings. A full multipl*e* fixed beam smart antenna (which is the simplest of the smart antenna family) needs separate transceiver chains for beam port and a fully adaptive smart antenna needs accurate real–time calibration. Also, the adaptive antenna beam-forming is computationally rigorous which means that smart antenna base stations must be equipped with very powerful digital signal processors which leads to a substantial increase in the cost of the system [45] which cannot be justified in terms of improved system capacity, Switched beam smart antennas could be implemented, but it is hard to incorporate the

antenna receiver structure into the mobile telecommunication base station electronics which increases complexity and cost and cannot provide any beam shape flexibility.

To be able to achieve the objectives of this research, the fundamental principles of mobile telecommunication networks, smart antenna systems and its building blocks had to be reviewed and discussed. It started by tracing the development of mobile systems, both in technical and commercial terms, from the earliest analogue systems to present day broadband systems and included anticipated future developments in chapter two. The chapter reviewed the current mobile communication network architectures (GMS and UMTS), challenges of the current mobile communication networks and identified the limitations of 3G networks. The fundamentals of smart antennas, benefits and cost/performance trade-offs were identified in chapter three. Smart antennas have the ability to provide enhanced range and capacity leading to reduced infrastructure costs in early deployments, enhanced link performance as the system is rolled out, and increased capacity in overloaded 3G networks. Smart antennas can enhance coverage and capacity simultaneously in 3G which cannot be done with conventional sector antenna systems for which coverage and capacity are inter-dependent.

Following this, chapter four presented the modelling and analysis of the new smart antenna concept which included multiple beam-forming and beam shaping methodology. Conventional multiple switched beam smart antennas require separate transceivers at each beam port to enable all the beams to be active simultaneously. The novel feed network to enable the smart antenna system to use one transceiver per polarisation was also introduced in chapter four. This network blends the narrow beams if the number of users within sector increases and also shapes the beam to enhance capacity in a sub-sector and maintains capacity in the remainder of the sector. In chapter five, the design of the major building block of the new smart antenna system were presented. The array antenna element, the array type, beam forming network and beam shaping network was discussed. The array element is a slant $\pm 45^0$ dual-polarised stacked patch antenna for simultaneous transmit/receive application. This design is an alternative to the old bulky combination of separate transmit and receive antenna systems. The two antenna ports will provide two orthogonal polarisations for polarisation diversity gain.

To verify the performance of the proposed smart antenna concept, a specific UK 3G network operator licence frequency sub-bands has been assumed. The orange UK sub-bands have been assumed as a practical example (downlink frequency band of 2.1597GHz

to 2.1697GHz and uplink frequency band 1.9697GHz to 1.9797GHz). The smart antenna system's major components incorporating an array of slant ± 45^0 dual-polarised stacked patch elements four columns wide excited by a multi-beam forming and beam shaping network has been simulated and results were presented in chapter six. It was demonstrated that using only three variable phase shifters within the beam shaping network provides effective dynamic beam flexibility.

For an ideal array (i.e. no mutual coupling and cosine element pattern) four narrow overlapping beams, one wide "broadcast channel" beam and right and left shaped beams can be provided. The later shaped beams are to provide enhanced capacity and maintain coverage in a specific narrow angular sub-sector while low capacity coverage is maintained over the remainder of a 120^0 sector. Results were presented for the simulation of this smart antenna system using CST EM simulation software which inherently includes mutual coupling and the effects of a truncated ground plane on the element patterns. The results show some significant changes to the desired set of coverage patterns. Mutual coupling effects and various mutual coupling compensation techniques have been reviewed in chapter seven. The two main factors which have been identified are mutual coupling between antenna elements and a variation of active reflection coefficients at each antenna element.

An improved design technique has been developed in chapter seven for compensating the performance degrading effects of mutual coupling and finite ground plane dimensions in microstrip antenna arrays. The essence of the technique is summarised as follows. The existence of mutual coupling between array elements in an array antenna causes two performance degrading effects. These are radiation pattern distortion (relative to the radiation pattern that would exist without mutual coupling) and variation of the active reflection coefficients at each array element. Furthermore, the radiation pattern performance is affected by the truncation of the finite ground plane. If only one fixed beam was required, then the mutual coupling effects could be compensated by changing the array excitation weights (to correct the radiation pattern) and by the inclusion of suitable fixed impedance matching networks at each array element. However, when dynamic multiple beam radiation patterns are required these simple compensating methods do not work. Hence, an improved technique is needed.

The improved technique utilises two previously known techniques in combination which to my knowledge has not been done before. These are: complex excitation weights compensation by inversion of the array mutual coupling scattering matrix and the incorporation of a wide angle impedance matching (WAIM) sheet. When these are implemented, an iterative optimisation of performance is required as each affects the compensating effects of the other. The effect of the finite ground plane truncation is to change both the mutual coupling coefficients and the edge array element radiation patterns and this has been taken into account.

The technique has been applied to a novel multi-beam Smart antenna array for use in 3G mobile networks to demonstrate the efficacy of the technique by electromagnetic simulation. In chapter eight, a demonstrator array has been constructed and tested to facilitate experimental verification of the simulation results which has yielded a positive conformation of the usefulness of the technique. The Smart antenna array excitation network consist of a Butler matrix multiple beam-forming network which is excited by a novel beam shaping network. The latter actually facilitates the correct compensated array excitation weights determined by the subject technique for optimum performance for each of the seven desired beams (achieved by adjusting of the three phase shifters within the beam shaping network).

For the developed demonstrator array which provides seven different beams (wide beam for broadcast channel, 4 narrow beams and left and right shaped beams), beam "footprints" have been predicted both for free space propagation and for urban propagation (using COST 259 model) to evaluate the dynamic capacity performance of the smart antenna in a 3G mobile communication network, presented in chapter nine. The results indicate that sector capacity can be dynamically tailored to user demand profiles by selection of the appropriate beam patterns provided by the novel Smart antenna array described. Strategic deployment of this smart antenna system into mobile telecommunication networks to the optimum techno-economic advantage of mobile network providers has been investigated in chapter ten. The best locations for smart antennas in the radio network and cost efficient deployment of smart antennas, using commercial radio network planning and optimisation tools was also highlighted in chapter ten.

This research has developed a smart antenna concept which has been designed, simulated, implemented and tested. The smart antenna concept represents a "half-way" house between

a multiple switched beam smart antenna system and the fully adaptive smart antenna system. This has been achieved by the development of a beam shaping network which essentially excites all beams of a multi-beam smart antenna simultaneously in the optimum "blend ratio" (and relative phase) to produce the desired shaped beams. The resultant antenna system represents an improvement in performance over a single multiple switched beam smart antenna without the cost and complexity of a fully adaptive smart antenna. The simulated and measured radiation patterns and active reflection coefficients over the UK 3G frequency sub-bands show that useful dynamic capacity & coverage enhancement can be implemented with the proposed smart antenna system in a mobile telecommunication network.

11.2 Recommendations for Future Work

Although the objectives listed in chapter one of this thesis have been fully achieved, the work was never envisaged to be fully comprehensive to cover all smart antenna system concepts development for mobile telecommunications research areas. Since the amount of work and time required to do so is beyond the scope of this thesis, the author recommends further works, which can be carried out to extend the work reported here.

In other to make this smart antenna system design into a commercial product, there is need to develop the variable phase shifters using mechanical motors because using electronic phase shifters would cause unacceptable inter-modulation distortion. The antenna array used in analysing the effect of mutual coupling is four elements, but for the full antenna system the array antenna comprises of four column arrays and each column has ten elements. Therefore, to implement this antenna for a commercial use the effects of mutual coupling need to be analysed for the full array antenna. It is expected that this will slightly alter performance, which could then be re-optimised.

Lastly, a control system could be developed which controls the adjustable phase shifters within the beam shaping network to achieve the desired dynamic beam shaping performance. An appropriate control algorithm would need to be implemented which monitors the traffic load distribution within a sector to determine the optimum beam shape at each time sample.

APPENDIX A - A PROGRAM TO DETERMINE THE ARRAY ELEMENT EXCITATIONS 'AE & ΦE' FOR ANY COMBINATION OF BEAM INPUTS TO THE BUTLER MATRIX BEING EXCITED WITH 'AB & ΦB'

A program to determine the array element excitations 'Ae & e' for any combination of beam Inputs being excited with 'Ab & b'

Beam1 Excitation

$n := 1, 2 .. 4$ $\quad Ae_{n,1} := -6.02$ $\quad \Phi e_{n,1} := 135 + (n - 1) \cdot -45$

$\Phi e_{n,1} =$

135
90
45
0

Beam2 Excitation

$n := 1, 2 .. 4$ $\quad Ae_{n,2} := -6.02$ $\quad \Phi e_{n,2} := 45 + (n - 1) \cdot 135$

$\Phi e_{n,2} =$

45
180
315
450

Beam3 Excitation

$n := 1, 2 .. 4$ $\quad Ae_{n,3} := -6.02$ $\quad \Phi e_{n,3} := 90 + (n - 1) \cdot -135$

$\Phi e_{n,3} =$

90
-45
-180
-315

Beam4 excitation

$n := 1, 2 .. 4$ $\quad Ae_{n,4} := -6.02$ $\quad \Phi e_{n,4} := 0 + (n - 1) \cdot 45$

$\Phi e_{n,4} =$

0
45
90
135

$$Ae = \begin{pmatrix} -6.02 & -6.02 & -6.02 & -6.02 \\ -6.02 & -6.02 & -6.02 & -6.02 \\ -6.02 & -6.02 & -6.02 & -6.02 \\ -6.02 & -6.02 & -6.02 & -6.02 \end{pmatrix}$$

$$\Phi e = \begin{pmatrix} 135 & 45 & 90 & 0 \\ 90 & 180 & -45 & 45 \\ 45 & 315 & -180 & 90 \\ 0 & 450 & -315 & 135 \end{pmatrix}$$

Input Beam Excitation

$m := 1, 2 .. 4$ $\quad Ab_1 := 0$ $\quad Ab_2 := -12$ $\quad Ab_3 := 0$ $\quad Ab_4 := -12$

$$AbTotal := 10 \cdot \log\left(\sum_{m=1}^{4} 10^{\frac{Ab_m}{10}} \right)$$

$Ab_m := Ab_m - AbTotal$

$$Ab = \begin{pmatrix} -3.276 \\ -15.276 \\ -3.276 \\ -15.276 \end{pmatrix}$$

$\Phi b_1 := 0$

$\Phi b_2 := -135$

$\Phi b_3 := -135$

$\Phi b_4 := 0$

$n := 1..4$

$$Ecomplex_n := \sum_{m=1}^{4} \left[\frac{Ab_m}{10^{20}} \left(\frac{Ae_{n,m}}{10^{20}} \right) e^{i \cdot \left(\frac{\pi}{180} \right) \cdot \left(\Phi b_m + \Phi e_{n,m} \right)} \right]$$

$$Ecomplex1_n := \frac{0}{10^{20}} \left(\frac{Ae_{n,1}}{10^{20}} \right) e^{i \cdot \left(\frac{\pi}{180} \right) \cdot \left(0 + \Phi e_{n,1} \right)}$$

$$Ecomplex2_n := \frac{0}{10^{20}} \left(\frac{Ae_{n,2}}{10^{20}} \right) e^{i \cdot \left(\frac{\pi}{180} \right) \cdot \left(0 + \Phi e_{n,2} \right)}$$

$$Ecomplex3_n := \frac{0}{10^{20}} \left(\frac{Ae_{n,3}}{10^{20}} \right) e^{i \cdot \left(\frac{\pi}{180} \right) \cdot \left(0 + \Phi e_{n,3} \right)}$$

$$Ecomplex4_n := \frac{0}{10^{20}} \left(\frac{Ae_{n,4}}{10^{20}} \right) e^{i \cdot \left(\frac{\pi}{180} \right) \cdot \left(0 + \Phi e_{n,4} \right)}$$

$n := 1..4$

$m := 1..4$

$$Ecomplex_n = \begin{pmatrix} 0.086 - 0.086i \\ -0.221 + 0.465i \\ 0.399 + 0.571i \\ 0.343 - 0.343i \end{pmatrix}$$

$$\Phi e = \begin{pmatrix} 135 & 45 & 90 & 0 \\ 90 & 180 & -45 & 45 \\ 45 & 315 & -180 & 90 \\ 0 & 450 & -315 & 135 \end{pmatrix}$$

$$Ae = \begin{pmatrix} -6.02 & -6.02 & -6.02 & -6.02 \\ -6.02 & -6.02 & -6.02 & -6.02 \\ -6.02 & -6.02 & -6.02 & -6.02 \\ -6.02 & -6.02 & -6.02 & -6.02 \end{pmatrix}$$

$$\Phi_n := \frac{180}{\pi} \arg\left(Ecomplex_n\right)$$

$$\Phi 1_n := \frac{180}{\pi} \arg\left(Ecomplex1_n\right)$$

$$\Phi 2_n := \frac{180}{\pi} \arg\left(Ecomplex2_n\right)$$

$$\Phi 3_n := \frac{180}{\pi} \arg\left(Ecomplex3_n\right)$$

$$\Phi 4_n := \frac{180}{\pi} \arg\left(Ecomplex4_n\right)$$

$$\left|Ecomplex_n\right|$$

0.122
0.515
0.697
0.485

$$\log\left(\left|Ecomplex_n\right|\right)$$

-0.914
-0.288
-0.157
-0.314

$$EdB_n := 20\log\left(\left|Ecomplex_n\right|\right)$$

$$EdB1_n := 20\log\left(\left|Ecomplex1_n\right|\right)$$

$$EdB2_n := 20\log\left(\left|Ecomplex2_n\right|\right)$$

$$EdB3_n := 20\log\left(\left|Ecomplex3_n\right|\right)$$

$$EdB4_n := 20\log\left(\left|Ecomplex4_n\right|\right)$$

$EdB_n =$

-18.286
-5.77
-3.141
-6.286

$\Phi_n =$

-45
115.443
55.072
-45

$s := 1..181$

$n := 1, 2..4$

$f := 2.164$

$\lambda := \frac{300}{f}$

$d := \frac{\lambda}{2}$

$k := 2 \cdot \frac{\pi}{\lambda}$

$\theta_s := -90 + (s - 1)$

$10^{.30105} = 2$

$10^{\frac{EdB_n}{20}} =$

0.122
0.515
0.697
0.485

$$E_s := 17.5 + 20 \cdot \log\left[\left|\cos\left(\frac{\pi}{180}\cdot\theta_s\right)^2 \cdot \left[\sum_{n=1}^{4}\left[\left[\left(10^{\frac{EdB_n}{20}}\right)\cdot\left(e^{i\cdot\Phi_n\cdot\frac{\pi}{180}}\right)\right]\cdot e^{i\cdot k\cdot d\cdot(n-1)\cdot\sin\left(\frac{\pi\cdot\theta_s}{180}\right)}\right]\right]\right|\right]$$

$$E1_s := 17.5 + 20 \cdot \log\left[\left|\cos\left(\frac{\pi}{180}\cdot\theta_s\right)^2 \cdot \left[\sum_{n=1}^{4}\left[\left[\left(10^{\frac{EdB1_n}{20}}\right)\cdot\left(e^{i\cdot\Phi 1_n\cdot\frac{\pi}{180}}\right)\right]\cdot e^{i\cdot k\cdot d\cdot(n-1)\cdot\sin\left(\frac{\pi\cdot\theta_s}{180}\right)}\right]\right]\right|\right]$$

$$E2_s := 17.5 + 20 \cdot \log\left[\left|\cos\left(\frac{\pi}{180}\cdot\theta_s\right)^2 \cdot \left[\sum_{n=1}^{4}\left[\left[\left(10^{\frac{EdB2_n}{20}}\right)\cdot\left(e^{i\cdot\Phi 2_n\cdot\frac{\pi}{180}}\right)\right]\cdot e^{i\cdot k\cdot d\cdot(n-1)\cdot\sin\left(\frac{\pi\cdot\theta_s}{180}\right)}\right]\right]\right|\right]$$

$$E3_s := 17.5 + 20 \cdot \log\left[\left|\cos\left(\frac{\pi}{180}\cdot\theta_s\right)^2 \cdot \left[\sum_{n=1}^{4}\left[\left[\left(10^{\frac{EdB3_n}{20}}\right)\cdot\left(e^{i\cdot\Phi 3_n\cdot\frac{\pi}{180}}\right)\right]\cdot e^{i\cdot k\cdot d\cdot(n-1)\cdot\sin\left(\frac{\pi\cdot\theta_s}{180}\right)}\right]\right]\right|\right]$$

$$E4_s := 17.5 + 20 \cdot \log\left[\left|\cos\left(\frac{\pi}{180}\cdot\theta_s\right)^2 \cdot \left[\sum_{n=1}^{4}\left[\left[\left(10^{\frac{EdB4_n}{20}}\right)\cdot\left(e^{i\cdot\Phi 4_n\cdot\frac{\pi}{180}}\right)\right]\cdot e^{i\cdot k\cdot d\cdot(n-1)\cdot\sin\left(\frac{\pi\cdot\theta_s}{180}\right)}\right]\right]\right|\right]$$

Emax:= max(E)

Emax= 20.065

$EN_s := E_s - Ema$

EN =

	1
1	-656.874
2	-78.688
3	-66.679
4	-59.689
5	-54.768
6	-50.989
7	-47.943
8	-45.41
9	-43.26
10	-41.408
11	-39.799
12	-38.393
13	-37.161
14	-36.081
15	-35.139
16	...

E =

	1
1	-636.809
2	-58.624
3	-46.615
4	-39.625
5	-34.703
6	-30.925
7	-27.879
8	-25.345
9	-23.195
10	-21.343
11	-19.735
12	-18.328
13	-17.096
14	-16.016
15	-15.074
16	...

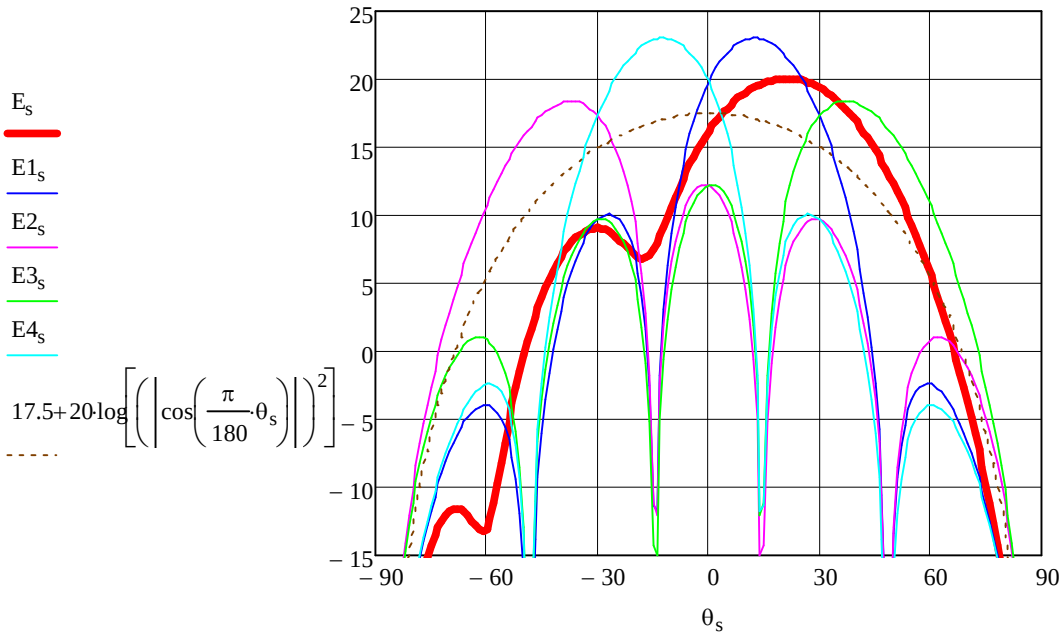
E_s
$E1_s$
$E2_s$
$E3_s$
$E4_s$
$17.5+20\cdot\log\left[\left(\left|\cos\left(\frac{\pi}{180}\cdot\theta_s\right)\right|\right)^2\right]-5$
25
20
15
10
5
0
– 5
– 10
– 15
– 90
– 60
– 30
0
30
60
90
θ_s

REFERENCES

[1] R. Steele, Mobile Radio Communication. London: PENTECH PRESS, 1992.

[2] R. L. Freeman, Telecommunications Transmission Handbook, Fourth ed. New York: John Wiley & sons, INC, 1998.

[3] B. Qi, G. L. Zysman, and H. Menkes, "Wireless mobile communications at the start of the 21st century," *Communications Magazine, IEEE,* vol. 39, pp. 110-116, 2001.

[4] J. De Vriendt, P. Laine, C. Lerouge, and X. Xiaofeng, "Mobile network evolution: a revolution on the move," *Communications Magazine, IEEE,* vol. 40, pp. 104-111, 2002.

[5] T. Ojanpera and R. Prasad, "An overview of third-generation wireless personal communications: a European perspective," *Personal Communications, IEEE,* vol. 5, pp. 59-65, 1998.

[6] J. Chuang and N. Sollenberger, "Beyond 3G: wideband wireless data access based on OFDM and dynamic packet assignment," *Communications Magazine, IEEE,* vol. 38, pp. 78-87, 2000.

[7] H. Gruber, "3G mobile telecommunications licenses in Europe: a critical review", info, Vol. 9 Iss: 6, pp.35 – 44, 2007

[8] H. Harri, T. Antti, "WCDMA for UMTS Radio Access for Third Generation Mobile Communication" Wiley, 2005.

[9] R. T. Derryberry, S. D. Gray, D. M. Ionescu, G. Mandyam, and B. Raghothaman, "Transmit diversity in 3G CDMA systems," *Communications Magazine, IEEE,* vol. 40, pp. 68-75, 2002.

[10] ‘‘The Future Mobile Market: Global Trends and Developments with a Focus on Western Europe,’’ UMTS Forum Report, 1999.

[11] Worldwide Cellular User forecasts (2004-2010) strategy Analytics December 2004

[12] B. A. Bjerke, "LTE-advanced and the evolution of LTE deployments," *Wireless Communications, IEEE,* vol. 18, pp. 4-5, October 2011.

[13] International Telecommunication Union: Information Society Statistical profiles-Africa 2009

[14] International Telecommunication Union: ICT FACTS AND FIGURES-www.itu.int/ITU, 2011

[15] C. A. Balanis, Analysis and Design Third Edition: John Wiley and Sons, 2005

[16] E. Z. Ahmed, Smart antenna engineering. London: Artech House, 2005.

[17] A. R. Mishra, "Advance Cellular Network Planning and Optimisation" Wiley & Sons, 2007.

[18] B. Christer , V. Johansson, S. Stefansson, *"Optimizing* Antenna Parameters for Sectorised W-CDMA *Networks'*, Proceedings of IEEE Vehicular Technology Conference, pp. 1524-1531, VTC2000.

[19] D. Tsilimantos, G. Tsoulos, and D. Kaklamani, "Radio Network Planning for UMTS with Smart Antennas," in Electromagnetics in Advanced Applications, ICEAA. International Conference on, pp. 415-418, 2007

[20] J. Niemela and J. Lempiainen, "Impact of the base station antenna beamwidth on capacity in WCDMA cellular networks," in *Vehicular Technology Conference, VTC 2003-Spring. The 57th IEEE Semiannual*, pp. 80-84 vol.1 2003

[21] K. Hiltunen and R. de Bernardi, "WCDMA downlink capacity estimation," in *Vehicular Technology Conference Proceedings, VTC-Spring Tokyo. IEEE 51st*, pp. 992-996 vol.2 2000

[22] W. Yangling, W. Fangfang, and L. Ming, "Investigation on Estimating Capacity for WCDMA Network," in *Knowledge Acquisition and Modeling Workshop, 2008. KAM Workshop. IEEE International Symposium on*, pp. 256-259, 2008

[23] F. Rayal, "Why have smart antennas not yet gained traction with wireless network operators?," *Antennas and Propagation Magazine, IEEE*, vol. 47, pp. 124-126, 2005.

[24] B. A. Bjerke, Z. Zvonar, and J. G. Proakis, "Antenna diversity combining schemes for WCDMA systems in fading multipath channels," *Wireless Communications, IEEE Transactions on,* vol. 3, pp. 97-106, 2004.

[25] T. S. Rappaport, *WIRELESS COMMUNICATIONS PRINCIPLES AND PRACTICE*, SECOND ed. Massachusetts: Prentice Hall PTR, 2008

[26] T. Frisanco, P. Tafertshofer, P. Lurin, and R. Ang, "Infrastructure sharing and shared operations for mobile network operators From a deployment and operations view," in *Network Operations and Management Symposium, NOMS IEEE*, 2008, pp. 129-136, *2008.*

[27] V.K. Garg and J.E. Wilkes, Wireless and Personal Communication Systems, prentice Hall PTR, Upper Saddle River, NJ, 1996.

[28] T. S. Yum and W. S. Wong, "Hot-spot traffic relief in cellular systems," IEEE Journal on Selected Areas in Communications, vol. 11, no. 6, pp. 934-940, August 1993.

[29] J. Peng, J. Bigham, and W. Jiayi, "Providing enhanced QoS differentiation to customers using geographic load balancing," in *Wireless Technology, The 9th European Conference on*, pp. 154-157, 2006

[30] A. Lindsay-Stewart, W. C. Y. Lee, M. A. Schulz, and C. Xu, "Incremental capacity gains for high blocking sites using dynamic channel sharing," *Vehicular Technology, IEEE Transactions on*, vol. 50, pp. 1-11, 2001.

[31] L. Junyi, N. B. Shroff, and E. K. P. Chong, "The study of a channel sharing scheme in wireless cellular networks including handoffs," in *INFOCOM '99. Eighteenth Annual Joint Conference of the IEEE Computer and Communications Societies. Proceedings. IEEE*, pp. 1179-1186 vol.3, 1999

[32] H. Shang-Ching, H. Shao-Yi, E. H. K. Wu, and C. Gen-Huey, "A Decentralized CR System Algorithm for Cognitive Borrowing Scheme from Primary Users," in *Personal, Indoor and Mobile Radio Communications, IEEE 17th International Symposium on*, pp. 1-5, *2006*

[33] Y. Argyropoulos, S. Jordan, and S. Kumar, Dynamic channel allocation in interference-limited cellular systems with uneven traffic distribution, *IEEE Transactions on Vehicular Technology*, vol. 48, no. 1, pp 224-232, January 1999.

[34] K. Bonghoe and K. Sung Lark, "A new soft handover scheme using punctured turbo codes in the wideband CDMA system," in *Vehicular Technology Conference, VTC Spring. IEEE VTS 53rd*, pp. 1420-1424 vol.2, 2001

[35] H.Wu, C. Qiao, S. De, and O. K. Tonguz, "Integrated cellular and ad-hoc relay systems: iCAR," *IEEE J. Select. Areas Commun.*, vol. 19, pp. 2105–2115, Oct. 2001.

[36] L. Zordan, N. Rutazihana, and N. Engelhart, "Capacity enhancement of cellular mobile network using a dynamic electrical down-tilting antenna system," in *Vehicular Technology Conference, VTC 1999 - Fall. IEEE VTS 50th*, pp. 1915-1918 vol.3, 1999

[37] J. Niemela, T. Isotalo, J. Borkowski, J. Lempiainen, "Sensitivity of optimum downtilt angle for geographical traffic load distribution in WCDMA", 62nd, IEEE Vehicular Technology Conference, VTC-Fall. Volume 2, Page(s):1202- 1206 Sept., 2005.

[38] T. Togo, I. Yoshii, and R. Kohno, "Dynamic cell-size control according to geographical mobile distribution in a ds/cdma cellular system," in *Proc. Ninth IEEE Int. Symp. Personal, Indoor and Mobile Radio Communications*, vol. 2, pp. 677–681, 1998.

[39] C. Lee, H. Kang, and T. Park, "Dynamic sectorization of microcells for balanced traffic in cdma: genetic algorithms approach," *IEEE Trans. Veh. Technol.*, vol. 51, pp. 63–72, Jan 2002.

[40] R. L. Haupt, "The development of smart antennas," in *Antennas and Propagation Society International Symposium. IEEE*, pp. 48-51 vol.4, *2001*

[41] E. Mitjana, X. Song, L. Lu, M. Haardt, C. Gessner, G. Lehmann, and M. Vollmer, "Performance of smart antenna in TD-SCDMA system," in *Communication Technology Proceedings, WCC - ICCT 2000. International Conference on*, pp. 152-155 vol.1, 2000.

[42] V. A. Sousa, Jr., C. H. M. de Lima, E. B. Rodrigues, F. R. P. Cavalcanti, and A. R. Brag, "Coverage and capacity of WCDMA systems with beam steering antennas," in *Vehicular Technology Conference, VTC 2003-Fall. IEEE 58th*, pp. 826-830 Vol.2, *2003*

[43] A. Chaaban and A. Sezgin, "On the capacity of a class of multi-user interference channels," in *Smart Antennas (WSA), International ITG Workshop on*, pp. 1-5 *2011*

[44] K. Hettak and G. Y. Delisle, "Smart antenna for capacity enhancement in indoor wireless communications at millimeter waves," in *Vehicular Technology Conference Proceedings, VTC-Spring Tokyo. 2000 IEEE 51st*, pp. 2152-2156 vol.3, 2000

[45] A. Osseiran, P. Skillermark, and M. Olsson, "Multi-Antenna SDMA in OFDM Radio Network Systems: Modeling and Evaluations," in *Personal, Indoor and Mobile Radio Communications, PIMRC 2007. IEEE 18th International Symposium on*, pp. 1-5, 2007

[46] K. A. Gotsis, K. Siakavara, and J. N. Sahalos, "On the Direction of Arrival (DoA) Estimation for a Switched-Beam Antenna System Using Neural Networks," *Antennas and Propagation, IEEE Transactions on*, vol. 57, pp. 1399-1411, 2009.

[47] M. D. Migliore, "A beamforming algorithm for adaptive antennas operating in crowded CDMA signal environment," *Antennas and Propagation, IEEE Transactions on*, vol. 54, pp. 1354-1357, 2006.

[48] L. Hongwei, K. Lingling, and S. Xiaodong, "An improved smart antenna algorithm," in *Wireless, Mobile and Multimedia Networks, IET International Conference on*, pp. 1-3, 2006.

[49] Y. Inoue and C. Keizo, "New smart antenna algorithm applied to autonomous area control for mobile radio network," in *Antennas and Propagation, EuCAP 3rd European Conference on*, pp. 2050-2054, 2009.

[50] A. Osseiran and M. Ericson, "On downlink admission control with fixed multi-beam antennas for WCDMA system," in *Vehicular Technology Conference, VTC 2003-Spring. The 57th IEEE Semiannual*, pp. 1203-1207 vol.2, 2003

[51] L. Du, J. Bigham, and L. Cuthbert, "A bubble oscillation algorithm for distributed geographic load balancing in mobile networks," in The Twenty-third Annual Joint Conference of the IEEE Computer and Communications, IEEE INFOCOM' Hong Kong: IEEE, March 2004.

[52] M. Luis Correia, 'Review of COST 259 European Co-operation in mobile Radio research', Wireless flexible personalized communication 2001.

[53] L. Du, J. Bigham and L. Cuthbert, Towards intelligent geographic load balancing for mobile cellular networks, *IEEE Transactions on Systems, Man and Cybernetics*, Part C, vol. 33, no. 4, pp. 480-491, November 2003.

[54] Na, Yao and L. Cuthbert,'' Resource management in 3G networks using case-based reasoning'' International Workshop on Modeling Analysis and Simulation of Wireless and Mobile Systems**,** Proceedings of the 8th ACM international symposium on Modeling, analysis and simulation of wireless and mobile systems Montreal, Quebec, Canada, pp 307-312 October 2005.

[55] A. Wang and V. Krishnamurthy, "Mobility Enhanced Smart Antenna Adaptive Sectoring for Uplink Capacity Maximization in CDMA Cellular Network," *Communications, IEEE Transactions on*, vol. 56, pp. 743-753, 2008.

[56] J. Dunlop and D.G. Smith 'Telecommunications engineering' - 3rd Edition, - Cheltenham: Stanley Thornes, 1998.

[57] A. R. Mishra, 'Fundamental of Cellular Network Planning & Optimisation' John Wiley &Sons Ltd, 2004

[58] Lal C. Godara, 'Application of Antenna Array to Mobile Communication, Part 1 performance Improvement, Feasibility and System Considerations'Proceeding of IEEE Vol. 85. No 7 1997.

[59] ETSI TS 125 401, .Universal Mobile Telecommunications System (UMTS): UTRAN Overall Description,. 3GPP TS 25.401 version 4.0.0 Release 4, March 2001

[60] TIA/EIA/1-A, 'Introduction to CDMA 2000 standard for spread spectrum systems' 2000.

[61] TIA/EIA/IS-200, 2-A 'Physical Layer standard for CDMA 2000 spread spectrum systems 2000.

[62] TIA/EIA-95B 'Mobile station-Base station compatibility standard for wideband spread spectrum cellular system' 1999.

[63] H. Holma And Toscala A., ''WCDMA for UMTS, New York'', John Wiley & Sons, 2004.

[64] 3GPP Technical specification 25.212 Multiplexing and channel coding (FDD) 2002.

[65] A. Wacker et al, 'WCDMA Radio Network Planning in Radio Network Planning and Optimisation for UMTS Edited by Laiho J et al second edition John Wiley & Sons LTD 2006.

[66] M. Rahnema 'Means to enhance Radio coverage and capacity in UMTS Network Planning Optimisation and Inter-operation with GSM' IEEE 2009.

[67] Y. J. Guo, *ADVANCES IN MOBILE RADIO ACCESS NETWORKS*. Boston, London: Artech House, 2004.

[68] D. Esmael, A. Kurochkin, S. Ketteni, 'UMTS Radio System Planning and Optimization' Bechtel Telecommunications Technical Journal Vol.1, No.1, December 2002.

[69] T. Kunz and R. Alhalimi, "Load-Balanced Routing in Wireless Networks: State Information Accuracy Using OLSR," in *Wireless and Mobile Computing, Networking and Communications, WiMOB. Third IEEE International Conference on*, pp. 83-83, *2007*.

[70] S. Mitra and S. DasBit, "A load balancing strategy using dynamic channel assignment and channel borrowing in cellular mobile environment," in *Personal Wireless Communications, IEEE International Conference on*, pp. 278-282, 2000

[71] A. Boukerche and R. E. De Grande, "Dynamic Load Balancing Using Grid Services for HLA-Based Simulations on Large-Scale Distributed Systems," in *Distributed Simulation and Real Time Applications, DS-RT '09. 13th IEEE/ACM International Symposium on*, pp. 175-183, 2009

[72] E. Yanmaz and O. K. Tonguz, "Dynamic load balancing and sharing performance of integrated wireless networks," *Selected Areas in Communications, IEEE Journal on*, vol. 22, pp. 862-872, 2004.

[73] K. Hamidian and J. Payne, "Performance analysis of a CDMA/FDMA cellular communication system with cell splitting," in *Computers and Communications, Proceedings, Second IEEE Symposium on*, 1997, pp. 545-550, *1997*

[74] H. G. Sandalidis, P. P. Stavroulakis, and J. Rodriguez-Tellez, "Borrowing channel assignment strategies based on heuristic techniques for cellular systems," *Neural Networks, IEEE Transactions on*, vol. 10, pp. 176-181, 1999.

[75] O. Yilmaz, S. Hamalainen, and J. Hamalainen, "Comparison of Remote Electrical and Mechanical Antenna Downtilt Performance for 3GPP LTE," in *Vehicular Technology Conference Fall (VTC 2009-Fall), IEEE 70th*, pp. 1-5, 2009

[76] W. Jung-Shyr, C. Jen-Kung, and W. Chang-Chung, "Performance study of traffic balancing via antenna-tilting in CDMA cellular systems," in *Vehicular Technology Conference, 'Mobile Technology for the Human Race., IEEE 46th*, pp. 1081-1085 vol.2, 1996

[77] RA UTRAN Iuant interface: General aspects and principles (Release 6*)*, 3GPP TS 25.460 V.6.2.0, March 2005.

[78] A. Alexiou and M. Haardt, "Smart antenna technologies for future wireless systems: trends and challenges," *Communications Magazine, IEEE,* vol. 42, pp. 90-97, 2004.

[79] J. C. Liberti, Jr., and T.S. Rappaport, Smart Antennas for wireless communications: IS-95 and Third Generation CDMA Applications, Prentice Hall PTR, Upper Saddle River, NJ 1999.

[80] H. Ming-Ju, H. Ming-Ju, G. L. Stuber, and M. D. Austin, "Performance of switched-beam smart antennas for cellular radio systems " *Vehicular Technology, IEEE Transactions on*, vol. 47, pp. 10-19, 1998.

[81] E. Siachalou, E. Vafiadis, S. S. Goudos, T. Samaras, C. S. Koukourlis, and S. Panas, "On the design of switched-beam wideband base stations," *Antennas and Propagation Magazine, IEEE*, vol. 46, pp. 158-167, 2004.

[82] G. V. Tsoulos, *Adaptive Antennas for Wireless Communications*. New York: IEEE Press, 2001.

[83] S. S. Haykin, Simon Saher, *Communication systems*, 4th ed. New York; Chichester: Wiley, 2000

[84] A. Osseiran and A. Logothetis, "Smart Antennas in a WCDMA Radio Network System: Modeling and Evaluations," *Antennas and Propagation, IEEE Transactions on*, vol. 54, pp. 3302-3316, 2006.

[85] A. Mahanfar, C. Menon, and R. G. Vaughan, "Smart antennas using electro-active polymers for deformable parasitic elements," *Electronics Letters*, vol. 44, pp. 1113-1114, 2008.

[86] N. Celik, M. F. Iskander, R. Emrick, S. J. Franson, and J. Holmes, "Implementation and Experimental Verification of a Smart Antenna System Operating at 60 GHz Band," *Antennas and Propagation, IEEE Transactions on*, vol. 56, pp. 2790-2800, 2008.

[87] P. Ioannides and C. A. Balanis, "Uniform circular arrays for smart antennas," *Antennas and Propagation Magazine, IEEE*, vol. 47, pp. 192-206, 2005.

[88] K. Y. Yazdandoost and K. Hamaguchi, "Antenna polarization mismatch in body area network communications," in *Antennas and Propagation (EuCAP), Proceedings of the Fourth European Conference on*, pp. 1-4, *2010*

[89] H. Moody, "The systematic design of the Butler matrix," *Antennas and Propagation, IEEE Transactions on*, vol. 12, pp. 786-788, 1964.

[90] J. Blass, "Multidirectional Antenna, a New Approach to Stacked Beams," *IRE International Conference Record*, Vol. 8, Part 1, pp 48-50, 1960

[91] W. Rotman and R. Turner, "Wide-angle microwave lens for line source applications," *IEEE Trans. Antennas Propagat.*, Vol. AP-11, No. 6, Nov., pp. 623–632, 1963.

[92] G. Leonakis, "Correction to "Wide-Angle Microwave Lens for Line Source Applications"," *Antennas and Propagation, IEEE Transactions on*, vol. 34, pp. 1067-1067, 1986.

[93]. Tayeb. A. Denidni and Tarob Eric Libar, Wide Band Four-Port Butler Matrix for switched Multibeam Atenna Arrays, the 14th IEEE international Symposium on Personal, Indoor and Mobile Radio Communication Proceedings, PP.2461-2464, 2003.

[94] N. J. G. Fonseca, "Printed S-Band 4X 4 Nolen Matrix for Multiple Beam Antenna Applications," *Antennas and Propagation, IEEE Transactions on*, vol. 57, pp. 1673-1678, 2009.

[95] T. Djerafi, N. J. G. Fonseca, and W. Ke, "Architecture and Implementation of Planar 4X4 Ku-Band Nolen Matrix in SIW Technology," *Microwave Theory and Techniques, IEEE Transactions on*, vol. 58, pp. 259-266, 2008.

[96] S. J. Foti and T. Macnamara, "Design of wideband Butler matrices using Schiffman lines," in *Multiple Beam Antennas and Beamformers, IEE Colloquium on*, pp. 5/1-5/8, 1989

[97] T. A. Denidni and T. E. Libar, "Wide band four-port butler matrix for switched multibeam antenna arrays," in *Personal, Indoor and Mobile Radio Communications, PIMRC 14th IEEE Proceedings on*, pp. 2461-2464 vol.3, 2003

[98] S. Gruszczynski, K. Wineza, and K. Sachse, "Compact broadband Butler matrix in multilayer technology for integrated multibeam antennas," *Electronics Letters*, vol. 43, pp. 635-636, 2007.

[99] H. Hayashi, D. A. Hitko, and C. G. Sodini, "Four-element planar Butler matrix using half-wavelength open stubs," *Microwave and Wireless Components Letters, IEEE*, vol. 12, pp. 73-75, 2002.

[100] M. Bona, L. Manholm, J. P. Starski, and B. Svensson, "Low-loss compact Butler matrix for a microstrip antenna," *Microwave Theory and Techniques, IEEE Transactions on*, vol. 50, pp. 2069-2075, 2002.

[101] C. Ting-Yueh, C. Sheng-Fuh, C. Chia-Chan, and W. Jen-Chieh, "A 24-GHz CMOS Butler Matrix MMIC for multi-beam smart antenna systems," in *Radio Frequency Integrated Circuits Symposium, RFIC 2008. IEEE*, pp. 633-636, 2008

[102] M. M. Alam, "Microstrip antenna array with four port Butler matrix for switched beam base station application," in *Computers and Information Technology, ICCIT '09. 12th International Conference on*, pp. 531-536, 2009

[103] C. Chia-Chan, L. Ruey-Hsuan, and S. Ting-Yen, "Design of a Beam Switching/Steering Butler Matrix for Phased Array System," *Antennas and Propagation, IEEE Transactions on*, vol. 58, pp. 367-374, 2010.

[104] B. Cetinoneri, Y. A. Atesal, and G. M. Rebeiz, "An 8X8 Butler Matrix in 0.13 micromilimetre CMOS for 5-6-GHz Multibeam Applications," *Microwave Theory and Techniques, IEEE Transactions on*, vol. 59, pp. 295-301, 2011.

[105] K. K. Chan, and S. K. Rao, "Design of a Rotman lens feed network to generate a hexagonal lattice of multiple beams," *IEEE Trans., Antennas Propagat.*, Vol. 50, No. 8, Aug. pp. 1099–1108, 2002

[106] R. C. Hansen, "Design trades for Rotman lenses," *IEEE Trans., Antennas Propagat.*, Vol. 39, No. 4, Apr. pp. 464–472, 1991

[107] J. Litva and T. K.-Y. Lo Digital Beamforming in Wireless Communications, Artech House, Boston 1996.

[108] D. M. Pozar, Microwave Engineering 3rd edition, John Wiley & Sons, 2005.

[109] A. Osseiran, M. Ericson, J. Barta, B. Goransson, and B. Hagerman, "Downlink capacity comparison between different smart antenna concepts in a mixed service W-CDMA system," in *Vehicular Technology Conference,. VTC Fall. IEEE VTS 54th*, pp. 1528-1532 vol.3, 2001

[110] G.L. Matthaei, L. Young and E.M.T Jones ‘‘Microwave Filters, Impedance-matching Networks, and coupling structures’’, Artech House, Dedham, mass, 1980.

[111] L. Besser and G. Rowan ‘Practical RF circuit design for Modern wireless systems Vol1 Artech House London, 2003.

[112] C. Kuo-Sheng, M. Ming-Chuan, C. Yi-Ping, and C. Yi-Chyun, "Closed-Form Equations of Conventional Microstrip Couplers Applied to Design Couplers and Filters Constructed With Floating-Plate Overlay," *Microwave Theory and Techniques, IEEE Transactions on*, vol. 56, pp. 1172-1179, 2008.

[113] L. Youngkwang and L. Hai-young, "Novel miniaturized branch-line coupler using bond-wire slow-wave structure," in *Microwave Conference, Asia-Pacific*, pp. 1-4, 2008

[114] F. Hosseini, M. K. A. Hosseini, and M. Yazdani, "Novel compact branch-line coupler using non-uniform transmission line," in *Microwave Conference, Asia Pacific*, 2009

[115] N. Celik, M. F. Iskander, and Z. Zhijun, "Experimental Verification of the Hybrid Smart Antenna Algorithm With Modulated Waveforms," *Antennas and Wireless Propagation Letters, IEEE*, vol. 8, pp. 236-239, 2009.

[116] A. Baharlouei, B. Abolhassani, and H. Oraizi, "A New Smart Antenna for CDMA using Nelder-Mead Simplex Algorithm and ESPAR Antenna," in *Information and Communication Technologies, ICTTA '06. 2nd*, pp. 2748-2753, 2006,

[117] Genesys RF and Microwave Design software, Genesys™ 2007, 2008, www.agilent.com

[118] CST STUDIO SUITE 2010™, www.cst.com

[119] D. H. S. David M. Pozar, "Microstrip Antennas: The Analysis and Design of Microstrip Antennas and Arrays " New Jersey: John Wiley & Sons, Inc., 1995.

[120] D. M. Pozar and B. Kaufman, "Design considerations for low sidelobe microstrip arrays," *Antennas and Propagation, IEEE Transactions on*, vol. 38, pp. 1176-1185, 1990.

[121] 3G Roadmap, *Microwave Eng. Eur.*, pp. 11–14, June 1999.

[122] B. Lindmark, S. Lundgren, J. R. Sanford, and C. Beckman, "Dual-polarized array for signal-processing applications in wireless communications," *Antennas and Propagation, IEEE Transactions on*, vol. 46, pp. 758-763, 1998.

[123] I. Acimovic, D. A. McNamara, and A. Petosa, "Dual-Polarized Microstrip Patch Planar Array Antennas With Improved Port-to-Port Isolation," *Antennas and Propagation, IEEE Transactions on*, vol. 56, pp. 3433-3439, 2008

[124] F. Bobor-Oyibo, D. Smith, and S. J. Foti, "The effects of a finite ground plane on the characteristics of printed patch antennas with and without a suspended patch," in *Communication Systems Networks and Digital Signal Processing (CSNDSP), 7th International Symposium on*, pp. 111-114, *2010*

[125] T. A. Patrick VAUDON, Philippe DUFRANE and Bernard JECKO, "Influence of ground plane structure on the radiation pattern of microstrip antennas," *Annals of Telecommunications*, vol. 48, pp. 319-329, 1993.

[126] McKinzie, et al, ‘‘Low Cost Trombone Line Beamformer’’, United States Patent, Patent No.: US 6,831,602,B2, Dec. 14,2004.

[127] L. Tingting, Z. Fei, S. Wei, and Q. Zuping, "Design of low cost 4 ports microstrip line phase shifter," in *Microwave and Millimeter Wave Technology (ICMMT), International Conference on*, pp. 1142-1144, 2010

[128] M. J. L. Alves and M. Sampaio de Alencar, "Effects of mutual coupling in smart antenna arrays," in *Microwave and Optoelectronics Conference, IMOC. SBMO/IEEE MTT-S International*, pp. 418-421, 2007

[129] K. R. Dandekar, L. Hao, and X. Guanghan, "Experimental study of mutual coupling compensation in smart antenna applications," *Wireless Communications, IEEE Transactions on*, vol. 1, pp. 480-487, 2002.

[130] I. Gupta and A. Ksienski, "Effect of mutual coupling on the performance of adaptive arrays," *Antennas and Propagation, IEEE Transactions on*, vol. 31, pp. 785-791, 1983.

[131] H. Hon Tat, "Reducing the mutual coupling effect in adaptive nulling using re-defined mutual impedance," *Microwave and Wireless Components Letters, IEEE*, vol. 12, pp. 178-180, 2002.

[132] R. M. Korany, I. E. Mohamed, B. Rajeev, H. Z.-D. Saber, and M. M. I. Sabry, "Analysis of uniform circular arrays for adaptive beamforming applications using particle swarm optimization algorithm," *International Journal of RF and Microwave Computer-Aided Engineering*, vol. 18, pp. 42-52, 2008.

[133] A. A. Maha and W. Parveen, "Effect of mutual coupling in adaptive arrays," *Microwave and Optical Technology Letters*, vol. 35, pp. 270-274, 2002.

[134] L. Min and Y. Luxi, "Blind Calibration and DOA Estimation With Uniform Circular Arrays in the Presence of Mutual Coupling," *Antennas and Wireless Propagation Letters, IEEE*, vol. 5, pp. 315-318, 2006.

[135] Y. Qiaowei, C. Qiang, and K. Sawaya, "Performance of adaptive array antenna with arbitrary geometry in the presence of mutual coupling," *Antennas and Propagation, IEEE Transactions on*, vol. 54, pp. 1991-1996, 2006.

[136] H. Zhiyong and C. A. Balanis, "The MMSE Algorithm and Mutual Coupling for Adaptive Arrays," *Antennas and Propagation, IEEE Transactions on*, vol. 56, pp. 1292-1296, 2008.

[137] H. Zhiyong, C. A. Balanis, and C. R. Birtcher, "Mutual Coupling Compensation in UCAs: Simulations and Experiment," *Antennas and Propagation, IEEE Transactions on*, vol. 54, pp. 3082-3086, 2006.

[138] L. G. Sodin, "Frequency-Independent Approximate Compensation of Mutual Coupling in a Linear Array Antenna," *Antennas and Propagation, IEEE Transactions on*, vol. 57, pp. 2293-2296, 2009.

[139] A. G. Demeryd, "Compensation of mutual coupling effects in array antennas," in *Antennas and Propagation Society International Symposium, AP-S. Digest*, pp. 1122-1125 vol.2, 1996

[140] E. Magill and H. Wheeler, "Wide-angle impedance matching of a planar array antenna by a dielectric sheet," *Antennas and Propagation, IEEE Transactions on*, vol. 14, pp. 49-53, 1966.

[141] A. J. Kelly, "Comment on Wide-Angle Impedance Matching of a Planar array Antenna by Dialectric Sheet," *IEEE Trans. Antenna Propag.*, vol. 14, pp. 636-637, 1966.

[142] M. Manteghi and Y. Rahmat-Samii, "Broadband characterization of the total active reflection coefficient of multiport antennas," in *Antennas and Propagation Society International Symposium, IEEE*, pp. 20-23 vol.3, 2003

[143] B. Allen and M. Beach, "On the analysis of switched-beam antennas for the W-CDMA downlink," *Vehicular Technology, IEEE Transactions on*, vol. 53, pp. 569-578, 2004.

[144] A. Paulraj, R. Nabar, and D. Gore, *Introduction to Space-Time Wireless Communications*, Cambridge Univ. Press, 2003.

[145] M. F. Iskander and Y. Zhengqing, "Propagation prediction models for wireless communication systems," *Microwave Theory and Techniques, IEEE Transactions on*, vol. 50, pp. 662-673, 2002.

[146] MatLab user's Guide, MatLab 7.11, the mathworks, 2010

[147] L. R. Maciel, H. L. Bertoni, and H. N. Xia, "Unified approach to prediction of propagation over buildings for all ranges of base station antenna height," *Vehicular Technology, IEEE Transactions on*, vol. 42, pp. 41-45, 1993.

[148] C. E. Shannon, A mathematical theory of communication, Bell Syst. Tech. J., Vol. 27, 379-423, July 1948; Vol. 27, 623-656, Oct. 1948

[149] M. Schwartz, *Mobile wireless communications* Cambridge UK: CAMBRIDGE UNIVERSITY PRESS, 2005.

[150] K. Nishimori, Y. Makise, M. Ida, R. Kudo, and K. Tsunekawa, "Channel Capacity Measurement of 8X2 MIMO Transmission by Antenna Configurations in an Actual Cellular Environment," *Antennas and Propagation, IEEE Transactions on,* vol. 54, pp. 3285-3291, 2006.

[151] A. Boukalov, S-G. Häggman. System Aspects of Smart Antennas Technology in Wireless Communications. Journal IEEE Transactions on Microwave Theory and Techniques, vol. 48, No.6, pp. 919-929, June 2000

[152] J. Lempiainen, M. Manninen (ed.), ”UMTS Radio Network Planning, Optimization and QoS Management”, Kluwer Academic Publishers, Dordrecht, 2003

[153] J. Itkonen, B. P. Tuzson, J. Lempi¨ainen, ”A Novel Network Layout for CDMA Cellular Networks with Optimal Base Station Antenna Height and Downtilt”, *Proc. of Vehicular Technology Conf.*, vol. 2, pp. 688-692, May 2006

[154] J. Itkonen, N. Rahmani, J. Lempi¨ainen, ”A Novel Network Topology for CDMA Networks Based on Modified Hexagonal Grid”, *Proc. of IEE Intl Conf. on 3G and Beyond*, pp. 1-5, November 2005

[155] W. C. Jakes, ”Microwave Mobile Communications”, New York IEEE Press, 1994.

[156] J. Niemel¨a and J. Lempi¨ainen, ”Impact of the Base Station Antenna Beamwidth on Capacity in WCDMA Cellular Networks”, *Proc. of Vehicular Technology Conf.* vol. 1, pp. 80-84, April 2003

[157] J. Perez-Romero, O. Sailent, R. Agusti, ”Impact of user location in W-CDMA downlink resource allocation”, *Proc. of IEEE Intl Symposium on Spread Spectrum Techniques and Applications*, vol. 2, pp. 420-424, September 2002

[158] Z. Ruzicka and S. Hanus, "Radio Network Dimensioning in UMTS Network Planning Process," in *Applied Electromagnetics and Communications, ICECom 18th International Conference,* pp. 1-4, 2005.

[159] K. Hiltunen and N. Binucci, "WCDMA downlink coverage: interference margin for users located at the cell coverage border," in *Vehicular Technology Conference, VTC Spring IEEE 55th*, pp. 270-274 vol.1, *2002*

[160] H. Holma, Z. Honkasalo, S. Hämäläinen, J. Laiho, K. Sipilä, A. Wacker, "Radio network planning," Chapter 8 in H. Holma and A. Toskala (ed.), *WCDMA for UMTS*, John Wiley & Sons, Revised Edition, 2001